Investigation of molecular states with charm and beauty hadrons

Chu-Wen Xiao

Departamento De Física Teórica

Universidad de Valencia

TESIS DOCTORAL

VALENCIA 2014

D. Eulogio Oset Báguena, Catedrático de Física Teórica de la Universidad de Valencia,

CERTIFICA: Que la presente Memoria *Investigation of molecular states with charm and beauty hadrons* ha sido realizada bajo mi dirección en el Departamento de Física Teórica de la Universidad de Valencia por D. Chu-Wen Xiao como Tesis para obtener el grado de Doctor en Física.

Y para que así conste presenta la referida Memoria, firmando el presente certificado.

Fdo: Eulogio Oset Báguena

Contents

Acknowledgment

After devoting several months, now I finish writing my Ph. D thesis, which is guided by my supervisor Prof. Eulogio Oset. During four years of my Ph. D studies, he taught me many things on theoretical physics and how to do research in nowadays particle physics. He is a nice man in the daily life, but is a rigorous professor in the academic study. Thus, he was always strict on me both in my research and in my study. Under his guidance in the world of particle physics, I have learned much about different theoretical approaches, and on how to do the research work. I also thank him for providing me so much happiness during the four years studied in Spain, far away from my hometown, since outside the work he is also a happy man in the daily life.

Secondly, I thank my master supervisor Prof. Wei-Hong Liang. During the three years studied in Guilin, she also taught me a lot in theoretical physics and other basic knowledge. She also gave me a good chance to study abroad. She was also strict on me in my study and made me improve during my master study, which opened the door of particle physics to me. She was also a good guide in my life.

For four years studying in the Valencia Group, the members of the group also helped me a lot and made my life happy. Prof. Manuel J. Vicente Vacas and Prof. Juan M. Nieves Pamplona taught me many skillful techniques in the calculation programs, and helped me a lot in my daily life. I also thank other members in the group for their helpful discussions and kind help, such as Luis Alvarez-Ruso, E. Javier Garzón, Francesca Aceti, En Wang, Toshitaka Uchino, Carlos Hidalgo, Astrid Hiller Blin, Tim Ledwig, and the former members, such as Melahat Bayar, Raquel Molina, Junko Yamagata-Sekihara, M. Pavon Valderrama, Ju-Jun Xie, Hua-Xing Chen, Ignacio Ruiz Simó. I sincerely appreciate the nice collaboration with Melahat Bayar,

Raquel Molina, Francesca Aceti and Toshitaka Uchino in several works. The visitors of our group, for example, Bao-Xi Sun, Altug Ozpineci and Miguel Albaladejo, were very kind to me and I appreciate their help and useful discussions. I also thank the nice collaboration with the Japanese fellows, such as Profs. T. Hyodo, A. Dote and M. Oka.

I acknowledge Prof. Angel Ramos, Prof. José Antonio Oller for useful discussions and kind help, and also thank Feng-Kun Guo, Alberto Martínez Torres, Kanchan Khemchandani, Daniel Gamermann and Michael Doering. I sincerely acknowledge the hospitality by Prof. Peng-Nian Shen when I applied for the visa in Beijing.

In addition, I thank my parents, my wife, my sisters and other relatives of my family, and my friends for accompanying me in the long way of my life and giving me encouragement continually.

Dear friends, maybe just saying "thank you" is not enough, but I should say it to you.

Finally, it is mandatory to acknowledge the held of the funding agencies that supported me and my work all this time. The work was partly supported by the Spanish Ministerio de Economia y Competitividad and European FEDER funds under Contract No. FIS2011-28853-C02-01 and the Generalitat Valenciana in the program Prometeo, 2009/090. I also acknowledge the support of the European Community-Research Infrastructure Integrating Activity Study of Strongly Interacting Matter (Hadron Physics 3, Grant No. 283286) under the Seventh Framework Programme of the European Union.

Gracias todos!

Chu-Wen Xiao
May, 2014

肖 楮 文

2014年五月 · 写于 IFIC， 瓦大

Introduction

The beginning of the last century brought two revolutions in physics: General Relativity and Quantum Mechanics that allowed physicists to dig into the universe of the large scales and small distances, respectively. A few significant physicists, see the picture in Fig. 1, helped to establish the new principles that challenged conventional wisdom. With the pass of the years the interconnection of the two worlds has become closer, with clear implications of the world of elementary particles in Astrophysics and Cosmology. The relationship about the two developed directions in nowadays physics

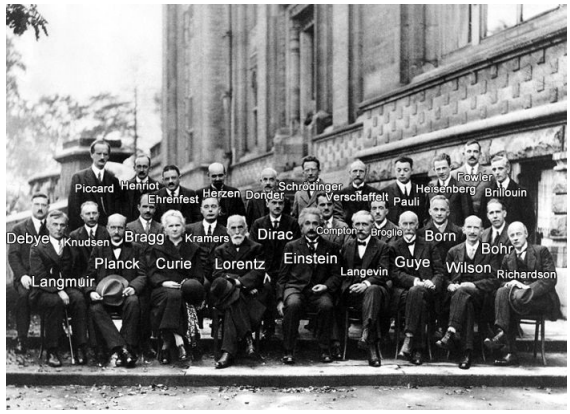

Figure 1: Solvay Conference on 1927.

can be visualized in the Cosmic Uroboros picture, seen in Fig. 2. From head to tail around the serpent in Fig. 2, the icons represent the size of the cosmic horizon (10^{28} cm), the size of a supercluster of galaxies (10^{25}), a single galaxy, the distance from Earth to the Great Nebula in Orion, the solar

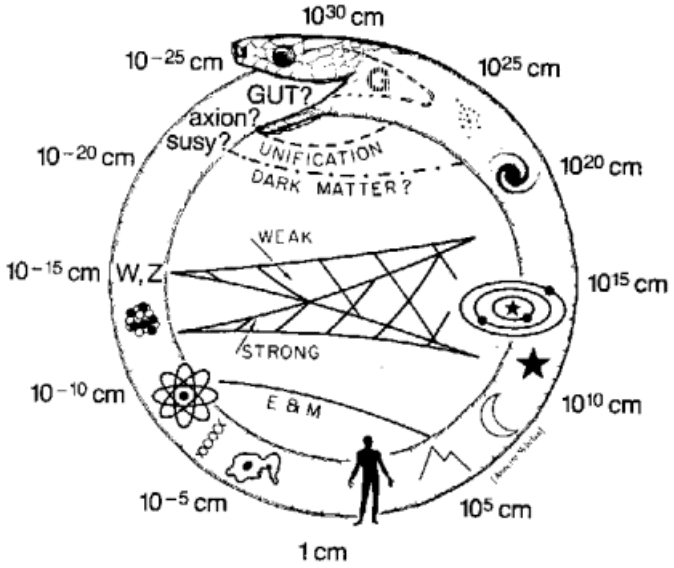

Figure 2: The scale of the modern physics.

system, the sun, the earth, a mountain, humans, a single-celled creature of the bacterium, a strand of DNA, an atom, a nucleus, the scale of the weak interactions (carried by the W and Z particles), and approaching the tail the extremely small size scales on which physicists hope to find massive dark matter particles ($10^{-17} - 10^{-25}$ cm), and on even smaller scales a Grand Unified Theory [1](GUT). We can see that particle physics (small size) and cosmology (large size) overlap each other at last, as the tail inside the head of the snake in the figure.

In the present work I shall concentrate on the region of $10^{-15} - 10^{-13}$ cm, where standard elementary particles find their place. In modern high energy physics it has been accepted generally that quarks are the basic building blocks of matter. With the Gell-Mann-Zweig quark model [2, 3] for the normal hadron states, mesons are made of a quark-antiquark pair, $q\bar{q}$, and baryons made of three quark components, qqq. The strong interaction between quarks and gluons is described by Quantum Chromodynamics (QCD). According to QCD theory, mesons and baryons are formed from color-singlet combinations of quarks. The need for the extra color degrees of freedom is

evidenced by the existence of the $\Delta^{++}(\frac{3}{2}^+)$. Its flavour-spin wave function is symmetric and one should introduce another color wave function to save Fermi statistics, an antisymmetric color wave function, which is made of three components, red, green and blue. Thus, with six basic quark components (flavour) combined with three colors, the wave functions of color-singlet combinations for hadrons are described as $SU(6)_{flavor} \otimes SU(3)_{color}$. The quark model was successfully motivated by the so-called "November revolution" [4, 5], with the discovery of the J/ψ particle nearly at the same time by two experimental groups in 1974, and drew the attention of many theoretical physicists later on [6–8]. After this discovery, both theory and experiment jumped to search for new states with charm, which are a good testimony for the QCD predictions. Therefore, with the new found states with charm, even though c quark is much heavier than the s, u, d quarks, meaning that symmetry is broken badly, we still can include the fourth quark, charm c, by extending SU(3) to SU(4). Thus, for $q\bar{q}$ mesons, we have $3 \otimes \bar{3} = 8 \oplus 1 \to 4 \otimes \bar{4} = 15 \oplus 1$. But, for qqq baryons, the configurations of 3-quark are more complicated than for mesons, and also the SU(4) symmetry is more strongly broken for the heavy c quark. Generally, most of the "ordinary" mesons and baryons with s, u, d and c can be included in SU(4) multiplets, as shown in Fig. 3. This is the success of QCD in the interpretation for the structure of the particles.

On the other hand, in the experiments, there are some states found, such as the mesons, $f_0(500)$, $f_0(980)$, $a_0(980)$, $\kappa(800)$, $f_0(1370)$, $f_0(1500)$ and $f_0(1710)$, *et al.*, the baryons, $\Lambda(1405)$, $N(1440)$, $N(1535)$, *et al.*, with structure and properties difficult to explain by the normal quark model. Thus, these states are called sometimes "exotic" states, although strictly speaking exotic states are those which can not be built with $q\bar{q}$ for mesons or qqq for baryons. Some recent experimental discussions are given in [10, 11]. What is the structure of these states? Under the Standard Model (SM) proposed by Glashow [12] and Weinberg [13], the strong interacting particles are colored quarks and gluons, described by the QCD, but, the visible particles in nature are color-singlet mesons and baryons. In theory, there are still some states expected to be color-singlet with multi-quark combinations, which are typically predicted by QCD-motivated models as non-$q\bar{q}$ mesons and non-qqq baryons. For example, similarly to the familiar meson octet of flavour-SU(3) combining a quark triplet with an antiquark antitriplet, two

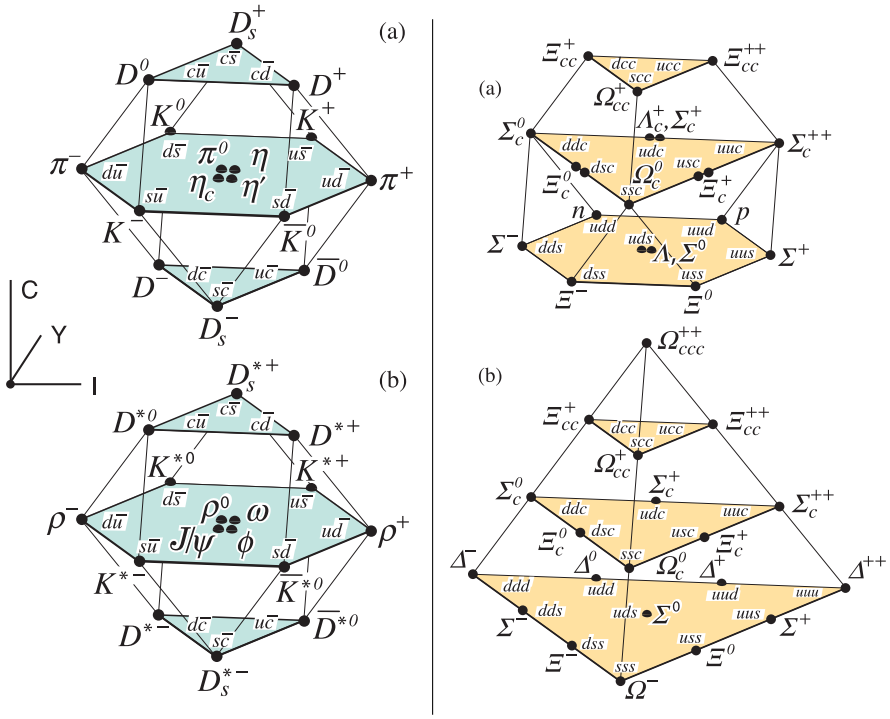

Figure 3: SU(4) multiplets of mesons (left) and baryons (right) [9]. Left: (a) for the 16-plets of pseudoscalar mesons; (b) for the 16-plets of vector mesons. Right: the 20-plet with an SU(3) octet; (b) the 20-plet with an SU(3) decuplet.

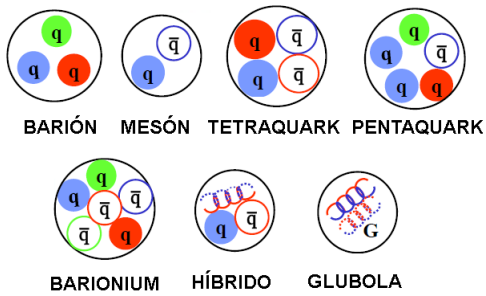

Figure 4: The diagram presentation of the "normal" and exotic states: baryon, meson, tetraquark, pentaquark, baryonium, hybrid and glueball (in Spanish).

quark triplets can be combined to form a "diquark" antitriplet and a sextet, or, green-red and blue-green diquarks form yellow (antiblue) and cyan (antired) antitriplets. In fact, these diquarks do not exist since they are not color-singlets [10]. But, the anticolored diquark antitriplets could combine with other colored antiquark antitriplets to make a more complicated structure forming multiquark color-singlet states. These so-called "exotic" color-singlet multiquark states are: tetraquark mesons (containing a diquark and diantiquark, 4-quark state $[\bar{q}\bar{q}][qq]$), pentaquark baryons (containing two diquarks and one antiquark, 5-quark state $\bar{q}qqqq$), the H-dibaryon (containing three diquarks, 6-quark state $qqqqqq$), glueballs (mesons made only from gluons, gg, ggg), hybrids (formed from a q, $\bar{q}$ and a gluon $\bar{q}qG$, or $qqqg$), and molecules (deuteron-like bound states made with two or more color-singlet "normal" hadrons, $q\bar{q}$ mesons or/and qqq baryons, by exchanging virtual mesons π, ρ, ω, $\cdots$, for example, meson-meson molecule $(q\bar{q})(q\bar{q})$, meson-baryon molecule $(q\bar{q})(qqq)$, baryon-antibaryon molecule called baryonium $(\bar{q}\bar{q}\bar{q})(qqq)$, and so on), some of them are illustrated in Fig. 4. One should note that theoretically the molecules are constructed from the long distance interaction force at the hadron level and are different from the other categories of exotic states at the quark level (short distance region).

Looking for these exotic state candidates, they have been the subject of many theoretical and experimental investigations in hadron physics. The structure of the lightest scalar mesons σ, κ, $a_0(980)$ and $f_0(980)$, *et al.*, is still a critical issue in the theoretical interpretation. Are their components

tetraquarks (see lattice QCD simulation [14]), mixing of scalar tetraquark and quarkonia states [15], mesonic molecules [16–20], or something else? A recent investigation of these states with tetraquarks, molecules, meson-meson scattering and disconnected contributions in lattice was done in Ref. [21], showing that whenever there are both connected and singly disconnected contributions, the disconnected part should never be dropped. The tetraquark $[\bar{q}\bar{q}][qq]$ potential was analysed in detail using SU(3) lattice QCD in Ref. [22]. Also there are some heavy states claimed recently as tetraquark states with QCD sum rules [23–26].

In the 2003, LEPS's experiment reported the existence of a peak in the K^+n invariant mass distribution in the reaction $\gamma n \to K^+K^-n$ [27] measured in nuclei, declared as an evidence of the pentaquark and called Θ^+ state (also seen in CLAS [28] and HERA-B [29]), which drew numerous theoretical attentions later: results with QCD sum rule [30, 31], SU(3) Skyrme model [32], lattice QCD [33], decay model [34, 35], chiral perturbation method [36, 37], and so on. But, later in high-statistices experiments of CLAS [38] and J-PARC [39], the signal of this state could not be reproduced. Therefore the existence of the pentaquark is still a questionable issue because of recent theoretical results in Effective Field Theory [40, 41], SU(3) lattice QCD [42, 43] and QCD sum rule [44] (a recent experimental review can be seen in Ref. [45]). Actually, the updated reaction of Ref. [27] performed in Ref. [46] with the $\gamma d \to npK^+K^-$ reaction, where a peak was also seen, was dismissed as a proof of a state in Ref. [47]. It was show there that a broad peak in the region of the K^+n invariant mass around 1540 MeV come artificially from the prescription given to calculate the momentum of the neutron which was not measured (nor the proton). It was shown there that the prescription failed to reproduce the actual neutron momentum. In addition it was shown that extra strength could be produced with a fluctuation. This was indeed the case and in the final accumulated strength with three times more statistics, the narrow peak has disappeared [48] and only the broad peak predicted in Ref. [47] remains.

The H-dibaryon was first predicted in 1977 by R.L. Jaffe with the quark bag model [49], which proposed a stable, flavor-singlet (strangeness $S = -2$) bound state dihyperon $H(2150)$ and another isosinglet dihyperon $H^*(2335)$ state (as a bump in the $\Lambda\Lambda$ invariant-mass distribution). After that, the six quark states were also investigated theoretically with a nonrelativistic

quark model [50], the Skyrme model [51], and recently lattice QCD [52,53], and chiral effective field theory [54]. To search for the H-dibaryon experimentally, the KEK-PS E224 Collaboration investigated the $\Xi^- {}^{12}C$ reaction at rest and found no strong evidence of H-dibaryon state in the observed Λ momentum spectrum [55]. With better statistics, the KEK-PS E522 Collaboration observed a bump near the $\Lambda\Lambda$ threshold in the new measurement data of the $\Lambda\Lambda$ invariant mass spectrum for the ${}^{12}C(K^+, K^-\Lambda\Lambda X)$ reactions, and still there was no significant enhancements observed above the level of the model predictions [56]. More recently Belle experiments with high-statistics looked for H-dibaryon production in inclusive $\Upsilon(1S)$ and $\Upsilon(2S)$ decays [57]. In their searched results there is no evidence of the $H \to \Lambda p\pi^-$ ($\bar{H} \to \bar{\Lambda}\bar{p}\pi^+$) signals in the inclusive $\Lambda p\pi^-$ ($\bar{\Lambda}\bar{p}\pi^+$) invariant mass distribution, and also of the $H \to \Lambda\Lambda$ ($\bar{H} \to \bar{\Lambda}\bar{\Lambda}$) signals in the $\Lambda\Lambda$ ($\bar{\Lambda}\bar{\Lambda}$) mass spectra. Therefore, until now, similarly to the pentaquark state, there is still no evidence for the H-dibaryon (or six-quark states) in nowadays experiments. Their existence is just at the level of the strong theoretical motivation in different models.

Therefore, at present, we still lack enough experimental evidence for the existence of so called "exotic" hadrons predicted by QCD-motivated models. But, for the molecules, the situation is different for there is much experimental support from hadron interactions. Strong evidence is found in high energy hadron experiments that many new particles are not simply explained in the normal quark model, such as baryoniums, and XYZ mesons which are charmonium-like and bottomonium-like states still not fitting into $c\bar{c}-$ and $b\bar{b}-$meson level schemes. Early in 1949, Fermi and Yang worked on the "elementary" particles to find out what particles are simple and what particles are complex, and theoretically proposed that the pion was a tightly bound state formed by a nucleon and an anti-nucleon [58], which is known as so-called baryonium (later, more theoretical discussions are seen in Refs. [59–61]). Many years later, the BESII collaboration reported the observation of a strong near-threshold mass enhancement in the invariant mass spectrum of $p\bar{p}$ in the radiative decay process $J/\psi \to \gamma p\bar{p}$ in 2003 [62], which observed a narrow peak close to low-mass $p\bar{p}$ system with the mass of $M = 1859^{+3}_{-10}(\text{stat})^{+5}_{-25}(\text{syst})$ MeV/c^2 and the width of $\Gamma < 30$ MeV/c^2 fitted by the S-wave Breit-Wigner resonance function. This possible new resonance is modified with a small shift on its mass and width by the BESIII

experiments in 2012, $M = 1832^{+19}_{-5}(\text{stat})^{+18}_{-17}(\text{syst}) \pm 19(\text{model})$ MeV/c^2 and $\Gamma < 76$ MeV/c^2 [63], using more J/ψ sample events and a partial wave analysis. This new hypothetical state is known as $X(1835)$, and has draw much theoretical attention by different models [64–71]. A search for this state in experiments was reviewed in Ref. [72], but it has also been questioned as a new state in [73], which concludes that the peak observed is a consequence of the final state interaction. Thus, the study of baryonium spectrum is a topic of hadron physics drawing much theory attention. In Ref. [74], using the one-boson-exchange potential model, the states of $Y(2175)$ and $\eta(2225)$ are declared as bound states of $\Lambda\bar{\Lambda}$ $^3S_1$ and $\Lambda\bar{\Lambda}$ $^1S_0$, respectively. However, in Ref. [75] the $Y(2175)$, now officially called $\phi(2170)$, is found as a three body resonance of $\phi K\bar{K}$, with the $K\bar{K}$ forming the $f_0(980)$. In the heavy quark sector, Ref. [76] concluded that the $Y(4630)$ and $Y(4660)$ are the first observation of charmed baryonium constituted by four quarks, by reanalyzing the Belle experimental data of $Y(4630) \to \Lambda_c\bar{\Lambda}_c$ and $Y(4660) \to \psi(2S)\pi\pi$. Using heavy baryon chiral perturbation theory, Ref. [77] investigated the heavy baryonium mass spectrum and searched for bound states by solving the Schrödinger equation with the two-pion exchange interaction potential. Analogously, with the same method, the heavy baryonium mass spectrum was revisited extrapolating the charm systems $\Lambda_c\bar{\Lambda}_c$, $\Sigma_c\bar{\Sigma}_c$ to the beauty sector of $\Lambda_b\bar{\Lambda}_b$ in Ref. [78].

In 2003, another well known particle was found, $X(3872)$, which was first discovered in the Belle experiment of the exclusive decay process $B \to K\pi^+\pi^- J/\psi$ [79]. In this decay process, a narrow peak was found in the $\pi^+\pi^- J/\psi$ invariant mass distribution, with mass $M = 3872.0 \pm 0.6(\text{stat}) \pm 0.5(\text{syst})$ MeV and width $\Gamma < 2.3$ MeV, which is very close the $m_{D^0} + m_{D^{*0}}$ threshold. Later, this new state, $X(3872)$, was confirmed in different experiments via different decay channels, CDF [80], DØ [81], BaBar [82], and its J^{PC} quantum numbers were also established recently in the Large Hadron Collider (LHC) experiment of the LHCb's results [83], as $J^{PC} = 1^{++}$. The $X(3872)$ is well know as a key member of the heavy quarkonium family (more discussion about this particle is seen in the review of Ref. [84]). One also has the so-called XYZ mesons, which can decay to final states containing a heavy quark Q (where Q is either a c or b quark) and a heavy antiquark $\bar{Q}$, but cannot be easily accommodated in an unfilled $Q\bar{Q}$ level. Normally, in the quark model, a heavy quark Q and a

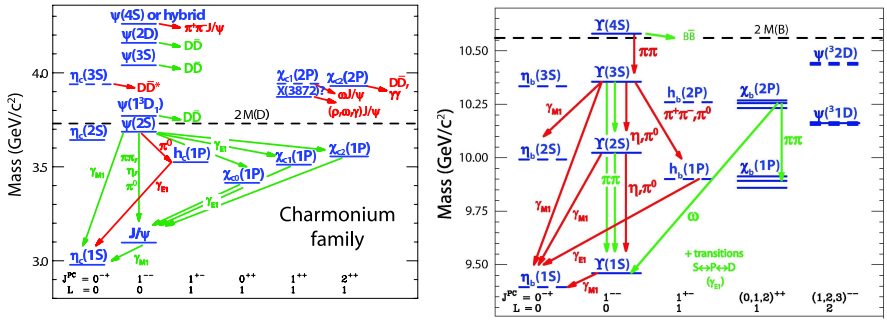

Figure 5: The spectrums of charmonium (left) and bottomonium (right).

heavy antiquark $\bar{Q}$ can construct $Q\bar{Q}$ particle systems, called conventional "quarkonium" mesons, such as charmonium (with Q as c) and bottomonium (with Q as b), and these systems can be reasonably well described by non-relativistic Quantum Mechanics (quarkonium model). For example, $\eta_c(1S)$, $h_c(1P)$, $\eta_c(2S)$, J/ψ, $\psi(3770)$, $\chi_{c0}(1P)$, $\chi_{c1}(1P)$, $\chi_{c2}(1P)$, $\psi(4040)(3S)$, $\psi(4160)(2D)$, $\psi(4415)(4S)$, *et al.*, are conventional charmonium states [85], and, $\eta_b(1S,\, 2S)$, $h_b(1P,\, 2P)$, $\chi_{bJ}(1P\, 2P)$, $\Upsilon(nS)$, *et al.*, are bottomonium states [86], as shown in Fig. 5. But, the properties of $X(3872)$ are not consistent with the normal charmonium, thus, it is just a charmonium like state, which has drawn much attention in theoretical discussions [87–96]. Motivated by the discovery of $X(3872)$, the experimental facilities of charm factories and B-factories, such as BABAR at PEP-II, Belle at KEKB, CLEO-III and CLEO-c at CESR, CDF and D at Fermilab, BESII and BESIII at BEPCII, KEDR at VEPP-4, and, MALICE, ATLAS, CMS, LHCb at the LHC, *et al.*, have looked for new heavy quarkonium states and have found many charmonium like and bottomonium like states in the last decade, for example, $X(3940)$, $X(4160)$, $Y(3915)$, $Y(4260)$, $Y(4360)$, $Z(4430)$, $Z_1(4050)$, $Z_2(4250)$, *et al.*. Even though there is no confirmation of the observation of $Z(4430)$, $Z_1(4050)$, $Z_2(4250)$ by the Belle collaboration [97, 98], a more exciting recent finding is the observation of the state $Z_c^+(3900)$ in the BESIII experiment $Y(4260) \to J/\psi\pi^+\pi^-$ decay [99], which was seen as a peak in the $\pi^\pm J/\psi$ mass spectrum, and was later confirmed by Belle collaboration [100] and the analysis of the CLEO-c data [101]. Not

soon later, the BESIII collaboration reported the results of related observations, with three more charged states, $Z_c^+(4025)$ [102], $Z_c^+(4020)$ [103], $Z_c^+(3885)$ [104]. But, up to now, the states $Z_c^+(3900)$ and $Z_c^+(3885)$, also $Z_c^+(4025)$ and $Z_c^+(4020)$, seem likely the same state but seen in different decay channels, and more investigations are needed before a firm conclusion can be drawn [10,105–107]. On the other hand, the $Y(4260)$ state, which was first discovered by BaBar in the initial-state radiation (isr) process $e^+e^- \to \gamma_{isr}\pi^+\pi^- J/\psi$, as a broad resonance peak in the invariant-mass spectrum of $\pi^+\pi^- J/\psi$ [108], was subsequently confirmed by CLEO [109], Belle [110]. Due to the large partial decay width of $\Gamma(Y(4260) \to \pi^+\pi^- J/\psi) > 1$ MeV, which is much larger than that for typical charmonium [111], as suggested by W. S. Hou in 2006 [112], the Belle collaboration was motivated to investigate whether or not there is a corresponding structure in the bottomonium mass region $\sqrt{s} \sim 10.87$ GeV. In this investigation the large anomalous cross section for $e^+e^- \to \pi^+\pi^-\Upsilon(nS)$, $(n = 1, 2, 3)$ and the partial widths $\Gamma(\Upsilon(5S) \to \Upsilon(mS)\pi^+\pi^-)$, $(m = 1, 2)$ obtained from the observed cross sections [113], may suggest the existence of a bottomonium like $b\bar{b}$ state around the energy range 10.89 GeV, as suggested in Ref. [112], which would be the equivalent of the $Y(4260)$. Therefore, continuing studies, Belle subsequently found the strong resonance signals in the mass spectra of the decay processes $\Upsilon(5S) \to \Upsilon(nS)\pi^+\pi^-$, $(n = 1, 2, 3)$ and $\Upsilon(5S) \to h_b(mP)\pi^+\pi^-)$, $(m = 1, 2)$ [114], which corresponded to two charged bottomonium-like states, the $Z_b(10610)$ and $Z_b(10650)$. The observation of $Z_c^+(3900)$, $Z_b(10610)$ and $Z_b(10650)$ in recent experiments has drawn much attention to theoretical discussions and comments [115–123]. In 2012, BESIII also observed seven N^* intermediate states in the decay channel $\psi(3686) \to p\bar{p}\pi^0$ [124], as $N(1440)$, $N(1520)$, $N(1535)$, $N(1650)$, $N(1720)$, and, two new resonances $N(2300)$ and $N(2570)$. There are also some predictions of the exotic baryons recently in theory, about resonant states formed by a heavy meson and a nucleon [125, 126], hidden charm baryons [127], hidden beauty baryons [128], and about baryon-baryon bound states [129].

Until now, the large number of new states found in the hadron experiments during the last few years in charmonium and bottomonium spectroscopy, seem to suggest that there are there too many XYZ states, as claimed in Ref. [130]. Furthermore, the properties of some of them are still

not easy to explain within the conventional quark model spectrum. The situation is that there are no compelling theoretical pictures that provide an unquestionable description of what is seen in the experiments. As the Quarkonium Working Group (QWG) concluded, there are still a lot of surprises and puzzles in the studies of heavy quarkonium [131] (more comments are also seen in the reviews of Refs. [132,133]). Although far away from the states reported so far, one cannot omit here the Higgs-like boson which was discovered by the ATLAS Collaboration and the CMS Collaboration in LHC experiments at CERN [134, 135]. This discovery is considered to be the most important advance in particle physics in the last half century, and justified the awarding of the Nobel Prize in Physics for 2013 to François Englert and Peter W. Higgs [136].

Thus, under the SM, the understanding of the properties of the particles found in the hadron experiments, such as structure, decay mode, production, and in-medium behaviour, *et al.*, and the search for new states of the hadron spectroscopy theoretically, is the motivation of the present thesis. What theories and methods do we exploit? I will give more details in the next chapter. Then, I will show our investigation results in the following three chapters, and finish with a chapter dedicated to the conclusion.

Chapter 1

Theoretical Approach

In this chapter, we will give a detail of the theories and approaches used in the present work. First, we make a short review of the QCD theory, such as its Lagrangian, running coupling, asymptotic freedom, confinement, chiral symmetry and its breaking, and so on. Following, I will make a summary on the interaction Lagrangian used in the present work. Next, one of the non-perturbative QCD methods, the chiral unitary approach will be discussed, including its extrapolation to higher partial waves. Then, we review one more extrapolation of the chiral unitary approach to the Faddeev equations for the three-body interaction, and its application under the Fixed Center Approximation (FCA). Finally, we make an overview of the heavy quark flavour-spin symmetry and Heavy Quark Effective Theory.

1.1 The QCD theory

The strong interaction is the strongest force of nature, which binds nucleons in nuclei. Quantum Chromodynamics (QCD) is the theory of strong interactions, a gauge field theory that describes the strong interactions of colored quarks and gluons. Nowadays, QCD has firmly occupied its place as part of the Standard Model (SM) of Particle Physics as a SU(3) component of the SU(3) $\times$ SU(2) $\times$ SU(1) gauge theory, where the SU(3) gauge group describes the strong color interactions among quarks and the SU(2) $\times$ SU(1) gauge group describes the electroweak interactions.

1.1.1 The QCD Lagrangian

In the framework of a constituent quark model, the spin 3/2 baryon, Δ^{++}, is composed of three identical up (u) quarks. Thus, together with spin, isospin, its wave function with spin third component 3/2 can be written as $|\Delta^{++}\rangle = |u\uparrow u\uparrow u\uparrow\rangle$, which is a completely symmetric wavefunction and is in contradiction with the spin-statistics theorem for a fermion. Therefore, the only way to construct a completely antisymmetric wavefunction for the Δ^{++} is to postulate an additional quantum number, which is called "color". Then, the quarks can exist in three different color states, called red, green and blue. Thus, we can make an antisymmetric wavefunction in color space, $|\Delta^{++}\rangle = \frac{1}{\sqrt{6}}\epsilon^{ijk}|u_i\uparrow u_j\uparrow u_k\uparrow\rangle$, where ϵ^{ijk} is the totally antisymmetric tensor. Since there are 3 dimensions for the color space, the context of QCD is based on the gauge group SU(3), a Special Unitary group with 3 complex dimensions. Now we can define a quark field in the 3-dimensional color space

$$\psi_q^i(x) = \begin{pmatrix} \psi_q^1(x) \\ \psi_q^2(x) \\ \psi_q^3(x) \end{pmatrix},$$

with a given flavour $q = u, d, s, ...$, which fulfils a colour gauge transformation,

$$\begin{aligned} \psi_q^i(x) &\to \psi_q'^i(x) = U_k^i(x)\psi_q^k(x)\,, \\ \bar{\psi}_{q\,i}(x) &\to \bar{\psi}'_{q\,i}(x) = \bar{\psi}_k U_i^{\dagger\,k}(x)\,, \end{aligned} \tag{1.1}$$

where the $U_k^i(x)$ is the usual exponential representation of the gauge transformation matrix, which is a 3×3 matrix and depends arbitrarily on the quark coordinates x, given by

$$U_k^i(x) = \exp\left[-i\sum_{a=1}^{8}\chi^a(x)\frac{(\lambda^a)_k^i}{2}\right], \tag{1.2}$$

where it contains eight independent and arbitrary functions $\chi^a(x)$ multiplied by eight reference matrices λ^a ($a = 1, ...8$), the Gell-Mann matrices [137].

The QCD Lagrangian has to be exactly symmetric with respect to the local gauge transformations of Eq. (1.1) and describes the interactions of quarks and gluons, which contains three parts,

$$\mathcal{L}_{QCD} = \mathcal{L}_{qua} + \mathcal{L}_{int} + \mathcal{L}_{glu}. \tag{1.3}$$

The first part of the Lagrangian, $\mathcal{L}_{qua}$, describes the propagation of free quarks, given by

$$\mathcal{L}_{qua}(x) = \sum_{q=u,d,s,\ldots} \left(\sum_{k=1,2,3} \bar{\psi}_{q\,k}(x)(i\partial_\mu \gamma^\mu - m_q)\psi_q^k(x) \right) , \tag{1.4}$$

where m_q is the quark mass, and γ^μ are the Dirac γ-matrices. The second part, $\mathcal{L}_{int}$, is a quark-gluon interaction term, as

$$\mathcal{L}_{int}(x) = g_s \sum_{q=u,d,s,\ldots} \bar{\psi}_{q\,i}(x) \frac{(\lambda^a)^i_k}{2} \gamma^\mu \psi_q^k(x) A_\mu^a(x) \, . \tag{1.5}$$

where g_s is the dimensionless coupling, and $A_\mu^a(x)$ correspond to the gluon fields. Then, the third part, $\mathcal{L}_{glu}$ is a gauge-invariant term describing the propagation of gluon fields, written

$$\mathcal{L}_{glu}(x) = -\frac{1}{4} F_{\mu\nu}^a(x) F^{a\,\mu\nu}(x) \, , \tag{1.6}$$

where

$$F_{\mu\nu}^a = \partial_\mu A_\nu^a - \partial_\nu A_\mu^a - g_s f^{abc} A_\mu^b A_\nu^c \, , \tag{1.7}$$

is the gluon field-strength tensor, and the f^{abc} are the structure constants of the SU(3) group, having $[\lambda^a, \lambda^b] = i f^{abc} \lambda^c$. Finally, the full form of the QCD Lagrangian is obtained by adding together the three pieces above

$$\mathcal{L}_{QCD} = \sum_q \bar{\psi}_q (i D_\mu \gamma^\mu - m_q)\psi_q - \frac{1}{4} G_{\mu\nu}^a G^{a\mu\nu} \, , \tag{1.8}$$

where we define $D_\mu = \partial_\mu - i g_s \frac{\lambda^a}{2} A_\mu^a$. We can see that, $\mathcal{L}_{QCD}$ describes not only quark-gluon interactions but also gluondynamics (the specific gluon self-interactions), and the fundamental parameters of QCD are the coupling g_s (or $\alpha_s = \frac{g_s^2}{4\pi}$ [9]) and the quark masses m_q.

1.1.2 Running coupling, asymptotic freedom and confinement

Now we will discuss about an important parameter of the QCD Lagrangian, the coupling in the quark-gluon interaction term, g_s. As an assumption or

approximation, if the strong coupling do not run, QCD would be a theory with a fixed coupling, the same at all scales, and is scale invariant, which is closely related to the class of angle-preserving symmetries (called conformal symmetries) and due to a property of light-cone scaling (called Bjorken scaling) [138].

On top of the underlying scaling behavior, the running coupling will introduce a dependence on the absolute scale, meaning that it is a function of an (unphysical) renormalization scale μ, as $\alpha_s = \frac{g_s^2}{4\pi} = \alpha_s(\mu^2)$ (for a given process, if one takes μ as the scale of the momentum transfer Q, then, $\alpha_s(\mu^2) = \alpha_s(Q^2)$). The running is logarithmic with energy, thus, the coupling is governed by the so-called beta function, a renormalization group equation, satisfying

$$\beta(\alpha_s) \;=\; \mu^2 \frac{\partial \alpha_s}{\partial \mu^2} \;=\; \frac{\partial \alpha_s}{\partial \ln\, \mu^2}, \tag{1.9}$$

where the function driving the energy dependence is defined as

$$\beta(\alpha_s) \;=\; -\sum_{n=0}^{\infty} b_n\, \alpha_s^{n+2} = -\alpha_s^2\,(b_0 + b_1\,\alpha_s^1 + b_2\,\alpha_s^2 + \cdots), \tag{1.10}$$

with $b_0,\ b_1,\ b_2, \cdots$ as the coefficients of leading order (one-loop), next to leading order (two-loop), next to next to leading order (three-loop), $\cdots$ (their values can be seen in Refs. [9, 138–140]). And a minus sign in Eq. (1.10) is consistent with the fact of asymptotic freedom, discussed later.

We can see that, the differential equation of Eq. (1.9) depends on the energy scale, since there will be an integrated constant μ_0, and also depends on how many loops are involved in the calculation from the loop coefficients b_i of Eq. (1.10). For example, working on one loop amplitude and a given scale of μ (or Q) as the mass of Z boson, $Q = m_Z$, one can determine the running coupling for the $b_0 > 0$ and the number of flavors $n_f \leq 16$,

$$\alpha_s(Q^2) \;=\; \frac{\alpha_s(m_Z^2)}{1 + b_0 \alpha_s(m_Z^2) \log(Q^2/m_Z^2) + \mathcal{O}(\alpha_s^2)}, \tag{1.11}$$

where $\alpha_s(m_Z) \simeq 0.12$ [140], which is a small value and means a weak coupled effect in the m_Z scale. Using Eq. (1.11), the running of the coupling constant is shown in Fig. 1.1 (so-called running coupling). As one can

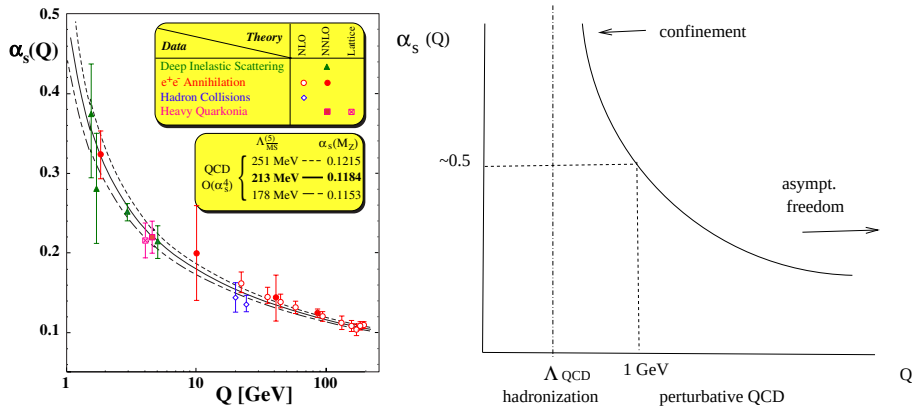

Figure 1.1: The running coupling constant $\alpha_s(Q^2)$ as a function of momentum transfer Q^2 [140] (left), and the schematic view of the α_s behavior at different scales [137] (right).

be seen in the left of this figure, there is a wide region spreading up to the scale $Q > 1$ GeV. In this region, the coupling α_s is small, $\alpha_s \sim 0.1 - 0.3$, thus, the strong coupling becomes weak for the "hard" processes [9, 141] involving large momentum transfers which correspond to short distances, $r \sim 1/Q$, and one can apply perturbative QCD. Furthermore, from Eq. (1.11) and Fig. 1.1, a most spectacular consequence is the vanishing of the running coupling in the limit of a very large energy (or momentum transfer),

$$\alpha_s(Q^2) \to 0 \qquad \text{for} \qquad Q^2 \to \infty. \tag{1.12}$$

This leads to the well known results of asymptotic freedom, discovered by D. Gross, F. Wilczek, and H. Politzer [142,143] (the Nobel prize in physics was awarded to them in 2004), which means that the QCD coupling effectively decreases with energy and then when the quarks are really close to each other, the force is so weak that they behave almost as free particles (more correctly, it is the coupling rather than the force which becomes weak as the distance decreases.) [138].

Conversely, quite a different situation takes place in the quark-gluon interactions at small momentum transfers (at long distances). According to Eq. (1.11) and Fig. 1.1, we also can see that when the scale is close to 1 GeV the coupling diverges rapidly, indicating that in the region of the scale

$Q < 1$ GeV (large-distance or low-momentum transfer) the perturbative QCD can not be applied. Therefore, this low momentum transfer region is also called non-perturbative region, where the coupling becomes very strong for the long distant interaction, and the fact is that the force between two quarks does not vanish as their separation (or distance) r increases, having

$$V(r) \rightarrow \infty \quad as \quad r \rightarrow \infty. \tag{1.13}$$

Thus, when the quarks move apart, the force becomes stronger since the distance increases. This force forbids the quarks to separate, then, in nature we can not see the free quarks, showing that quarks are confined at rather short distances ($\sim$ 1 fm), the fact of confinement. It is true that at long distances quarks and antiquarks strongly interact and form hadrons, which is a characteristic for QCD at low energy scale. In QCD, the non-observation of free colour-charged particles (quarks, antiquarks and gluons) is arranged in a form of the colour confinement principle, postulating that all observable states, i.e., all hadrons, have to be colour-neutral [137]. To work on this region, we should use nonperturbative methods, for example, Effective Field Theory (EFT) [144–147] (we will discuss it later), of which the underlying ideas is to extrapolate the QCD Lagrangian symmetry to construct the interaction Lagrangian with the "confinement" hadrons of the color singlet instead of the unseen and unfree (even until now) quarks and gluons.

1.1.3 Chiral symmetry and its breaking

Nowadays, we know that there are six quark flavors with different masses, the three light quarks u, d, and s and the three heavy flavors c, b, and t,

$$\begin{pmatrix} m_u = 0.002 \text{ GeV} \\ m_d = 0.005 \text{ GeV} \\ m_s = 0.095 \text{ GeV} \end{pmatrix} \ll 1\,\text{GeV} \leq \begin{pmatrix} m_c = 1.275 \text{ GeV} \\ m_b = 4.650 \text{ GeV} \\ m_t = 173.5 \text{ GeV} \end{pmatrix},$$

where 1 GeV is the scale of QCD as discussed before. Thus, for small momentum transfer, $Q < 1$ GeV $< m_{c,b,t}$, the heavy quarks should not have any influence on the dynamics, which will lead to a new flavor symmetry of QCD, chiral symmetry (on the other hand, conversely, for the heavy quark sector, the approximation to take the $m_Q \rightarrow \infty$ limit of QCD will lead to another symmetry, spin-flavor heavy quark symmetry, discussed

later). Containing only the light-flavor quarks in the so-called chiral limit, $m_u, m_d, m_s \to 0$ ($m_q \to 0$), the QCD Lagrangian of Eq. (1.8) is therefore invariant under the independent transformations of right- and left-handed fields ("chiral rotations") :

$$\psi_{q_l}^R = \frac{1}{2}(1+\gamma_5)\psi_{q_l}; \qquad \psi_{q_l}^L = \frac{1}{2}(1-\gamma_5)\psi_{q_l}, \tag{1.14}$$

where q_l are only light quark fields. With the absence of the heavy quarks and the massless of light quarks, the QCD Lagrangian in the chiral limit can then be written as

$$\mathcal{L}_{QCD}^0 = \sum_{q_l}(\bar{\psi}_{q_l}^R i D_\mu \gamma^\mu \psi_{q_l}^R + \bar{\psi}_{q_l}^L i D_\mu \gamma^\mu \psi_{q_l}^L) - \frac{1}{4} G_{\mu\nu}^a G^{a\mu\nu}\,, \tag{1.15}$$

which is invariant under independent global $SU(3)_L \times SU(3)_R$ symmetry.

In fact, the light quarks, u, d, and s, have not exact zero masses. Therefore, the chiral symmetry of the strong interactions is broken by the particularly non-zero quark masses. Taking into account finite light quark masses, the quark mass term mixes left- and right-handed fields,

$$\mathcal{L}_M = -\bar{\psi}_{q_l} M \psi_{q_l} = -(\bar{\psi}_{q_l}^R M \psi_{q_l}^L + \bar{\psi}_{q_l}^L M \psi_{q_l}^R)\,, \tag{1.16}$$

which is an explicit symmetry-breaking term when it transforms under $SU(3)_L \times SU(3)_R$ (more discussions can be seen in Ref. [148]).

Furthermore, the chiral symmetry $SU(3)_L \times SU(3)_R$ spontaneously breaks down to $SU(3)_V$ and, according to Goldstone theorem [149, 150], an octet of pseudoscalar massless bosons appears in the theory, which is the Chiral Perturbation Theory and discussed in next section.

1.2 Interaction Lagrangian

According to field theory, the interaction information can be obtained from the Lagrangian. In this section, I will discuss about the Lagrangians used in the present work, which are under the framework of the Chiral Perturbative Theory (ChPT) and Local Hidden Gauge (LHG), as discussed below.

1.2.1 The lowest order of ChPT Lagrangian

As discussed before, the chiral $SU(3)_L \times SU(3)_R$ symmetry in the massless limit will be broken by the finite masses of light quark, and this symmetry of the QCD Lagrangian also spontaneously leads to $SU(3)_V$ symmetry of the ground state, with the Goldstone bosons, which is an octet of the pseudoscalar mesons, (π, K, η). This is because the eight broken $SU(3)_L \times SU(3)_R$ generators transform the composite field $\bar{\psi}^R_{q_l}\psi^L_{q_l}$ along symmetry directions, and thus, fluctuations in field space along these eight directions are eight massless Goldstone bosons. The spontaneous symmetry breaking means that the ground state of the system is no longer invariant under the full symmetry group of the Hamiltonian. This is well described by one of the EFT, ChPT. The ChPT provides a systematic method for discussing the consequences of the global flavor symmetries of QCD at low energies by means of the EFT. Because of the QCD confinement, in the low energy region, we should use the non-perturbative QCD and work with the EFT as discussed before. More systematic discussions about the ChPT can be seen in Refs. [148, 151–154].

In the framework of mesonic ChPT, the most general chiral Lagrangian describing the dynamics of the Goldstone bosons is organized as a string of terms with an increasing number of derivatives (or, equivalently, in terms of increasing powers of momentum) and quark mass terms,

$$\mathcal{L}^M_{\text{eff}} = \mathcal{L}^M_2 + \mathcal{L}^M_4 + \mathcal{L}^M_6 + \cdots , \tag{1.17}$$

where the subscripts refer to the order in the momentum and quark mass expansion, and, parity conservation requires an even number of derivatives. To lowest order (leading order), the effective chiral Lagrangian is uniquely given by

$$\mathcal{L}^M_2 = \frac{f^2}{4}\langle \nabla_\mu U \nabla^\mu U^\dagger + \chi U^\dagger + U\chi^\dagger \rangle, \tag{1.18}$$

where f is the pion-decay constant and $\langle\,\rangle$ denotes the trace of the matrix. In Eq. (1.18), the meson fields are described by a unitary 3×3 matrix,

$$U(x) \;=\; u(x)^2 \;=\; \exp\Big\{ i\sqrt{2}\Phi(x)/f \Big\}, \tag{1.19}$$

which gives a very convenient parametrization of the Goldstone fields,

$$\Phi(x) = \sum_{a=1}^{8} \lambda_a \phi_a = \begin{pmatrix} \frac{1}{\sqrt{2}}\pi^0 + \frac{1}{\sqrt{6}}\eta_8 & \pi^+ & K^+ \\ \pi^- & -\frac{1}{\sqrt{2}}\pi^0 + \frac{1}{\sqrt{6}}\eta_8 & K^0 \\ K^- & \bar{K}^0 & -\frac{2}{\sqrt{6}}\eta_8 \end{pmatrix}; \quad (1.20)$$

the field χ embodies two of the scalar and pseudoscalar external fields (s, p),

$$\chi = 2B_0(s + ip), \quad (1.21)$$

where B_0 is a constant and one of the two free parameters (the other one is f), which is also not fixed by symmetry requirements alone; and, the covariant derivative $\nabla_\mu U$ contains the couplings to two gauge fields (v_μ, a_μ), the external vector and axial fields,

$$\nabla_\mu U = \partial_\mu U - i r_\mu U + i U l_\mu \,, \quad (1.22)$$

with $r_\mu = (v_\mu + a_\mu)$ and $l_\mu = (v_\mu - a_\mu)$. The higher order terms of the mesonic ChPT Lagrangian are out of the discussion in the present work, which have more free parameters.

In the low-energy EFT, the interaction of baryons with the Goldstone bosons is described as well by the external fields at low energies. To be specific, we consider the octet of the $\frac{1}{2}^+$ baryons, which are described in a complex, four-component Dirac field, given by a traceless 3×3 matrix,

$$B = \sum_{a=1}^{8} \lambda_a B_a = \begin{pmatrix} \frac{1}{\sqrt{2}}\Sigma^0 + \frac{1}{\sqrt{6}}\Lambda & \Sigma^+ & p \\ \Sigma^- & -\frac{1}{\sqrt{2}}\Sigma^0 + \frac{1}{\sqrt{6}}\Lambda & n \\ \Xi^- & \Xi^0 & -\frac{2}{\sqrt{6}}\Lambda \end{pmatrix}. \quad (1.23)$$

Since the power counting is different from the mesonic Lagrangian, the lowest order of the baryonic Lagrangian, for the meson-baryon interaction, is written as

$$\mathcal{L}_1^B = \langle \bar{B}(i\gamma^\mu \nabla_\mu - M_B)B \rangle + \frac{D}{2} \langle \bar{B}\gamma^\mu \gamma_5 \{u_\mu, B\} \rangle + \frac{F}{2} \langle \bar{B}\gamma^\mu \gamma_5 [u_\mu, B] \rangle, \quad (1.24)$$

where the D and F are the axial SU(3) coupling constants, with the values, $D = 0.85$, $F = 0.52$ [153], and, M_B denotes the mass of the baryon octet

in the chiral limit (the masses of baryons do not vanish in the chiral limit). But now, ∇_μ is defined as

$$\nabla_\mu B \equiv \partial_\mu B + [\Gamma_\mu, B]\,, \tag{1.25}$$

with

$$\Gamma_\mu = \frac{1}{2}\left[u^\dagger(\partial_\mu - ir_\mu)u + u(\partial_\mu - il_\mu)u^\dagger\right], \tag{1.26}$$

where the matrix field u is defined in Eq. (1.19), and r_μ, l_μ are given in Eq. (1.22). Finally, another Hermitian building block, the field u_μ also includes the external gauge fields, defined as

$$u_\mu = i\left[u^\dagger(\partial_\mu - ir_\mu)u - u(\partial_\mu - il_\mu)u^\dagger\right]. \tag{1.27}$$

Notice that from the point of view of chiral power counting $\nabla_\mu B$ and $M_B B$ are $\mathcal{O}(1)$, but $i\gamma^\mu\nabla_\mu B - M_B B$ is $\mathcal{O}(p)$ [153, 154].

In the present work, we only use the lowest order of ChPT Lagrangian since it contains just a few free parameters and is enough with the complement of the unitary of the scattering amplitude (this is proved by the results of Refs. [16–19, 155]), which will be discussed in the next section.

1.2.2 Local hidden gauge Lagrangian

Before, I have discussed the effective chiral Lagrangians describing the pseudoscalar meson (π, K, η) interaction and the pseudoscalar meson-baryon interaction, which do not contain any vector meson (ρ, ω, ϕ, K^*) fields. How to include massive spin $S = 1$ particles in the effective low-energy Lagrangian? In theory, the vector mesons can be included in the chiral Lagrangian by treating them as vector fields [156–160] or tensor fields [161, 162], and, as gauge bosons [156–159] or not gauge bosons [160–162]. Thus, normally there are two types of theoretical approach distinguished by the way of including the vector fields, the massive Yang-Mills approach (vector mesons as heavy gauge particles of the Yang-Mills type) and the hidden symmetry scheme (vector mesons as dynamical gauge bosons), which are equivalent by the proof in Ref. [161, 163] (more discussions and clarifications can be seen in Ref. [164], also some discussions can be found in Refs. [165, 166]). In the present work, we use the LHG formalism, which treat the vector mesons

as dynamical gauge bosons of the hidden local symmetry in the non-linear $U(3)_L \times U(3)_R/U(3)_V$ sigma model with a chiral Lagrangian.

We summarize the formalism of the hidden gauge interaction for vector mesons which we take from Refs. [156, 159, 163] (see also useful Feynman rules in Ref. [167] extended to SU(4), which is done in Ref. [127, 168]). The Lagrangian accounting for the interaction of vector mesons amongst themselves is given by

$$\mathcal{L}_{III} = -\frac{1}{4}\langle V_{\mu\nu} V^{\mu\nu} \rangle \ , \tag{1.28}$$

where the $\langle\rangle$ symbol represents the trace in the SU(4) space and $V_{\mu\nu}$ is given by

$$V_{\mu\nu} = \partial_\mu V_\nu - \partial_\nu V_\mu - ig[V_\mu, V_\nu] \ , \tag{1.29}$$

with the coupling of the theory given by $g = \frac{m_V}{2f}$ where $f = 93$ MeV is the pion decay constant and m_V the mass of vector meson, taking $m_V = m_\rho$. The magnitude V_μ is the SU(4) matrix of the vectors of the meson 15-plet + singlet, given by [93, 169]

$$V_\mu = \begin{pmatrix} \frac{\rho^0}{\sqrt{2}} + \frac{\omega}{\sqrt{2}} & \rho^+ & K^{*+} & \bar{D}^{*0} \\ \rho^- & -\frac{\rho^0}{\sqrt{2}} + \frac{\omega}{\sqrt{2}} & K^{*0} & D^{*-} \\ K^{*-} & \bar{K}^{*0} & \phi & D_s^{*-} \\ D^{*0} & D^{*+} & D_s^{*+} & J/\psi \end{pmatrix}_\mu \ . \tag{1.30}$$

The interaction of $\mathcal{L}_{III}$ provides a contact term which comes from $[V_\mu, V_\nu][V_\mu, V_\nu]$

$$\mathcal{L}_{III}^{(c)} = \frac{g^2}{2}\langle V_\mu V_\nu V^\mu V^\nu - V_\nu V_\mu V^\mu V^\nu \rangle \ , \tag{1.31}$$

as well as to a three vector vertex from

$$\mathcal{L}_{III}^{(3V)} = ig\langle (\partial_\mu V_\nu - \partial_\nu V_\mu) V^\mu V^\nu \rangle = ig\langle (V^\mu \partial_\nu V_\mu - \partial_\nu V_\mu V^\mu) V^\nu \rangle \ , \tag{1.32}$$

which, thus, can be simplified as

$$\mathcal{L}_{VVV} \equiv \mathcal{L}_{III}^{(3V)} = ig \ \langle [V_\nu, \partial_\mu V_\nu] V^\mu \rangle. \tag{1.33}$$

It is worth recalling the analogy with the coupling of vectors to pseudoscalars given in the same formalism by

$$\mathcal{L}_{VPP} = -ig \ \langle [P, \partial_\mu P] V^\mu \rangle, \tag{1.34}$$

where P is the SU(4) matrix of the pseudoscalar fields extended the SU(3) representation of Eq. (1.20),

$$P = \begin{pmatrix} \frac{\pi^0}{\sqrt{2}} + \frac{\eta_8}{\sqrt{6}} + \frac{\tilde{\eta}_c}{\sqrt{12}} + \frac{\tilde{\eta}'_c}{\sqrt{4}} & \pi^+ & K^+ & \bar{D}^0 \\ \pi^- & -\frac{\pi^0}{\sqrt{2}} + \frac{\eta_8}{\sqrt{6}} + \frac{\tilde{\eta}_c}{\sqrt{12}} + \frac{\tilde{\eta}'_c}{\sqrt{4}} & K^0 & D^- \\ K^- & \bar{K}^0 & \frac{-2\eta_8}{\sqrt{6}} + \frac{\tilde{\eta}_c}{\sqrt{12}} + \frac{\tilde{\eta}'_c}{\sqrt{4}} & D_s^- \\ D^0 & D^+ & D_s^+ & -\frac{3\tilde{\eta}_c}{\sqrt{12}} + \frac{\tilde{\eta}'_c}{\sqrt{4}} \end{pmatrix} . \tag{1.35}$$

where $\tilde{\eta}_c$ stands for the SU(3) singlet of the 15th SU(4) representation and we denote $\tilde{\eta}'_c$ for the singlet of SU(4) (see quark content in Ref. [168]). The physical η_c can be written as [168]

$$\eta_c = \frac{1}{2}(-\sqrt{3}\tilde{\eta}_c + \tilde{\eta}'_c) \ . \tag{1.36}$$

In the present work, we also need the vertex of the hidden gauge Lagrangian

$$\mathcal{L}_{PVV} = \frac{G'}{\sqrt{2}} \ \epsilon^{\mu\nu\alpha\beta} \ \langle \partial_\mu V_\nu \partial_\alpha V_\beta P \rangle, \tag{1.37}$$

where $G' = 3m_V^2/(16\pi^2 f^3)$ [96, 170].

The baryonic vertex when the baryons belong to the octet of SU(3) is given in terms of the Lagrangian [171, 172]

$$\mathcal{L}_{BBV} = g \left(\langle \bar{B}\gamma_\mu [V^\mu, B] \rangle + \langle \bar{B}\gamma_\mu B \rangle \langle V^\mu \rangle \right), \tag{1.38}$$

where B is now the SU(3) matrix of the baryon octet [154, 173]. Similarly, one has also a Lagrangian for the coupling of the vector mesons to the baryons of the decuplet, which can be found in Ref. [174].

Extrapolating to the heavy quark sector the lower vertex VBB does not have such a simple representation as in SU(3) and in practice one evaluates the matrix elements using SU(4) symmetry by means of Clebsch-Gordan coefficients and reduced matrix elements. This is done in Refs. [127, 168] (a discussion on the accuracy of the SU(4) symmetry is done there). Since the 20 representation for baryon states of $3/2^+$ is not considered there, we

must consider these matrix elements in the present work too. Once again one uses SU(4) symmetry for this vertex to evaluate the matrix elements, as done in Refs. [127, 168]. Alternatively, one can use results of SU(3) symmetry substituting a s quark by a c quark, or make evaluations using wave functions of the quark model [175], substituting the s quark by the c quark.

1.3 Chiral unitary approach

ChPT has been successful in the interpretation of the particle properties in the low energy region of the hadron interaction as a nonperturbative QCD approach. But, there are some limitations of using it widely. As shown in the discussion of the lowest order ChPT Lagrangian above, we can see that there are only two free parameters in the lowest order (leading order) Lagrangian. In fact, when going up to next to leading order, $\mathcal{O}(p^4)$ for the mesonic ChPT Lagrangian there will be 12 parameters, and for next-next-leading order $\mathcal{O}(p^6)$ there are more than 100 parameters. Therefore, the theoretical power is lost in the higher order expansion. To overcome these limitations, one should implement others nonperturbative method, such as effective field theory [144–147], Lattice QCD [176–179], QCD sum rule [91,180–182], Dyson-Schwinger equations [183–185], chiral quark model [186, 187], chiral unitary approach (ChUA) [16–19, 155], and so on. In the present work, we use the ChUA, but, as discussed in Ref. [166], there are three different ways to construct a unitary T-matrix for extending chiral symmetry, the inverse amplitude method [17,18], N/D method [19] and the Bethe-Salpeter (BS) equation [16,155] (a overview can be seen in Refs. [188, 189]). We choose one of them, the BS equation, to perform our investigation (its wide application to the low energy interaction will be discussed in later chapters of our study results), and show some details of the method below. We give one more step and also extrapolate this approach from s-wave to higher partial wave interaction.

1.3.1 The BS equation

Since the interaction supposedly produces a state below the threshold (a bound state), a certain class of diagrams needs to be summed to infinite

order to produce a pole at the appropriate energy, but, then ChPT expansion for the scattering amplitude is not applicable, thus, Ref. [190] adopts a potential model approach to investigate the $\Lambda(1405)$ state in the $\bar{K}N$ and its coupled channels interaction, constructing a pseudo-potential in the Born approximation from the ChPT Lagrangian and then iterates in a Lippmann-Schwinger equation solving analytically the T-matrix. Along the same line, Ref. [191] interprets the properties of the $N^*(1535)$ resonance with the interaction of πN and its coupled channels. Following the spirit of the approach of Refs. [190, 191], in Ref. [16] the kernel of the interaction (potential V) of pseudoscalar mesons was evaluated starting from the chiral Lagrangians [151–154, 173], and then, implementing unitarity in coupled channels, simplifying the Lippmann-Schwinger equation as a algebraic BS equation, the scalar meson resonances σ [or $f_0(500)$], $f_0(980)$, $a_0(980)$ were dynamically produced using only one free parameter, with phase shifts, inelasticities, mass distributions of given channels consistent with the experimental data (the consistency of the results with QCD sum rules can be seen in Refs. [192, 193]). The same idea is also extrapolated to the meson-baryon interaction in Ref. [155] to interpret the dynamics properties of $\Lambda(1405)$ state.

In Refs. [16, 155], the potential V is derived from the lowest order ChPT Lagrangian, then, inserted into the coupled channels Lippmann-Schwinger equations to calculate the scattering amplitudes,

$$t_{ij} = V_{ij} + V_{il}\, G_l\, t_{lj}, \tag{1.39}$$

where the indices i, j run over all possible channels for the meson-baryon interaction case

$$V_{il}\, G_l\, t_{lj} = i \int \frac{d^4q}{(2\pi)^4} \frac{M_l}{E_l(\vec{q})} \frac{V_{il}(k,q)\, T_{lj}(q,k')}{k^0 + p^0 - q^0 - E_l(\vec{q}) + i\epsilon} \frac{1}{q^2 - m_l^2 + i\epsilon}, \tag{1.40}$$

where M_l, E_l correspond to the mass and energy of the intermediate baryon and m_l to the mass of the intermediate meson. Eq. (1.39) is depicted by the series of diagrams of Fig. 1.2, which sums up automatically all of the diagrams and contains the dynamics to produce a resonance [190]. In principle one would have to solve the integrals in Eq. (1.39) by taking t and V off shell. In fact, for s-wave, we only need the on shell information,

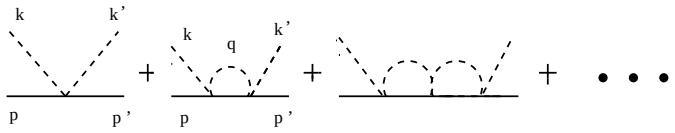

Figure 1.2: Diagrammatic representation of the Lippmann-Schwinger equations of Eq. (1.39) for $\bar{K}N$ scattering [155].

and we can simplify the coupled integral equations. The argument goes as follows.

Taking the one loop diagram of Fig. 1.2 with equal masses in the external and intermediate states for simplicity, we have

$$\begin{aligned} V_{\rm off}^2 &= C(k^0+q^0)^2 = C(2k^0+q^0-k^0)^2 \\ &= C(2k^0)^2 + 2C(2k^0)(q^0-k^0) + C(q^0-k^0)^2 \\ &= V_{\rm on}^2 + 2C(2k^0)(q^0-k^0) + C(q^0-k^0)^2, \end{aligned} \tag{1.41}$$

where C a proportionality constant and the first term in the last expression $V_{\rm on}^2$ is the on shell contribution, with $V_{\rm on} \equiv C2k^0$. Neglecting $p^0 - E(-\vec{q})$ in Eq. (1.40), a typical approximation in the heavy baryon formalism, the one loop integral for the second term of Eq. (1.41) becomes

$$\begin{aligned} & 2iV_{\rm on} \int \frac{d^3q}{(2\pi)^3} \int \frac{dq^0}{2\pi} \frac{M_l}{E_l(\vec{q})} \frac{q^0-k^0}{k^0-q^0} \frac{1}{q^{02}-\omega(\vec{q})^2+i\epsilon} \\ = \; & -2V_{\rm on} \int \frac{d^3q}{(2\pi)^3} \frac{M_l}{E_l(\vec{q})} \frac{1}{2\omega(\vec{q})} \sim V_{\rm on}\, q_{\rm max}^2 \end{aligned} \tag{1.42}$$

with $\omega(\vec{q})^2 = \vec{q}^{\,2} + m_l^2$. This term, proportional to $V_{\rm on}$, has the same structure as the tree level term in the Bethe-Salpeter series and it can be reabsorbed in the lowest order Lagrangian by a suitable renormalization of the parameter f. Similarly, the term proportional to $(q^0-k^0)^2$ in the last term of Eq. (1.41) cancels the baryon propagator in Eq. (1.40) while the remaining factor gives rise to another term proportional to k^0 (and hence $V_{\rm on}$) and a term proportional to q^0, which vanishes for parity reasons.

These arguments can be extended to coupled channels and higher order loops with the conclusion that V_{il} and t_{lj} factorize with their on shell values out of the integral in Eq. (1.40), reducing the problem to one of solving a

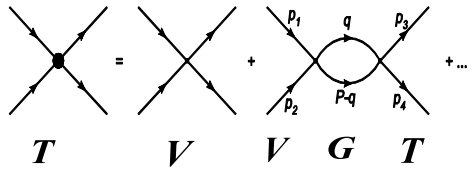

Figure 1.3: Diagrammatic representation of the BS equation.

set of algebraic equations, the BS equation, written in matrix form as

$$T = V + V\,G\,T, \tag{1.43}$$

or equivalently

$$T = [1 - V\,G]^{-1}\,V, \tag{1.44}$$

with G a diagonal matrix with its element for l channel given by

$$G_l(s) = i \int \frac{d^4q}{(2\pi)^4} \frac{m_f}{(P-q)^2 - m_1^2 + i\varepsilon} \frac{1}{q^2 - m_2^2 + i\varepsilon}, \tag{1.45}$$

where m_1, m_2 are the masses of the hadrons, q is the four-momentum of one meson, and P is the total four-momentum of the systems, thus, $s = P^2$. Besides, m_f is a mass factor, taking $m_f = 1$ for meson-meson loop and $m_f = 2M_B = 2m_1$ when m_1 is the baryon mass (M_B) in the meson-baryon loop. Then, the BS equation is also represented by a series of diagrams, as shown in Fig. 1.3. The integral for the G function, Eq. (1.45), is logarithmically divergent. There are two methods to regularize it. One is the dimensional regularization and the analytic expression can be seen in Ref. [194] with a scale μ and the subtraction constant $a(\mu)$ as free parameter,

$$\begin{aligned} G_l(s) \;=\; & \frac{m_f}{16\pi^2}\Big\{a_\mu + \ln\frac{m_1^2}{\mu^2} + \frac{m_2^2 - m_1^2 + s}{2s}\ln\frac{m_2^2}{m_1^2} \\ & + \frac{q_{cm}}{\sqrt{s}}\Big[\ln(s - (m_1^2 - m_2^2) + 2q_{cm}\sqrt{s}) \\ & + \ln(s + (m_1^2 - m_2^2) + 2q_{cm}\sqrt{s}) \\ & - \ln(-s - (m_1^2 - m_2^2) + 2q_{cm}\sqrt{s}) \\ & - \ln(-s + (m_1^2 - m_2^2) + 2q_{cm}\sqrt{s})\Big]\Big\}\,, \end{aligned} \tag{1.46}$$

where q_{cm} is the three-momentum of the intermediate mesons in the center mass frame. As discussed in Ref. [194], for μ at low energy scale, the "natural" value of a_μ is around -2, and μ, a_μ are not independent. The other method to regularize it is using a cut-off momentum, performing the integration

$$G_l(s) = m_f \int_0^{q_{max}} \frac{d^3\vec{q}}{(2\pi)^3} \frac{\omega_1 + \omega_2}{2\omega_1\omega_2} \frac{1}{P^{0\,2} - (\omega_1 + \omega_2)^2 + i\varepsilon}, \tag{1.47}$$

where $\omega_i = \sqrt{\vec{q}^{\,2} + m_i^2}$, $(i = 1\,2)$, and q_{max} is the cut-off of the three-momentum, the free parameter. Also the analytic formula of Eq. (1.47) can be seen in Refs. [18,195]. Normally at low energies, the two regularization methods are compatible and there are relationships between these free parameters, $a(\mu)$, μ and q_{max} [194] (see also Eq. (52) of Ref. [196]).

Furthermore, we want to discuss the unitary properties of the coupled channel BS equation. According to the Mandl and Shaw normalization [197], the unitarity in coupled channels implies

$$\text{Im } T_{ij} = T_{in}\, \sigma_{nn}\, T^*_{nj}, \tag{1.48}$$

where σ is a real diagonal matrix whose elements are given by

$$\sigma_{nn} \equiv \text{Im } G_n = -m_f \frac{q_{cm}}{8\pi\sqrt{s}} \theta(s - (m_1 + m_2)^2)). \tag{1.49}$$

The coupled channel BS equation fulfils the normalization requirement of the unitarity, thus, it is one of the ChUA. This unitarity is important when extrapolating the loop function G to the second Riemann sheet above the threshold for searching the pole of the resonance (a detail of the second Riemann sheet for the pole can be seen in Refs. [16, 198, 199]), written

$$G_l^{II}(s) = G_l^I(s) + i\, m_f \frac{q_{cm}}{4\pi\sqrt{s}}. \tag{1.50}$$

Finally, the on shell approximation of the BS equation, which has been proved reasonable [16,155] as discussed above, works well in the low energy region and is successfully explored to explain the properties of resonances (we will come back its wide application in later chapters). The on-shell factorization is accurate enough for the theoretical reproduction of the resonances. A different justification is given in [194], where staring from Eq.

(1.48), a subtracted dispersion relation is used to obtain T^{-1}, which provides the result of the BS equation when one neglects the contribution of the left hand cut. This contribution is usually quite energy independent in the physical region of interest, and hence can be easily accommodated by means of the subtraction constant. A systematic investigation of the ChUA is carried on Ref. [200], which also compared the contribution for both the on-shell approximation and full off-shell effects in the scattering of $\pi\pi$ and its coupled channels. The results of Refs. [127, 168] in the charm sector with the on-shell BS equation is consistent with the results of Ref. [201] using several coupled-channel models, also with the results of chiral quark model in Ref. [202]. Recently, no qualitative difference between the on-shell and off-shell approaches for the BS equation is observed in the low energy interaction using the Lattice QCD data in Ref. [203].

1.3.2 The partial wave BS equation

To distinguish the nature of a resonance whether it is a "composite" or "genuine" state [204], the works of Refs. [95, 205] develop the coupled channel approach to establish the relationship of the couplings of the states in different channels versus the wave function. A further generalization to higher partial waves was done in Ref. [206].

Following Ref. [206] one uses the set of coupled Schrödinger equations

$$\begin{aligned} |\Psi\rangle &= |\Phi\rangle + \frac{1}{E - H_0} V |\Psi\rangle \\ &= |\Phi\rangle + \frac{1}{E - M_i - \frac{\vec{p}^{\,2}}{2\mu_i}} V |\Psi\rangle \ , \end{aligned} \tag{1.51}$$

where H_0 is the free Hamiltonian, μ_i is the reduced mass of the system of total mass $M_i = m_{ai} + m_{bi}$, and

$$|\Psi\rangle = \begin{Bmatrix} |\Psi_1\rangle \\ |\Psi_2\rangle \\ \vdots \\ |\Psi_N\rangle \end{Bmatrix} \ , \qquad |\Phi\rangle = \begin{Bmatrix} |\Phi_1\rangle \\ 0 \\ \vdots \\ 0 \end{Bmatrix} \ , \tag{1.52}$$

where $|\Phi_1\rangle$ represents the only channel present at $t = -\infty$ taken as a plane

wave. V is the potential chosen as

$$\langle \vec{p}|V|\vec{p}\,'\rangle \equiv (2l+1)\ v\ \Theta(\Lambda-p)\Theta(\Lambda-p')|\vec{p}|^l|\vec{p}\,'|^l P_l(\cos\theta)\ , \tag{1.53}$$

where v is a $N\times N$ matrix with N the number of channels, Λ is a cutoff in the momentum space, and $P_l(\cos\theta)$ is the Legendre function. Note that the functions inherent to a l-wave character have been explicitly taken into account in V and hence v is considered as a constant in Eq. (1.53).

As shown in Ref. [206] one can see that the T-matrix can be written in the form of Eq. (1.53) and one finds

$$\langle \vec{p}|T|\vec{p}\,'\rangle \equiv (2l+1)\ t\ \Theta(\Lambda-p)\Theta(\Lambda-p')|\vec{p}|^l|\vec{p}\,'|^l P_l(\cos\theta)\ , \tag{1.54}$$

with

$$t=(1-vG)^{-1}v\ , \tag{1.55}$$

where G is the loop function for the two intermediate hadron states, which differs technically from the one more commonly used in the chiral unitary approach [19] in that it contains the factor $|\vec{p}|^{2l}$ in the integral, since this factor has been removed from v (see Eq. (1.53)). Hence

$$G_{ii}=\int_{|\vec{p}|<\Lambda} d^3\vec{p}\,\frac{|\vec{p}|^{2l}}{E-M_i-\frac{\vec{p}^{\,2}}{2\mu_i}+i\epsilon}\ . \tag{1.56}$$

For more details we refer to Ref. [206].

1.4 Three-body interaction

Some discovered particles, such as the $\phi(2170)$ (also called $X(2175)$, $Y(2175)$), $Y(4260)$, $N^*(1710)$, *et. al.*, look like having a more complicate structure and would come from multi-body hadron interaction. The simplest multi-body interaction is the three-body interaction, which is a subject of study in hadron physics, drawing much attention for a long time [207–211]. Thus, in this section, we will discuss about how to extend the ChUA formalism to the three-body interaction.

1.4.1 The Faddeev equations with ChUA

We have discussed the ChUA above for the two-body interaction, which is rather successful and plays an important role in the description of the hadronic properties in the studies of the meson-meson and meson-baryon interactions. Developing the ChUA for the three-body interaction is the main motivation of the work in Ref. [212], which combine the three-body Faddeev equations with chiral dynamics and has reported several S-wave $J^P = \frac{1}{2}^+$ resonances qualifying as two mesons-one baryon molecular states. This combination of Faddeev equations and chiral dynamics produces results consistent with QCD sum rules in the investigation of the $DK\bar{K}$ system in the work of Ref. [213]. The details of this extension of the ChUA is systematically discussed in Ref. [214] and a short review is given below [1].

For the three-body interaction as Faddeev suggested in Ref. [208], the scattering amplitude of T-matrix can be written as a sum of three partitions,

$$T = T^1 + T^2 + T^3, \tag{1.57}$$

where T^i ($i = 1, 2, 3$) includes all the possible interactions contributing to the three-body T-matrix with the particle i being a spectator in the last interaction. Obviously, as shown in Fig. 1.4 the sum of T^1, T^2 and T^3 contains all the possible diagrams obtained by permutations of the different interactions between the three particles. The series T^1, T^2 and T^3 can be rewritten to get the Faddeev equations,

$$\begin{aligned} T^1 &= t^1 + t^1 G\big[T^2 + T^3\big], \\ T^2 &= t^2 + t^2 G\big[T^1 + T^3\big], \\ T^3 &= t^3 + t^3 G\big[T^1 + T^2\big], \end{aligned} \tag{1.58}$$

where t^i ($i = 1, 2, 3$) correspond to the two-body t-matrix in ChUA and G is the Green-function of the three-body system.

Within unitary chiral dynamics, combining with the ChUA formalism, the Faddeev partitions T^i are given by

$$T^i = \tilde{\delta}^3(\vec{k}_i - \vec{k}_i')t^i + \sum_{i=1}^{3}\sum_{j\neq i=1}^{3} T_R^{ij}, \tag{1.59}$$

[1] We thank Alberto Martínez Torres for useful discussions and kind help.

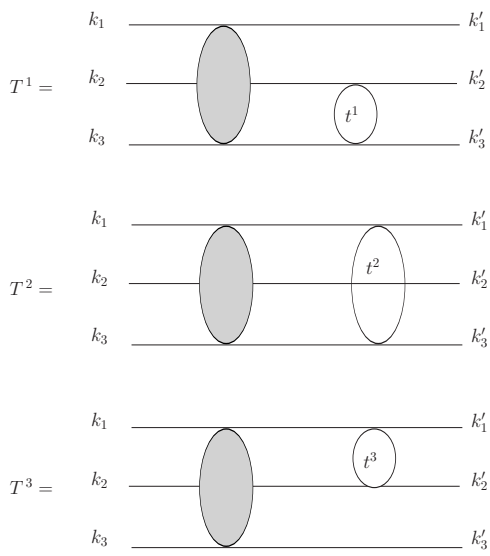

Figure 1.4: Diagrammatic representation of the Faddeev partitions [214].

with $j \neq k \neq i = 1,\, 2,\, 3$ and $\tilde{\delta}^3(\vec{k}_i - \vec{k}'_i) \equiv \left[(2\pi)^3 \tilde{N}_i \delta^3(\vec{k}_i - \vec{k}'_i)\right]$, where

$$\tilde{N}_i = \begin{cases} \sqrt{2\omega(\vec{k}_i)}\sqrt{2\omega(\vec{k}'_i)}\,, & i = 1, 2, \\ \left(\sqrt{2\omega(\vec{k}_i)}\sqrt{2\omega(\vec{k}'_i)}\right) \Big/ \left(\sqrt{2m_i}\sqrt{2m'_i}\right)\,, & i = 3, \end{cases}$$

for a two meson-one baryon system and

$$\tilde{N}_i = \sqrt{2\omega(\vec{k}_i)}\sqrt{2\omega(\vec{k}'_i)}\,, \quad i = 1, 2, 3,$$

for a three meson system, with the three-momentum, the mass and the energy of the incoming (outgoing) particle, $\vec{k}_i$ ($\vec{k}'_i$), m_i (m'_i) and $\omega(\vec{k}_i)$, ($\omega(\vec{k}'_i)$) respectively. In Eq. (1.59), the T_R^{ij} matrices are summing all the diagrams

with the same last two t-matrices,

$$\begin{aligned}
T_R^{12} &= t^1 g^{12} t^2 + t^1 \big[G^{121} T_R^{21} + G^{123} T_R^{23} \big], \\
T_R^{13} &= t^1 g^{13} t^3 + t^1 \big[G^{131} T_R^{31} + G^{132} T_R^{32} \big], \\
T_R^{21} &= t^2 g^{21} t^1 + t^2 \big[G^{212} T_R^{12} + G^{213} T_R^{13} \big], \\
T_R^{23} &= t^2 g^{23} t^3 + t^2 \big[G^{231} T_R^{31} + G^{232} T_R^{32} \big], \\
T_R^{31} &= t^3 g^{31} t^1 + t^3 \big[G^{312} T_R^{12} + G^{313} T_R^{13} \big], \\
T_R^{32} &= t^3 g^{32} t^2 + t^3 \big[G^{321} T_R^{21} + G^{323} T_R^{23} \big],
\end{aligned} \tag{1.60}$$

where all the loop dependence is assembled in the loop function G^{ijk}, therefore, they are algebraic equations. The loop function G^{ijk} are generally defined as,

$$G^{ijk} = \int \frac{d^3k''}{(2\pi)^3} \hat{g}^{ij}(s_{lm}, \vec{k}'') F^{ijk}(\vec{k}'', \vec{k}'_j, \vec{k}_k, s^{k''}_{l'k'}), \tag{1.61}$$

with $i \neq j$, $j \neq k = 1, 2, 3$, $l \neq m \neq i$, $l' \neq k' \neq j$, where the elements of the $\hat{g}^{ij}$ matrix are given by,

$$\hat{g}^{ij}_{\xi} = \frac{N_l}{2E_l(\vec{k}'')} \frac{N_m}{2E_m(\vec{k}'')} \times \frac{1}{\sqrt{s_{lm}} - E_l(\vec{k}'') - E_m(\vec{k}'') + i\epsilon}, \tag{1.62}$$

and the matrix,

$$\begin{aligned}
F^{ijk}(\vec{k}'', \vec{k}'_j, \vec{k}_i, s^{k''}_{l'k'}) = t^j(s^{k''}_{l'k'}) \times g^{jk}(\vec{k}'', \vec{k}_k) \\
\times [g^{jk}(\vec{k}'_j, \vec{k}_k)]^{-1} [t^j(s_{l'k'})]^{-1},
\end{aligned} \tag{1.63}$$

with the variable of the invariant mass s_{lm} in the center mass frame of the subsystem with l and m particles. And for the definition of the T_R^{ij} matrices, which should sum all the possible diagrams with the elements of the t-matrix, for example, the T_R^{12} element is the series as,

$$\begin{aligned}
T_R^{12} \equiv & t^1 g^{12} t^2 + t^1 G^{121} t^2 g^{21} t^1 + t^1 G^{121} t^2 G^{212} t^1 g^{12} t^2 + \cdots \\
& + t^1 G^{123} t^2 g^{23} t^3 + t^1 G^{123} t^2 G^{232} t^3 g^{32} t^2 + \cdots .
\end{aligned} \tag{1.64}$$

Thus, the full three-body T-matrix is given by,

$$T = \sum_{i=1}^{3} T^i = \sum_{i=1}^{3} t^i \tilde{\delta}^3(\vec{k}'_i - \vec{k}_i) + \sum_{i=1}^{3} \sum_{j \neq i=1}^{3} T_R^{ij}. \tag{1.65}$$

As comment in Ref. [214], the obtained six coupled equations of Eq. (1.60), which appear as a reformulation of the Faddeev equations, are algebraic equations instead of integral equations. The solution of these equations have been simplified with the ChUA and can be looked for the correspondence of the peaks found in the amplitude to poles of the physical states. Thus, this extension for the Faddeev equations has been successful to interpret the structure and properties of the states found in the experiments, such as, $X(2175)$ in the $\phi K\bar{K}$ system [75], $N^*(1710)$ in the $\pi\pi N$ system [215], $Y(4260)$ in the $J/\psi K\bar{K}$ system [216], and others, as the low lying Λ^* and Σ^* states of $J^P = 1/2^+$ [212].

1.4.2 The FCA to Faddeev equations

We have given the formalism for the three-body interaction with the ChUA extension to Faddeev equation above. Furthermore, when there are resonances (or bound states) appearing in the two-body subsystem of the three-body interaction, we can take the FCA [208, 218–222] to the Faddeev equations. The FCA assumes that a cluster is formed by two particles and is not much modified by the interaction of a third particle with this cluster. Multiple scattering of the third particle with the components of the cluster is then taken into account. By taking the FCA to Faddeev equations, several multi-$\rho(770)$ states are dynamically produced in Ref. [223], in which the resonances $f_2(1270)(2^{++})$, $\rho_3(1690)(3^{--})$, $f_4(2050)(4^{++})$, $\rho_5(2350)(5^{--})$, and $f_6(2510)(6^{++})$ are theoretically found as basically molecules of an increasing number of $\rho(770)$ particles with parallel spins. Analogously, in Ref. [224], the resonances $K_2^*(1430)$, $K_3^*(1780)$, $K_4^*(2045)$, $K_5^*(2380)$ and a new K_6^* could be explained as molecules with the components of an increasing number of $\rho(770)$ and one $K^*(892)$ meson. With the same approach, the $\Delta_{\frac{5}{2}^+}(2000)$ puzzle is solved in Ref. [225] in the study of the $\pi - (\Delta\rho)$ interaction. The FCA to Faddeev equations is technically simple, and allows one to deal with three-body hadron interactions which would be otherwise rather cumbersome [226–228]. As discussed in Ref. [227], this method is accurate when dealing with bound states, and gets consistent results with the full Faddeev equation evaluation without taking FCA [229], or a variational calculation with a nonrelativistic three-body potential model [230] (more discussions can be seen in Ref. [231]). One should also know the limits of the applica-

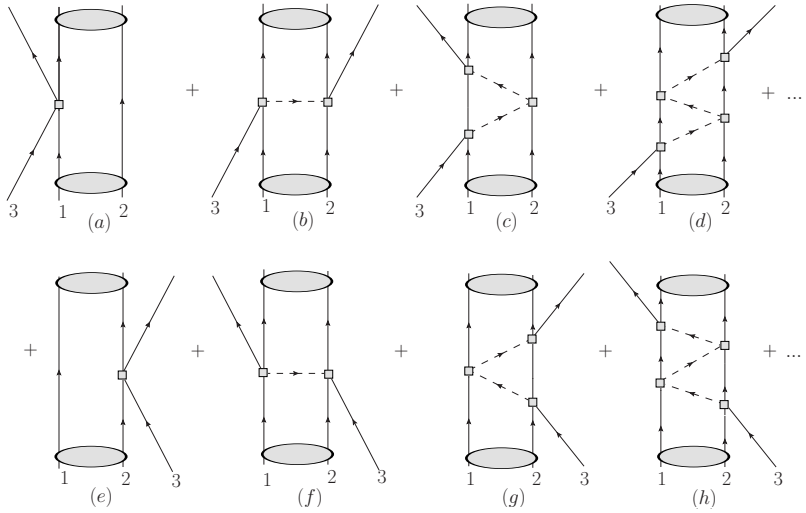

Figure 1.5: Diagrammatic representation of the FCA to Faddeev equations.

bility of the FCA, and one should avoid the case in which the states have enough energy to excite its components in intermediate states [232], which is the case of resonances above threshold. Thus, the Faddeev equations under the FCA are an effective tool to deal with multi-hadron interaction, more details given below.

The FCA to Faddeev equations assumes a pair of particles (1 and 2) forming a cluster. Then particle 3 interacts with the components of the cluster, undergoing all possible multiple scattering with those components. This is depicted in Fig. 1.5. With this basic idea of the FCA, we can write the Faddeev equations easily. For this one defines two partition functions T_1 and T_2, which sum all diagrams of the series of Fig. 1.5 which begin with the interaction of particle 3 with particle 1 of the cluster (T_1), or with the particle 2 (T_2). The equations then read

$$T_1 = t_1 + t_1 G_0 T_2, \tag{1.66}$$

$$T_2 = t_2 + t_2 G_0 T_1, \tag{1.67}$$

$$T = T_1 + T_2, \tag{1.68}$$

where T is the total three-body scattering amplitude that we are looking for. The amplitudes t_1 and t_2 represent the unitary scattering amplitudes

with coupled channels for the interactions of particle 3 with particle 1 and 2, respectively. And G_0 is the propagator of particle 3 between the components of the two-body system.

For the unitary amplitudes corresponding to single-scattering contribution one must take into account the isospin structure of the cluster and write the t_1 and t_2 amplitudes in terms of the isospin amplitudes of the (3,1) and (3,2) systems. Besides, because of the normalization of Mandl and Shaw [197] which has different weight factors for the particle fields, we must take into account how these factors appear in the single scattering and double scattering and in the total amplitude. This is easy and is done in detail in Refs. [224,226]. We show below the details for the case of a meson cluster (also particles 1 and 2) and a meson as scattering particle (the third particle). In this case, following the field normalization of Ref. [197] we find for the S matrix of single scattering, Fig. 1.5 (a),

$$\begin{aligned} S_1^{(1)} =& - it_1(2\pi)^4\,\delta(k+k_R-k'-k'_R) \\ & \times \frac{1}{\mathcal{V}^2}\frac{1}{\sqrt{2\omega_3}}\frac{1}{\sqrt{2\omega'_3}}\frac{1}{\sqrt{2\omega_1}}\frac{1}{\sqrt{2\omega'_1}}, \end{aligned} \tag{1.69}$$

$$\begin{aligned} S_2^{(1)} =& - it_2(2\pi)^4\,\delta(k+k_R-k'-k'_R) \\ & \times \frac{1}{\mathcal{V}^2}\frac{1}{\sqrt{2\omega_3}}\frac{1}{\sqrt{2\omega'_3}}\frac{1}{\sqrt{2\omega_2}}\frac{1}{\sqrt{2\omega'_2}}, \end{aligned} \tag{1.70}$$

where, k, k' (k_R, k'_R) refer to the momentum of initial, final scattering particle (R for the cluster), ω_i, ω'_i are the energies of the initial, final particles, $\mathcal{V}$ is the volume of the box where the states are normalized to unity and the subscripts 1, 2 refer to scattering with particle 1 or 2 of the cluster.

The double scattering diagram, Fig. 1.5 (b), is given by,

$$\begin{aligned} S^{(2)} =& - i(2\pi)^4\delta(k+k_R-k'-k'_R)\frac{1}{\mathcal{V}^2}\frac{1}{\sqrt{2\omega_3}}\frac{1}{\sqrt{2\omega'_3}}\frac{1}{\sqrt{2\omega_1}}\frac{1}{\sqrt{2\omega'_1}}\frac{1}{\sqrt{2\omega_2}}\frac{1}{\sqrt{2\omega'_2}} \\ & \times \int \frac{d^3q}{(2\pi)^3}F_R(q)\frac{1}{q^{0\,2}-\vec{q}^{\,2}-m_3^2+i\,\epsilon}t_1t_2, \end{aligned} \tag{1.71}$$

where $F_R(q)$ is the cluster form factor that we shall discuss below. Similarly, the full S matrix for scattering of particle 3 with the cluster will be given

by,

$$S = -i\,T\,(2\pi)^4\delta(k + k_R - k' - k'_R) \times \frac{1}{\mathcal{V}^2}\frac{1}{\sqrt{2\omega_3}}\frac{1}{\sqrt{2\omega'_3}}\frac{1}{\sqrt{2\omega_R}}\frac{1}{\sqrt{2\omega'_R}}. \quad (1.72)$$

In view of the different normalization of these terms by comparing Eqs. (1.69), (1.70), (1.71) and (1.72), we can introduce suitable factors in the elementary amplitudes,

$$\tilde{t_1} = \frac{2M_R}{2m_1}\,t_1, \qquad \tilde{t_2} = \frac{2M_R}{2m_2}\,t_2, \quad (1.73)$$

with $m_1,\ m_2,\ M_R$ the masses of the particles 1,2 and the cluster, respectively, where we have taken the approximations, suitable for bound states, $\frac{1}{\sqrt{2\omega_i}} = \frac{1}{\sqrt{2m_i}}$, and sum all the diagrams by means of,

$$T = T_1 + T_2 = \frac{\tilde{t_1} + \tilde{t_2} + 2\,\tilde{t_1}\,\tilde{t_2}\,G_0}{1 - \tilde{t_1}\,\tilde{t_2}\,G_0^2}. \quad (1.74)$$

When $\tilde{t_1} = \tilde{t_2}$ in some cases, it can be simplified as,

$$T = \frac{2\,\tilde{t_1}}{1 - \tilde{t_1}\,G_0}. \quad (1.75)$$

The function G_0 in Eqs. (1.74) and (1.75) is given by,

$$G_0(s) = \frac{1}{2M_R}\int \frac{d^3\vec{q}}{(2\pi)^3}F_R(q)\frac{1}{q^{02} - \vec{q}^{\,2} - m_3^2 + i\,\epsilon}, \quad (1.76)$$

where $F_R(q)$ is the form factor of the cluster of particles 1 and 2. Note that, when the cluster, the particles 1 and 2, one of them is a baryon, the factors in Eqs. (1.73) and (1.76), $2m_i$ ($i = 1,\ 2$) and $2M_R$ should be replaced by 1 by taking the baryonic field factor approximation $\sqrt{\frac{2M_B}{2E_B}} \approx 1$. We must use the form factor of the cluster consistently with the theory used to generate the cluster as a dynamically generated resonance. This requires to extend to the wave functions the formalism of the chiral unitary approach developed for scattering amplitudes. This work has been done in Refs. [95, 205, 206] for S-wave bound states, S-wave resonant states and states with arbitrary angular momentum, respectively. Here we only need the expressions for

S-wave bound states, and then the expression for the form factors is given in section 4 of Ref. [205] by,

$$F_R(q) = \frac{1}{\mathcal{N}} \int_{|\vec{p}|<\Lambda', |\vec{p}-\vec{q}|<\Lambda'} d^3\vec{p}\, \frac{1}{2E_1(\vec{p})} \frac{1}{2E_2(\vec{p})} \frac{1}{M_R - E_1(\vec{p}) - E_2(\vec{p})} \frac{1}{2E_1(\vec{p}-\vec{q})} \frac{1}{2E_2(\vec{p}-\vec{q})} \frac{1}{M_R - E_1(\vec{p}-\vec{q}) - E_2(\vec{p}-\vec{q})}, \tag{1.77}$$

$$\mathcal{N} = \int_{|\vec{p}|<\Lambda'} d^3\vec{p} \left(\frac{1}{2E_1(\vec{p})} \frac{1}{2E_2(\vec{p})} \frac{1}{M_R - E_1(\vec{p}) - E_2(\vec{p})} \right)^2, \tag{1.78}$$

where E_1 and E_2 are the energies of the particles 1, 2 and M_R the mass of the cluster. The parameter Λ' is a cut off that regularizes the integrals of Eqs. (1.77) and (1.78). This cut off is the same that one needs in the regularization of the loop function of the two particle propagators in the study of the interaction of the two particles of the cluster [205]. As done in Refs. [224, 226], we take the value of Λ' the same as the cutoff q_{max} used to generate the resonance in the two-body interaction. Thus we do not introduce any free parameters in the present procedure.

In addition, q^0, the energy carried by particle 3 in the rest frame of the three particle system, is given by,

$$q^0(s) = \frac{s + m_3^2 - M_R^2}{2\sqrt{s}}. \tag{1.79}$$

Note also that the arguments of the amplitudes $T_i(s)$ and $t_i(s_i)$ are different, where s is the total invariant mass of the three-body system, and s_i are the invariant masses in the two-body systems. The value of s_i is given by [224],

$$s_i = m_3^2 + m_i^2 + \frac{(M_R^2 + m_i^2 - m_j^2)(s - m_3^2 - M_R^2)}{2M_R^2}, (i, j = 1, 2,\ i \neq j) \tag{1.80}$$

where m_l ($l = 1, 2, 3$) are the masses of the corresponding particles in the three-body system and M_R the mass of two body resonance or bound state (cluster).

The Faddeev equations under the FCA are a useful tool to deal with three-body interaction. They are particularly suited to study system in

which a pair of particles cluster together and the cluster is not much modified by the third particle. Even if there is a sizeable modification of the cluster, the method is useful in combination with information from other sources on how the cluster can be modified by the presence of the third particle [227]. The assumption of a small modification of the cluster wave function seems to imply that the mass of the third particle should be smaller than that of the cluster components, but this can also happen if the cluster is strongly bound, independent of the masses. In any case, in an exploratory study of the systems under consideration, where uncertainties of even 50 MeV are readily acceptable, the FCA proves to be a sufficiently accurate tool, and relatively simple to use, once comparison with more accurate tools has shown that the same results are obtained within a few MeV of difference.

1.5 Heavy quark flavour-spin symmetry

In subsection Sub. 1.1.3 before, we have discussed in the limit of taking the light quark mass $m_q \to 0$ that QCD has an $SU(3)_L \times SU(3)_R$ chiral symmetry. But, for the heavy quark sector, since the heavy quark masses $m_Q > 1$ GeV, which are larger than the scale of nonperturbative QCD, this implies a different property for the hadrons containing a single heavy quark, leading to the Heavy Quark Spin-Flavor Symmetry [233–236]. Considering a meson with heavy-light quarks $Q\bar{q}$, the typical momentum transfer (< 1 GeV) between the heavy and light quarks leads to an important consequence, that the velocity v of the heavy quark is almost unchanged by such interaction since $\Delta v = \Delta p/m_Q \sim 0$. Therefore, in the limit of $m_Q \to \infty$, the heavy quark behaves like a static external source, as a spectator in the interaction, and the meson dynamics reduces to that of light degrees of freedom interacting with this external source. Thus, this leads to Heavy Quark Flavor Symmetry: the dynamics is unchanged under the exchange of heavy quark flavors. Besides, in this limit, the static heavy quark can only interact with gluons via its chromoelectric charge, which is spin independent. This leads to another symmetry, Heavy Quark Spin Symmetry (HQSS): the dynamics is unchanged under arbitrary transformations on the spin of the heavy quark. Both of them are so-called the Heavy Quark Spin-Flavor Symmetry in the heavy quark QCD.

HQSS predicts that all types of spin interactions vanish for infinitely

massive quarks. The spin-dependent interactions are proportional to the chromomagnetic moment of the heavy quark, and hence, they are of the order of $1/m_Q$. The total angular momentum $\vec{J}$ of the hadron is always a conserved quantity, but in this case the spin of the heavy quark $\vec{S}_Q$ is also conserved in the $m_Q \to \infty$ limit. Consequently, the spin of the light degrees of freedom $\vec{S}_l = \vec{J} - \vec{S}_Q$ is a conserved quantity in that limit. Thus, heavy hadrons come in doublets (unless $s_l = 0$), containing states with total spin $j_\pm = s_l \pm 1/2$ (with $\vec{S}_l^{\,2} = s_l(s_l+1)$ and $\vec{J}^{\,2} = j(j+1)$) obtained by combining the spin of the light degrees of freedom with the spin of the heavy quark $s_Q = 1/2$. These doublets are degenerate in the $m_Q \to \infty$ limit. This is the case for the ground state mesons D and D^* or D_s and D_s^* which are composed of a charm quark with $s_Q = 1/2$ and light degrees of freedom with $s_l = 1/2$, forming a multiplet of negative parity hadrons with spin 0 and 1. The entire multiplet of degenerate states should be treated in any HQSS inspired formalism as a single field that transforms linearly under the heavy quark symmetries [235, 236]. For finite charm quark mass, the pseudoscalar and vector D meson masses differ in about just one pion mass (actually one has $m_D - m_{D^*} = \mathcal{O}(1/(m_D + m_{D^*}))$), even less for the strange charmed mesons, thus it is reasonable to expect that the coupling $DN \to D^*N$ might play an important role. This is indeed what happens when SU(8) symmetry is used [237, 238].

As discussed before, the strong interaction in the low energy region is described by the effective theory, the nonperturbative approach. Of course, the strong interactions for the heavy quark with light quarks and gluons can be described by an effective theory, which is invariant under changes of the flavor and spin of the heavy quark. The theoretical framework for such interactions is provided by the so-called Heavy Quark Effective Theory [146, 239]. Considering a heavy quark with velocity v interacting with external fields, where the velocity of an on-shell quark is defined by $p = m_Q v$, the effective Lagrangian is formulated by the velocity-dependent fields $h_v(x)$, called large component field, together with small component field $H_v(x)$, which are defined as

$$h_v(x) = \exp(im_Q\, v\cdot x) P_+ Q_v(x), \quad H_v(x) = \exp(im_Q\, v\cdot x) P_- Q_v(x), \tag{1.81}$$

where $P_\pm$ are the velocity-dependent projection operator, $P_\pm = \frac{1}{2}(1 \pm \not{v})$,

and $Q_v(x)$ is the original field at tree level,

$$Q_v(x) = \exp(-im_Q\, v\cdot x)[h_v(x) + H_v(x)]. \tag{1.82}$$

Then, the effective Lagrangian related to heavy quarks is given by [235,236]

$$\mathcal{L}^Q_{eff} = \bar{h}_v(iv\cdot D)h_v - \bar{H}_v(iv\cdot D + 2m_Q)H_v + \bar{h}_v i\not{D}' H_v + \bar{H}_v i\not{D}' h_v, \tag{1.83}$$

with $D'_\mu = D_\mu - v_\mu\, v\cdot D$.

In fact, the small component field H_v is related to the large scale m_Q and dependent on the large component field $h_v(x)$. By solving the generating functional of QCD Green functions, the H_v field is worked out

$$H_v = \frac{1}{iv\cdot D + 2m_Q - i\epsilon}\, i\not{D}' h_v, \tag{1.84}$$

which indicates that the small component field H_v is indeed of order $1/m_Q$, so called "small" component [235,240]. Hence, one can establish the desired heavy mass expansion for the effective Lagrangian of Eq. (1.83) in terms of the $1/m_Q$ terms [235,236,241,242]

$$\begin{aligned}\mathcal{L}^Q_{eff} &= \bar{h}_v(iv\cdot D)h_v + \frac{1}{2m_Q}\bar{h}_v(iD')^2 h_v + \frac{g}{4m_Q}\bar{h}_v\sigma_{\mu\nu}G^{\mu\nu}h_v + \mathcal{O}(\frac{1}{m_Q^2}) + \cdots \\ &= \mathcal{L}^Q_0 + \mathcal{L}^Q_1 + \cdots,\end{aligned} \tag{1.85}$$

where using the identity $[D^\mu, D^\nu] = igG^{\mu\nu}$, the definition $\sigma_{\mu\nu} = i[\gamma^\mu, \gamma^\nu]/2$, the lowest order Lagrangian and the next leading order term are defined as

$$\begin{aligned}\mathcal{L}^Q_0 &= \bar{h}_v(iv\cdot D)h_v\,, \\ \mathcal{L}^Q_1 &= \frac{1}{2m_Q}\bar{h}_v(iD')^2 h_v + \frac{g}{4m_Q}\bar{h}_v\sigma_{\mu\nu}G^{\mu\nu}h_v\,.\end{aligned} \tag{1.86}$$

Similarly, one can also make a mass expansion for the original field

$$\begin{aligned}Q_v(x) &= \exp(-im_Q\, v\cdot x)\left(1 + \frac{1}{iv\cdot D + 2m_Q - i\epsilon}\, i\not{D}'\right) h_v \\ &= \exp(-im_Q\, v\cdot x)(1 + \not{D}'/2m_Q + \cdots)h_v.\end{aligned} \tag{1.87}$$

More discussion about the higher order $1/m_Q$ expansion can be referred to the reviews of Refs. [235,240].

Analogously, heavy hadrons chiral perturbation theory can be derived from the spontaneously broken $SU(3)_L \times SU(3)_R$ chiral symmetry on the light quarks, considering the spin-flavor symmetry on the heavy quarks. For the low momentum strong interactions of the ground states with the $s_\ell = 1/2$ spin symmetry doublet of heavy mesons P and P^*, containing only one heavy quark Q, we first need to introduce a superfield describing the combined doublet of the two P and P^* fields,

$$H_a^{(Q)} = \frac{1+\not{v}}{2}[P^{*(Q)}_{a\,\mu}\gamma^\mu - P_a^{(Q)}\gamma_5]. \tag{1.88}$$

But, we do not make more discussion on its chiral Lagrangian for its complication and in the present work we use another approach on this issue, seen later. Further discussions and applications can be seen in Refs. [236, 243–247].

Chapter 2

The study of the three-body interaction

Now we use the three-body formalism, as discussed in Sec. 1.4, to investigate some multibody hadron system interactions. First, we investigate some charm systems with one nucleon, for example NDK, $\bar{K}DN$ and $ND\bar{D}$ interactions, and also with two nucleons, the DNN system. Then, we investigate the D^*-multi-ρ systems for the multi-hadron interaction with the same formalism. Besides, we also study some three-body systems with light quarks, such as $\eta K\bar{K}$, $\eta' K\bar{K}$ and $\rho K\bar{K}$ interactions.

2.1 NDK, $\bar{K}DN$ and $ND\bar{D}$ molecules

While the three baryon system has been a subject of intense theoretical study [248–250], it has only been recently that attention was brought to systems with two mesons and one baryon, with unexpected results. Indeed, states with two pseudoscalar mesons and one baryon were studied in Ref. [212]. The same happened with the low lying $J^P = 1/2^+$ N^* states [215]. Independently, and using variational techniques, a N^* state around 1920 MeV was predicted in Ref. [230] as a molecule of $NK\bar{K}$, corroborated in coupled channels Faddeev equations in Refs. [229, 251]. A different calculation also predicts a quasibound $\pi\bar{K}N$ system, with the difference that the $N\pi$ interaction is in p-wave [252]. Systems of bound or quasibound three mesons did not wait long and in Ref. [75] the X(2175)

(now the $\phi(2170)$) was explained as a resonant $\phi K\bar{K}$ system, also described as such in a phenomenological way in Ref. [253]. In a similar way, the $K(1460)$ is explained as a $KK\bar{K}$ state in Ref. [254] and more recently the $\pi(1300)$ is described as a $\pi K\bar{K}$ molecule in Ref. [255].

The charm sector has not yet been explored for such three body systems. For this purpose we have selected systems that have a nucleon and a D meson. The DN system, in collaboration with coupled channels, leads to the formation of a dynamically generated state, the $\Lambda_c(2595)$ [237,256–258]. On top of it we add a $K, \bar{K}$ or $\bar{D}$ meson and we study the stability of the system. The case of scattering of N on the DK cluster, which is known to generate the $D_{s0}^*(2317)$ [259–261] is also considered. On the other hand, the $D\bar{D}$ system leads to a bound state in isospin I=0 [261], which might have already been observed [262], in analogy to the $f_0(980)$ made of $K\bar{K}$ [16, 17, 263–267]. We add a nucleon to it and study the interaction of the three body system. The system obtained would be the analogous to the one found in Refs. [229, 230, 251] as a $NK\bar{K}$. In all cases we find bound or quasibound states with masses around 3100 MeV in the first cases and 4400 MeV in the case of $ND\bar{D}$.

We use the FCA to the Faddeev equations, seen in subsection 1.4.2. The method has proved to be rather reliable for cases like K-deuteron scattering very close to threshold (see Ref. [222] and the earlier work [218]). In a closer problem to the present one, diverting a bit from threshold in the bound region, the FCA has been applied to the study of the $NK\bar{K}$ system in Ref. [226] and the results compare favorably with those of the Faddeev approach in Ref. [229] and those of the variational approach in [230]. Similarly the FCA has been applied to an analogous problem, the one of the $\bar{K}NN$ system [227]. Yet, it has been reassuring to see in that paper that the results of the FCA are qualitatively in agreement with those of other approaches [268–273], and remarkably similar to those obtained in the variational approach of Refs. [271,272] which use the same input as in Ref. [227]. The differences between Ref. [271, 272] and Ref. [227] are at the level of a few MeV in the binding.

2.1.1 Considering the isospin structure

We follow the FCA to the Faddeev equations of subsection 1.4.2, and one more thing that we should take into account is the isospin components

of the two-body interaction amplitudes. Thus, we turn to the amplitudes corresponding to single-scattering contribution, Fig. 1.5 (a). One must take into account the isospin structure of the cluster and write the t_1 and t_2 amplitudes in terms of the isospin amplitudes of the (3,1) and (3,2) systems. Details can be seen in Refs. [223, 224] and our paper [274]. In the present case this is particularly easy. Whether we have the $\bar{K}DN$, KDN, NDK or $ND\bar{D}$ system, where the first particle is labelled 3 and the last two particles are making the cluster (particles 1, 2), the bound state of 1, 2 is in $I = 0$ from former studies and the total spin is then $I = \frac{1}{2}$. Then, for all four cases we find

$$t_1 = \frac{3}{4}\, t_{31}^{I=1} + \frac{1}{4}\, t_{31}^{I=0}, \tag{2.1}$$

$$t_2 = \frac{3}{4}\, t_{32}^{I=1} + \frac{1}{4}\, t_{32}^{I=0}, \tag{2.2}$$

in which $t_{31}^{I=1}$ is the two-body unitary scattering amplitude of isospin $I = 1$ between particle 3 and 1 evaluated with its coupled channels, and similarly for the other cases. We show below the explicit evaluation for the $ND\bar{D}$ case. The derivation for the other systems is identical. Here we take the case of $I_{D\bar{D}} = 0$ and $I_{total} \equiv I_{ND\bar{D}} = 1/2$. We have

$$|D\bar{D}>^{(0,0)} = \sqrt{\frac{1}{2}}|(\frac{1}{2},-\frac{1}{2})> -\sqrt{\frac{1}{2}}|(-\frac{1}{2},\frac{1}{2})>, \tag{2.3}$$

where $|(\frac{1}{2},-\frac{1}{2})>$ denote $|(I_z^1, I_z^2)>$ which shows the I_z components of particles 1 and 2. Then we obtain

$$\begin{aligned}
t &= < ND\bar{D}|\,\hat{t}\,|ND\bar{D}> \\
&= (< D\bar{D}|^{(0,0)} \otimes < N|^{(\frac{1}{2},\frac{1}{2})})\,(\hat{t}_{31}+\hat{t}_{32})\,(|D\bar{D}>^{(0,0)} \otimes |N>^{(\frac{1}{2},\frac{1}{2})}) \\
&= \left[\sqrt{\frac{1}{2}}\left(<(\frac{1}{2},-\frac{1}{2})| - <(-\frac{1}{2},\frac{1}{2})|\right) \otimes < N|^{(\frac{1}{2},\frac{1}{2})}\right](\hat{t}_{31}+\hat{t}_{32})\left[\sqrt{\frac{1}{2}}\left(|(\frac{1}{2},-\frac{1}{2})> \right.\right. \\
&\quad \left.\left. - |(-\frac{1}{2},\frac{1}{2})>\right) \otimes |N>^{(\frac{1}{2},\frac{1}{2})}\right] \\
&= \left[\sqrt{\frac{1}{2}} < (1,1),-\frac{1}{2}| - \sqrt{\frac{1}{2}}\left(\sqrt{\frac{1}{2}} < (1,0),\frac{1}{2}| - \sqrt{\frac{1}{2}} < (0,0),\frac{1}{2}|\right)\right]\hat{t}_{31}\left[\sqrt{\frac{1}{2}}\right. \\
&\quad \left. \times |(1,1),-\frac{1}{2}> -\sqrt{\frac{1}{2}}\left(\sqrt{\frac{1}{2}}|(1,0),\frac{1}{2}> -\sqrt{\frac{1}{2}}|(0,0),\frac{1}{2}>\right)\right] + \left[\sqrt{\frac{1}{2}}\right.
\end{aligned}$$

$$\times \left(\sqrt{\frac{1}{2}} < (1,0), \frac{1}{2}| - \sqrt{\frac{1}{2}} < (0,0), \frac{1}{2}|\right) - \sqrt{\frac{1}{2}} < (1,1), -\frac{1}{2}|\Big] \hat{t}_{32} \Big[\sqrt{\frac{1}{2}}$$
$$\times \left(\sqrt{\frac{1}{2}}|(1,0), \frac{1}{2} > -\sqrt{\frac{1}{2}}|(0,0), \frac{1}{2} > \right) - \sqrt{\frac{1}{2}}|(1,1), -\frac{1}{2} > \Big]$$
$$= \Big(\frac{3}{4} t_{ND}^{I=1} + \frac{1}{4} t_{ND}^{I=0}\Big) + \Big(\frac{3}{4} t_{N\bar{D}}^{I=1} + \frac{1}{4} t_{N\bar{D}}^{I=0}\Big), \tag{2.4}$$

where the notation of the states followed in the terms is $|(1,1), -\frac{1}{2} > \equiv |(I^{31}, I_z^{31}), I_z^2 >$ for t_{31}, and $|(I^{32}, I_z^{32}), I_z^1 >$ for t_{32}.

2.1.2 The case of $\bar{K}DN$ interaction

Our strategy proceeds as follows: first we generate the resonance or bound state in the compound system and determine the value of the parameter Λ, then calculate the form factor and G_0 propagator and take the t_1 and t_2 amplitudes from the unitary coupled channel approach, finally the total scattering amplitude T is evaluated. For the $\bar{K}DN$ scattering, the first thing we do is to reproduce the work of Refs. [257,275] in coupled channels for the DN system. The coupled channels used are $\pi\Sigma_c$, DN, $\eta\Lambda_c$, $K\Xi_c$, $K\Xi_c'$, $D_s\Lambda$, $\eta'\Lambda_c$ and the dynamics is obtained from the exchange of vector mesons between the pseudoscalar meson and the baryon. This procedure, based on the LHG approach [156,159,163], leads to the chiral Lagrangians in the SU(3) sector. One gets as dynamically generated resonance the $\Lambda_c(2595)$, which couples most strongly to the DN channel and is interpreted as a DN bound state. As shown in Fig. 2.1, the method generates a pole in the DN scattering amplitude in $I = 0$ in the first Riemann Sheet at $(2595 + i0)$ MeV. Since the works of Refs. [257, 275] use dimensional regularization for the loops, and we need a cut off to obtain the wave function and form factor, the equivalent cut off must be obtained. There are three methods to do this. One of them is to compare the value of the G propagator (the loop function of two particles propagator which appears in the BS equation of Eq. (1.43)) at threshold using the dimensional regularization formula [276] with the one of the cut off which can be taken from Ref. [155] (Ref. [16] for meson-meson interaction) or the analytic expression in Ref. [195]. Another method is to compare the pole position using different regularization schemes. The third one is to use the relation between the subtraction constant $a(\mu)$ and the cut off Λ of Eq. (52) in Ref. [196]. The best fitting results by these methods

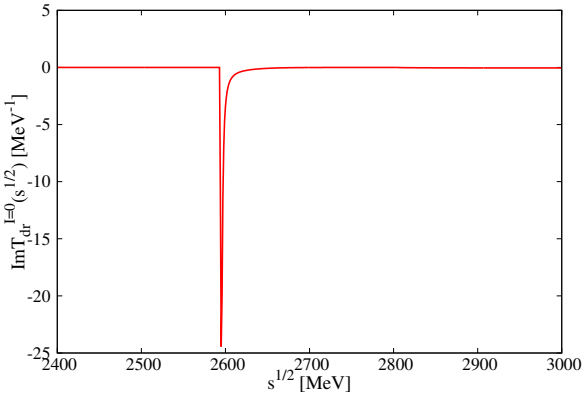

Figure 2.1: Imaginary part of the DN amplitude for isospin $I = 0$.

give us a value of $\Lambda = 973$ MeV. The imaginary part of the DN amplitude in $I = 0$ is shown in Fig. 2.1. The $\Lambda_c(2595)$ form factor using this cut off is shown in Fig. 2.2. In the next step we evaluate G_0 by means of Eq. (1.76) (for the baryon cluster) and we show its real and imaginary parts in Fig. 2.3.

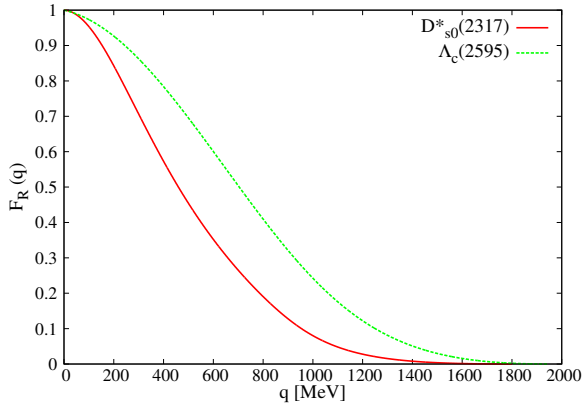

Figure 2.2: Form factors of $\Lambda_c(2595)$ and $D^*_{s0}(2317)$.

In the final calculation we also need to know the two-body unitary scattering amplitudes in different isospin states. For the $\bar{K}DN$ interac-

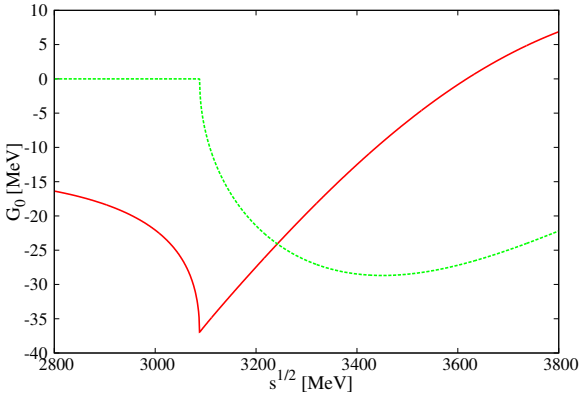

Figure 2.3: Real(solid line) and imaginary(dashed line) parts of G_0 in $\bar{K}DN$.

tion, the amplitudes of $\bar{K}D$ and $\bar{K}N$ are needed. For the $\bar{K}D$ interaction we have taken the results of Ref. [261]. On the other hand, the $\bar{K}N$ scattering has been evaluated using the chiral unitary approach of Ref. [155] with the dimensional regularization scheme of Ref. [276], using $\mu = 630$ MeV, $a_i(\mu) = -1.84$ for all channels. This scheme leads to the generation of the two $\Lambda(1405)$ states reported in Ref. [277].

In Fig. 2.4 we show the results of $|T|^2$ for the $\bar{K}\Lambda_c(2595)$ scattering. We find a peak around 3150 MeV, slightly above the threshold of the $\Lambda_c(2595) + \bar{K}$ mass (3088 MeV) and below the threshold of the $\bar{K}DN$ system (3298 MeV). The width of the peak is about 50 MeV, which indicates the width of the state that we obtain. In our study of the system $\bar{K}DN$, where we have chosen the DN system in $I = 0$, since this is the channel with strong attraction leading to the $\Lambda_c(2595)$ resonance, the quantum numbers of the $\bar{K}DN$ state are $C = 1, S = -1$ and $J^P = \frac{1}{2}^+$ since we only consider the interaction among the components in $L = 0$. The mass of this state is very close to that of the $\Xi_c(3123)$, of unknown spin and parity, but its decay width is larger than that of the $\Xi_c(3123)$, 4 ± 4 MeV [9]. The larger width, tied to the $\pi\Sigma$ decay of the $\bar{K}N$ system, seems unavoidable, and this indicates that the resonance that we find could most probably correspond to a resonance not yet found.

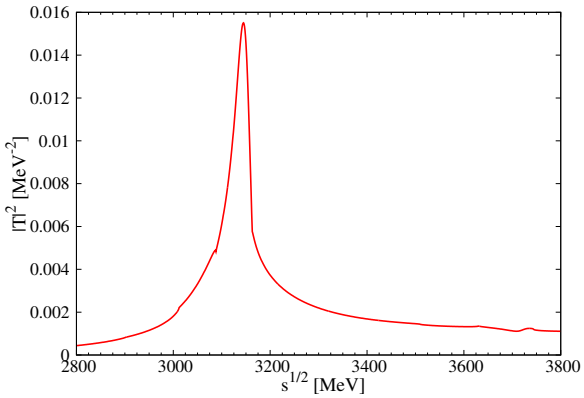

Figure 2.4: Modulus squared of the $\bar{K}\Lambda_c(2595)$ scattering amplitude.

2.1.3 Investigating the NDK interaction

The two body KD and DN interactions were studied by the coupled channel with ChUA in Refs. [261] and [257, 275], respectively. It was found that the resonance $D_{s0}^*(2317)$ is dynamically generated in $I = 0$ from KD scattering and the $\Lambda_c(2595)$ is produced in $I = 0$ from the DN interaction, as we mentioned above. Hence there are two possible cases of three body scattering in the NDK system. One is the $N-(DK)_{D_{s0}^*(2317)}$ and the other one is the $K-(DN)_{\Lambda_c(2595)}$.

First, we are going to investigate the three body scattering for the $N-(DK)_{D_{s0}^*(2317)}$. In order to calculate this, in a first step we obtain the DN amplitude, t_1 from Refs. [257,275] and the KN amplitude, t_2 from the chiral unitary approach of Ref. [155]. For the DN matrix element the result of Ref. [257] is reproduced and the imaginary part of the DN matrix element that we obtain is shown in Fig. 2.1. In the case of the KN system, the interaction is repulsive in $I = 1$ and has vanishing interaction in $I = 0$. We take the parameters for the loop function from Ref. [276]. For the next step, in order to get the total scattering amplitude T, we need to know the form factor for $D_{s0}^*(2317)$ and $G_0(s)$. Here the cut off is determined by comparing the value of the G function that one obtains from the dimensional regularization [276] and the cut off scheme [155] at threshold. In this way $\Lambda = 900$ MeV is obtained for the cut off of the $D_{s0}^*(2317)$ form factor. The

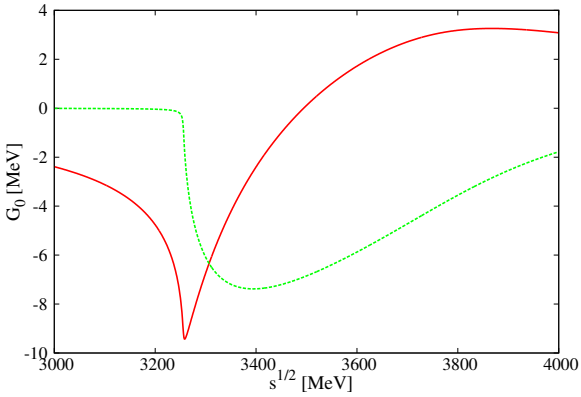

Figure 2.5: Real(solid line) and imaginary(dashed line) parts of G_0 in $N - DK$.

form factor of the $D_{s0}^*(2317)$ is plotted in Fig. 2.2 and the $G_0(s)$ function for this case is represented in Fig. 2.5.

Using the aforementioned total three-body scattering amplitude T, we obtain $|T|^2$ for the $ND_{s0}^*(2317)$ scattering shown in Fig. 2.6. We found a peak around 3050 MeV which is about 200 MeV below the $D_{s0}^*(2317)$ and N threshold. This reflects the strong attraction in the DN system that leads to the $\Lambda_c(2595)$. The width of the state is smaller than 10 MeV. We do not find a counterpart in the PDG and the quantum numbers, with positive strangeness, correspond to an exotic state.

As an alternative possibility, the three body scattering in the KDN system can also be formed as $K-(DN)_{\Lambda_c(2595)}$, with the $\Lambda_c(2595)$ assumed as a two body cluster. Now we need the two body matrix elements KD and KN. The latter one is calculated using the chiral unitary approach that was mentioned before. The KD matrix element, as also mentioned above, is investigated in Ref. [261]. In order to calculate the form factor for the $\Lambda_c(2595)$, the cut off is needed. With the aforementioned strategy the value of $\Lambda = 973$ MeV is obtained and it was already used in section 2.1.2. Using this cut off value, the $G_0(s)$ function is the same as in section 2.1.2 when we had scattering of a $\bar{K}$ on the cluster of $\Lambda_c(2595)$, since the masses of $\bar{K}$ and K are the same. The $G_0(s)$ function is, thus, the one plotted in Fig. 2.3. Ultimately the total three-body scattering amplitude for the

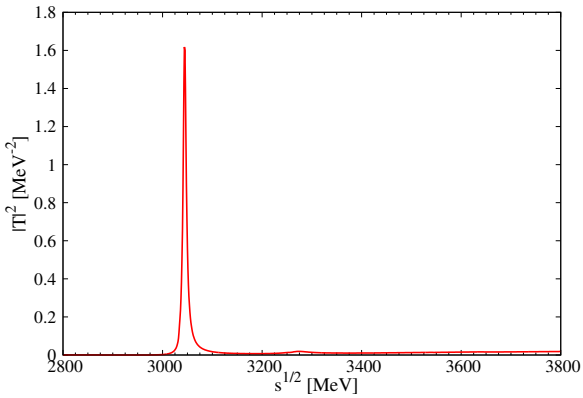

Figure 2.6: Modulus squared of the $ND^*_{s0}(2317)$ scattering amplitude.

$K\Lambda_c(2595)$ scattering is evaluated and the result of $|T|^2$ is represented in Fig. 2.7. There is an explicit narrow peak at 3100 MeV.

One may try to investigate the structure of the peak in Fig. 2.7, but it would only distract us from the main point, which is that the weight of $|T|^2$ in Fig. 2.7 is very small compared with the one in Fig. 2.6 for the $N-(DK)_{D^*_{s0}(2317)}$ configuration. Note that a proper comparison requires to take into account the different field normalizations. Indeed, the S matrix for $N-(DK)_{D^*_{s0}(2317)}$ goes as

$$S \simeq 1 - iT \frac{1}{\sqrt{2\omega_{D^*_{s0}(2317)}}} \frac{1}{\sqrt{2\omega'_{D^*_{s0}(2317)}}} \sqrt{\frac{2M_N}{2E_N}} \sqrt{\frac{2M_N}{2E'_N}}, \qquad (2.5)$$

while for $K-(DN)_{\Lambda_c(2595)}$ it goes as

$$S \simeq 1 - iT \frac{1}{\sqrt{2\omega_K}} \frac{1}{\sqrt{2\omega'_K}} \sqrt{\frac{2M_{\Lambda_c}}{2E_{\Lambda_c}}} \sqrt{\frac{2M_{\Lambda_c}}{2E'_{\Lambda_c}}}. \qquad (2.6)$$

Hence, the proper comparison is $\frac{T}{2m_{D^*_{s0}}}$ in the first case versus $\frac{T}{2m_K}$ in the second, or $T(K(DN))$ versus $\frac{m_K}{m_{D^*_{s0}}} \times T(N(DK))$. Considering this, the

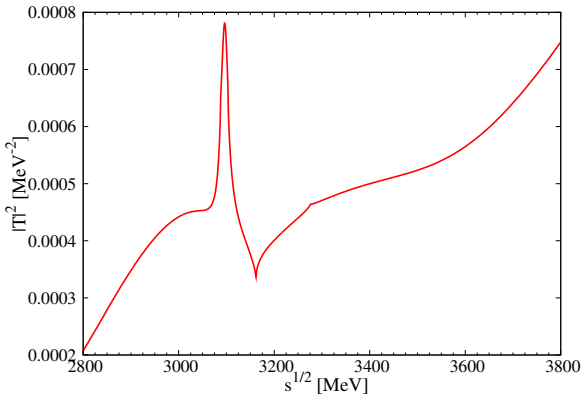

Figure 2.7: Modulus squared of the $K\Lambda_c(2595)$ scattering amplitude.

strength of the peak for $|T(K(DN))|^2$ is about a factor 90 smaller than for $|T(N(DK))|^2$. This means that the $K(DN)$ configuration in the wave function of the KDN system has a very small weight. Hence, we predict a bound state of NDK mostly made of a N orbiting around a bound DK cluster forming the $D_{s0}^*(2317)$.

2.1.4 $NDar{D}$ interaction results

The two-body $D\bar{D}$ interaction was investigated in Refs. [261, 262, 278] and a resonance called $X(3700)$, was dynamically generated. This resonance would be the analogue one to the $f_0(980)$ which is basically a $K\bar{K}$ bound state [16, 17, 263–267]. In our procedure we also reproduce this $D\bar{D}$ state successfully, getting the pole as $(3718 + i0)$ MeV with the same parameters as in Ref. [261]. We take a value of $\Lambda = 850$ MeV from Ref. [262], which is consistent with the methods mentioned above. Then we can calculate the form factor of the $X(3700)$ with Eq. (1.77) by means of this cut off. Next we evaluate the G_0 by means of Eq. (1.76), for N propagating between the D and $\bar{D}$, and its results are shown in Fig. 2.8.

The nucleon interaction with the $D, \bar{D}$ mesons was studied by the coupled channels two-body scattering equations in Refs. [257, 258]. For the DN scattering amplitude, as mentioned before, we followed the procedure of Ref. [257]. For the $I = 1$ sector there are eight coupled channels and we

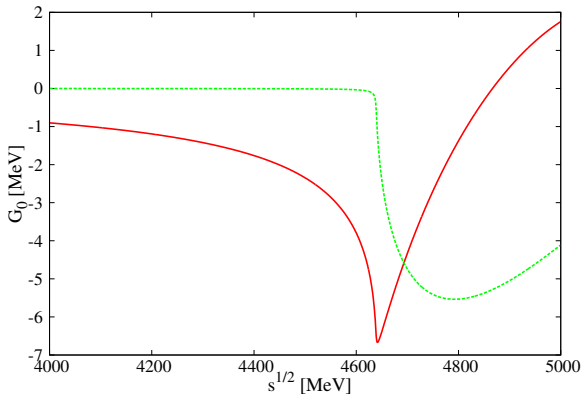

Figure 2.8: Real(solid line) and imaginary(dashed line) parts of G_0 in $ND\bar{D}$.

have used the same parameters as in $I = 0$ which reproduced the $\Lambda_c(2595)$ resonance. The $\bar{D}N$ interaction, which is similar to the KN channel [257], is repulsive in $I = 1$ and vanishes for $I = 0$. As in [258], we took the same parameter as for the DN interaction. Finally we obtain the T matrix, for the $ND\bar{D}$ interaction by means Eq. (1.68), and show the results of $|T|^2$ in Fig. 2.9. From this figure we can see that there is a clear peak of $|T|^2$

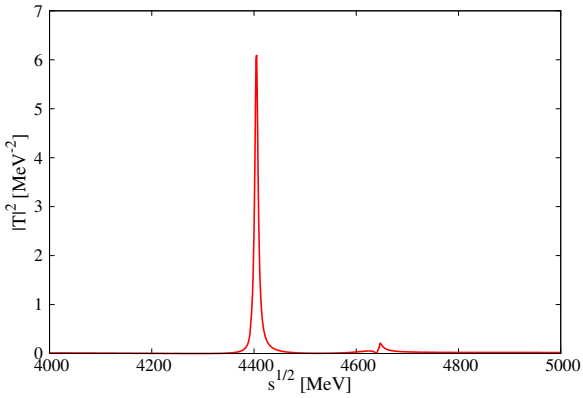

Figure 2.9: Modulus squared of the $NX(3700)$ scattering amplitude.

around 4400 MeV and the width is very small, less than 10 MeV. The peak

appears below the $ND\bar{D}$ and $NX(3700)$ thresholds and corresponds to a bound state of $NX(3700)$. This would be a hidden charm baryon state of $J^P = \frac{1}{2}^+$ which appears in the same region of energies as other hidden charm states of $J^P = \frac{1}{2}^-$ obtained from the $\bar{D}\Lambda_c$, $\bar{D}\Sigma_c$ and $\bar{D}^*\Lambda_c$, $\bar{D}^*\Sigma_c$ in Refs. [127, 168]. In these latter works some reactions were suggested to observe those states in future Facilities. The same or similar reactions could be used to observe these states of positive parity.

2.1.5 Conclusions

We have investigated three body systems that have one D meson or $D\bar{D}$, together with one baryon. The systems are $\bar{K}DN$, NDK and $ND\bar{D}$. Concretely, for $\bar{K}DN$ we study the scattering of $\bar{K}$ with the D and N components of the cluster of DN that makes the $\Lambda_c(2595)$ resonance. In the second case, NDK, we find that the important configuration corresponds to N scattering over the cluster of KD that makes the $D^*_{s0}(2317)$. In the case of the $ND\bar{D}$ we look at N scattering on the $D\bar{D}$ cluster that is supposed to generate a bound state called X(3700). In all cases we find bound or quasibound states, relatively narrow, with energies 3150 MeV, 3050 MeV and 4400 MeV, respectively. All these states have $J^P = 1/2^+$ and isospin $I = 1/2$ and differ by their charm or strangeness content, $S = -1, C = 1$, $S = 1, C = 1$, $S = 0, C = 0$, respectively.

2.2 DNN quasi-bound state

The interaction of mesons with nuclei and the property of mesonic bound states are one of the most important topics in the nuclear-hadron physics [279–284]. Bound states of pions and K^- have been investigated for long and have revealed the roles of strong interactions in the hadron-nucleus bound states. A step forward in the experimental observation of the most deeply bound pionic states was given using the $(d,^3\mathrm{He})$ reaction [285], and also, although less clearly, using the coherent radiative π^- capture [286] in Ref. [287]. The deeply bound kaon atoms had been studied theoretically using the optical potentials [288–292]. Because of the large imaginary part, the width of the bound states is larger than the energy separation between the levels [283, 293], so that the experimental observation is not obvious (see also Refs. [294, 295]).

The simplest of the many-body kaonic nuclear system is the $\bar{K}NN$. Because the $\Lambda(1405)$ resonance is interpreted as a quasi-bound state of the $\bar{K}N$ system in the $\pi\Sigma$ continuum [155, 190, 194, 277, 296–299], one expects a quasi-bound $\bar{K}NN$ system driven by the attractive $\bar{K}N$ interaction in the isospin $I = 0$ channel. Various approaches have resulted in a rather general consensus that the quasi-bound state is obtained above the $\pi\Sigma N$ threshold and the width is larger than the binding [227, 228, 231, 268–273, 300–302]. Thus, the experimental identification of this system would be difficult.

What we report here is the analogous state of the $\bar{K}NN$, substituting the $\bar{K}$ by a D meson. The DN interaction in $I = 0$ dynamically generates the $J^P = 1/2^-$ excited state, $\Lambda_c(2595)$ [237, 256–258]. The $\Lambda_c(2595)$ resonance is rather narrow ($\Gamma < 1.9$ MeV), in contrast to the analogous $\Lambda(1405)$ with the widths of 30-60 MeV [277,298,299]. While the large width of the $\Lambda(1405)$ is responsible for the large width of the $\bar{K}NN$ state, the analogous state DNN, where the $\Lambda_c(2595)$ plays the role of the $\Lambda(1405)$ in the $\bar{K}NN$ state, has much better chances to survive as a long lived and observable state.

The interaction of the D mesons with nuclei has been addressed in Refs. [237, 257, 303] and the possibility of making bound atomic states of D mesons in nuclei has been considered in Ref. [304]. However, few-body systems like DNN are less affected by the Coulomb repulsion particularly for the total isospin $I_{\mathrm{tot}} = 1/2$. With this in mind we tackle the DNN system from two different approaches: the FCA to the Faddeev equations, as done in Refs. [227, 228, 231] for the $\bar{K}NN$ system, and the variational

method as done in Refs. [271,272]. In order to gain confidence that the state found is narrow, we have also evaluated the width of the state coming from the absorption of the D by a pair of nucleons going to the $\Lambda_c N$ system in the FCA, analogous to the absorption of $\bar{K}$ by a pair of nucleons as considered in Refs. [272, 289, 305, 306].

2.2.1 DN scattering and interaction

We consider the two-body DN scattering based on the model in Ref. [257]. This is a coupled-channel approach to the s-wave meson-baryon scattering in the vector-meson exchange picture. The negative parity $\Lambda_c(2595)$ resonance is dynamically generated as a quasi-bound state of the DN system in the $I = 0$ channel, just like the $\Lambda(1405)$ resonance in the strangeness sector [155, 190, 194, 277, 297–299].

We consider seven (eight) coupled channels in the isospin $I = 0$ ($I = 1$) sector, DN, $\pi\Sigma_c$, $\eta\Lambda_c$, $K\Xi_c$, $K\Xi_c'$, $D_s\Lambda$, and $\eta'\Lambda_c$ (DN, $\pi\Lambda_c$, $\pi\Sigma_c$, $\eta\Sigma_c$, $K\Xi_c$, $K\Xi_c'$, $D_s\Sigma$, and $\eta'\Sigma_c$). The scattering amplitude t_{ij} is obtained from the ChUA as discussed in subsection 1.3.1

$$t^{(I)} = ((v^{(I)})^{-1} - g^{(I)})^{-1}, \tag{2.7}$$

with the dimensional regularization for the loop function $g^{(I)}$ in the present work. The diagonal components of the s-wave scattering amplitudes in the DN channel, which are complex above the πY_c ($Y_c = \Lambda_c, \Sigma_c$) threshold, are shown in Fig. 2.10, where the $\Lambda_c(2595)$ of the $I = 0$ resonance is dynamically generated and the other resonance in $I = 1$ is also generated at ~ 2760 MeV.

Now we construct an effective single-channel potential, which will be used in the variational calculation of the DNN system. We utilize the method in Ref. [307], first constructing a single-channel framework which is equivalent to Eq. (2.7) and then translating the result into a local and energy-dependent potential in coordinate space.

The effective interaction $v^{\rm eff}$ is constructed to reproduce the original amplitude t_{11}, given by

$$t_{11} = [(v^{\rm eff})^{-1} - g_1]^{-1}. \tag{2.8}$$

It is shown that the $v^{\rm eff}$ is given by the sum of the bare interaction in channel

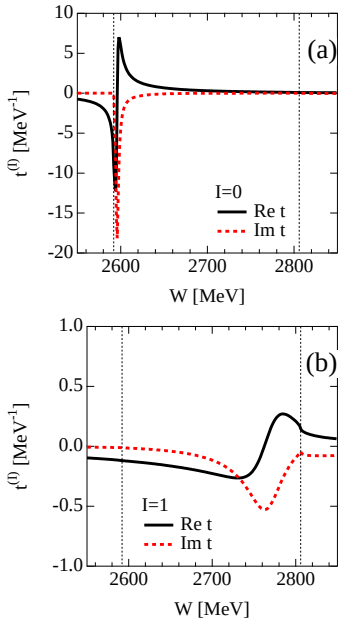

Figure 2.10: (Color online) S-wave DN scattering amplitude in the coupled-channel model (2.7); (a): $I = 0$ channel, (b): $I = 1$ channel. Vertical dotted lines represent the threshold energies of $\pi\Sigma_c$ and DN channels.

1 (v_{11}) and the term with coupled-channel effects as [307]

$$v^{\rm eff} = v_{11} + \sum_{m=2}^{N} v_{1m} g_m v_{m1} + \sum_{m,l=2}^{N} v_{1m} g_m t_{ml}^{(N-1)} g_l v_{l1}, \tag{2.9}$$

where $t_{ml}^{(N-1)} = [(v^{(N-1)})]^{-1} - g^{(N-1)}]^{-1}$ is the $(N-1) \times (N-1)$ matrix of the coupled-channel amplitude without the DN channel.

We then translate $v^{\rm eff}$ into the local potential in coordinate space. Thus, the two-body potential can be written as

$$v_{DN}(r; W) = \frac{M_N}{2\pi^{3/2} a_s^3 \tilde{\omega}(W)} \times [v^{\rm eff}(W) + \Delta v(W)] \exp[-(r/a_s)^2], \tag{2.10}$$

where $a_s = 0.4$ fm is the range parameter of the potential and $\tilde{\omega}(W)$ is the reduced energy of the DN system. This complex and energy-dependent potential reproduces the scattering amplitude t_{11} when the Schrödinger equation with this potential is self-consistently solved. The strength of the potential $v_{DN}(r; W)$ at $r = 0$ is shown in Fig. 2.11. One finds that the real part (imaginary part) is larger (smaller) than that of the $\bar{K}N$ potential [307], which demonstrate the differences of the interaction kernel.

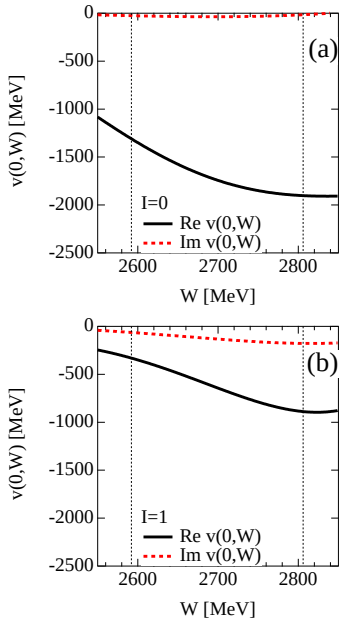

Figure 2.11: (Color online) Strength of the effective potential $v_{DN}(r, W)$ at $r = 0$ by Eq. (2.10); (1): $I = 0$ channel, (b): $I = 1$ channel. The range parameter is chosen to be $a_s = 0.4$ fm. Vertical dotted lines represent the threshold energies of $\pi\Sigma_c$ and DN channels.

2.2.2 The FCA for the DNN system

The FCA to the Faddeev equations has been used with success as discussed above. The method has been used with success in the study of K^- scattering with the deuteron in Refs. [218, 221, 308, 309] (see a review in Ref. [222]

for comparison with full Faddeev calculations). In the present case, where we want to study the DNN system, we have also the precedent of the work of Refs. [227, 228], where the $\bar{K}NN$ system was studied within this approximation and found to provide results in qualitative agreement with those of the variational calculations [271, 272]. The condition that the interacting particle (D meson) is lighter than those of the two-body cluster (nucleon) is not fulfilled in this case. This certainly introduces larger uncertainties than in other cases studied but we still expect that one can get good results at a qualitative level. We already mentioned in the section Sec. 2.1 that the FCA is still a sensible tool in this case when dealing with bound states.

In the FCA to the Faddeev equations for the DNN three body system, one takes the NN as a cluster and D scatters from that cluster. We consider the DNN system with total isospin $I_{\rm tot} = 1/2$ and with the total spin-parity $J^P = 0^-$ and $J^P = 1^-$. In this approach, all the two-body pairs are in s wave.

First we make the evaluation for the case of $J^P = 0^-$, which corresponds to the spin (isospin) of the NN pair as $S_{NN} = 0$ ($I_{NN} = 1$). To have total isospin $I_{\rm tot} = 1/2$, the dominant component of the DN system is $I = 0$, where the $\Lambda_c(2595)$ resonance appears.

The T matrix for the three-body DNN scattering is labeled by the DN isospins in the entrance channel I and the exit channel I', $T_{I,I'}$. We denote the two-body (s-wave) DN scattering amplitudes by $t^{(0)}$ for $I = 0$ and $t^{(1)}$ for $I = 1$. Then the T matrix satisfies

$$T_{I,I'} = t^{(I)}\delta_{I,I'} + t^{(I)}G^{tr}_{I,I''}G_0T_{I'',I'}P_{ex}, \tag{2.11}$$

which is diagrammatically represented in Fig. 2.12. In Eq. (2.11), G_0 is the meson exchange propagator

$$G_0 = \int \frac{d^3q}{(2\pi)^3}F_{NN}(q)\frac{1}{q^{0\,2} - \vec{q}^{\,2} - m_D^2 + i\epsilon}, \tag{2.12}$$

where $F_{NN}(q)$ is the form factor, representing the momentum distribution of the NN system. P_{ex} is the isospin exchange factor, which depends on the total isospin of the nucleon, I_{NN}, in the final state, $P_{ex} = (-1)^{I_{NN}+1} = 1$ for $J = 0$, and $= -1$ for $J = 1$. And, the transition matrix G is given by

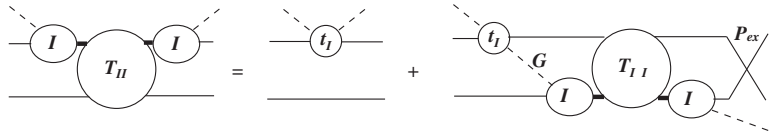

Figure 2.12: Diagrammatic illustration of the three-body equation (2.11).

$$G^{tr}_{I,I''} = \begin{pmatrix} \frac{1}{2} & \frac{\sqrt{3}}{2} \\ \frac{\sqrt{3}}{2} & -\frac{1}{2} \end{pmatrix}.$$

The three-body amplitude $T_{I,I'}$ is obtained by solving Eq. (2.11):

$$\begin{aligned} T = &\left[1 - \frac{1}{2}(t^{(0)} - t^{(1)})G_0 P_{ex} - t^{(0)}t^{(1)}G_0^2\right]^{-1} \\ &\times \begin{pmatrix} t^{(0)} + \frac{1}{2}t^{(1)}G_0 t^{(0)}P_{ex} & \frac{\sqrt{3}}{2}t^{(0)}t^{(1)}G_0 P_{ex} \\ \frac{\sqrt{3}}{2}t^{(0)}t^{(1)}G_0 P_{ex} & t^{(1)} - \frac{1}{2}t^{(0)}G_0 t^{(1)}P_{ex} \end{pmatrix}. \end{aligned}$$

In calculating the T matrix for the scatterings in the $J = 0$ and $J = 1$ channels, we take the linear combinations, with a factor 2 for the choice of the first nucleon, as

$$\begin{aligned} T(J=0) &= 2\begin{pmatrix} \frac{\sqrt{3}}{2} & \frac{1}{2} \end{pmatrix}\begin{pmatrix} T_{00} & T_{01} \\ T_{10} & T_{11} \end{pmatrix}\begin{pmatrix} \frac{\sqrt{3}}{2} \\ \frac{1}{2} \end{pmatrix}, \\ T(J=1) &= 2\begin{pmatrix} -\frac{1}{2} & \frac{\sqrt{3}}{2} \end{pmatrix}\begin{pmatrix} T_{00} & T_{01} \\ T_{10} & T_{11} \end{pmatrix}\begin{pmatrix} -\frac{1}{2} \\ \frac{\sqrt{3}}{2} \end{pmatrix}. \end{aligned}$$

Substituting the T matrix and replacing P_{ex} by $+1$ for $J = 0, I_{NN} = 1$

scattering and -1 for $J = 1, I_{NN} = 0$, we obtain

$$T(J=0) = \left(\frac{3}{2}t^{(0)} + \frac{1}{2}t^{(1)} + 2t^{(0)}t^{(1)}G_0\right) \times \left[1 - \frac{1}{2}(t^{(0)} - t^{(1)})G_0 - t^{(0)}t^{(1)}G_0^2\right]^{-1}, \quad (2.13)$$

$$T(J=1) = \left(\frac{1}{2}t^{(0)} + \frac{3}{2}t^{(1)} + 2t^{(0)}t^{(1)}G_0\right) \times \left[1 + \frac{1}{2}(t^{(0)} - t^{(1)})G_0 - t^{(0)}t^{(1)}G_0^2\right]^{-1}. \quad (2.14)$$

These results coincide with those derived in the charge basis with the formalism of the FCA [228, 231] (more details are seen in the appendix of our paper [310]).

We can see that Eq. (2.12) contains the folding of the D intermediate propagator with the form factor of the NN system. Eq. (2.12) requires the NN form factor. In order to estimate the NN size one can rely upon the results of Ref. [272] in the study of the $\bar{K}NN$ system, where the NN repulsion at short distance was explicitly taken into account. In practical terms we use the same expression for the form factor as for the deuteron [311]

$$F(q) = \int_0^\infty d^3p \sum_{j=1}^{11} \frac{C_j}{\vec{p}^2 + m_j^2} \sum_{i=1}^{11} \frac{C_i}{(\vec{p} - \vec{q})^2 + m_i^2}, \quad (2.15)$$

but with the parameters m_i rescaled such as to give an average separation of the nucleons of $R_{NN} \simeq 2$ fm [272]. They are shown in Fig. 2.13. The validity of this NN form factor will be examined by the result of the variational calculation, where the average distance of the NN pair in the DNN system will be optimized in the three-body dynamics.

We need the argument s_1 of the DN amplitude, $t(\sqrt{s_1})$. To evaluate it we adopt a common procedure of dividing the binding energy into the three particles proportionally to their masses. The energy of the nucleon and the D meson are given by

$$E_N = M_N \frac{\sqrt{s}}{2M_N + m_D}\ ,\ E_D = m_D \frac{\sqrt{s}}{2M_N + m_D},$$

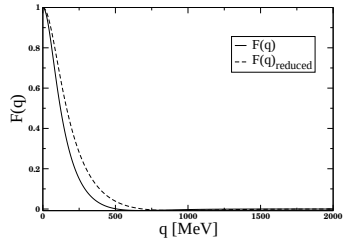

Figure 2.13: Form factor of the deuteron, and the one corresponding to an NN system with a reduced radius from Ref. [272].

so the total energy of the two-body system can be calculated as

$$s_1 = (p_D + p_{N_1})^2 = s\,\left(\frac{M_N + m_D}{2M_N + m_D}\right)^2 - \vec{p}^{\,2}_{N_2}. \tag{2.16}$$

The approximate value of $\vec{p}^{\,2}_{N_2}$ can be obtained by assuming

$$\frac{\vec{p}^{\,2}_{N_2}}{2M_N} \simeq B_{N_2}; \quad B_{N_2} = M_N - M_N \frac{\sqrt{s}}{2M_N + m_D}, \tag{2.17}$$

which provides a rough estimate for bound systems with the strong interaction.

We use here a different prescription for s_1 than the one used in Ref. [227]. The latter one was based on the calculation of $s_1 = (p_A + p_1)^2 = m_A^2 + m_{b_1}^2 + 2p_A \cdot p_1$ and further steps to calculate $p_A \cdot p_1$, where A is the interacting particle and b_1 one of the particles of the cluster. However, when the binding of the system is large, like in the present case, assuming $p_A^2 = m_A^2$ and $p_1^2 = m_{b_1}^2$ grossly underestimated the binding of the particles and we have introduced the new, more realistic prescription of Eq. (2.16).

2.2.3 Evaluation of the $D(NN)$ Absorption

As we shall see later, we obtain a DNN bound system with a very small width. This is related to the small width of the $\Lambda_c(2598)$ state which is generated in DN interaction in $I = 0$. Yet, this calculation only takes into account the decay channel $DN \to \pi\Sigma_c$ for which there is little phase space and $DN \to \pi\Lambda_c$ channel which comes from the subdominant DN $I = 1$

component in the DNN system. Now we allow the D to be absorbed by two nucleons, in analogy to the $\bar{K}NN \to \Lambda N$ considered in Refs. [289,305,306]. Here the channel will be $DNN \to N\Lambda_c$ whose absorption process is shown diagrammatically in Fig. 2.14 (other mechanisms and decay channels will be discussed in the end of this section). We calculate only the first diagram in Fig. 2.14. The second one gives an identical contribution and they sum incoherently: there is no interference since the $N\Lambda_c$ and $\Lambda_c N$ are orthogonal states. Hence, the total width will be twice the one obtained from just one diagram.

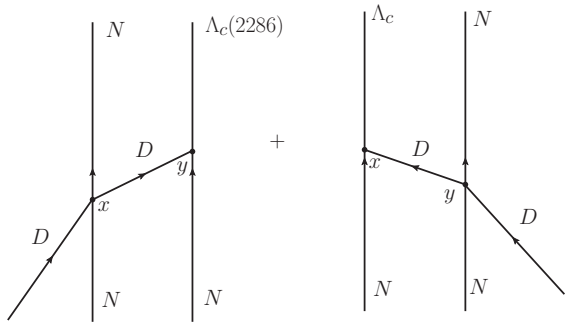

Figure 2.14: Diagrammatic representation of the $D(NN)$ absorption.

The S-matrix for the diagram is given by

$$\begin{aligned} S &= \int d^4x \int d^4y (-i) t_{DN\to DN} \\ &\times \frac{1}{\sqrt{2\omega_D}} \varphi_D(\vec{x}) e^{-i\omega_D x^0} e^{iE'_{N_1} x^0} e^{-iE_{N_1} x^0} \varphi^*_{N'_1}(\vec{x}) \varphi_{N_1}(\vec{x}) \\ &\times \int \frac{d^4q}{(2\pi)^4} e^{-iq(y-x)} \frac{i}{q^2 - m_D^2 + i\epsilon} \\ &\times V_y \vec{\sigma}\vec{q}\, e^{iE_{\Lambda_c} y^0} e^{-iE_{N_2} y^0} \varphi^*_{\Lambda_c}(\vec{y}) \varphi_{N_2}(\vec{y}), \end{aligned}$$

where V_y is the Yukawa vertex. We take the same coupling as $K^- p \to \Lambda$ since in the D and Λ_c the c quark plays the role of the s quark in the $\bar{K}$ and Λ. In Ref. [312], the V_y is given as

$$V_y = -\frac{1}{\sqrt{3}} \frac{3F + D}{2f},$$

with $D = 0.795$, $F = 0.465$ [313]. After performing the integrations, the S-matrix is written as follows

$$\begin{aligned} S &= \frac{1}{V^2}\int \frac{d^3q}{(2\pi)^3}\frac{1}{\sqrt{2\omega_D}} t_{DN\to DN}\frac{1}{q^2-m_D^2+i\epsilon} \\ &\quad \times V_y \vec{\sigma}\vec{q}\;\tilde{\varphi}(\vec{q}-\vec{p}_{\Lambda_c}+\frac{\vec{P}}{2})(2\pi)^4\delta^4(p_i-p_f) \\ &\equiv -iT\frac{1}{\sqrt{2\omega_D}}\frac{1}{V^2}(2\pi)^4\delta^4(p_i-p_f). \end{aligned} \tag{2.18}$$

Taking an approximation to the D propagator in Eq. (2.18),

$$\frac{1}{q^2-m_D^2} \to \frac{1}{(q^0)^2-\vec{p}_{\Lambda_c}^{\,2}-m_D^2}, \tag{2.19}$$

where $q^0 = E_{\Lambda_c} - E_{N_2}$ and $p_{\Lambda_c} \approx \lambda^{1/2}(M_{NND}^2, M_N^2, M_{\Lambda_c}^2)/2M_{NND}$, and defining of $\vec{q}-\vec{p}_{\Lambda_c} \equiv \vec{q}\,'$, the square of the total matrix element is obtained as follow:

$$\begin{aligned} |T|^2 &= V_y^2\vec{p}_{\Lambda_c}^{\,2}\left(\frac{1}{(q^0)^2-p_{\Lambda_c}^2-m_D^2}\right)^2 \\ &\quad \times\left|\frac{1}{2\pi^2}\int q'^2dq'\tilde{\varphi}(\vec{q}\,')t_{DN,DN}(\sqrt{s'})\right|^2, \end{aligned} \tag{2.20}$$

With this T matrix we evaluate the cross section for the process of Fig. 2.14 (left) and we obtain

$$\sigma_{\rm abs} = \frac{1}{2\pi}\frac{M_{NN}M_{\Lambda_c}M_N}{M_{NND}^2}\frac{p_{\Lambda_c}}{p_D}|T|^2.$$

It is interesting to relate this cross section to the imaginary part of the forward $D(NN)\to D(NN)$ amplitude from the diagram of Fig. 2.15 using the optical theorem. We find

$$\text{Im } T_{D(NN)} = -\frac{p_D\sqrt{s}}{M_{NN}}\sigma_{\rm abs} = -\frac{1}{2\pi}\frac{M_{\Lambda_c}M_N}{M_{NND}}p_{\Lambda_c}|T|^2.$$

The next step is to convert the absorption diagram of the Fig. 2.15 (a) into a "many body" diagram of Fig. 2.15 (b) where the nucleon where the D

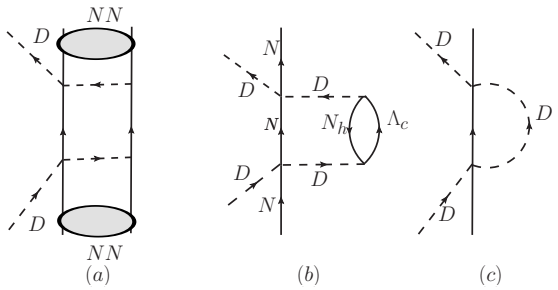

Figure 2.15: $D(NN)$ absorption.

is absorbed, the only occupied state of the "many body" system, is converted into a hole state in the many body terminology [314]. Once this is done, one observes that if we remove the amplitude t_{DN} in the expression of T, the expression that we obtain for Im $T_{D(NN)}$ corresponds to the evaluation of the imaginary part of the two-body loop function g of a nucleon and a D meson [Fig. 2.15 (c)] but with a D selfenergy insertion accounting for the $(\Lambda_c N_h)$ excitation of the D meson. We call this $\delta\tilde{g}$. The Feynman rules to evaluate Im $\delta\tilde{g}$ and Im $T_{D(NN)}$ are identical, except that $t_{DN,DN}$ is removed in the evaluation of Im $\delta\tilde{g}$. Hence we obtain

$$i\text{Im } \delta\tilde{g} = -i\frac{1}{2\pi}\frac{M_{\Lambda_c}M_N}{M_{NND}}p_{\Lambda_c}|\tilde{T}|^2.$$

with $|\tilde{T}|^2$ is given by Eq. (2.20) removing $t_{DN,DN}$. This simplifies the expression since

$$\begin{aligned}\frac{1}{2\pi^2}\int q'^2 dq' \tilde{\varphi}(\vec{q}\,') = &\lim_{r\to 0}\int \frac{d^3q'}{(2\pi)^3}e^{i\vec{q}\,'\vec{r}}\tilde{\varphi}(\vec{q}\,') \\ =&\varphi(r=0).\end{aligned} \tag{2.21}$$

Thus $|\tilde{T}|^2$ is given by

$$|\tilde{T}|^2 \;=\; V_y^2\vec{p}_{\Lambda_c}^{\,2}\frac{1}{[(q^0)^2 - p_{\Lambda_c}^2 - m_D^2]^2}|\varphi(0)|^2.$$

Finally $\vec{p}_{\Lambda_c}^{\,2}$ accompanying V_y^2 in the former expression requires a small correction. The factor comes from the non relativistic $\vec{\sigma}\vec{q}$ form of the $DN\Lambda_c$

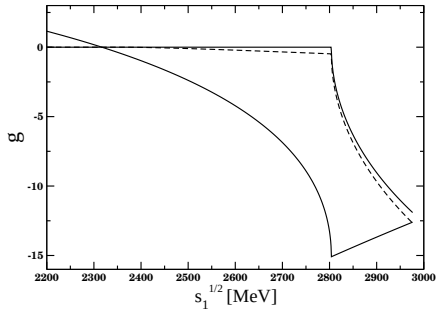

Figure 2.16: The meson-baryon loop function g_{DN} in the DN channel (solid line) and with the effect of the two-body absorption iIm $\delta\tilde{g}$ added (dashed line).

vertex. If we take instead the relativistic Yukawa vertex of the type $\gamma^\mu\gamma^5$, then we find the easy prescription to account for the relativistic correction,

$$V_y^2 \vec{p}_{\Lambda_c}^{\,2} \quad \to \quad V_y^2 \frac{1}{4m_{\Lambda_c}^2}(M_N + M_{\Lambda_c})^2 \vec{p}_{\Lambda_c}^{\,2}.$$

The next step is to reevaluate the $t_{DN,DN}$ amplitude used as input in the fixed center formulas. As we mentioned, it was obtained using the method of Ref. [257] with several coupled channels and the formula (2.7). We redo the evaluation by replacing the loop function in the DN channel as

$$g_{DN} \to g_{DN} + i \text{ Im } \delta\tilde{g} \tag{2.22}$$

to take into account the D absorption by two nucleons or, analogously, the $\Lambda_c N_h$ excitation of the D meson. When doing this, the DN amplitude becomes complex below the DN threshold and the narrow $\Lambda_c(2598)$ resonance acquires now a moderate width due to the D absorption with a second nucleon. The second process of Fig. 2.14 (right) is accounted for when we consider the three-body amplitude T in the FCA formula with the first D scattering with the second nucleon.

Let us numerically investigate the effect of the absorption. In Fig. 2.16, we show the meson-baryon loop function g_{DN} in the DN channel together with the two-body absorption contribution to the imaginary part, iIm $\delta\tilde{g}$. We can see that the imaginary part of the total g function is no longer

zero below the DN threshold due to D absorption. In Fig. 2.17, we show the modulus of the two-body amplitude $|t|$ for the DN channel for $I = 0$ using g_{DN} and $g_{DN} + i\text{Im}\,\delta\tilde{g}$ of Eq. (2.22). As we can see, the inclusion of the absorption mechanism induces an increase in the width of the peak of $\Lambda_c(2595)$ in $|t|$ which will have repercussion in the width of the DNN system.

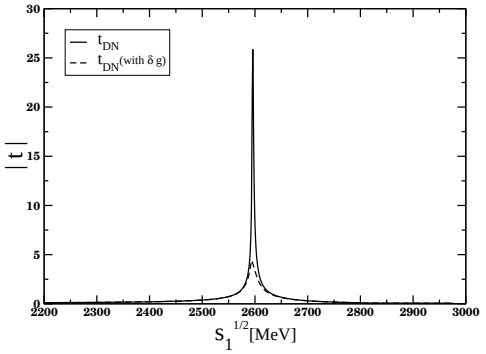

Figure 2.17: Modulus of the two-body amplitude $DN \to DN$ (solid line) and with the effect of the two-body absorption $i\text{Im}\,\delta\tilde{g}$ added (dashed line).

2.2.4 Variational calculation of the DNN system

Here we calculate the energy of the DNN system with a variational approach formulated for the $\bar{K}NN$ system in Refs. [271, 272]. As in the case of the FCA, we consider the DNN system with total isospin $I = 1/2$ and the total spin-parity either $J^P = 0^-$ or $J^P = 1^-$. The trial wave function for the $J^P = 0^-$ state is prepared with two components:

$$|\,\Psi^{J=0}\,\rangle = (\mathcal{N}^0)^{-1}[|\,\Phi^0_+\,\rangle + C^0|\,\Phi^0_-\,\rangle],$$
$$|\,\Psi^{J=1}\,\rangle = (\mathcal{N}^1)^{-1}[|\,\Phi^1_+\,\rangle + C^1|\,\Phi^1_-\,\rangle],$$

where $\mathcal{N}^0$, $\mathcal{N}^1$ are the normalization constants, C^0, C^1 are the mixing coefficients, $|\,\Phi^0_+\,\rangle$, $|\,\Phi^1_+\,\rangle$ are the main component, and $|\,\Phi^0_-\,\rangle$, $|\,\Phi^1_-\,\rangle$ are the mixture components. Note that only the main component of $|\,\Phi^{J=0,1}_+\,\rangle$ is taken into account in the FCA calculation. The wave functions are expanded in terms of gaussians in coordinate space, and we minimize the total energy

of the system with the Hamiltonian given below. Detailed explanation of the variational method can be found in Ref. [272].

We consider the following Hamiltonian in this study:

$$\hat{H} = \hat{T} + \hat{V}_{NN} + \mathrm{Re}\ \hat{V}_{DN} - \hat{T}_{\mathrm{c.m.}}, \tag{2.23}$$

where $\hat{T}$ is the total kinetic energy, $\hat{V}_{DN}$ is the DN potential term which is the sum of the contributions from two nucleons, and $\hat{T}_{\mathrm{c.m.}}$ is the energy of the center-of-mass motion. For the NN potential $\hat{V}_{NN}$, we use three models: HN1R which is constructed from Hasegawa-Nagata No.1 potential [315], the Minnesota force [316], and the gaussian-fitted version of the Argonne v18 potential [317]. We have examined three kinds of NN interactions. Because we work in the isospin symmetric limit, the Coulomb interaction is not included in all cases. In Fig. 2.18, we show the spatial form of the potentials in the ${}^1S_0$ channel. The phase shifts of the NN scattering in the ${}^1S_0$ channel are shown in Fig. 2.19 in comparison with experimental data.

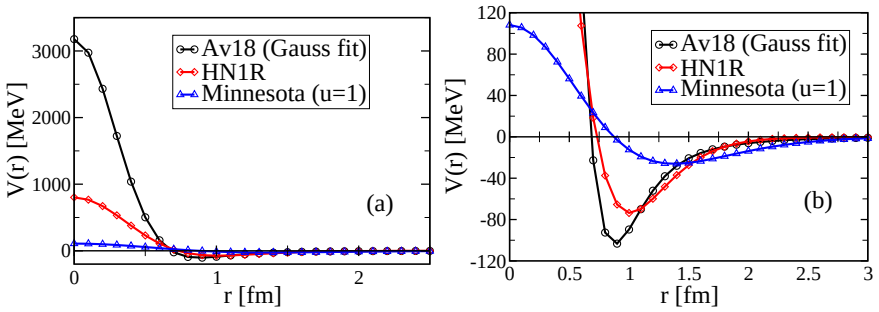

Figure 2.18: (Color online) (a): Coordinate space NN potentials in the ${}^1S_0$ channel. (b): Detail of the lower part of the panel (a).

We take the real part of the DN potential for the energy variation, and the imaginary part will be used to estimate the mesonic decay width. The energy dependence of the interaction was treated self-consistently in the study of $\bar{K}NN$ system [272]. In addition, the self-consistent treatment requires some assumption on the energy fraction of the DN pair in the three-body system, which cannot be determined unambiguously. In this study, therefore, we refrain from the self-consistent treatment of the energy of the DN subsystem and set the strength of the potential at the energy of

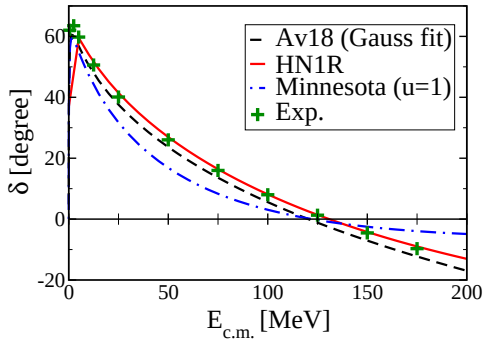

Figure 2.19: (Color online) NN phase shifts in the ${}^1S_0$ channel calculated by the NN potentials.

the Λ_c^* resonance:

$$\text{Re } v_{DN}(r=0; W=M_{\Lambda_c^*}) = \begin{cases} -1336 \text{ MeV} & (I=0) \\ -343 \text{ MeV} & (I=1) \end{cases}, \tag{2.24}$$

with $M_{\Lambda_c^*} = 2597.1$ MeV. In this case, the $M_{\Lambda_c^*}$ in $I=0$ channel is correctly reproduced, while the $I=1$ resonance disappears, because the strength of the DN potential (2.10) reduces at the lower energy region as seen in Fig. 2.11.

It is useful to introduce one- and two-body densities in order to extract the spatial structure of the DNN bound state. We first define the one-body densities as

$$\begin{aligned} \rho_N(r) =& \langle\, \Psi \,|\, \sum_{i=1,2} \delta^3(|\boldsymbol{r}_i - \boldsymbol{R}_G| - r) |\, \Psi \,\rangle, \\ \rho_D(r) =& \langle\, \Psi \,|\delta^3(|\boldsymbol{r}_D - \boldsymbol{R}_G| - r) |\, \Psi \,\rangle, \\ \rho_T(r) =& \rho_N(r) + \rho_D(r), \end{aligned}$$

where $\boldsymbol{R}_G$ is the center-of-mass coordinate of the three-body system. We also define the two-body correlation densities as

$$\begin{aligned} \rho_{NN}(x) =& \langle\, \Psi \,|\delta^3(|\boldsymbol{r}_1 - \boldsymbol{r}_2| - x) |\, \Psi \,\rangle, \\ \rho_{DN}(x) =& \langle\, \Psi \,|\, \sum_{i=1,2} \delta^3(|\boldsymbol{r}_D - \boldsymbol{r}_i| - x) |\, \Psi \,\rangle, \end{aligned}$$

which stand for the probabilities of finding NN or DN pair at relative distance x.

In this setup, since the imaginary part of the DN potential is not included, the Λ_c^* appears as a stable bound state. Thus, in the variational approach, the DNN three-body bound state can be found in the energy region below the $\Lambda_c^* N$ threshold $\sqrt{s} \sim 3536$ MeV. If the three-body (quasi-)bound state exists above the $\Lambda_c^* N$ threshold, the variational calculation will find the $\Lambda_c^* N$ two-body scattering state as the ground state of the three-body system.

A three-body bound state above the $\pi\Lambda_c N$ threshold $\sqrt{s} \sim 3363$ MeV has a mesonic decay width. The three-body decay width can be estimated by the matrix element of the imaginary part of the DN potential as

$$\Gamma_{\pi Y_c N} = -2\langle \Psi | \mathrm{Im}\ \hat{V}_{DN} | \Psi \rangle,$$

where $|\Psi\rangle$ is the obtained wave function of the ground state. As seen in Fig. 2.11, the imaginary part of the DN potential is much smaller than the real part.

2.2.5 Results with the FCA approach

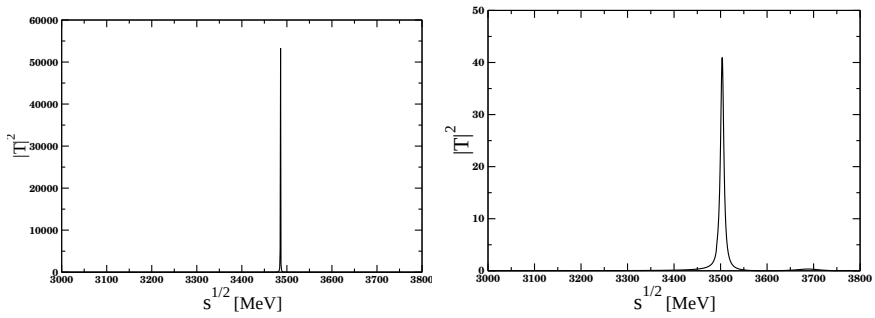

Figure 2.20: Modulus squared of the three-body scattering amplitude for $I = 1/2$ and $J = 0$ (left), $J = 1$ (right) with reduced size of the NN radius.

We first study the quasi-bound state found in the FCA calculation. In Figs. 2.20 we show the results for $|T|^2$ as functions of the total energy $\sqrt{s}$

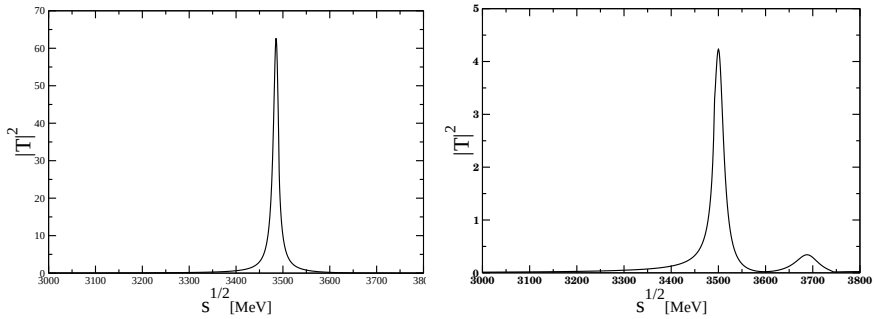

Figure 2.21: Modulus squared of the three-body scattering amplitude for $I = 1/2$ and $J = 0$ (left), $J = 1$ (right) with reduced NN radius (with $\delta\tilde{G}$).

assuming the NN system to have reduced size. Both for $I_{NN} = 0$, $I_{NN} = 1(J = 1,\ J = 0)$, we obtain a neat peak. The resonance energy for $J = 0$ is about 3486 MeV and the width is extremely small. In the case of $J = 1$ we have a smaller binding and the energy is about 3500 MeV, with a width of around 9 MeV. We should note that the binding is similar for both the spin channels.

Next we include $\delta\tilde{g}$ to account for absorption and plot $|T|^2$ for the DNN system in Figs. 2.21 for $J = 0$ ($I_{NN} = 1$) and $J = 1$ ($I_{NN} = 0$). The difference of the peak position by the absorption effect is only a few MeV (2-4 MeV) which is certainly within our uncertainties. The novelty, which is welcome, is that $|T|^2$ has become now wider and acquires a width of about 20-25 MeV. We are now in a position to compare the strength of these two amplitudes and we see that in the case of $J = 0$ the strength of $|T|^2$ at the peak is about a factor 15 larger than that for $J = 1$. This means that the state that we find at $J = 1$ should be more difficult to see, or alternatively we should see the small strength as an indication that this state is more uncertain in our approximation, as should be the smaller shoulder that one can see at higher energies for $J = 1$ in Fig. 2.21 (right).

2.2.6 Results with the variational approach

Now we investigate the same system in the variational approach. We first adopt HN1R potential for the nuclear force. As a result of the variational

calculation, we have found that the total spin $J = 1$ system ($I_{NN} = 0$) is unbound with respect to the $\Lambda_c^* N$ threshold. A bound state of the spin $J = 0$ system ($I_{NN} = 1$) is found at $B \sim 225$ MeV measured from the DNN threshold (~ 3745 MeV). This corresponds to the total energy of the three-body system as $M_B \sim 3520$ MeV. We also examine the Minnesota force and Av18 potential. The results are summarized in Table 2.1, together with the contributions from the individual terms in Eq. (2.23).

Table 2.1: Results of the energy compositions in the variational calculation for the ground state of the DNN system with total isospin $I = 1/2$ (range parameter $a_s = 0.4$ fm). Terms "bound" and "unbound" are defined with respect to the $\Lambda_c^* N$ threshold. All the numbers are given in MeV.

	HN1R		Minnesota	Av18
	$J = 1$	$J = 0$	$J = 0$	$J = 0$
	unbound	bound	bound	bound
B	208	225	251	209
M_B	3537	3520	3494	3536
$\Gamma_{\pi Y_c N}$	-	26	38	22
$E_{\rm kin}$	338	352	438	335
$V(NN)$	0	-2	19	-5
$V(DN)$	-546	-575	-708	-540
$T_{\rm nuc}$	113	126	162	117
E_{NN}	113	124	181	113
P(Odd)	75.0 %	14.4 %	7.4 %	18.9 %

As seen in the Table 2.1, the DNN system in the $J = 0$ channel is bound below the $\Lambda_c^* N$ threshold ($B \sim 209$ MeV) for all the NN potentials employed. A large kinetic energy of the deeply bound system is overcome by the strong attraction of the DN potential, while the NN potential adds a small correction. Comparing the results with three different nuclear forces, we find that the binding energy is smaller when the NN potential has a harder repulsive core (see the potential in Fig. 2.18).

In the $J = 1$ channel, the ground state energy is obtained slightly above

the $\Lambda_c^* N$ threshold. The fact that the $J = 1$ channel is unbound is confirmed by changing the parameter μ in the trial wave function, which controls the size of the total system [272]. We also examine the $J = 1$ channel with the Minnesota force. Although the repulsive core is soft in this case, no bound $\Lambda_c^* N$ is found.

Using the imaginary part of the DN potential, we evaluate the mesonic decay width of the quasi-bound state in the $J = 0$ channel, $\Gamma_{\pi Y_c N}$. The results are 20-40 MeV as shown in Table 2.1. This corresponds to the result of FCA without the D absorption, where the width is less than 10 MeV. Note, however, that in the variational approach we have evaluated the width perturbatively, while in the FCA the evaluation is done nonperturbatively. In this sense, $\Gamma_{\pi Y_c N}$ obtained in the variational approach can only be regarded as an estimation of the mesonic decay width.

2.2.7 Structure of the DNN quasi-bound state

To further investigate the structure of the DNN systems, we calculate the expectation values at various distances of the obtained wave function. The results of the root-mean-square radii and the relative distances are shown in Table 2.2. Except for the Av18 case where the wave function spreads due to the weaker binding, the size of the DNN bound state in the $J = 0$ channel is smaller than that of the $\bar{K}NN$ system, in which the NN and $\bar{K}N$ distances are $R_{NN} \sim 2.2$ fm and $R_{\bar{K}N} \sim 1.9$ fm. It is, on the other hand, acceptable to use the reduced size of Eq. (2.15) for the NN distribution in the FCA calculation, given the uncertainty that arises from the choice of the NN interaction. The large relative distances in the $J = 1$ channel also reflect the nature of the scattering state in this channel.

In view of the different values of R_{NN} obtained from the use of different NN potentials (see Table 2.2) and the different binding obtained in each case (see Table 2.1), we redo the calculations in the FCA changing the NN form factor of Eq. (2.15). We find a change in the binding from $R_{NN} = 2.62$ fm to 1.55 fm of 10 MeV (more bound) versus 16 MeV in Table 2.1. In the case of R_{NN} from $R_{NN} = 2.62$ fm to 1.03 fm the change is 28 MeV (more bound) versus 42 MeV in Table 2.1. The effects of the binding go in the same direction in both cases and they also agree in absolute value at the qualitative level.

In Fig. 2.22, we show the one-body densities of the nucleon and D meson

Table 2.2: Structure of the DNN ground state (range parameter $a_s = 0.4$ fm). $\sqrt{\langle r^2\rangle_T}$, $\sqrt{\langle r^2\rangle_D}$ and $\sqrt{\langle r^2\rangle_N}$ mean the root-mean-square radius of the distribution of total system, nucleons and D meson, respectively. R_{NN} (R_{DN}) is the mean distance between two nucleons (D meson and a nucleon) in the DNN. $R_{DN}(I)$ is the mean distance of a DN component with isospin I. All the numbers are given in fm.

	HN1R		Minnesota	Av18
	$J=1$	$J=0$	$J=0$	$J=0$
$\sqrt{\langle r^2\rangle_T}$	4.81	0.75	0.50	1.26
$\sqrt{\langle r^2\rangle_N}$	5.61	0.88	0.59	1.47
$\sqrt{\langle r^2\rangle_D}$	2.52	0.41	0.28	0.67
R_{NN}	10.04	1.55	1.03	2.62
R_{DN}	7.11	1.12	0.76	1.87
$R_{DN}(I=0)$	4.52	0.83	0.62	1.28
$R_{DN}(I=1)$	10.03	1.57	1.03	2.65

of the quasi-bound state with the HN1R potential. It is clear that the D meson distributes more compactly than the nucleons. This result indicates a schematic picture where the D meson sits at the center and nucleons circulate around it.

It is instructive to look at the DN correlation in more detail. In Fig. 2.23, we show the DN two-body correlation density as well as its isospin decomposition. It is seen that the $I = 0$ component distributes more compactly than the $I = 1$ component, which reflects the strength of the attraction in each channel [see Eq. (2.24)]. Moreover, the $I = 0$ component is similar to the distribution of the relative distance of the DN two-body bound state $\rho_{\Lambda_c^*}(r)$. This indicates that the structure of the Λ_c^* is maintained even in the three-body system. This feature has also been found in the $\bar{K}NN$ system [272, 318].

As in the case of the $\bar{K}NN$ system, the survival of the Λ_c^* in the three-body system opens the possibility of the "Λ_c^*-hypernuclei", in which the Λ_c^* is treated as an effective degree of freedom [319, 320]. In fact, this picture is

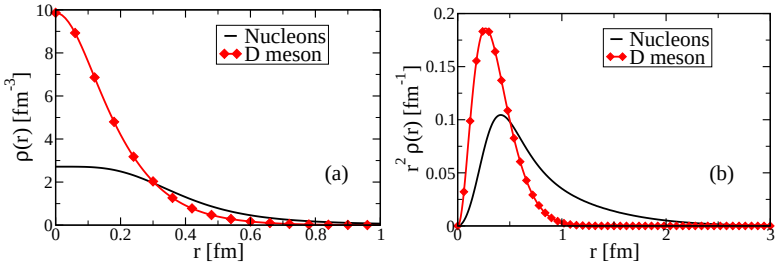

Figure 2.22: (Color online) (a): One-body densities $\rho_N(r)$ and $\rho_D(r)$ in the $J = 0$ channel with HN1R potential. (b): the same plot of the densities multiplied by r^2.

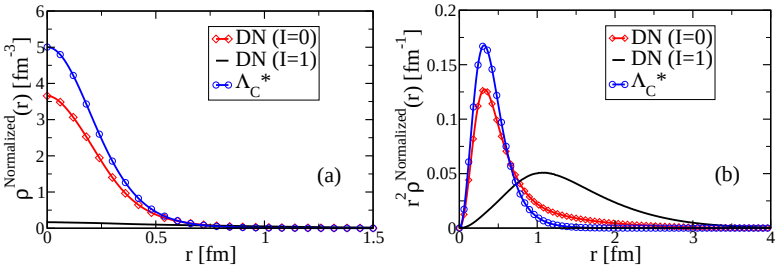

Figure 2.23: (Color online) (a): Normalized DN two-body correlation density $\rho_{DN}(r)$ with isospin decomposition. The $I = 0$ DN bound state (Λ_c^*) correlation density is also shown for comparison. (b): the same plot of the densities multiplied by r^2.

more suitable in the charm sector, since the width of the Λ_c^* is smaller than that of the Λ^*, so the effect of the imaginary part in the calculation should be smaller. Note also that the binding of the DN system is as large as 200 MeV, while the binding of the $\Lambda_c^* N$ is much smaller, especially for the case of the realistic Av18 potential.

We have examined theoretical uncertainties in the construction of the potential. The range parameter of the DN potential a_s is introduced in Eq. (2.10) and chosen to be 0.4 fm. When we adopt $a_s = 0.35$ fm, the binding energy changes by a few MeV, and the size changes less than 0.1 fm. The Minnesota potential has a parameter u which controls the strength of the NN odd force [316]. The effect of the slight inclusion of the odd force

($u = 0.95$) turns out to be very small, less than 1 MeV. We thus conclude that these uncertainties are much smaller than the dependence on the choice of the NN potential. The variation of the values in Tables 2.1 and 2.2 can be regarded as the theoretical uncertainties in the present calculation.

2.2.8 Discussions

- Comparison of two approaches

  We have presented the results of two approaches, the Faddeev FCA calculation and the variational calculation. In the total spin $J = 0$ channel, both approaches find a quasi-bound state around 3500 MeV which is below the $\Lambda_c^* N$ threshold. The assumed NN distribution in the FCA turns out to be similar to that found in the variational calculation by minimizing the total energy. It is therefore reasonable to conclude that these approaches find the same quasi-bound state.

  The spin $J = 1$ channel, on the other hand, has differences in the two approaches. The lowest-energy state obtained in the variational calculation is a $\Lambda_c^* N$ scattering state, while a narrow peak is found in the FCA amplitude below the $\Lambda_c^* N$ threshold, although the signal strength is not so significant as the $J = 0$ case. A major reason of this discrepancy may be traced back to the DN interaction in the isospin $I = 1$ channel. The difference of the results in the two approaches also stems from the odd component of the NN state, which is included only in the variational calculation. In addition, we should also remember that the two approaches employ different approximations.

- Comparison with $\bar{K}NN$ results

  It is instructive to compare the DNN quasi-bound state with the corresponding $\bar{K}NN$ state in Ref. [272]. In both cases, we obtain a quasi-bound state, but the DNN system has a larger binding energy and a narrower width. This is in parallel with the properties of the DN and $\bar{K}N$ two-body quasi-bound states, and they are closely related through the DN and $\bar{K}N$ interactions.

  The D meson can be more strongly bound in a nucleus than $\bar{K}$ meson by two reasons: the coupling itself is stronger, and, the heavier mass of the D meson is advantageous to increase the binding. So,

we can consider two hypothetical variants between the DNN system ($B \sim 230$ MeV) and $\bar{K}NN$ system ($B \sim 30$ MeV)[1]; case I: kinematics of the DNN system with the $\bar{K}N$ potential ($m = m_D, V = V_{\bar{K}}$), and case II: kinematics of the $\bar{K}NN$ system with the DN potential ($m = m_{\bar{K}}, V = V_D$). The result of the variational calculation shows that $B \sim 40$ MeV for case I and $B \sim 190$ MeV for case II. As summarized in Table 2.3, the suppression of the kinetic energy by the heavy D mass is more important for the strong binding of the DNN system. One should note that in the present case, the strength of the two-body interaction is fixed at the energy of the two-body quasi-bound state. Since the DN two-body bound state locates 200 MeV below the DN threshold, the strength of the potential is reduced, as seen in Fig. 2.10. Thus, in the present prescription, the attractive strength of the DN potential is not very much different from the $\bar{K}N$ one, and the result of case I does not very much deviate from the $\bar{K}NN$ quasi-bound state. The narrow width of the DNN system is a consequence of the narrow width of the $\Lambda_c^*(2595)$.

Table 2.3: Binding energies of the three-body bound state in $J = 0$ channel measured from the three-body threshold with different meson mass and different meson-nucleon potential.

	$m = m_{\bar{K}}$	$m = m_D$
$V = V_{\bar{K}}$	~ 30 MeV	~ 190 MeV
$V = V_D$	~ 40 MeV	~ 230 MeV

2.2.9 Possible experiments to produce the DNN state

The very narrow width of the DNN system is qualitatively different to the $\bar{K}NN$ one where the width was so large as to make its experimental observation practically unfeasible. In the present case there is a clear situation and there are no problems in principle for the observation of the state.

[1]Here we also set the strength of the $\bar{K}N$ potential at the energy of the Λ^* for comparison with the DNN calculation.

In the FCA calculation, we observe that the two-nucleon absorption width is larger than the three-body decay width. This indicates that the DNN quasi-bound state can be more easily seen in the two-baryon final states such as $\Lambda_c N$. The findings of the present work should stimulate efforts to find suitable reactions where this state could be found.

As a suggestion in this direction we can think of the $\bar{p}\ ^3\mathrm{He} \to \bar{D}^0 D^0 pn \to \bar{D}^0[DNN]$ reaction, which could be done by FAIR at GSI. With a $\bar{p}$ beam of 15 GeV/c there is plenty of energy available for this reaction and the momentum mismatch of the D^0 with the spectator nucleons of the ^{3}He can be of the order of 550 MeV/c, equivalent to an energy of 80 MeV for the D, small compared with the scale of the binding ($\gtrsim$ 200 MeV). With an estimate of $\sigma \simeq 10 - 20$ nb for $\bar{p}p \to \bar{D}^0 D^0$ production [321, 322] one would expect several thousand events per day for the background of the proposed reaction [323]. A narrow peak could be visible on top of this background corresponding to the DNN bound state formation.

Another possibility is the high-energy π induced reaction. An analogous reaction is $\pi^- d \to D^- D^+ np \to D^-[DNN]$ where the relevant elementary process is $\pi^- N \to D^+ D^- N$. Since the DN pair in the DNN system is strongly clustering as the Λ_c^*, the reaction $\pi^- d \to D^- \Lambda_c^* n \to D^-[DNN]$ is also another candidate. The elementary reaction $\pi^- p \to D^- \Lambda_c^*$ is relevant in this case. Such reactions may be realized in the high-momentum beamline project at J-PARC.

A different strategy is to look for the formation of the quasi-bound state in the heavy ion collisions. It has been shown that the hadronic molecular states with charm quark are abundantly produced at RHIC and LHC [324, 325]. Although a deeply bound DNN state has smaller production yield, it can also be produced *via* coalescence of the $\Lambda_c^* N$ with much smaller binding. A peak structure of the DNN state may be seen, for instance, in the invariant mass spectrum of the $\Lambda_c \pi^- p$ or $\Lambda_c p$ final state.

2.2.10 Conclusions

We have used two methods to investigate the DNN system with $I = 1/2$. Both the FCA for the Faddeev equations and the second one employs the variational approach with hadronic potentials in coordinate space, have found that the system is bound and rather stable, with a width of about 20-40 MeV. In both cases, we have found a bound state with an energy around

3500 MeV in the $J = 0$ channel. This corresponds to 250 MeV binding from the DNN threshold. The $J = 1$ channel is more subtle, and the precise DN amplitude in the $I = 1$ channel is important for a robust prediction in this channel. The mesonic decay width of the quasi-bound state turned out to be less than 40 MeV.

The small width of the DNN quasi-bound state is advantageous for the experimental identification. The search for the DNN quasi-bound state can be done by $\bar{p}$ induced reaction at FAIR, π^- induced reaction at J-PARC, and relativistic heavy ion collisions at RHIC and LHC.

2.3 A study of D^*-multi-ρ states

One of the important aims in the study of the strong interaction is to understand the nature and structure of hadronic resonances. The search for new resonances is another goal both in theories and experiments. At low energy, using the input of chiral Lagrangians [151–154, 173] and implementing unitarity in coupled channels, one develops a theoretical tool, chiral unitarity theory, which explains the two-body interaction very successfully [16, 18, 19, 155, 190, 194, 195, 260, 277, 326–328]. For the three-body interaction, the pioneer work of Ref. [212] combined Faddeev equations and chiral dynamics and reported several S-wave $J^P = \frac{1}{2}^+$ resonances which qualify as two mesons-one baryon molecular states. Furthermore, the FCA [208, 219–221] to Faddeev equations for multi-$\rho(770)$ states, was given in Ref. [223], in which the resonances $f_2(1270)$, $\rho_3(1690)(3^{--})$, $f_4(2050)(4^{++})$, $\rho_5(2350)(5^{--})$, and $f_6(2510)(6^{++})$ were explained as basically molecules of an increasing number of $\rho(770)$ particles with parallel spins. Similarly, it was also found in Ref. [224] that the resonances $K_2^*(1430)$, $K_3^*(1780)$, $K_4^*(2045)$, $K_5^*(2380)$ and a new K_6^* could be understood as molecules made of an increasing number of $\rho(770)$ and one $K^*(892)$ meson.

Using effective Lagrangians of the LHG theory [156, 159, 163, 329] of the subsection 1.2.2, the $\rho\rho$ interaction was studied in Ref. [330] with on-shell factorized BS equations. It was found that the $\rho\rho$ interaction was attractive in the isospin zero, spin 0 and 2 channels, particularly in the tensor channel where it led to the formation of a $\rho\rho$ quasibound state or molecule that could be associated to the $f_2(1270)$ ($I(J^{PC}) = 0(2^{++})$). With the same formalism, the composite systems of light (ρ and ω) and heavy (D^*) vector mesons were studied in Ref. [331]. In that work, a strong attraction was found in the isospin, spin channels $(I, S) = (1/2, 0), (1/2, 1)$ and $(1/2, 2)$, with positive parity, leading to bound $\rho(\omega)D^*$ states, one of them identified as the $D_2^*(2460)$ ($I(J^P) = \frac{1}{2}(1^-)$). Therefore, the resonance $D_2^*(2460)$ was generated as a ρD^* quasibound state or molecule by the strong and attractive ρD^* interaction. As discussed in Ref. [223], because of the large binding energy per ρ meson in spin 2, it is possible to obtain bound systems with several ρ mesons as building blocks. As mentioned in Ref. [331], the ρD^* interaction is also very strong and can bind the system.

Therefore, in our present work, based on the two-body interaction results

of Refs. [330, 331], we follow the main ideas of Refs. [223, 224] to search D^*-multi-ρ resonances in the charm sector. Thus, the main aim in the present work is, first, to study the three-body interaction of D^* and two ρ mesons, for which we have two options, the clusters $D^* - f_2(1270)(\rho\rho)$ and $\rho - D_2^*(2460)(\rho D^*)$, in order to see if there are some resonance structures in the scattering amplitudes. If this is the case, one can predict a not-yet-discovered D_3^* resonance, and we could continue our study extending these ideas to include more ρ mesons as building blocks of the many-body system. Then we repeat the test in the four-body system and so forth, which is analogous to the K^*-multi-ρ systems [224].

The D^*-multi-ρ interactions that we investigate in the present work are listed in Table 2.4, and are explained as follows. First, we need to investigate the two-body interaction to look for a bound state as the cluster of the FCA, which will be studied in the next subsection, the $\rho\rho$ and ρD^* interactions. For the three-body interaction, we have two options: particle $3 = D^*$, cluster or resonance $R = f_2$ (particle $1 = \rho,\ 2 = \rho$) and $3 = \rho$, $R = D_2^*$ $(1 = \rho,\ 2 = D^*)$. For four-body, we also have two cases: $3 = f_2$, $R = D_2^*$ $(1 = \rho,\ 2 = D^*)$ and $3 = D_2^*$, $R = f_2$ $(1 = \rho,\ 2 = \rho)$. For five-body, $3 = D^*$, $R = f_4$ $(1 = f_2,\ 2 = f_2)$ and $3 = \rho$, $R = D_4^*$ $(1 = f_2,\ 2 = D_2^*)$. For six-body, $3 = D_2^*$, $R = f_4$ $(1 = f_2,\ 2 = f_2)$ and $3 = f_2$, $R = D_4^*$ $(1 = f_2,\ 2 = D_2^*)$. We describe all these cases in detail below (more details can be referred to our paper [332]).

Table 2.4: The cases considered in the D^*-multi-ρ interactions.

particles:	3	R (1,2)	amplitudes
Two-body	ρ	D^*	$t_{\rho D^*}$
	ρ	ρ	$t_{\rho\rho}$
Three-body	D^*	$f_2\ (\rho\rho)$	$T_{D^*-f_2}$
	ρ	$D_2^*\ (\rho D^*)$	$T_{\rho-D_2^*}$
Four-body	D_2^*	$f_2\ (\rho\rho)$	$T_{D_2^*-f_2}$
	f_2	$D_2^*\ (\rho D^*)$	$T_{f_2-D_2^*}$
Five-body	D^*	$f_4\ (f_2 f_2)$	$T_{D^*-f_4}$
	ρ	$D_4^*\ (f_2 D_2^*)$	$T_{\rho-D_4^*}$
Six-body	D_2^*	$f_4\ (f_2 f_2)$	$T_{D_2^*-f_4}$
	f_2	$D_4^*\ (f_2 D_2^*)$	$T_{f_2-D_4^*}$

2.3.1 $\rho\rho$ and ρD^* two-body interactions

To evaluate the Faddeev equations under the FCA (seen in the formalism in subsection 1.4.2), we need to search the cluster of the FCA, and input the two-body scattering amplitudes, corresponding to the third particle colliding with the two components of the cluster. Thus the starting point of our work is the two-body $\rho\rho$ and ρD^* interactions, which were studied in Refs. [330] and [331] with the LHG formalism [156,159,163,329] (seen in the discussions in subsection 1.2.2) and the unitary coupled channels method [16,18,19,155, 190,194,195,260,277,326–328] (seen in the discussions in subsection 1.3.1). We briefly summarize the model of Refs. [330] and [331] here to explain how to obtain the unitarized $\rho\rho$ and ρD^* scattering amplitudes, evaluating the $\rho\rho$ and ρD^* scattering amplitudes with the coupled channels unitary approach, the BS equation in coupled channels, seen in subsection 1.3.1. The details can be seen in Refs. [330, 331].

To construct the three-body system we start from the clusters $f_2(1270)$ ($I(J^{PC}) = 0(2^{++})$) and $D_2^*(2460)$ ($I(J^P) = \frac{1}{2}(1^-)$) and add to them a D^* or a ρ respectively. The new particles are introduced with their spins aligned with that of the cluster such that the total spin adds one unity. Thus we only need to take into account the potential of spin $S = 2$ for $\rho\rho$ and ρD^* interactions,

$$
\begin{aligned}
V_{\rho\rho}^{(I=0,S=2)}(s) &= -4g^2 - 8g^2\Big(\frac{3s}{4m_\rho^2} - 1\Big), \\
V_{\rho\rho}^{(I=2,S=2)}(s) &= 2g^2 + 4g^2\Big(\frac{3s}{4m_\rho^2} - 1\Big), \\
V_{\rho D^*(11)}^{(I=1/2,S=2)}(s) &= -\frac{5}{2}g^2 - 2\frac{g^2}{m_\rho^2}(k_1+k_3)\cdot(k_2+k_4) - \frac{1}{2}\frac{\kappa g^2}{m_\rho^2}(k_1+k_4)\cdot(k_2+k_3), \\
V_{\rho D^*(12)}^{(I=1/2,S=2)}(s) &= \frac{\sqrt{3}}{2}g^2 + \frac{\sqrt{3}}{2}\frac{\kappa g^2}{m_\rho^2}(k_1+k_4)\cdot(k_2+k_3), \\
V_{\rho D^*(22)}^{(I=1/2,S=2)}(s) &= \frac{1}{2}g^2 + \frac{1}{2}\frac{\kappa g^2}{m_\rho^2}(k_1+k_4)\cdot(k_2+k_3), \\
V_{\rho D^*}^{(I=3/2,S=2)}(s) &= 2g^2 + \frac{g^2}{m_\rho^2}(k_1+k_3)\cdot(k_2+k_4) + \frac{\kappa g^2}{m_\rho^2}(k_1+k_4)\cdot(k_2+k_3),
\end{aligned}
\tag{2.25}
$$

where $g = M_V/2f_\pi$, with M_V the vector meson mass and f_π the pion decay

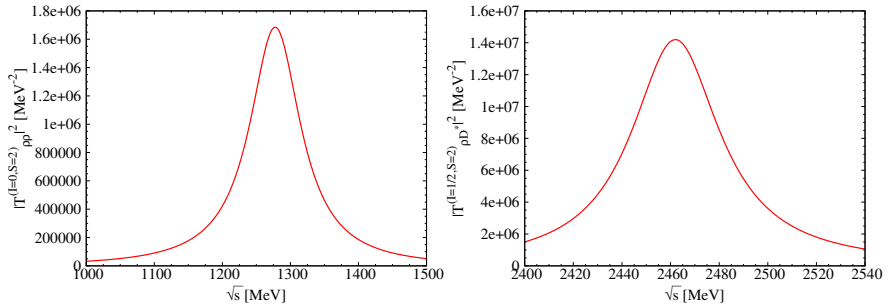

Figure 2.24: Modulus squared of the scattering amplitudes. Left: $|t^{I=0}_{\rho\rho}|^2$, $f_2(1270)$; Right: $|t^{I=1/2}_{\rho D^*}|^2$, $D^*_2(2460)$.

constant. In these equations k_i, $i = 1, 2, 3, 4$ are the initial, $(1, 2)$, and final $(3, 4)$ momenta of the particles. The quantity $\kappa = m_\rho^2/m_{D^*}^2$ appears because in some transitions one is exchanging a heavy vector instead of a light one. Note that in isospin $I = 1/2$ there are two coupled channels, 1 is ρD^* and 2 is ωD^*.

As mentioned in Refs. [330, 331], we also should take into account the contribution of the box diagram with two pseudoscalar mesons in the intermediate state. We only add the imaginary part of the box diagram contribution to the potential V, which is not accounted for by the coupled channels [127, 168], and neglect the real part which is very small. Note that we also take into account the ρ mass distribution by replacing the G function in the corresponding channel by its convoluted form, which is done by considering the mass distribution of the ρ mesons in the loop as done in Refs. [330, 331].

Finally, considering the box diagram contribution to the potential V and the convolution of the ρ mass distribution in the loop function G, we show the evaluated results of $\rho\rho$ and ρD^* scattering amplitudes in Fig. 2.24, which are consistent with Refs. [330, 331]. The structure of the resonances $f_2(1270)$ and $D^*_2(2460)$ are clear in the peak of the modulus squared of the amplitudes. The nonresonant amplitudes $t^{(I=0,S=2)}_{\rho\rho}$ and $t^{(I=3/2,S=2)}_{\rho D^*}$ are not shown here.

2.3.2 Three-body interaction

For three-body interaction, we have two options of structure: $D^* - f_2(\rho\rho)$ and $\rho - D_2^*(\rho D^*)$, which means $3 = D^*$, $R = f_2$ $(1 = \rho,\ 2 = \rho)$ and $3 = \rho$, $R = D_2^*$ $(1 = \rho,\ 2 = D^*)$. Thus, to evaluate these scattering amplitudes, we need as input the t_1 and t_2 amplitudes of the (3,1) and (3,2) systems, $t_1 = t_2 = t_{\rho D^*}$ for $D^* - f_2(\rho\rho)$ and $t_1 = t_{\rho\rho},\ t_2 = t_{\rho D^*}$ for $\rho - D_2^*(\rho D^*)$. We should calculate the two-body $\rho\rho$ and ρD^* amplitudes.

As mentioned before, the isospin structure of the cluster should be considered for the t_1 and t_2 amplitudes. For the case of $D^* - f_2(\rho\rho)$, the cluster of f_2 has isospin $I = 0$. Therefore the two ρ mesons are in an $I = 0$ state, and we have

$$|\rho\rho>^{(0,0)} = \frac{1}{\sqrt{3}}\Big(|(1,-1)> + |(-1,1)> - |(0,0)>\Big), \tag{2.26}$$

where $|(1,-1)>$ denote $|(I_z^1, I_z^2)>$ which shows the I_z components of particles 1 and 2, and $|\rho\rho>^{(0,0)}$ means $|\rho\rho>^{(I,I_z)}$. The third particle is a D^* meson taken $|I_z^3)> = |\frac{1}{2}>$. Then we obtain

$$t_1 = t_{\rho D^*} = \frac{1}{3}\big(2t_{31}^{I=3/2} + t_{31}^{I=1/2}\big), \quad t_2 = t_1. \tag{2.27}$$

But for the case of $\rho - D_2^*(\rho D^*)$, the situation is different. Because the isospins of ρ and D_2^* are $I_\rho = 1$ and $I_{D_2^*} = \frac{1}{2}$, the total isospin of the three-body system are $I_{total} \equiv I_{\rho\rho D^*} = \frac{1}{2}$ or $I_{total} \equiv I_{\rho\rho D^*} = \frac{3}{2}$, and then we have

$$\begin{aligned} |\rho D_2^*>^{(\frac{1}{2},\frac{1}{2})} &= |\rho\rho D^*>^{(\frac{1}{2},\frac{1}{2})} = \sqrt{\frac{2}{3}}|(1,-\frac{1}{2})> - \sqrt{\frac{1}{3}}|(0,\frac{1}{2})>, \\ |\rho D_2^*>^{(\frac{3}{2},\frac{1}{2})} &= |\rho\rho D^*>^{(\frac{3}{2},\frac{1}{2})} = \sqrt{\frac{1}{3}}|(1,-\frac{1}{2})> + \sqrt{\frac{2}{3}}|(0,\frac{1}{2})>, \end{aligned} \tag{2.28}$$

where we have taken $I_z = \frac{1}{2}$ for convenience. Therefore the $|\rho D^*>$ states inside the D_2^* for the $I_z = -\frac{1}{2}$ and $I_z = +\frac{1}{2}$ are given by

$$\begin{aligned} |\rho D^*>^{(\frac{1}{2},-\frac{1}{2})} &= \sqrt{\frac{1}{3}}|(0,-\frac{1}{2})> - \sqrt{\frac{2}{3}}|(-1,\frac{1}{2})>, \\ |\rho D^*>^{(\frac{1}{2},\frac{1}{2})} &= \sqrt{\frac{2}{3}}|(1,-\frac{1}{2})> - \sqrt{\frac{1}{3}}|(0,\frac{1}{2})>. \end{aligned} \tag{2.29}$$

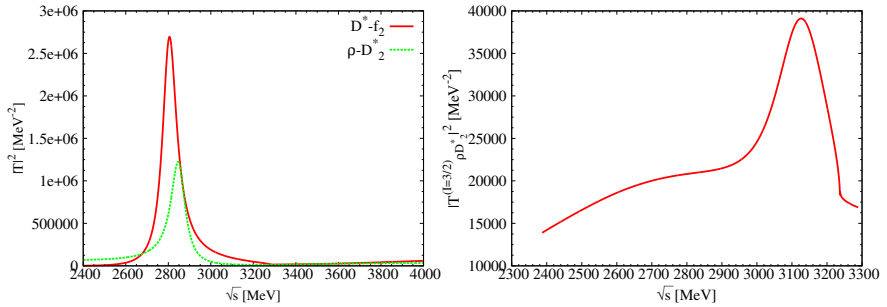

Figure 2.25: Modulus squared of the T_{D^*-f2} and $T_{\rho-D_2^*}$ scattering amplitudes. Left: $I_{total} = \frac{1}{2}$; Right: $I_{total} = \frac{3}{2}$.

For the two possibilities, combining Eqs. (2.28) and (2.29), we obtain

$$\begin{aligned} T^{(I=1/2)}_{\rho-D_2^*}: \quad & t_1 = t_{\rho\rho} = \frac{2}{3} t^{(I=0)}_{31}, \quad t_2 = t_{\rho D^*} = \frac{1}{9}\left(8 t^{I=3/2}_{32} + t^{I=1/2}_{32}\right); \\ T^{(I=3/2)}_{\rho-D_2^*}: \quad & t_1 = t_{\rho\rho} = \frac{5}{6} t^{(I=2)}_{31}, \quad t_2 = t_{\rho D^*} = \frac{1}{9}\left(5 t^{I=3/2}_{32} + 4 t^{I=1/2}_{32}\right). \end{aligned} \tag{2.30}$$

We show our results in Fig. 2.25. In Fig. 2.25 (left) we show the modulus squared of the amplitudes for $|T^{I=1/2}_{D^*-f_2}|^2$ and $|T^{I=1/2}_{\rho-D_2^*}|^2$, and we find that there are clear peaks around the energy $2800-2850$ MeV which is about 400 MeV lower than the $D^* - f_2$ threshold. The bindings are large because they scale with the mass of the mesons and we have now a D^* interacting with two ρ mesons. The strength of the peak of $|T^{I=1/2}_{D^*-f_2}|^2$ is two times bigger than for $|T^{I=1/2}_{\rho-D_2^*}|^2$, and we see that the $D^* - f_2$ component is a bit more bound than the $\rho - D_2^*$ one. We expect that a real state would be an admixture of both with a binding in between that of the individual components. In Fig. 2.25 (right) we show $|T^{I=3/2}_{\rho-D_2^*}|^2$, and there is a clear resonant structure about 3120 MeV, the strength of which is 30 times smaller than that of $|T^{I=1/2}_{\rho-D_2^*}|^2$ in the left figure and less bound. We are concerned with the lowest lying states and hence we concentrate on the predicted new D_3^* state with a structure formed by a mixture of $D^* - f_2$ and $\rho - D_2^*$, with a mass about $2800 - 2850$ MeV and a width about $60 - 100$ MeV.

2.3.3 Four-body interaction

There are also two possibilities in the four-body interaction as we have shown in Table 2.4: particle $3 = f_2$, $R = D_2^*$ ($1 = \rho$, $2 = D^*$) or particle $3 = D_2^*$, $R = f_2$ ($1 = \rho$, $2 = \rho$). Because $I_{f_2} = 0$ and $I_{D_2^*} = \frac{1}{2}$, the total isospin of the four-body system is only $I_{total} = \frac{1}{2}$. In the first case, f_2 collides with the D_2^*, the amplitude $t_1 = t_{f_2\rho} = T_{\rho - f_2}$ has been evaluated in Ref. [223] and is reproduced in our work, and $t_2 = t_{f_2 D^*} = T_{D^* - f_2}$, which has been evaluated in the former subsection 2.3.2. For the second case, D_2^* collides with the f_2, and the amplitudes $t_1 = t_2 = t_{D_2^*\rho} = T_{\rho - D_2^*}$ have been evaluated in the former subsection 2.3.2. We must now consider that the three-body amplitude $T_{\rho - D_2^*}$ is also combined with different isospins as mentioned in subsection 2.3.2. This situation is similar to the case when the D^* collides with the f_2, because the isospins of both the D_2^* and D^* are $I = \frac{1}{2}$, thus from Eq. (2.27) we have

$$t_1 = T_{\rho D_2^*} = \frac{1}{3}\big(2T_{31}^{I=3/2} + T_{31}^{I=1/2}\big), \quad t_2 = t_1. \tag{2.31}$$

The results are shown in Fig. 2.26. The left of Fig. 2.26 is $|T_{D_2^* - f_2}^{I=1/2}|^2$. We find that there is a clear peak at an energy of 3200 MeV, the width of which is about 200 MeV. The right plot of Fig. 2.26 shows $|T_{f_2 - D_2^*}^{I=1/2}|^2$ and there is a resonant peak around the energy 3075 MeV with a large width of nearly 400 MeV. The strength of the peak of $|T_{f_2 - D_2^*}^{I=1/2}|^2$ is about two times bigger than the one of $|T_{D_2^* - f_2}^{I=1/2}|^2$ and the energy of the peak is more bound too. But from the former results, subsection 2.3.2, we found that $|T_{D_2^* - f_2}^{I=1/2}|^2$ has more strength and is more bound than $|T_{f_2 - D_2^*}^{I=1/2}|^2$. We have investigated that this occurs because of the contribution of $|T_{\rho - D_2^*}^{I=3/2}|^2$, even though the strength of $|T_{\rho - D_2^*}^{I=3/2}|^2$ is much smaller and less bound than the one of $|T_{\rho - D_2^*}^{I=1/2}|^2$ from the former results. When we removed the contribution of $|T_{\rho - D_2^*}^{I=3/2}|^2$ in Eq. (2.31), the strength of the peak was enhanced by a factor five and was more bound. Therefore, within the uncertainty of the theory, we find a new D_4^* resonance, of a mass about $3075 - 3200$ MeV and a width about $200 - 400$ MeV.

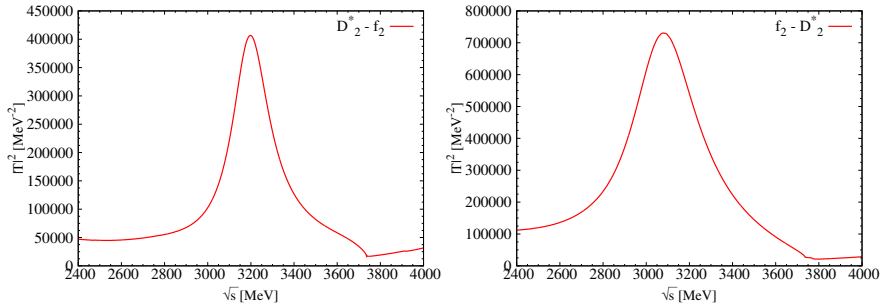

Figure 2.26: Modulus squared of the $T_{D_2^*-f2}$ (left) and $T_{f_2-D_2^*}$ (right) scattering amplitudes.

2.3.4 Five-body interaction

For the five-body interaction, we also have two options for the cluster, one of which is the particle f_4 studied in Ref. [223] and the other one the resonance D_4^* obtained in the four-body interaction, subsection 2.3.3. Thus letting the third particle (D^* or ρ) collide with them, we have $3 = D^*$, $R = f_4$ ($1 = f_2$, $2 = f_2$) or $3 = \rho$, $R = D_4^*$ ($1 = f_2$, $2 = D_2^*$). Because the isospin $I_{f_4} = 0$ and $I_{D_4^*} = \frac{1}{2}$, the total isospin of the five-body system is only $I_{total} = \frac{1}{2}$ in the $D^* - f_4$ structure, but $I_{total} = \frac{1}{2}$ or $I_{total} = \frac{3}{2}$ in the $\rho - D_4^*$ structure. Thus the situation is similar to the three-body interaction discussed before, D^* (or ρ) collide with f_2 (or D_2^*). Therefore in the first case, the D^* collides with the f_4, and the amplitudes $t_1 = t_2 = t_{D^* f_2} = T^{(I=1/2)}_{D^*-f_2}$ have been evaluated in subsection 2.3.2. For the second case, the ρ collides with the D_4^*, which is similar to $\rho - D_2^*$ in the three-body interaction, thus, we have

$$\begin{aligned} T^{(I=1/2)}_{\rho-D_4^*}: \quad & t_1 = t_{\rho f_2} = T^{(I=1)}_{31}, \quad t_2 = t_{\rho D_2^*} = T^{I=1/2}_{32}; \\ T^{(I=3/2)}_{\rho-D_4^*}: \quad & t_1 = t_{\rho f_2} = T^{(I=1)}_{31}, \quad t_2 = t_{\rho D_2^*} = T^{I=3/2}_{32}, \end{aligned} \tag{2.32}$$

where the $T^{(I=1)}_{31}$ is the same as $T_{\rho-f_2}$ in the subsection 2.3.3 reproducing the results of Ref. [223], and $T^{I=1/2}_{\rho-D_2^*}$ and $T^{I=3/2}_{\rho-D_2^*}$ have also been evaluated in subsection 2.3.2.

In Fig. 2.27 we show our results. The left of Fig. 2.27 is $|T^{I=1/2}_{D^*-f_4}|^2$ and we observe a resonant peak around the energy 3375 MeV with a width of less

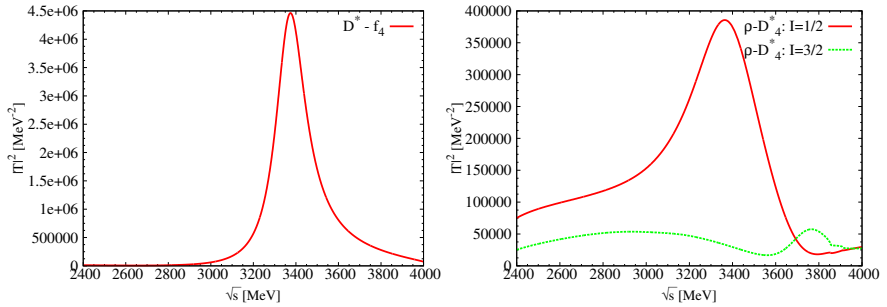

Figure 2.27: Modulus squared of the $T_{D^*-f_4}$ (left) and $T_{\rho-D_4^*}$ (right) scattering amplitudes.

than 200 MeV. The right plot of Fig. 2.27 is $|T^{I=1/2}_{\rho-D_4^*}|^2$ and $|T^{I=3/2}_{\rho-D_4^*}|^2$. We find that there is a resonant structure in $|T^{I=1/2}_{\rho-D_4^*}|^2$ at the energy 3360 MeV, the width of which is about 400 MeV, and the position is very close to the one of $|T^{I=1/2}_{D^*-f_4}|^2$. But the strength of $|T^{I=1/2}_{\rho-D_4^*}|^2$ is one order smaller than the one $|T^{I=1/2}_{D^*-f_4}|^2$. For $|T^{I=3/2}_{\rho-D_4^*}|^2$ there is no resonant structure. Therefore, within uncertainties, we also find a new D_5^* resonance, with a mass about $3360-3375$ MeV and a width about $200-400$ MeV.

2.3.5 Six-body interaction

Similarly to the five-body interaction, we also have two options of the cluster for the six-body interaction, the particle f_4 studied in Ref. [223] and the resonance D_4^* obtained in subsection 2.3.3. Now letting a resonance (D_2^* or f_2) be the third particle and collide with them, we have $3 = D_2^*$, $R = f_4$ ($1 = f_2$, $2 = f_2$) or $3 = f_2$, $R = D_4^*$ ($1 = f_2$, $2 = D_2^*$). Because $I_{f_2} = I_{f_4} = 0$ and $I_{D_2^*} = I_{D_4^*} = \frac{1}{2}$, the total isospin of the six-body system is only $I_{total} = \frac{1}{2}$. Thus, in the first case, the D_2^* collides with the f_4, the amplitudes $t_1 = t_2 = t_{D_2^* f_2} = T^{(I=1/2)}_{D_2^*-f_2}$ have been evaluated in subsection 2.3.3. For the second case, the f_2 collides with the D_4^*, the amplitudes $t_1 = t_{f_2 f_2} = T_{f_2-f_2}$ reproduce the results from Ref. [223], and $t_2 = t_{f_2 D_2^*} = T_{f_2-D_2^*}$ has been calculated in subsection 2.3.3.

Our results are shown in Fig. 2.28. The left plot of Fig. 2.28 is $|T^{I=1/2}_{D_2^*-f_4}|^2$

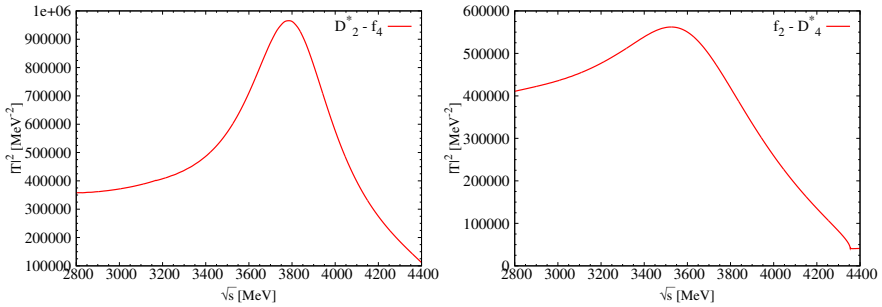

Figure 2.28: Modulus squared of the $T_{D_2^*-f_4}$ (left) and $T_{f_2-D_4^*}$ (right) scattering amplitudes.

where we see a peak around the energy 3775 MeV with a large width of nearly 400 MeV. The right of Fig. 2.28 is $|T^{I=1/2}_{f_2-D_4^*}|^2$, and there we find that there is not a clear peak at the energy 3550 MeV. It looks like the resonant structure of $f_2 - D_4^*$ is not as stable as the $D_2^* - f_4$ one. From these results, we could predict a new D_6^* resonance with more uncertainty, with a mass of about 3775 MeV and a width about 400 MeV.

2.3.6 Considering the width of the cluster

It should be stated that we have taken into account the width of the ρ in the evaluation of the amplitudes. This is done through the amplitudes $\tilde{t}_1$, $\tilde{t}_2$ which are the input in our T amplitude (see Eq. (1.74)). Let us take the three body cases of Table 2.4. In one of them we have $D^* - f_2(\rho\rho)$ scattering. In this case the $D^*\rho$ amplitude ($t_{\rho D^*}$) needed has been evaluated in [331] and the width of the ρ has been explicitly taken into account in the calculations by convoluting the the loop function of the $D^*\rho$ intermediate states in the scattering by the mass distribution of the ρ. However, the f_2 width is not explicitly considered. We can do so by replacing M_R in Eqs. (1.77), (1.78) by $M_R - i\frac{\Gamma_R}{2}$. The new results are compared with the old ones in Fig. 2.29. We can see that the effects are small and barely change the width of the peak. The fact that $F_R(q)$ is normalized to 1 at $q = 0$ minimizes the effect of this width.

For the second case we have $\rho - D_2^*(\rho D^*)$. In this case we implement the width of the D_2^* as before, but in addition we also add an imaginary part

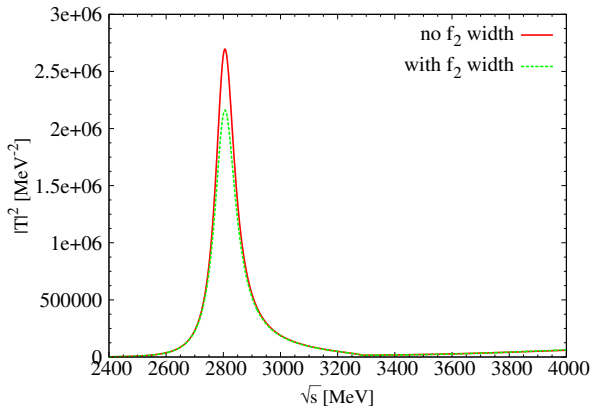

Figure 2.29: Comparison of $|T|^2$ for the $D^* - f_2(\rho\rho)$ case considering or not the width of the f_2 in the form factor.

$im_\rho\Gamma_\rho$ in the denominator of the ρ propagator in Eq. (1.76). The results can be seen in Fig. 2.30. Once again we see that the changes are very small. In this case the exchanged ρ is below threshold and the effect of the ρ width in the $G_0(s)$ function is indeed very small.

Thus, the important effects from the ρ width are taken into account in the amplitudes $\tilde{t}_i$ and are an important factor for the width of the states that we obtain.

2.3.7 Discussion

At this point we would like to comment on the relationship and possible mixing with states of $q\bar{q}$ or other possible quark configurations. A valid approach is to start from a seed of $q\bar{q}$ (quenched approximation) and unitarize this seed with coupled channels of meson-meson (or other possible configurations). For the scalar mesons it is found that meson-meson components take over and the original $q\bar{q}$ component becomes of minor importance [333–336]. The dynamically generated resonance that we deal with corresponds to cases where the $q\bar{q}$ components are of minimal relevance. A thorough discussion of this issue is provided in section IIA of Ref. [337]. Another useful recent overview is given in Ref. [338], with emphasis on charmed and hidden charm states.

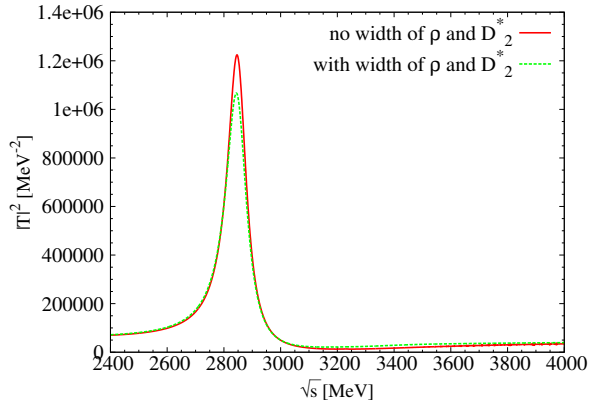

Figure 2.30: Same as in Fig. 2.29 for the case of $\rho - D_2^*(\rho D^*)$ scattering.

The mixture of meson-meson components in mesons or meson-baryon components in baryons is unavoidable and even the most stable baryon, the proton, has 36% admixture of πN component as determined from Drell Yan and deep inelastic process [339–341]. Certainly other baryons will have much larger meson baryon components, and those where these components are absolutely dominant qualify as molecular states dynamically generated from the meson-baryon interaction, the two $\Lambda(1405)$ states [277] being a good example of it. As to the possibility of having multiquark components, recent studies conclude that the clustering of the quarks in hadronic molecules is advantageous in most cases [342–344]. In our case, by concentrating on problems where hadron-hadron interaction is very strong and leads to bound systems, we are choosing cases where the hadronic components will be dominant, rendering of minor importance quark components which in quark model would appear at much higher energies.

2.3.8 Conclusions

In the present work, we show the results of our investigation of the D^*-multi-ρ systems. Our idea is based on the fact that the two-body interactions of $\rho\rho$ and ρD^* in spin $S = 2$ are so strong as to bind the particles forming the resonances$f_2(1270)$ [330] and $D_2^*(2460)$ [331] respectively. So we could study the many-body D^*-multi-ρ systems in an iterative way, looking at the

structure of the amplitudes and observing clear peaks that become wider as the number of ρ mesons increase.

The D^*-multi-ρ states with spins aligned combined to give some new charmed resonances, D_3^*, D_4^*, D_5^* and D_6^*, which are basically made of one D^* meson and an increasing number of $\rho(770)$ mesons and are not found in the list of PDG [9]. Their masses are predicted around $2800 - 2850$ MeV, $3075 - 3200$ MeV, $3360 - 3375$ MeV and 3775 MeV respectively. And their widths are about $60-100$ MeV, $200-400$ MeV, $200-400$ MeV and 400 MeV respectively. The analogy with the states already known in the strange and non-strange sector, from the study of multi-ρ systems in Ref. [223] and the work of Ref. [224] about the K^*-multi-ρ systems, together with the stronger interaction of the D^* mesons, make our predictions solid within the uncertainties admitted.

2.4 The study of $\eta K\bar{K}$ and $\eta' K\bar{K}$ interaction

Understanding the nature and structure of hadronic resonances is a main topic in high energy physics, which attracts the attention of both theory and experiment. With the advent of quantum chromodynamics (QCD) and the standard model, modern hadron physics is developing fast. The traditional picture for the internal structure of hadrons is that a meson is made of $q\bar{q}$ and a baryon of qqq, and quark models describe them well. On the other hand, with the development of the experiments, some states have been found experimentally whose properties cannot be explained by the standard way and may be of more complex structures, like tetraquarks and hybrids including possible glueballs for mesons, pentaquarks and heptaquarks for the baryons, or molecular states (see recent reviews in Refs. [345,346]). For the low energy region where the abnormal states showed up, nonperturbative QCD should be explored, for example, the ChUA [16, 155], as discussed in the subsection 1.3.1. Chiral dynamics for meson-meson and meson-baryon interaction has played an important role in understanding the nature and structure of hadronic resonances, and it has shown that many known resonances are generated dynamically as a natural consequence of the hadron-hadron interaction. The ChUA has successfully explained both the experimental data for the light scalar mesons [16, 18, 347, 349] (such as $a_0(980)$, $f_0(980)$, σ, and κ [or $K^*(800)$]) and the light baryons [155, 190, 194, 277, 326, 328, 348], two $\Lambda(1405)$, $\Lambda(1670)$, $N^*(1535)$, $\Delta(1620)$, etc. Extrapolation of this dynamics to the charm sector has also produced many meson states, as the $D^*_{s0}(2317)$, $D^*_0(2400)$, $X(3700)$, $X(3872)$, etc [93, 259–261, 350], as well as baryon states like the $\Lambda_c(2595)$ [256–258]. More work on the $K\pi$ interaction is done in Refs. [19, 195, 351], where the S-wave $K\pi$ elastic scattering amplitude is evaluated and good agreement with the experimental phase shifts is obtained. In addition, the scalar resonance κ is generated dynamically, which is also seen in the final state interaction in some reactions [352].

The three-body interaction is another subject in hadron physics which is also drawing much attention. In our present work we will use the FCA to Faddeev equations of the formalism in the subsection 1.4.2 to investigate the $\eta K\bar{K}$ and $\eta' K\bar{K}$ systems. When studied in S-wave, provided the strength of the interaction allows for it, this systems could give rise to η states. There are many η excited states, the lowest ones the $\eta(1295)$, $\eta(1405)$ and $\eta(1475)$.

Since we do not want states too far from threshold, the $\eta(1475)$ could be in principle a candidate for the $\eta K\bar{K}$ system. For the $\eta' K\bar{K}$ system we would have to look for an η state around 1930 MeV. There are two η states around this energy in the Particle Data Group (PDG) [9], the $\eta(1760)$ and the $\eta(2225)$, both far away from the $\eta' K\bar{K}$ threshold mass. There is a peak seen at 1870 MeV in the $J/\psi \to \eta\pi^+\pi^-$ in Ref. [353], but its quantum numbers are not well determined. Similarly, there is another peak seen in the $J/\psi \to \eta'\pi^+\pi^-$ reaction that peaks around 1836 MeV [$X(1835)$], with a large width of about 190 MeV [354]. We shall explore the possibility that the $\eta' K\bar{K}$ could be responsible for any of such states, although we anticipate that the interaction is too weak to lead to such strongly bound systems.

The $\eta K\bar{K}$ and $\eta' K\bar{K}$ systems have been investigated before in Ref. [355], following the lines of Ref. [253], where it was concluded that the $\eta K\bar{K}$ system could be the $\eta(1475)$ resonance, and the $\eta' K\bar{K}$ the $X(1835)$. Yet, in Ref. [232] it was discussed that the method of Ref. [253] contains some element of uncertainty which makes it most opportune to perform calculations with a different method and contrast the predictions. Certainly, there are also other options for these resonances using quark models and other approaches and a detailed discussion on it can be found in the Introduction of Ref. [355]. In the present work we will explore the possible molecular structure of these three body systems (which is done in our paper [356]).

2.4.1 $K\bar{K}$ and $\eta K\,(\eta'\bar{K})$ two-body interactions

To evaluate the Faddeev equations under the FCA, we need to define the two-body cluster and then let the third particle collide with the cluster. Thus, the starting point of our work is to look for the cluster in the two-body interactions. Following the formalism of Ref. [16], by taking into account the chiral dynamics and the unitary coupled channels approach [16, 18, 19, 155, 190, 194, 195, 260, 277, 326, 328, 357], we should reproduce the resonances $f_0(980)$ and $a_0(980)$ as the cluster of FCA. We briefly summarize the method of Ref. [16] here.

To calculate the scattering amplitudes with the ChUA of the subsection 1.3.1, the BS equation in coupled channels, with the factorized on shell potentials [16, 194] is used, seen Eq. (1.44). In the present work, the kernel V is a matrix of the interaction potentials between the channels, given

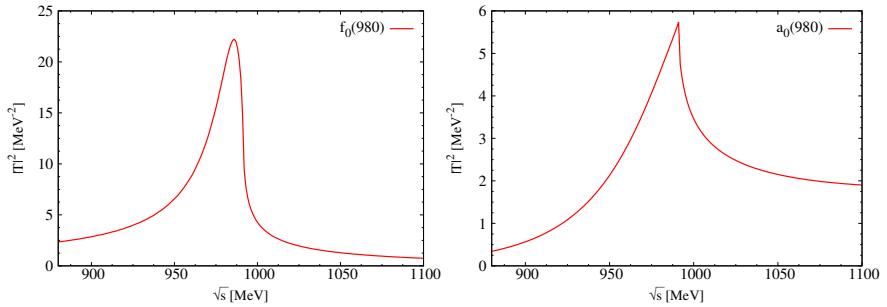

Figure 2.31: Modulus squared of the scattering amplitudes. Left: $|t_{12}^{I=0}|^2/10^3$, $f_0(980)$; Right: $|t_{22}^{I=1}|^2/10^3$, $a_0(980)$.

by [16]

$$\begin{aligned} V_{11}^{I=0}(s) &= -\frac{1}{2f_\pi^2}(2s-m_\pi^2), \quad V_{12}^{I=0}(s) = -\frac{\sqrt{3}}{4f_\pi^2}s, \quad V_{22}^{I=0}(s) = -\frac{3}{4f_\pi^2}s, \\ V_{11}^{I=1}(s) &= -\frac{1}{3f_\pi^2}m_\pi^2, \quad V_{12}^{I=1}(s) = \frac{\sqrt{6}}{36f_\pi^2}(9s-8m_K^2-m_\pi^2-3m_\eta^2), \\ V_{22}^{I=1}(s) &= -\frac{1}{4f_\pi^2}s, \end{aligned} \tag{2.33}$$

with f_π the pion decay constant. Note that in isospin $I=0$, there are two coupled channels, 1 is $\pi\pi$ and 2 is $K\bar{K}$; for $I=1$, channel 1 denotes $\pi^0\eta$ and 2 as $K\bar{K}$.

Taking $\Lambda = 1.03$ GeV and $\Lambda = \sqrt{q_{max}^2 + m_K^2}$ as done in Ref. [16] for the loop function G, we get $q_{max} = 903$ MeV. Our results are shown in Fig. 2.31. In Fig. 2.31, we produce the resonances of $f_0(980)$ and $a_0(980)$, which are consistent with Ref. [16] and form the clusters of the $\eta K\bar{K}$ and $\eta' K\bar{K}$ three-body interactions in our present work.

To perform the evaluation of Faddeev equations under the FCA, we need the calculation of the two-body interaction amplitudes ($\tilde{t}_1$ and $\tilde{t}_2$) of ηK and $\eta\bar{K}$ for the $\eta K\bar{K}$ system ($\eta' K$ and $\eta'\bar{K}$ for the $\eta' K\bar{K}$ system) which are investigated in Refs. [19,195,351] as mentioned before. The former input is needed to construct the form factor of the cluster entering Eq. (1.76).

Next we address the ηK, $\eta\bar{K}$ and $\eta' K$, $\eta'\bar{K}$ interaction. Since we are involving the η', it is convenient to take the three coupled channels πK, ηK

and $\eta' K$, labeled by channel 1, 2 and 3 respectively. Thus, the potentials are [195]

$$V_{11}^{I=1/2}(s) = -\frac{1}{4f_\pi^2}(4s+3t-4m_\pi^2-4m_K^2), \tag{2.34}$$

$$V_{12}^{I=1/2}(s) = -\frac{\sqrt{2}}{6f_\pi^2}(-3t+2m_K^2+m_\eta^2), \tag{2.35}$$

$$V_{13}^{I=1/2}(s) = \frac{1}{12f_\pi^2}(-3t+3m_\pi^2+8m_K^2+m_{\eta'}^2), \tag{2.36}$$

$$V_{22}^{I=1/2}(s) = -\frac{2}{9f_\pi^2}(3t-m_K^2-2m_\eta^2), \tag{2.37}$$

$$V_{23}^{I=1/2}(s) = \frac{\sqrt{2}}{18f_\pi^2}(3t-3m_\pi^2+2m_K^2-m_\eta^2-m_{\eta'}^2), \tag{2.38}$$

$$V_{33}^{I=1/2}(s) = -\frac{1}{36f_\pi^2}(3t-6m_\pi^2+32m_K^2-2m_{\eta'}^2), \tag{2.39}$$

where there is a minus sign difference with Refs. [19,355] in some nondiagonal matrix elements resulting from taking different phase conventions [2]. As done in Ref. [195], we take

$$\mu = m_K, \qquad a(\mu) = -1.383, \tag{2.40}$$

in the loop function for all channels, and we obtain the same results as in Ref. [195], seen in Fig. 2.32, which agree fairly well with the data except at the higher energies.

With these parameters, we also find the pole of κ [or $K^*(800)$], $(743.72 - i275.36)$ MeV, which is consistent with the result of Ref. [195], $(0.742 - i0.273)$ GeV. Then, using these parameters, we can get the ηK and $\eta' K$ scattering amplitudes. Because of charge conjugation symmetry, the amplitudes for $\eta\bar{K}$, $\eta'\bar{K}$ are the same as those for ηK, $\eta' K$.

2.4.2 $\eta K\bar{K}$ and $\eta' K\bar{K}$ three-body interactions

As discussed in the former section, we calculate the ηK and $\eta\bar{K}$ ($\eta' K$ and $\eta'\bar{K}$) amplitudes using the same parameters, and then we use Eq. (1.75) to evaluate the three-body amplitude of the $\eta K\bar{K}$ ($\eta' K\bar{K}$) system. Also,

[2] The final scattering amplitudes are the same, as pointed out by J. A. Oller.

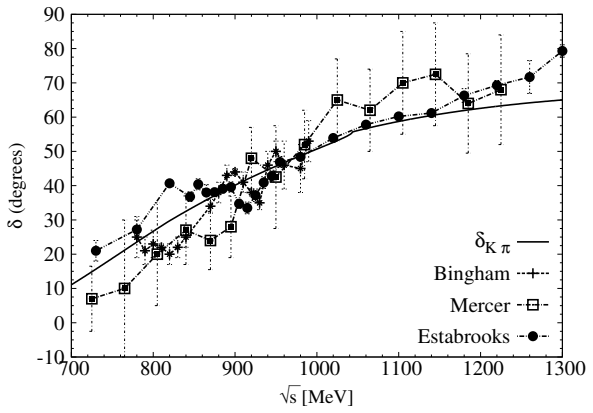

Figure 2.32: The S-wave $K\pi$ phase shifts in isospin $I = 1/2$. The experiments data are taken from: Mercer [358], Bingham [359], Estabrooks [360].

as discussed in the former section, the Λ' of Eq. (1.77) can be taken as $q_{max} = 903$ MeV for the cluster of $f_0(980)$ or $a_0(980)$.

In Fig. 2.33 (left), we can see a clear resonance structure in the modulus squared of the $\eta K\bar{K}$ scattering amplitude, which is around 1490 MeV, with the width of about 100 MeV, and about 38 MeV below the threshold of $\eta\, f_0(980)$. This result is consistent with the one found in Ref. [355]. From the PDG [9], this resonance may be the $\eta(1475)$ of $I = 0$, with mass 1476 ± 4 MeV and width 85 ± 9 MeV. Comparing our results with the PDG, both the mass and the width are consistent with the experimental values if we assume 10-15 MeV uncertainties in our calculated results.

Since the masses of the $K\bar{K}$ bound states $f_0(980)$ and $a_0(980)$ are the same and only their isospins are different, the three-body amplitudes of $\eta K\bar{K}$ and $\eta' K\bar{K}$ in our formalism are degenerated in isospin $I = 0$ and $I = 1$. This means that if we predict a bound state for the $\eta f_0(980)$ system, we also have the same for $\eta a_0(980)$. This is so, assuming that the $f_0(980)$ and $a_0(980)$ resonances are predominantly $K\bar{K}$ molecules. But, as we have discussed, in the construction of the $f_0(980)$ resonance we need the $\pi\pi$ and $K\bar{K}$ channels, and the $\pi\pi$ is marginal in the structure of the resonance, it simply provides a decay mode. However, this is not the case for the $a_0(980)$ where the $\pi\eta$ channel already plays an important role in the build up of the resonance. Then a more elaborate, and technically complex, study of the

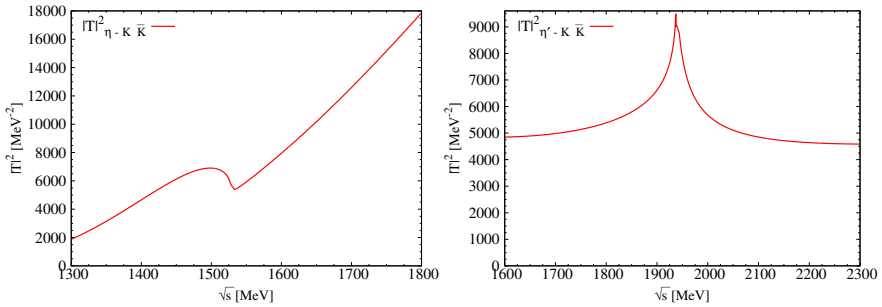

Figure 2.33: Modulus squared of the three-body interaction amplitudes. Left: $|T_{\eta K\bar{K}}|^2$; Right: $|T_{\eta' K\bar{K}}|^2$.

η, η' interacting with this system, would have much contribution from $\eta\eta$, which only comes from coupled channels and is very weak, and $\eta\pi$ which is also weak. The signal that we get in Fig. 2.33 would be much diluted and we do not expect an I=1 state.

We also see an obvious peak in Fig. 2.33 (right) for the $\eta' K\bar{K}$ interaction. But the mass position of the peak is about 1940 MeV, which is very close to threshold, 1942 MeV. Therefore, this peak should be an enhancement effect of the threshold, a cusp effect, and we will check it further in the next section.

2.4.3 Further discussions

We showed the results of our investigation of the $\eta K\bar{K}$ and $\eta' K\bar{K}$ systems in the former section. For the $\eta K\bar{K}$ scattering, we find one resonance structure in the modulus squared of the amplitude. But, for the other one, the clear peak of the $\eta K\bar{K}$ amplitude turns into an enhancement effect at the threshold in the $\eta' K\bar{K}$ amplitude, a cusp effect reflecting the cusp of the $\tilde{t}_1$ amplitude, used in Eq. (1.75), at threshold. In all these results we did not take into account the width of $f_0(980)$ as done in the former work. In the PDG, the width of the $f_0(980)$ is 40 to 100 MeV, which is not small compared to the binding energy found.

As done in the former work, in the last subsection, we can take into account the width of the $f_0(980)$ in the three-body scattering amplitudes, just by replacing M_R in Eqs. (1.77), (1.78) by $M_R - i\frac{\Gamma_R}{2}$. The new results

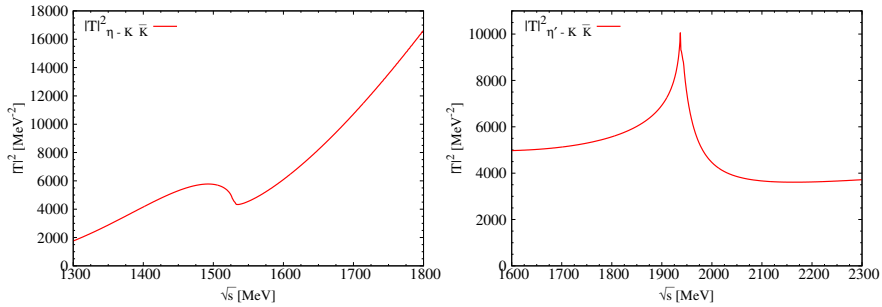

Figure 2.34: Modulus squared of the three-body interaction amplitudes with the considering the contribution of the width of $f_0(980)$ [or $a_0(980)$]. Left: $|T_{\eta K\bar{K}}|^2$; Right: $|T_{\eta' K\bar{K}}|^2$.

are given in Fig. 2.34, where we just take the width as 60 MeV. For the $\eta K\bar{K}$ amplitude we can see in Fig. 2.34 (left), comparing with Fig. 2.33 (left), that the strength of the amplitude is reduced and the peak position is still not changed, but the width becomes a little larger (around 120 MeV), which is in the line with the finding in the last subsection. For the $\eta' K\bar{K}$ amplitude, shown in Fig. 2.34 (right), by comparing to Fig. 2.33 (right), we can see that the strength at the peak is a bit increased and the shape changes a bit when considering the contribution of the width $f_0(980)$. The important thing, however, is that the shape of the $\eta' K\bar{K}$ amplitude continues to be that of a cusp effect. In summary, as discussed in the last subsection, we can conclude that the effects of the contribution of the cluster's width are small and do not change the relevant features found before.

Next, we want to check the uncertainties in Eq. (1.75) when we make a small change in the parameters in the evaluation of $\tilde{t}_1$. Following Ref. [195], we can only change $a(\mu)$. This parameter was chosen in Ref. [195] to fit the experimental data of the $K\pi$ phase shifts. Then, we change 50 % up and down the parameter $a(\mu)$ of Eq. (2.40), to a point where the $K\pi$ phase shifts are not too good, as shown in Fig. 2.35 (left). From Fig. 2.35 (right), we can see that the resonance structure in $\eta K\bar{K}$ scattering is not changed so much even with these extreme changes in the input, and both the peak position and the width have practically not changed. This gives us confidence that the results that we get are rather solid and do not change

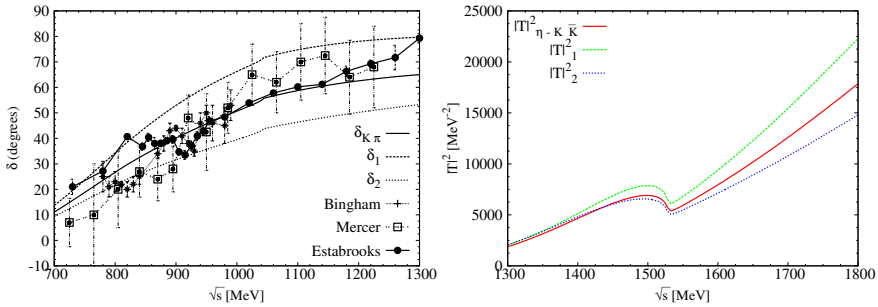

Figure 2.35: The results for the change of the parameter in Eq. (2.40). Left: the $K\pi$ phase shifts, solid line is the fit one, the two dash line of $\delta_1,\ \delta_2$ are with 50 % changes; Right: $|T_{\eta K\bar{K}}|^2$, solid line is with fit parameter, the two dash line of $T_1,\ T_2$ are with 50 % changes of the fit.

with small variations of the parameters. The same changes only affect in a minor way the $\eta' K\bar{K}$ amplitude and the cusp effect at threshold is the only relevant feature of the amplitude.

At this point one must comment on the results of [355]. In that work the interaction of the η with the $K\bar{K}$ cluster is done as here, although the formalism seems rather different. There the primary amplitude for the η interaction with the components of the cluster is evaluated and then the η and the cluster propagate similarly to the propagation of the meson meson components in the G function. The caveat is that while the regularization parameters are fitted to data on meson meson scattering, here one does not have this information for the scattering of η and $f_0(980)$ and one must make assumptions on how this new loop is regularized. As a consequence, there is an element of uncertainty and usually what one makes is to assume that the interaction gives rise to a certain resonance to fix the parameters, although they are kept within a natural range; there is, hence, not a genuine prediction. In that work, the $\eta f_0(980)$ gives rise to the $\eta(1475)$ as we have also claimed here. But the $\eta' f_0(980)$ is claimed to produce the $X(1835)$ resonance, something that our approach does not give.

The difference between the $\eta K\bar{K}$ and $\eta' K\bar{K}$ systems could be qualitatively understood by recalling that the ηK, together with the πK system, generate the broad κ resonance, but the $\eta' K$ amplitude has no structure around the $\eta' K$ energies (up to the unavoidable cusp at threshold) and is

small and smooth around these energies. In order to see how far we are from creating a resonance structure in the $\eta' K\bar{K}$ system, we artificially multiply V_{33} of Eq. (2.39) by a factor and look at the $\eta' K\bar{K}$ amplitude. We must multiply by a factor four the V_{33} potential to see the peak move a bit (by about 6 MeV) below the threshold. Since the uncertainties of the model are by no means that large (we can accept about 20 % uncertainties in the potentials), the former exercise tells us about the cusp character of the $\eta' K\bar{K}$ amplitude is quite a stable result and we cannot associate a physical η state to it.

We should comment on the paper [255], where using the Faddeev approach in the version of Ref. [212], one peak in $|T|^2$ for $\pi K\bar{K}$ is found around 1400 MeV, which is associated to the $\pi(1300)$. It is mentioned there that the $\eta K\bar{K}$ system is also investigated and no clear signal is seen. The coupled channels approach used there contains πK and ηK but not $\eta' K$. We have checked that removing the $\eta' K$ channel does not change qualitatively the $\eta K\bar{K}$ amplitude, although the distribution of $|T|^2$ in energy has a broader shape. Consideration of the $\eta' K$ channel makes the energy distribution a little sharper. The fact that no clear peak for the $\eta K\bar{K}$ amplitude appears is somewhat unexpected, since one usually gets qualitative agreement between the FCA and the Faddeev calculations for bound states. For instance, the three body $\bar{K}NK$ scattering amplitude was calculated using the FCA to the Faddeev equations in Ref. [225] and the results of that work are in good agreement with the other theoretical works [229, 230] evaluated using variational and Faddeev approaches, respectively. The same can be said when one studies the $\bar{K}NN$ system in the FCA [228] or in Faddeev calculations [301], or variational calculations [272]. The DNN system is another case of agreement between the FCA and variational calculation [310]. We state the present situation and call for further calculations of the $\eta K\bar{K}$ system using different approaches in order to clarify the situation.

2.4.4 Conclusions

In our work, we study the three-body systems of $\eta K\bar{K}$ and $\eta' K\bar{K}$, by using the fixed center approximation to the Faddeev equations. The clusters of $f_0(980)$ for the fixed center approximation is successfully reproduced by the chiral unitary approach. With this approach, the experimental S-wave $K\pi$ phase shifts of isospin $I = 1/2$ are also well fitted. For the three-body scat-

tering we find a resonant structure in the $\eta K\bar{K}$ scattering amplitude, which may correspond to the $\eta(1475)$ state for $I = 0$. This finding is consistent with the result of Ref. [355]. We also make an estimation of our theoretical uncertainties for this state by taking into account the contribution of the cluster's width and reasonable changes in the free parameters, and we get stable results. As for the $\eta' K\bar{K}$ scattering, we only get an enhancement effect at the threshold in the modulus squared of the interaction amplitude and we can not claim that this can be associated to any resonance.

2.5 The investigation of the $\rho K\bar{K}$ system

One of the most important aims of hadron physics is getting a better understanding of the strong interaction through the study of hadronic resonances. Besides the constituent quark model, recently the rich spectrum of hadronic resonances is studied actively from various viewpoints. Among them, hadronic molecules, dynamically generated states through the hadronic interaction, attracts plenty of attention. At low energies, the dynamics of light hadrons can be described in terms of chiral symmetry [151–154, 160, 161, 173]. By using the leading order of the chiral Lagrangians as input, a powerful tool, the chiral unitary approach, implementing unitarity in coupled channels, has been developed and it has provided great success in describing many resonances for meson-meson or meson-baryon systems [16, 18, 19, 155, 190, 194, 260, 277, 326–328].

In order to explore multi-hadron systems, the application of the FCA to Faddeev equations has been implemented [208, 218–222]. Under the condition where the cluster structure in three-body systems is not varied so much against the collision of the other particle, that approximation will work fine, as discussed in Refs. [223, 224, 227, 232]. More discussions can be seen in the subsection 1.4.2.

In the present work, we study the $\rho K\bar{K}$ system in the sector $I^G(J^{PC}) = 1^+(1^{--})$ within the FCA to obtain the $\rho(1700)$ resonance. Namely, a pair of $K\bar{K}$ is assumed to form the scalar cluster, the $f_0(980)$ resonance. Since the $K\bar{K}$ component in $f_0(980)$ is found to be dominant [16], this assumption seems to work well. The amplitude needed in the present work is the ρK unitarized scattering amplitude. In Ref. [164], interactions including vector mesons are reviewed. In order to obtain the ρK amplitude, we follow the schemes given by Refs. [362, 363] and extend them to the isospin $I = 3/2$ sector.

2.5.1 The two-body ρK unitarized amplitude

To implement the Faddeev equation within the FCA, we need the two-body unitarized amplitude. Namely in the present case of the $\rho K\bar{K}$ system, the ρK ($\rho\bar{K}$) unitarized amplitude is necessary. In the previous work [362, 363], the vector-pseudoscalar interaction in the sector with strangeness $S = 1$ and isospin $I = 1/2$ was studied within the framework of the chiral unitary

approach and that interaction was shown to generate two resonance poles corresponding to the $K_1(1270)$ resonance. This work has been extended in the recent work of Ref. [364] including the effect of higher order terms. It is found there that the introduction of the new terms barely affects the results of the lowest order Lagrangians. Here we are going to follow the scheme of Refs. [362, 363] and pick up only the essence for simplicity.

Following the BS approach, we have the VP two-body scattering amplitude as

$$T = [1 + V\hat{G}]^{-1}(-V)\vec{\epsilon}\cdot\vec{\epsilon}', \tag{2.41}$$

where V is an interaction kernel which will be discussed later, $\hat{G}$ is $(1 + \frac{1}{3}\frac{q_l^2}{M_l^2})G$ being a diagonal matrix and $\vec{\epsilon}(\vec{\epsilon}')$ represents a polarization vector of the incoming (outgoing) vector-meson. We also take the dimensional regularization for the G function, seen in Eq. (1.46), and also found in our paper [365].

Before the derivation of the VP interaction, it is worth referring to a finite width of the vector mesons in the loop function. In Ref. [363], the effect of the propagation of unstable particles is taken into account in terms of the Lehmann representation. That is done with the dispersion relation with its imaginary part

$$D(s) = \int_{s_{\rm th}}^{\infty} ds_V \left(-\frac{1}{\pi}\right) \frac{{\rm Im}D(s_V)}{s - s_V + i\epsilon}, \tag{2.42}$$

where $s_{\rm th}$ stands for the square of the threshold energy. Now the spectral function is taken as

$${\rm Im}D(s_V) = {\rm Im}\left\{\frac{1}{s_V - M_V^2 + iM_V\Gamma_V}\right\}, \tag{2.43}$$

where the width Γ_V is assumed to be a constant physical value. Substituting Eqs. (2.42) and (2.43) into the original loop function Eq. (1.46), we have

$$\begin{aligned}\tilde{G}_l(\sqrt{s}) &= \frac{1}{C_l}\int_{(M_l-2\Gamma_l)^2}^{(M_l+2\Gamma_l)^2} ds_V G_l(\sqrt{s}, \sqrt{s_V}, m_l) \\ &\times \left(-\frac{1}{\pi}\right){\rm Im}\left\{\frac{1}{s_V - M_l^2 + iM_l\Gamma_l}\right\},\end{aligned} \tag{2.44}$$

with the normalization for the lth component

$$C_l = \int_{(M_l-2\Gamma_l)^2}^{(M_l+2\Gamma_l)^2} ds_V \times \left(-\frac{1}{\pi}\right) \mathrm{Im}\left\{\frac{1}{s_V - M_l^2 + iM_l\Gamma_l}\right\}, \tag{2.45}$$

with m_l, M_l, Γ_l, the mass of the pseudoscalar meson, mass of the vector and width of the vector respectively. Replacing G_l by $\tilde{G}_l$ in Eq. (2.41), we include the width effect of vector mesons.

We do the convolution for the ρ and K^*. In order to strictly respect the analytical properties of the amplitude, the integral of Eq. (2.44) should fill up all the space available for the decay of the ρ and the K^* and thus the lower limit should be $(2m_\pi)^2$ for the ρ and $(m_\pi + m_K)^2$ for the K^*. This is important to have the branch points at the proper place, as discussed in Ref. [366]. Also, the width should not be constant but should be energy dependent. Later, we shall come back to make improvements on the present prescription which is often used in the literature [362].

In order to obtain the VP interaction kernel in terms of the $SU(3)$ chiral symmetry, we start from the following Lagrangian of Eq. (1.28). In the WCCWZ approach [160, 161, 367], this Lagrangian stems from a nonlinear realization of chiral symmetry. Expanding Eq. (1.28) up to two pseudoscalar fields, we have the leading order contribution of the four point $VVPP$ interaction Lagrangian

$$\mathcal{L}_{VVPP} = -\frac{1}{4f^2}\left\langle [V^\mu, \partial^\nu V_\mu]\,[P, \partial_\nu P]\right\rangle. \tag{2.46}$$

From Eq. (2.46), the VP potential projected over s-wave, can be obtained as

$$\begin{aligned} V_{ij}(s) &= -\frac{\vec{\epsilon}\cdot\vec{\epsilon}'}{8f^2}C_{ij}\left[3s - (M_i^2 + m_i^2 + M_j^2 + m_j^2)\right. \\ &\quad \left. -\frac{1}{s}(M_i^2 - m_i^2)(M_j^2 - m_j^2)\right], \end{aligned} \tag{2.47}$$

where the index $i(j)$ represents the VP channel of the incoming (outgoing) particles. The coefficients C_{ij} in Eq. (2.47) for the $I = 1/2$ sector and the

$I = 3/2$ sector are given in Refs. [362, 363]. In order to have an appropriate unitarized amplitude, we use the following parameter set chosen to reproduce $K_1(1270)$ in Ref. [363]

$$\mu = 900 \text{ MeV}, \ a(\mu) = -1.85, \ f = 115 \text{ MeV}. \tag{2.48}$$

In Ref. [362], two poles were obtained for the $K_1(1270)$ which were further studied in Ref. [363], where it was shown that available experimental information gives support to the existence of these two poles. In Ref. [363] the two poles were found at $1195-i123$ MeV and $1289-i73$ MeV. The second pole, corresponding to a narrower state, was shown to couple strongly to ρK, while the first pole coupled strongly to $K^*\pi$ and not so much to ρK. In the formalism that we study, the ρK system is allowed to decay into $K^*\pi$, but we do not propagate further these particles. Although a coupled channel approach with FCA is possible, we find it unnecessary for the study of the $\rho K\bar{K}$ system. Indeed, while the coupling of the higher resonance to ρK is $g_{\rho K} = 4821$ MeV, the coupling to $K^*\pi$ is $g_{K^*\pi} = 1401$ MeV. Since the $\rho K \to \rho K$ amplitude goes as $g^2_{\rho K}$ and the $K^*\pi \to K^*\pi$ as $g^2_{K^*\pi}$, it is clear that processes involving the ρK amplitude will dominate the amplitude and in the multiple scattering we just consider ρK rescattering.

2.5.2 The $\rho K\bar{K}$ three-body scattering

Once the unitarized ρK amplitude is obtained, let us go to the $\rho K\bar{K}$ three-body system. As mentioned above, we study this system by solving the Faddeev equation within the FCA of the formalism in the subsection 1.4.2.

In the present work, the particles 1, 2 and 3 correspond to K, $\bar{K}$ and ρ respectively, and thus $t = t_1 = t_2$. Therefore, from now on we will not specify the particle 1 or 2, and use the Eq. (1.75) to evaluate the three-body amplitude. From Ref. [16], we take $q_{\max} = \sqrt{\Lambda^2 - m_K^2}$ and $\Lambda = 1030$ MeV for getting the $f_0(980)$ from the $K\bar{K}$ cluster, thus, it is the same cutoff for the form factor, seen Eq. (1.77). Note that in the region $q > 2q_{\max}$, F_{f_0} vanishes identically. Therefore the integration in Eq. (1.76) has a limit $2q_{\max}$. In Fig. 2.36, the form factor for the $f_0(980)$ resonance and the G_0 function are shown, respectively. In the form factor the strong suppression of high energy momentum is seen and the threshold effect appears in the G_0 function.

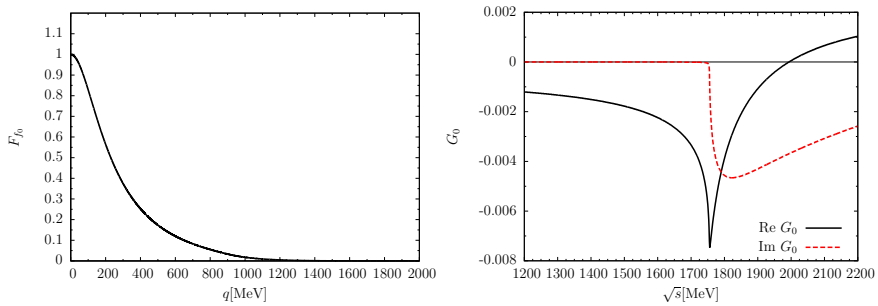

Figure 2.36: The results of form factor (left) and the G_0 function (right).

At the end of this section, we refer to the conversion of the basis of the unitarized amplitude t. Since the $\rho[K\bar{K}]_{I=0}$ system is studied in the sector $I(J^P) = 1(1^-)$, now we focus on the scattering in the $I_z = +1$ channel, $\rho^+[K\bar{K}]_{I=0}$. With the phase convention, we have

$$|K\bar{K}\rangle_{I=0} = -\frac{1}{\sqrt{2}}\left(\left|K^+K^-\right\rangle + \left|K^0\bar{K}^0\right\rangle\right). \tag{2.49}$$

Following the same phase convention, we have

$$\begin{aligned} t &= \left\langle\rho^+\right| \otimes \left\langle[K\bar{K}]_{I=0}\right| \hat{t}_{\rho K} \left|[K\bar{K}]_{I=0}\right\rangle \otimes \left|\rho^+\right\rangle \\ &= \frac{1}{2}\left(\left\langle\rho^+K^+K^-\right| + \left\langle\rho^+K^0\bar{K}^0\right|\right) \hat{t}_{\rho K} \times \left(\left|\rho^+K^+K^-\right\rangle + \left|\rho^+K^0\bar{K}^0\right\rangle\right) \\ &= \frac{1}{2}\left(\left\langle\rho^+K^+\right| \hat{t}_{\rho K} \left|\rho^+K^+\right\rangle + \left\langle\rho^+K^0\right| \hat{t}_{\rho K} \left|\rho^+K^0\right\rangle\right), \end{aligned} \tag{2.50}$$

where $\bar{K}$ acts as a spectator. Therefore the interaction kernel is given as a mixture of different isospin sectors

$$t = \frac{1}{3}\left(2t_{\rho K}^{I=3/2} + t_{\rho K}^{I=1/2}\right), \tag{2.51}$$

where $t_{\rho K}$ is the ρK unitarized scattering amplitude given by Eq. (2.41).

2.5.3 Results

Now we have the $\rho K\bar{K}$ three-body amplitude within the FCA. To see the effect of the multiple scattering, the full amplitude is compared with the

single scattering amplitude $T = 2\tilde{t}$. Furthermore, as discussed in the previous work [363], the inclusion of the vector meson width is found to be much important. Therefore, we also consider the width of the ρ, $\Gamma_\rho \sim 150$ MeV, in the G_0 function. By using the following replacement for the ρ propagator in Eq. (1.76)

$$\frac{1}{q^{02} - \vec{q}^2 - m_\rho^2 + i\epsilon} \to \frac{1}{q^{02} - \vec{q}^2 - m_\rho^2 + i m_\rho \Gamma_\rho}, \tag{2.52}$$

we include the ρ width into the G_0 function. Once again, the use of the constant ρ width can spoil precise analytical properties tied to the unstable ρ, as discussed in Ref. [366], but we shall see later on that the strict use of the ρ spectral function has about the same effect.

In Fig. 2.37, the $\rho^+[K\bar{K}]_{I=0}$ amplitude is shown and there one can see that a peak appears in each case. In the single scattering amplitude, the

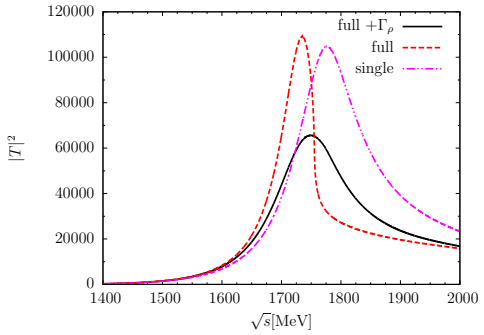

Figure 2.37: The $\rho K\bar{K}$ amplitude where "single", "full", "full + Γ_ρ" denote the amplitude of the single scattering, full scattering, full scattering with the ρ width effect, respectively.

peak exists around the threshold of ρ and $f_0(980)$. Through the multiple scattering, the peak position shifts lower while the width is getting smaller because the $\rho f_0(980)$ channel becomes closed. With the ρ width effect, that peak is getting much wider while the shift of the peak position is not so large. The masses (or a peak position in the amplitude) and full widths at half maximum of the dynamically generated state are listed with the experimental data in Table. 2.5, where the amplitudes are given by the single scattering, the full scattering and the full scattering with the ρ width

effect respectively. Compared with the experimental data, the consideration of the ρ width is found to be important.

Table 2.5: The masses and widths of dynamically generated states.

	single	full	full + Γ_ρ	PDG [9]
Mass (MeV)	1777.9	1734.8	1748.0	1720 ± 20
Width (MeV)	144.4	63.7	160.8	250 ± 100

As shown above, the present study seems to work for generating the resonance which might correspond to $\rho(1700)$. In addition, we consider the width of the $f_0(980)$ too. The $K\bar{K}$ component in the $f_0(980)$ resonance is found to be dominant while the decay width into the $\pi\pi$ channel is not so small. Therefore we consider the inclusion of the width into our framework. In order to keep the FCA, here we give a naive prescription that the eigenvalue of the $K\bar{K}$ system is now a complex value. Namely the mass of the cluster M_{f_0} in Eqs. (1.77) and (1.78) is replaced by $M_{f_0} - i\Gamma_{f_0}/2$. Then the form factor becomes a complex function which might represent the effect of the wave function of the unstable cluster. The amplitude with the $f_0(980)$ and ρ width effect is shown in Fig. 2.38 and the masses and widths of the dynamically generated state are listed in Table 2.6. Taking into

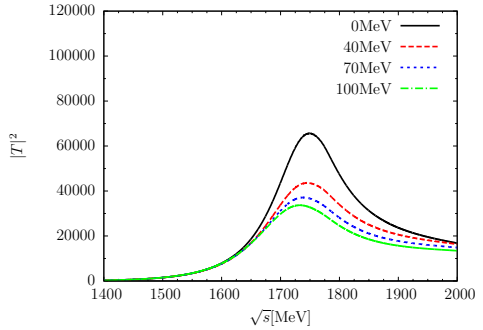

Figure 2.38: The $\rho K\bar{K}$ amplitude with the ρ and $f_0(980)$ width effect, taking Γ_{f_0} as 0, 40, 70 and 100 MeV, respectively.

account the ambiguity of the $f_0(980)$ width, as a value of Γ_{f_0}, a maximum

Table 2.6: The masses and widths of dynamically generated states with the ρ and $f_0(980)$ width effects. (in MeV)

	$\Gamma_{f_0}=0$	$\Gamma_{f_0}=40$	$\Gamma_{f_0}=70$	$\Gamma_{f_0}=100$
Mass	1748.0	1743.6	1739.2	1734.8
Width	160.8	216.4	227.2	224.6

and minimum value of the experimental data and their average are taken. It is shown that the inclusion of the $f_0(980)$ width induces a suppression of the magnitude of the peak and the peak becomes broader as the width of the $f_0(980)$ increases. Furthermore it is also a remarkable feature that the peak position is not so affected by this prescription. By taking $\Gamma_{f_0}=70$ MeV which is between 40 MeV and 100 MeV as quoted in the PDG [9], we find the mass at 1739 MeV and the width of 227 MeV (see Table 2.6), which agrees very well with the experimental properties of the $\rho(1700)$ (see Table 2.5).

2.5.4 Peaks in the three-body scattering amplitude

We find it interesting to discuss here the meaning of Eq. (1.75) and of Fig. 2.37. Eq. (1.75) bears resemblance to the BS equation for two interacting particles that leads to bound states or resonances

$$T=\frac{V}{1-VG}. \tag{2.53}$$

There are however some differences. In general V is a smooth function of the energy and poles of the T matrix appear for $1-VG=0$. One might correspondingly think that the poles of the three body system come from a zero in the denominator of Eq. (1.75), $1-\tilde{t}G_0=0$, but this is not the case. The difference of Eq. (1.75) with Eq. (2.53) with a smooth potential is that $\tilde{t}(\sqrt{s'})$ already has a pole corresponding to a dynamically generated K_1 resonance [362, 363]. In this case the situation is similar to the one of the BS equation in the presence of a genuine resonance, which is taken into account by means of a CDD pole [368]. To clarify situation let us just take

V of Eq. (2.53) that contains a CDD pole as

$$V = \frac{g^2}{s - s_c}. \tag{2.54}$$

Then, the T matrix of Eq. (2.53) can be recast as

$$T = \frac{1}{V^{-1} - G} = \frac{1}{\frac{s-s_c}{g^2} - G} = \frac{g^2}{s - s_c - g^2 G}, \tag{2.55}$$

which develops a pole at $s = s_c + g^2 G$. The coupling of the CDD pole to the interacting components shifts the position of the original CDD pole. Here, we have a similar situation. For the discussion purpose one can approximate $\tilde{t}(\sqrt{s'})$ by its pole term and then

$$\tilde{t}(\sqrt{s'}) \quad \sim \quad \frac{\tilde{g}^2}{s' - s_K}, \tag{2.56}$$

with s_K, the mass squared of the K_1 state. Then

$$T(\sqrt{s}) \quad = \quad 2\frac{\tilde{g}^2}{s' - s_K - \tilde{g}^2 G_0(\sqrt{s})}, \tag{2.57}$$

and thus, the multiple scattering of the ρ with K and $\bar{K}$, shifts the position of the original ρK pole. This is what is seen in Fig. 2.37. The single term $\tilde{t}$ already gives rise to a resonant structure, but the multiple scattering of the ρ shifts the peak to lower energies and produces a more bound three body system.

It is also worthwhile to discuss these results from the physical point of view. What we see in Fig. 2.37 is similar to what happens with the binding of atomic molecules. The subject is discussed in Quantum Mechanics books using two attractive δ functions in just one dimension [369]. If the two δ functions are separated one binds a particle with either of the δ potentials. This would correspond to our results with just the numerator in Eq. (1.75). The interesting thing to observe is that the two δ potentials bind a particle even in this case. Here, we can say that, even without multiple scattering of the ρ, the $K\bar{K}\rho$ system already appears bound if the ρK system binds the K_1, although this has to be seen in the context where the ρ has a mass

distribution and there are decay channels. In our case, with the attractive $K\bar{K}$ interaction, the formation of the molecule is further supported.

What we observe in Fig. 2.37 is exactly this situation. With just the single scattering we already get a peak, which corresponds to the bound state of ρK (or $\rho\bar{K}$) in the presence of another $\bar{K}$ (K). Allowing the interaction of the ρ with the two K, the ρ can orbit around the two K centers and produces an extra binding in the system, reflected by the peak that appears at lower energies. This corresponds to the case where the two δ functions are closer, such that the particle can orbit around the two centers of the potential.

The points made before need still a further discussion. In the case that there is a resonance of the external particle with one of the clusters, the cross section in the impulse approximation will show this peak. The experimental π deuteron cross section [374] shows clearly a peak corresponding to the formation of a $\Delta(1232)$ from the πN scattering. Can we interpret this in a similar way to the $\rho K\bar{K}$ system? There are obvious differences: we cannot claim that we have obtained a πN bound state in addition to the second nucleon. Also the peak seen in the experiment does not indicate a further binding of the Δ with the second nucleon, and can be interpreted as a ΔN propagating on shell. Actually, this kind of discussion has been raised in the Literature, and the bound K^-pp system that is obtained theoretically in many works [228,271,301,302] is reinterpreted in Ref. [320] as a bound state of a $\Lambda(1405)$ and a nucleon. Conversely, from our calculations we observe that the rescattering of the ρ with the second kaon leads to extra attraction that allows us to interpret the result as the formation of a $K_1\bar{K}$ bound state from the perspective of Ref. [320] and the discussion of the molecule done before. We see that, in any case, a bound $\rho K\bar{K}$ state, more bound than a $K_1\bar{K}$ system propagating on shell, appears in our approach.

2.5.5 Inclusion of the vector meson width

Next we come back to the discussion on improvements concerning the consideration of the ρ width.

In Eq. (2.44) we took a range of $m_\rho \pm 2\Gamma$ in the range of the ρ invariant mass to construct the $\tilde{G}$ function. This leaves out some phase space for $\rho \to \pi\pi$, which begins at $m_V = 2m_\pi$. Increasing 2Γ to 3Γ practically accounts for all the phase space and we can compare the results obtained.

We do the same for the K^*. At the same time we consider now the energy dependence of the width. For later use we define the on-shell momentum $\bar{q}$ of two particles a and b at the energy $\sqrt{s}$ of center mass frame

$$q_{cm}(\sqrt{s}, m_a, m_b) = \frac{\lambda^{1/2}(s, m_a^2, m_b^2)}{2\sqrt{s}}, \tag{2.58}$$

with the Källen function $\lambda(x, y, z) = x^2 + y^2 + z^2 - 2xy - 2yz - 2zx$ and masses of particles, m_a, m_b. With the nominal width $\Gamma^{\rm phys}$ (*e. g.*, $\Gamma_\rho^{\rm phys} \sim 150$ MeV), we utilize the following width in the spectral function of Eq. (2.44)

$$\tilde{\Gamma}_l = \Gamma_l^{\rm phys} \left(\frac{q_l}{q_l^{\rm on}} \right)^3, \tag{2.59}$$

where the momenta used are

$$\begin{aligned} q_\rho &= q_{cm}(\sqrt{s_V}, m_\pi, m_\pi)\theta(\sqrt{s_V} - 2m_\pi), \\ q_\rho^{\rm on} &= q_{cm}(m_\rho, m_\pi, m_\pi), \end{aligned} \tag{2.60}$$

for the ρ, and

$$\begin{aligned} q_{K^*} &= \bar{q}(\sqrt{s_V}, m_\pi, m_K)\theta(\sqrt{s_V} - m_\pi - m_K), \\ q_{K^*}^{\rm on} &= \bar{q}(m_{K^*}, m_\pi, m_K), \end{aligned} \tag{2.61}$$

for the K^*.

Similarly we reconsider the unstable ρ propagation in the G_0 function by using the Lehmann representation of the ρ propagator instead of the simple replacement of Eq. (2.52). Hence, Eq. (1.76) is then replaced by

$$\begin{aligned} \tilde{G}_0(\sqrt{s}) =& \frac{1}{C_\rho} \int_{(m_\rho - 3\Gamma_\rho)^2}^{(m_\rho + 3\Gamma_\rho)^2} ds_V G_0(\sqrt{s}, \sqrt{s_V}) \\ & \times \left(-\frac{1}{\pi} \right) {\rm Im} \left\{ \frac{1}{s_V - m_\rho^2 + i m_\rho \tilde{\Gamma}_\rho} \right\} \\ =& \frac{1}{C_\rho 2M_{f_0}} \int_{(m_\rho - 3\Gamma_\rho)^2}^{(m_\rho + 3\Gamma_\rho)^2} ds_V \end{aligned}$$

$$\times \int \frac{d^3q}{(2\pi)^3} F_{f_0}(q) \frac{1}{q^{02}(\sqrt{s},\sqrt{s_V}) - q^2 - s_V + i\epsilon}$$
$$\times \left(-\frac{1}{\pi}\right) \mathrm{Im}\left\{\frac{1}{s_V - m_\rho^2 + i m_\rho \tilde{\Gamma}_\rho}\right\}, \qquad (2.62)$$

with the normalization C_ρ given in Eq. (2.45) with the extended range in the integration. It should be noted that here we use the energy dependent width, $\tilde{\Gamma}_\rho$, given by Eq. (2.59). With these ingredients we show the new results in Fig. 2.39, which compared to Fig. 2.37 shows only small quantitative differences but does not change the results and conclusions drawn so far.

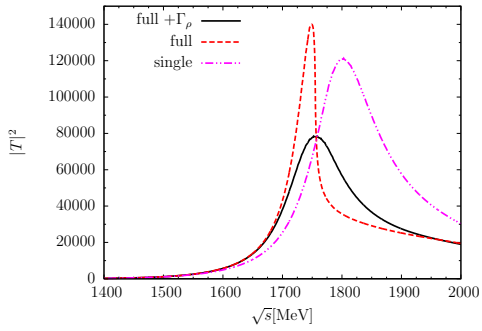

Figure 2.39: The $\rho K\bar{K}$ amplitude with the reconsideration of the phase space in the G and G_0 functions.

Step by step, the changes that we see are the following : *a*) when we extend the convolution with a range of 3Γ rather than 2Γ and use the energy dependent width, the pole for the ρK and coupled system changes from $1282 - i74$ MeV to $1298 - i72$ MeV; *b*) on the other hand when we replace the prescription of Eq. (2.52) to include the ρ width into the G_0 function, by the more accurate method of considering the spectral function of the ρ, then we obtain the results of Table 2.7, replacing tables 2.5 and 2.6. There has been a reduction of the binding by 10 MeV and of the width by 20 MeV. The changes done, however, have a bigger effect when, in addition, we consider the width of the $f_0(980)$ in the form factor of the cluster. A reduction of the mass of about 25 MeV takes place, while before it was about 10 MeV. On the other hand the width is now increased by about

22 MeV, while before it was increased by about 60 MeV. With the more accurate prescription to account for the width of the states we predict a mass of about 1732 MeV and a width of about 161 MeV. Both numbers are compatible within errors with those in the PDG.

Table 2.7: The masses and widths of dynamically generated states with the improvement of the phase space and the f_0 width, $\Gamma_{f_0} = 70.$ (in MeV)

	single	full	full + Γ_ρ	full+ $\Gamma_\rho + \Gamma_{f_0}$
Mass	1802.6	1749.2	1758.0	1732.4
Width	150.0	39.9	139.8	161.4

Another aspect that we should consider is the application of the FCA in a situation when the particle that rescatters is heavier than the one of the constituents of the cluster. The use of the FCA in that case can be unrealistic when one studies the three body system at energies above the threshold of the three particle mass. This was the case of the $\phi K\bar{K}$ system at energies around 2170 MeV, almost 170 MeV above the $\phi K\bar{K}$ threshold, as shown in Ref. [232]. The reason is that the ϕ has then enough energy to excite the $K\bar{K}$ system breaking it and spoiling the basic starting point of the FCA. The full Faddeev calculations, however, produce a resonant state which was identified with $\phi(2170)$ in Ref. [75]. Yet, if we have a three body system which is bound, the scattering particle has now no available energy for the excitation of the cluster and the FCA becomes meaningful again. This was shown in the study of the DNN system discussed before, where the NN was the cluster and the D made the multiple scattering [310]. There the ratio of the masses is $m_D/m_N \sim 2$, ever bigger than $m_\rho/m_K = 1.56$.

Another relevant information comes from the study of the $NK\bar{K}$ system, which is very close to the one studied here, with N heavier than the ρ. This system was studied in Ref. [226] using the FCA and the results were similar to those obtained by Faddeev equation in Ref. [229], leading to a N^* resonance around 1920 MeV for which experimental support could already be seen in the $\gamma p \to K^*\Lambda$ cross section around this energy [375].

We can also invoke different arguments. It is known that the FCA neglects specific steps where the $K\bar{K}$ would interact in between some initial

and final $\rho K(\rho\bar{K})$ interactions. The corrections are known as recoil corrections, and have been studied in the literature [370–372]. In Ref. [372] they are studied for the $\bar{K}NN$ system and found to go as $(m_K/m_N)^{1/2}$, leading in that case to corrections of the order of $10-15$ % of the main term. Taking this as an indication of the size of the corrections for the case of $\rho K\bar{K}$, where $(m_\rho/m_K)^{1/2}$ is 1.7 times larger than $(m_K/m_N)^{1/2}$, we could expect corrections of the order of $17-25$ %. Admitting about 30 % corrections to the main term in multiple scattering, which leads to the shift of the peak in Fig. 2.37 by about 40 MeV, we would get a correction of about 12 MeV, an uncertainty that must be certainly admitted in our approach and which is still smaller than the experimental uncertainty in the experimental mass of the $\rho(1700)$.

Finally, we would like to say some words about the possible poles in the complex plane associated to the peak of Fig. 2.37. The analytical structure of the G function for stable particles, with the cusp at threshold, leads to poles or resonances in the complex plane. If one of the particles can itself decay into two other particles, like the ρ into $\pi\pi$, the analytical structure gets complicated with branch points which are studied in detail in Ref. [366]. The poles can still appear or not and the structure in the real axis can not be trivially associated to the particular singularities of the new amplitude [366]. Sometimes poles still appear like in Ref. [362] and other times they disappear like in Ref. [373]. The analytical structure of the three body T-matrix of Eq. (1.75) is then further complicated by the analytical structure of G_0 in the denominator and the further need to account for the width of the unstable ρ particle. This is the reason why in former works of the FCA poles were not searched for. After all, the only thing that is physical is the amplitude in the real axis and the peaks that they produce, which is what the experimentalist observe. In this particular case the $\rho(1700)$ is experimentally claimed from broad peaks in cross sections of different experiments [9]. It should also be mentioned that the main decay mode is $\rho\pi\pi$, as would also come from our model when the $f_0(980)$ decays into $\pi\pi$.

2.5.6 Conclusion

Through the present paper, we construct the $\rho K\bar{K}$ three-body amplitude by means of the FCA. In our framework, a pair of $K\bar{K}$ is considered to form a scalar meson cluster $f_0(980)$, based on Ref. [16]. We use the ρK unitarized

amplitude provided by Refs. [362, 363] which respects chiral symmetry. In the three-body amplitude, we have a peak at the energy around 1732 MeV rather independent of the width of the $f_0(980)$. Besides, it is seen that the inclusion of the ρ and $f_0(980)$ width makes the peak wider and gives a good agreement with the experimental data of the $\rho(1700)$, both for the position and the width. Since the ρ decays into $\pi\pi$ mostly, the above results might be related to the dominant decay mode of the $\rho(1700)$, $\rho\pi\pi$ and 4π. Our approach to the $\rho K\bar{K}$ system provides the description of the $\rho(1700)$ as a dynamically generated state and then we conclude that the building block of the $\rho(1700)$ resonance are the ρ and $f_0(980)$.

Chapter 3

HQSS in heavy hadronic states

In the section Sec. 1.5, we have discussed about this subject. Now, along this line, we explore the ChUA, and combine the heavy quark spin symmetry (HQSS) and the local hidden gauge (LHG) symmetry, to investigate the hidden charm baryon coupled channels interaction, then, extrapolate to the hidden beauty sectors, hidden beauty baryons and hidden beauty mesons. With one more step, we also make an incursion in the open beauty and open charm sectors with these two combinations.

The LHG model is a good representation of QCD at low energies. In the pseudoscalar sector it contains the lowest order chiral Lagrangian [376, 377] and, in addition, the hidden gauge Lagrangian provides the interaction between vectors and their coupling to pseudoscalars, seen in the subsection 1.2.2. It implements the vector meson dominance hypothesis of Sakurai [378] and, within this assumption, it also provides the second order Lagrangian for pseudoscalar-pseudoscalar interaction of [377], as shown in Ref. [161]. The use of the LHG Lagrangian in connection with ChUA allows to study vector meson interactions in the intermediate energy range. This is the case for the $\rho\rho$ interaction, from where one obtains the $f_2(1270)$ and $f_0(1370)$ resonances [330] and its extension to the interactions of vectors of the ρ nonet [379], from where the $f_0(1710)$, $f_2'(1525)$ and $K_2^*(1430)$ were dynamically generated. The properties of the resonances obtained are shown to be consistent with the radiative decay to two photons [380] and to two-photon and one photon-

one vector meson in Ref. [337]. Similarly, consistency with experiment has been shown in $J/\psi \to \phi(\omega)R$ [381], with R any of the resonances of Ref. [379], and in J/ψ radiative decays in Ref. [382]. The extension of these ideas to the charm and hidden charm sector have also shown that some of the excited D states and X,Y,Z states recently reported could be explained as molecules involving charm mesons [331, 383–388].

The extension of the LHG approach to the baryon sector has also been tackled: the interaction of vector mesons with the decuplet of baryons is studied in Ref. [389] and with the octet of baryons in Ref. [390]. In both cases some dynamically generated resonances are obtained which can be associated to reported resonances in the PDG [9]. One step forward in this direction is the consideration of vector-baryon and pseudoscalar-baryon simultaneously in the interaction, which has been done in Ref. [391]. A thorough work in this direction has also been done in Refs. [392–394]. A review of the hidden gauge approach for vector-baryon and vector-nucleus interaction can be seen in Ref. [395].

As discussed in section Sec. 1.5, an element missing in principle in these works is the consideration of HQSS [233–236], which should be a good symmetry when working with mesons and baryons with charm. Work along these lines was done in Refs. [237, 238, 396, 397], where an extended Weinberg-Tomozawa (WT) interaction to four flavors is derived. The model for four flavors includes all basic hadrons (pseudoscalar and vector mesons, and $\frac{1}{2}^+$ and $\frac{3}{2}^+$ baryons) and it reduces to the WT interaction in the sector where Goldstone bosons are involved, while it incorporates HQSS in the sector where charm quarks participate. Charmed and strange baryons are studied in Ref. [238], where among other results, a HQSS doublet is associated to the three stars $\Xi_c(2790)$ and $\Xi_c(2815)$ pair of resonances. Moreover, the model derived in Ref. [238] also accommodates naturally the three stars charmed resonances $\Lambda_c(2595)$ and $\Lambda_c(2625)$. The $\Lambda_c(2595)$ was previously dynamically generated in other schemes based on t-channel vector-meson-exchange models [256, 257, 406, 407], but in Ref. [238], as first pointed out in Ref. [237], a large (dominant) ND^* component in its structure was claimed. This is in sharp contrast with the findings of the former references, where it was generated mostly as one ND bound state, since the ND^* channel was not considered in the coupled channels space. The work of Ref. [398] takes advantage of the underlying spin-flavor extended WT structure of the

couplings of the model of Refs. [237, 238] and it is used to study odd parity bottom-flavored baryon resonances by replacing a $c-$quark by a $b-$quark. Two resonances $\Lambda_b(5912)$ and $\Lambda_b(5920)$, which are HQSS partners, are predicted in Ref. [398] and turn out to be in excellent agreement with the two narrow baryon resonances with beauty recently observed by the LHCb Collaboration [399]. Finally, in Ref. [397] the model of Ref. [238] is extended to the hidden charm sector, where seven odd parity $N-$like and three $\Delta-$like states with masses around 4 GeV, most of them as bound states, are predicted, which are almost degenerate in mass. However, the HQSS does not determine the potential, simply puts some constraints in it, so the determination in the works of [237, 238, 396–398] is made assuming extra elements of SU(8) spin-isospin symmetry.

The work with baryons along these lines has run parallel to work in the meson sector [246, 247, 400–402]. In these works, an Effective Field Theory (EFT) that implements leading order (LO) HQSS constrains is constructed and its consequences are derived. The scheme, however, neither relies on SU(4) symmetry nor on spin symmetry in the light sector. Many dynamically generated resonances are obtained as HQSS partners of the $X(3872)$, $Z_b(10610)$, and the $Z_b(10650)$, some of which can be associated to known resonances, but most are predictions. Our works along these line can be seen below.

3.1 The study of hidden charm baryons

Now we investigate hidden charm baryons which come from the interaction of mesons with baryons, with the system containing a $c\bar{c}$ component. This can come from pseudoscalar-baryon or vector-baryon interactions, which was faced in Refs. [127, 168] and relatively narrow N^* and Λ^* resonances were predicted around 4.3 GeV with an extrapolation to SU(4) of the LHG dynamics used for SU(3) [156, 159, 163].

Work in the charm sector for meson-baryon interaction has been done along different lines, which share similarities with the LHG approach [256, 403–405]. A different approach is done in Ref. [406], where one uses the analogy of the work of the $\bar{K}N$ interaction and replaces a s-quark by the c-quark. As mentioned in Ref. [257], while the potentials obtained are fine with this prescription, in the coupled channel approach one is missing chan-

nels that mix charm and strangeness in that approach. In Refs. [257, 407] the work of Ref. [403] is retaken and appropriate modifications are done in the potentials and the regularization scheme. Similar work is also done by the Jülich group in Refs. [408–410]. All these works share the dynamical generation of the $\Lambda_c(2595)$, which comes mostly from the interaction of the DN channel. Some hidden charm baryonic states are also generated in Ref. [256], albeit with a binding of the order of 1000 MeV, difficult to accommodate with the generated potentials as discussed in Refs. [127, 168].

In the present work we use the LHG approach and introduce D^* and the members of the 20-plet of the Δ, as demanded by HQSS, but the dynamics linking the different pseudoscalar-baryon and vector-baryon states is taken from the hidden gauge approach. We look again in the hidden charm baryon sector, where the matrix elements obtained with the dynamics of the LHG approach respect the HQSS for the dominant terms in the mass of the heavy quarks, something that was not known so far.

3.1.1 Lowest order HQSS constraints

We study baryons with hidden charm and $I = 1/2,\ 3/2,\ J = 1/2,\ 3/2,\ 5/2$. We take as coupled channels states with $\eta_c,\ J/\psi$ and a N or a Δ, and states with $\bar{D},\ \bar{D}^*$ and $\Lambda_c,\ \Sigma_c$ or Σ_c^*. Attending to the spin quantum number we have thus 17 orthogonal states in the physical basis. Thus, we have the following space states sorted by the different $I,\ J$ quantum numbers.

1) $J = 1/2,\ I = 1/2$
   $\eta_c N,\ J/\psi N,\ \bar{D}\Lambda_c,\ \bar{D}\Sigma_c,\ \bar{D}^*\Lambda_c,\ \bar{D}^*\Sigma_c,\ \bar{D}^*\Sigma_c^*$.

2) $J = 1/2,\ I = 3/2$
   $J/\psi\Delta,\ \bar{D}\Sigma_c,\ \bar{D}^*\Sigma_c,\ \bar{D}^*\Sigma_c^*$.

3) $J = 3/2,\ I = 1/2$
   $J/\psi N,\ \bar{D}^*\Lambda_c,\ \bar{D}^*\Sigma_c,\ \bar{D}\Sigma_c^*,\ \bar{D}^*\Sigma_c^*$.

4) $J = 3/2,\ I = 3/2$
   $\eta_c\Delta,\ J/\psi\Delta,\ \bar{D}^*\Sigma_c,\ \bar{D}\Sigma_c^*,\ \bar{D}^*\Sigma_c^*$.

5) $J = 5/2,\ I = 1/2$

$\bar{D}^*\Sigma_c^*$.

6) $J = 5/2,\ I = 3/2$
$J/\psi\Delta,\ \bar{D}^*\Sigma_c^*$.

Next, we will introduce a different basis, that we will call HQSS basis, for which it is straightforward to implement the LO HQSS constraints. Thus, in present case, the 17 orthogonal states in the HQSS basis are given by

- $|S_{c\bar{c}}=0,\,\mathcal{L}=\frac{1}{2}\,;J=\frac{1}{2}\rangle_{(\ell_M=0,\,\ell_B=\frac{1}{2})}$, $|S_{c\bar{c}}=0,\,\mathcal{L}=\frac{1}{2}\,;J=\frac{1}{2}\rangle_{(\ell_M=1/2,\,\ell_B=0)}$, $|S_{c\bar{c}}=0,\,\mathcal{L}=\frac{1}{2}\,;J=\frac{1}{2}\rangle_{(\ell_M=1/2,\,\ell_B=1)}$
- $|S_{c\bar{c}}=1,\,\mathcal{L}=\frac{1}{2}\,;J=\frac{1}{2}\rangle_{(\ell_M=0,\,\ell_B=\frac{1}{2})}$, $|S_{c\bar{c}}=1,\,\mathcal{L}=\frac{1}{2}\,;J=\frac{1}{2}\rangle_{(\ell_M=1/2,\,\ell_B=0)}$, $|S_{c\bar{c}}=1,\,\mathcal{L}=\frac{1}{2}\,;J=\frac{1}{2}\rangle_{(\ell_M=1/2,\,\ell_B=1)}$
- $|S_{c\bar{c}}=1,\,\mathcal{L}=\frac{1}{2}\,;J=\frac{3}{2}\rangle_{(\ell_M=0,\,\ell_B=\frac{1}{2})}$, $|S_{c\bar{c}}=1,\,\mathcal{L}=\frac{1}{2}\,;J=\frac{3}{2}\rangle_{(\ell_M=1/2,\,\ell_B=0)}$, $|S_{c\bar{c}}=1,\,\mathcal{L}=\frac{1}{2}\,;J=\frac{3}{2}\rangle_{(\ell_M=1/2,\,\ell_B=1)}$
- $|S_{c\bar{c}}=0,\,\mathcal{L}=\frac{3}{2}\,;J=\frac{3}{2}\rangle_{(\ell_M=0,\,\ell_B=\frac{3}{2})}$, $|S_{c\bar{c}}=0,\,\mathcal{L}=\frac{3}{2}\,;J=\frac{3}{2}\rangle_{(\ell_M=1/2,\,\ell_B=1)}$
- $|S_{c\bar{c}}=1,\,\mathcal{L}=\frac{3}{2}\,;J=\frac{1}{2}\rangle_{(\ell_M=0,\,\ell_B=\frac{3}{2})}$, $|S_{c\bar{c}}=1,\,\mathcal{L}=\frac{3}{2}\,;J=\frac{1}{2}\rangle_{(\ell_M=1/2,\,\ell_B=1)}$
- $|S_{c\bar{c}}=1,\,\mathcal{L}=\frac{3}{2}\,;J=\frac{3}{2}\rangle_{(\ell_M=0,\,\ell_B=\frac{3}{2})}$, $|S_{c\bar{c}}=1,\,\mathcal{L}=\frac{3}{2}\,;J=\frac{3}{2}\rangle_{(\ell_M=1/2,\,\ell_B=1)}$
- $|S_{c\bar{c}}=1,\,\mathcal{L}=\frac{3}{2}\,;J=\frac{5}{2}\rangle_{(\ell_M=0,\,\ell_B=\frac{3}{2})}$, $|S_{c\bar{c}}=1,\,\mathcal{L}=\frac{3}{2}\,;J=\frac{5}{2}\rangle_{(\ell_M=1/2,\,\ell_B=1)}$

where, J is the total spin of the meson-baryon system; $\mathcal{L}$, total spin of the light quarks system; $S_{c\bar{c}}$, total spin of the $c\bar{c}$ subsystem; ℓ_M, total spin of the light quarks in the meson; and ℓ_B, total spin of the light quarks in the baryon. Note that we assume that all orbital angular momenta are zero, since we are dealing with ground state baryons. The approximate HQSS of QCD leads to important simplifications when the HQSS basis is used:

$$\begin{aligned}&{}_{(\ell'_M,\ell'_B)}\langle S'_{c\bar{c}},\,\mathcal{L}';J',\,\alpha'|\hat{H}|S_{c\bar{c}},\,\mathcal{L};J,\,\alpha\rangle_{(\ell_M,\ell_B)}\\&=\delta_{\alpha\alpha'}\delta_{JJ'}\delta_{S'_{c\bar{c}}S_{c\bar{c}}}\delta_{\mathcal{L}\mathcal{L}'}\langle\ell'_M\ell'_B\mathcal{L};\alpha||\hat{H}||\ell_M\ell_B\mathcal{L};\alpha\rangle\ ,\end{aligned}\tag{3.1}$$

where α stands for other quantum numbers (isospin and hypercharge), which are conserved by QCD. Note that the reduced matrix elements do not depend on $S_{c\bar{c}}$, because QCD dynamics is invariant under separate spin rotations of the charm quark and antiquark. Thus, in a given α sector, we have a total of nine unknown low energy constants (LEC's):

- Three LEC's associated to $\mathcal{L} = 3/2$

$$\begin{aligned}
\lambda_1^\alpha &= \left\langle \ell'_M = 0,\, \ell'_B = \frac{3}{2},\, \mathcal{L} = 3/2; \alpha || \hat{H} || \ell_M = 0,\, \ell_B = \frac{3}{2},\, \mathcal{L} = 3/2; \alpha \right\rangle \\
\lambda_2^\alpha &= \left\langle \ell'_M = 1/2,\, \ell'_B = 1,\, \mathcal{L} = 3/2; \alpha || \hat{H} || \ell_M = 1/2,\, \ell_B = 1,\, \mathcal{L} = 3/2; \alpha \right\rangle \\
\lambda_{12}^\alpha &= \left\langle \ell'_M = 0,\, \ell'_B = \frac{3}{2},\, \mathcal{L} = 3/2; \alpha || \hat{H} || \ell_M = 1/2,\, \ell_B = 1,\, \mathcal{L} = 3/2; \alpha \right\rangle
\end{aligned}$$

- Six LEC's associated to $\mathcal{L} = 1/2$

$$\begin{aligned}
\mu_1^\alpha &= \left\langle \ell'_M = 0,\, \ell'_B = \frac{1}{2},\, \mathcal{L} = 1/2; \alpha || \hat{H} || \ell_M = 0,\, \ell_B = \frac{1}{2},\, \mathcal{L} = 1/2; \alpha \right\rangle \\
\mu_2^\alpha &= \left\langle \ell'_M = 1/2,\, \ell'_B = 0,\, \mathcal{L} = 1/2; \alpha || \hat{H} || \ell_M = 1/2,\, \ell_B = 0,\, \mathcal{L} = 1/2; \alpha \right\rangle \\
\mu_3^\alpha &= \left\langle \ell'_M = 1/2,\, \ell'_B = 1,\, \mathcal{L} = 1/2; \alpha || \hat{H} || \ell_M = 1/2,\, \ell_B = 1,\, \mathcal{L} = 1/2; \alpha \right\rangle \\
\mu_{12}^\alpha &= \left\langle \ell'_M = 0,\, \ell'_B = \frac{1}{2},\, \mathcal{L} = 1/2; \alpha || \hat{H} || \ell_M = 1/2,\, \ell_B = 0,\, \mathcal{L} = 1/2; \alpha \right\rangle \\
\mu_{13}^\alpha &= \left\langle \ell'_M = 0,\, \ell'_B = \frac{1}{2},\, \mathcal{L} = 1/2; \alpha || \hat{H} || \ell_M = 1/2,\, \ell_B = 1,\, \mathcal{L} = 1/2; \alpha \right\rangle \\
\mu_{23}^\alpha &= \left\langle \ell'_M = 1/2,\, \ell'_B = 0,\, \mathcal{L} = 1/2; \alpha || \hat{H} || \ell_M = 1/2,\, \ell_B = 1,\, \mathcal{L} = 1/2; \alpha \right\rangle
\end{aligned}$$

This means that in the HQSS basis, the $\hat{H}$ is a block diagonal matrix, i.e, up to $\mathcal{O}(\Lambda_{QCD}/m_Q)$ corrections, $\hat{H} = \mathrm{Diag}(\mu^\alpha, \mu^\alpha, \mu^\alpha, \lambda^\alpha, \lambda^\alpha, \lambda^\alpha, \lambda^\alpha)$, where μ^α and λ^α are symmetric matrices of dimension 3 and 2, respectively.

To exploit Eq. (3.1), one should express hidden charm uncoupled meson–baryon states in terms of the HQSS basis. For those states composed of hidden charm mesons ($\ell_M = 0$) the relations are trivial,

$$\begin{aligned}
|\eta_c N; J = \frac{1}{2}\rangle &= |S_{c\bar{c}} = 0,\, \mathcal{L} = \frac{1}{2}\,; J = \frac{1}{2}\rangle_{(\ell_M = 0,\, \ell_B = \frac{1}{2})} \\
|\eta_c \Delta; J = \frac{3}{2}\rangle &= |S_{c\bar{c}} = 0,\, \mathcal{L} = \frac{3}{2}\,; J = \frac{3}{2}\rangle_{(\ell_M = 0,\, \ell_B = \frac{3}{2})} \\
|J_\Psi N; J = \frac{1}{2}\rangle &= |S_{c\bar{c}} = 1,\, \mathcal{L} = \frac{1}{2}\,; J = \frac{1}{2}\rangle_{(\ell_M = 0,\, \ell_B = \frac{1}{2})}
\end{aligned}$$

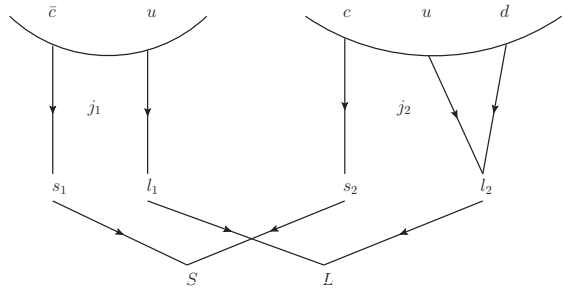

Figure 3.1: Diagrams for the 9-j coefficients evaluation.

$$
\begin{aligned}
|J_\Psi N; J=\frac{3}{2}\rangle &= |S_{c\bar{c}}=1,\ \mathcal{L}=\frac{1}{2}; J=\frac{3}{2}\rangle_{(\ell_M=0,\,\ell_B=\frac{1}{2})}\\
|J_\Psi \Delta; J=\frac{1}{2}\rangle &= |S_{c\bar{c}}=1,\ \mathcal{L}=\frac{3}{2}; J=\frac{1}{2}\rangle_{(\ell_M=0,\,\ell_B=\frac{3}{2})}\\
|J_\Psi \Delta; J=\frac{3}{2}\rangle &= |S_{c\bar{c}}=1,\ \mathcal{L}=\frac{3}{2}; J=\frac{3}{2}\rangle_{(\ell_M=0,\,\ell_B=\frac{3}{2})}\\
|J_\Psi \Delta; J=\frac{5}{2}\rangle &= |S_{c\bar{c}}=1,\ \mathcal{L}=\frac{3}{2}; J=\frac{5}{2}\rangle_{(\ell_M=0,\,\ell_B=\frac{3}{2})}
\end{aligned}
\tag{3.2}
$$

while for the other states, one needs to use 9-j symbols.

The 9-j symbols are used to relate two basis where the angular momentums are coupled in a different way. Taking two particles with $\vec{l}_1,\ \vec{s}_1$ and $\vec{l}_2,\ \vec{s}_2$, we can combine them to $\vec{j}_1,\ \vec{j}_2$ and finally $\vec{j}_1,\ \vec{j}_2$ to total $\vec{J}$. Alternatively we can couple $\vec{l}_1,\ \vec{l}_2$ to $\vec{L}$, $\vec{s}_1,\ \vec{s}_2$ to $\vec{S}$, and then $\vec{L},\ \vec{S}$ to total $\vec{J}$. These two bases are related as [411]

$$
\begin{aligned}
|l_1 s_1 j_1; l_2 s_2 j_2; JM\rangle = &\sum_{S,L}[(2S+1)(2L+1)(2j_1+1)(2j_2+1)]^{1/2}\\
&\times \left\{ \begin{array}{ccc} l_1 & l_2 & L \\ s_1 & s_2 & S \\ j_1 & j_2 & J \end{array} \right\} |l_1 l_2 L; s_1 s_2 S; JM\rangle,
\end{aligned}
\tag{3.3}
$$

where the symbol $\{\}$ stands for the 9-j coefficients.

As an example take a meson(M)-baryon(B) state of the type $\bar{D}^{(*)}B_c$ and look at the recombination scheme on Fig. 3.1. Thus in this case we have

the correspondence,

generic:	l_1	l_2	s_1	s_2	j_1	j_2	L	S	J
HQSS:	$\ell_M(\frac{1}{2})$	ℓ_B	$\frac{1}{2}$	$\frac{1}{2}$	$J_M(0,1)$	$J_B(\frac{1}{2},\frac{3}{2})$	$\mathcal{L}$	$S_{c\bar{c}}$	$J(\frac{1}{2},\frac{3}{2},\frac{5}{2})$.

with J_M and J_B the total spin of the meson and baryon respectively. Then one easily finds the physical states expressed by the HQSS basis, for example (more details seen our paper [412])

$$\begin{aligned} |\bar{D}\Lambda_c\rangle &= \frac{1}{2}|S_{c\bar{c}}=0,\,\mathcal{L}=\frac{1}{2}\,;J=\frac{1}{2}\rangle_{(\ell_M=1/2,\,\ell_B=0)} \\ &+ \frac{\sqrt{3}}{2}|S_{c\bar{c}}=1,\,\mathcal{L}=\frac{1}{2}\,;J=\frac{1}{2}\rangle_{(\ell_M=1/2,\,\ell_B=0)}, \end{aligned} \tag{3.4}$$

$$\begin{aligned} |\bar{D}\Sigma_c\rangle &= \frac{1}{2}|S_{c\bar{c}}=0,\,\mathcal{L}=\frac{1}{2}\,;J=\frac{1}{2}\rangle_{(\ell_M=1/2,\,\ell_B=1)} \\ &- \frac{1}{2\sqrt{3}}|S_{c\bar{c}}=1,\,\mathcal{L}=\frac{1}{2}\,;J=\frac{1}{2}\rangle_{(\ell_M=1/2,\,\ell_B=1)} \\ &+ \sqrt{\frac{2}{3}}|S_{c\bar{c}}=1,\,\mathcal{L}=\frac{3}{2}\,;J=\frac{1}{2}\rangle_{(\ell_M=1/2,\,\ell_B=1)}, \end{aligned} \tag{3.5}$$

Ignoring hidden strange channels, we find the following interactions, taking $J=1/2$, $I=1/2$ and $J=1/2$, $I=3/2$ for example:

- $J=1/2$, $I=1/2$

$$
\begin{array}{c}
\begin{array}{ccccccc}
\quad\eta_c N & \quad J_\Psi N & \quad \bar{D}\Lambda_c & \quad \bar{D}\Sigma_c & \quad \bar{D}^*\Lambda_c & \quad \bar{D}^*\Sigma_c & \quad \bar{D}^*\Sigma_c^*
\end{array}
\\
\left(\begin{array}{ccccccc}
\mu_1 & 0 & \frac{\mu_{12}}{2} & \frac{\mu_{13}}{2} & \frac{\sqrt{3}\mu_{12}}{2} & -\frac{\mu_{13}}{2\sqrt{3}} & \sqrt{\frac{2}{3}}\mu_{13} \\
0 & \mu_1 & \frac{\sqrt{3}\mu_{12}}{2} & -\frac{\mu_{13}}{2\sqrt{3}} & -\frac{\mu_{12}}{2} & \frac{5\mu_{13}}{6} & \frac{\sqrt{2}\mu_{13}}{3} \\
\frac{\mu_{12}}{2} & \frac{\sqrt{3}\mu_{12}}{2} & \mu_2 & 0 & 0 & \frac{\mu_{23}}{\sqrt{3}} & \sqrt{\frac{2}{3}}\mu_{23} \\
\frac{\mu_{13}}{2} & -\frac{\mu_{13}}{2\sqrt{3}} & 0 & \frac{1}{3}(2\lambda_2+\mu_3) & \frac{\mu_{23}}{\sqrt{3}} & \frac{2(\lambda_2-\mu_3)}{3\sqrt{3}} & \frac{1}{3}\sqrt{\frac{2}{3}}(\mu_3-\lambda_2) \\
\frac{\sqrt{3}\mu_{12}}{2} & -\frac{\mu_{12}}{2} & 0 & \frac{\mu_{23}}{\sqrt{3}} & \mu_2 & -\frac{2\mu_{23}}{3} & \frac{\sqrt{2}\mu_{23}}{3} \\
-\frac{\mu_{13}}{2\sqrt{3}} & \frac{5\mu_{13}}{6} & \frac{\mu_{23}}{\sqrt{3}} & \frac{2(\lambda_2-\mu_3)}{3\sqrt{3}} & -\frac{2\mu_{23}}{3} & \frac{1}{9}(2\lambda_2+7\mu_3) & \frac{1}{9}\sqrt{2}(\mu_3-\lambda_2) \\
\sqrt{\frac{2}{3}}\mu_{13} & \frac{\sqrt{2}\mu_{13}}{3} & \sqrt{\frac{2}{3}}\mu_{23} & \frac{1}{3}\sqrt{\frac{2}{3}}(\mu_3-\lambda_2) & \frac{\sqrt{2}\mu_{23}}{3} & \frac{1}{9}\sqrt{2}(\mu_3-\lambda_2) & \frac{1}{9}(\lambda_2+8\mu_3)
\end{array}\right)_{I=1/2}
\end{array}
\tag{3.6}
$$

- $J = 1/2$, $I = 3/2$

$$
\begin{array}{c}
\begin{array}{cccc} J_\Psi\Delta & \bar{D}\Sigma_c & \bar{D}^*\Sigma_c & \bar{D}^*\Sigma_c^* \end{array} \\
\left(\begin{array}{cccc}
\lambda_1 & \sqrt{\frac{2}{3}}\lambda_{12} & \frac{\sqrt{2}\lambda_{12}}{3} & -\frac{\lambda_{12}}{3} \\
\sqrt{\frac{2}{3}}\lambda_{12} & \frac{1}{3}(2\lambda_2+\mu_3) & \frac{2(\lambda_2-\mu_3)}{3\sqrt{3}} & \frac{1}{3}\sqrt{\frac{2}{3}}(\mu_3-\lambda_2) \\
\frac{\sqrt{2}\lambda_{12}}{3} & \frac{2(\lambda_2-\mu_3)}{3\sqrt{3}} & \frac{1}{9}(2\lambda_2+7\mu_3) & \frac{1}{9}\sqrt{2}(\mu_3-\lambda_2) \\
-\frac{\lambda_{12}}{3} & \frac{1}{3}\sqrt{\frac{2}{3}}(\mu_3-\lambda_2) & \frac{1}{9}\sqrt{2}(\mu_3-\lambda_2) & \frac{1}{9}(\lambda_2+8\mu_3)
\end{array} \right)_{I=3/2}
\end{array}
\tag{3.7}
$$

Note, once more, that μ and λ only depend on isospin and are independent of J.

In the present work, there is a total of 7 ($6\mu's$ and λ_2) independent LEC's for $I = 1/2$, while for $I = 3/2$, we have 4 ($3\lambda's$ and μ_3) LEC's. Thus, when one neglects open and hidden strange channels, we have a total of 11 LEC's. The extension of the WT model, using SU(8) spin-flavor symmetry [397], provides predictions for all these LEC's. Namely,[1]

$$
\begin{aligned}
I = 1/2 \quad &\rightarrow \quad \mu_1 = 0,\ \mu_2 = \mu_3 = 1,\ \mu_{12} = -\mu_{13} = \sqrt{6},\ \mu_{23} = -3,\ \lambda_2 = -2; \\
I = 3/2 \quad &\rightarrow \quad \mu_3 = -2,\ \lambda_1 = 0,\ \lambda_{12} = 2\sqrt{3},\ \lambda_2 = 4,
\end{aligned}
\tag{3.8}
$$

up to an overall $\frac{1}{4f^2}(k^0+k'^0)$ factor, being k^0 and k'^0 the center mass energies of the incoming and outgoing mesons. The extension of the LHG approach to the charm sector provides different values, as we discuss below.

3.1.2 Review of the LHG formalism

We make a short review of the formalism of the hidden gauge interaction for vector mesons which we have discussed in the subsection 1.2.2.

The philosophy of the LHG in the meson-baryon sector is that the interaction is driven by the exchange of vector mesons, as depicted in Fig. 3.2. Eqs. (1.33) and (1.34) provide the upper vertex of these Feyman diagrams.

[1] We thank L. L. Salcedo.

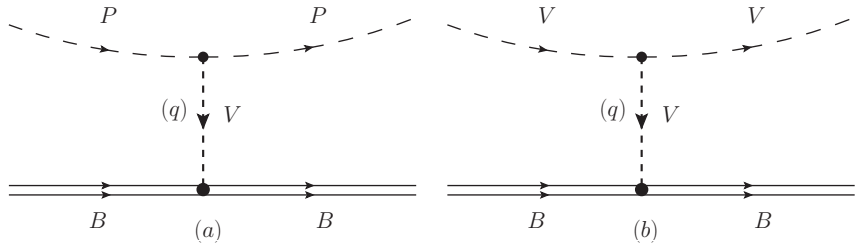

Figure 3.2: Diagrams obtained in the effective chiral Lagrangians for interaction of pseudoscalar [a] or vector [b] mesons with the octet or decuplet of baryons.

It was shown in Ref. [390] that the vertices of Eqs. (1.33) and (1.34) give rise to the same expression in the limit of small three momenta of the vector mesons compared to their mass, a limit which is also taken in our calculations. The lower vertex when the baryons belong to the octet of SU(3) is given in terms of the Lagrangian of Eq. (1.38). In the charm sector the lower vertex VBB does not have such a simple representation as in SU(3) and in practice one evaluates the matrix elements using SU(4) symmetry by means of Clebsch-Gordan coefficients and reduced matrix elements [127, 168].

The γ^μ matrix of the VBB vertex (see Eq. (1.38)) gets simplified in the approach, where we neglect the three momenta versus the mass of the particles (in this case the baryon). Thus, only the γ^0 becomes relevant, which can be taken as unity within the baryon states of positive energy that we consider. Then the transition potential corresponding to the diagram of Fig. 3.2(b) is given by

$$V_{ij} = -C_{ij} \frac{1}{4f^2} (k^0 + k'^0) \vec{\epsilon}\, \vec{\epsilon}\,', \tag{3.9}$$

where k^0, k'^0 are the energies of the incoming and outgoing vector mesons, and C_{ij} numerical coefficients evaluated as described above. The expression is the same for the pseudoscalar baryon matrix elements for the same quark content of pseudoscalar and vector mesons, omitting the $\vec{\epsilon}\, \vec{\epsilon}\,'$ factor.

The scattering matrix is evaluated by solving the coupled channels BS equation in the on shell factorization approach, Eq. (1.44), seen in the subsection 1.3.1. The iteration of diagrams produced by the BS equation

in the case of the vector mesons keeps the $\vec{\epsilon}\,\vec{\epsilon}\,'$ factor in each of the terms. Hence, the factor $\vec{\epsilon}\,\vec{\epsilon}\,'$ appearing in the potential V factorizes also in the T matrix for the external vector mesons. A consequence of this is that the interaction is spin independent and one finds degenerate states having $J^P = 1/2^-$ and $J^P = 3/2^-$. In the present work, with HQSS constraints, we shall include in the coupled channels dynamics, the pseudoscalars, vectors, baryons of spin $J = 1/2$ and $J = 3/2$, seen in Eqs. (3.6) and (3.7).

3.1.3 Evaluation of the HQSS LEC's in the LHG approach

Let us examine first the $I = 1/2$ sector. As an example let us take $\bar{D}\Lambda_c \to \bar{D}\Lambda_c$ and $\bar{D}^*\Lambda_c \to \bar{D}^*\Lambda_c$. These two interactions are equal as we discussed. This is in agreement with the general HQSS constraints explicited in Eq. (3.6) for $J = 1/2$, $I = 1/2$, where both matrix elements are equal to the LEC's μ_2. So we see that the HQSS is respected there by the LHG results. In addition the interactions of $\bar{D}\Sigma_c \to \bar{D}\Sigma_c$ and $\bar{D}^*\Sigma_c \to \bar{D}^*\Sigma_c$ are also equal. This does not contradict Eq. (3.6), it simply forces

$$\frac{1}{3}(2\lambda_2 + \mu_3) = \frac{1}{9}(2\lambda_2 + 7\mu_3), \tag{3.10}$$

which has as a solution,

$$\lambda_2 = \mu_3. \tag{3.11}$$

This has as a consequence that the matrix element of $\bar{D}^*\Sigma_c^* \to \bar{D}^*\Sigma_c^*$ is also equal to λ_2. The evaluation of this later matrix element using SU(4) Clebsch-Gordan coefficients also gives the same result as the one of $\bar{D}^*\Sigma_c \to \bar{D}^*\Sigma_c$. Once again we can see that the constraints of HQSS are fulfilled by the hidden gauge formalism, only that it gives us $\lambda_2 = \mu_3$, which is a result different to the one obtained in the approach of Ref. [397] (see Eq. (3.8)).

Let us look at the coefficient μ_1. It is related to the $\eta_c N \to \eta_c N$ or $J/\psi N \to J/\psi N$ matrix elements. In this case with the diagram of Fig. 3.3, since η_c or J/ψ have $c\bar{c}$, there is no vector that can be exchanged in Fig. 3.3 and hence this leads to

$$\mu_1 = 0. \tag{3.12}$$

This also occurs in the approach of Ref. [397] and it is a consequence of the OZI rule, that is implemented in both schemes. Let us now look at the μ_{12} parameter. This enters in $\eta_c N \to \bar{D}\Lambda_c$ transition which is depicted the

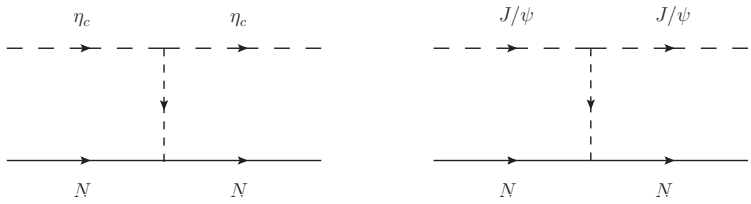

Figure 3.3: Diagrams for the $\eta_c N \to \eta_c N$ and $J/\psi N \to J/\psi N$ interactions. No vector meson exchanged is allowed.

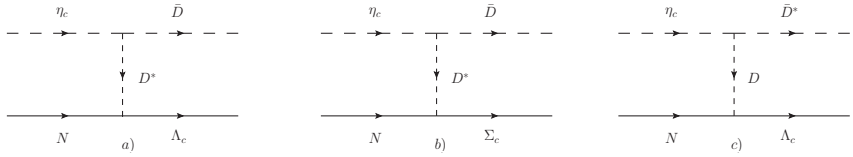

Figure 3.4: Diagrams for the $\eta_c N \to \bar{D}\Lambda_c, \bar{D}\Sigma_c, \bar{D}^*\Lambda_c$ interaction.

diagram of Fig. 3.4 a). Within the hidden gauge model, the diagram forces the exchange of a D^* and is subleading in the m_Q counting ($\mathcal{O}(m_Q^{-2})$). In the limit of $m_Q \to \infty$ this term would vanish. We, however, keep it and take it from Refs. [127,168]. Yet, because it is subleading we shall not expect the LO HQSS restrictions to hold. We also evaluate the diagram of Fig. 3.4 b), and using again SU(4) symmetry for the $D^* N \Sigma_c$ vertex (see Refs. [127,168]) we find that

$$\frac{\mu_{13}}{2} = -\frac{\mu_{12}}{2} \;\Rightarrow\; \mu_{13} = -\mu_{12}, \tag{3.13}$$

which also occurs in Ref. [397].

As to the transition from $\eta_c N \to \bar{D}^* \Lambda_c$, they are mediated by the exchange of a D meson, see Fig. 3.4 c). This term is doubly suppressed because of the D propagator and because of the Yukawa coupling, $\vec{\sigma} \cdot \vec{q}$, in $DN\Lambda_c$ vertex, where the three momentum is small compared with m_D. In Eq. (3.6) we see that this term is proportional to μ_{12}, showing again that the LO HQSS constraints does not hold for these subleading terms in the m_Q counting. In practice keeping this term, and those for $\eta_c N \to \bar{D}^* \Sigma_c$, $\bar{D}^* \Sigma_c^*$ or ignoring them has no practical repercussion on the final results.

With the dynamics of the LHG approach only the pion exchange in the

Figure 3.5: Diagrams for the pion exchange in the transition of $\bar{D}$, $\bar{D}^*$. Panels (a) and (b) correspond to the $\bar{D}\Lambda_c \to \bar{D}^*\Lambda_c$ and $\bar{D}\Lambda_c \to \bar{D}^*\Sigma_c$ transitions, respectively.

t-channel is allowed in this case, see Fig. 3.5. The $\bar{D}\Lambda_c \to \bar{D}^*\Lambda_c$ transition is zero because the π exchange is zero in the $\pi\Lambda_c\Lambda_c$ vertex. This agrees with the result of the matrix of Eqs. (3.6). However the transition $\bar{D}\Lambda_c \to \bar{D}^*\Sigma_c$ is not null and we evaluate it here.

The $\pi\Lambda_c\Sigma_c$ vertex can be obtained by analogy to the $\pi\Lambda\Sigma$ vertex in SU(3) (exchanging c and s quark) and using the Lagrangian,

$$\mathcal{L} = \frac{1}{2} D \langle \bar{B}\gamma^\mu\gamma_5\{u_\mu, B\}\rangle + \frac{1}{2} F \langle \bar{B}\gamma^\mu\gamma_5[u_\mu, B]\rangle, \tag{3.14}$$

where $u_\mu = iu^\dagger\partial_\mu U u^\dagger$, $u^2 = U = e^{i\sqrt{2}\phi/f}$ with $D = 0.80$, $F = 0.46$ from Ref. [313]. The $\bar{D}\bar{D}^*\pi$ vertex is evaluated from Eq. (1.34). We find at the end projecting over s-wave,

$$-it = \frac{1}{\sqrt{6}} \frac{M_V}{2f} \frac{2}{5} \frac{D+F}{2f} \vec{q}^{\,2}\ \vec{\sigma}\cdot\vec{\epsilon}\ \frac{i}{q^{0\ 2} - \vec{q}^{\,2} - m_\pi^2}, \tag{3.15}$$

with $\vec{q}$ the momentum transfer.

One can also prove that the matrix element of $\vec{\sigma}\cdot\vec{\epsilon}$ is $\sqrt{3}$ [391]. If we compare this contribution of this diagram with that of the $\bar{D}\Lambda_c \to \bar{D}\Lambda_c$ transition from Refs. [127,168], we find a contribution of the order of 7%. If one looks at diagonal matrix elements in the final scattering T-matrix, the non diagonal terms of the transition potentials come squared and then we can safely neglect this contribution. Thus we take

$$\mu_{23} = 0. \tag{3.16}$$

Note that the transitions $\bar{D}\Sigma_c \to \bar{D}^*\Sigma_c$, $\bar{D}^*\Sigma_c^*$ also require the pion exchange and should be taken zero. This is consistent with the matrix of Eq.

(3.6) since these matrix elements are proportional to $\lambda_2 - \mu_3$ but we saw before that $\lambda_2 = \mu_3$.

When evaluating the pion exchange mechanism in the $VB \to VB$ transition one has to consider the equivalent contact term that in the case of $\gamma N \to \pi N$ scattering is known as the Kroll Ruderman term. Explicit expressions to obtain it can be found from Refs. [391–394] and is of the same order of magnitude as the pion exchange term, with usually destructive interference.

With this exercise we have proved that the dynamics of the LHG approach is fully consistent with the HQSS requirements for the matrix of Eq. (3.6). The values for the parameters that we obtain from Refs. [127, 168], together with those determined here, are

$$\begin{aligned} \mu_2 &= \frac{1}{4f^2}(k^0 + k'^0), \quad \mu_3 = -\frac{1}{4f^2}(k^0 + k'^0), \\ \mu_{12} &= -\sqrt{6}\ \frac{m_\rho^2}{p_{D^*}^2 - m_{D^*}^2}\ \frac{1}{4f^2}\ (k^0 + k'^0), \\ \mu_1 &= 0, \quad \mu_{23} = 0, \quad \lambda_2 = \mu_3, \quad \mu_{13} = -\mu_{12}. \end{aligned} \tag{3.17}$$

μ_{12} is small, of the order of 15%. But we keep it since this term is the only one that allows the scattering $\eta_c N \to \eta_c N$ ($J/\psi N \to J/\psi N$) through intermediate inelastic states. As we discussed before, μ and λ only depend on isospin and are independent of spin J, therefore, Eq. (3.17) is general for all isospin $I = 1/2$ sectors with different J.

The matrix of Eq. (3.7) for $J = 1/2$, $I = 3/2$ is equally analyzed. We find

$$\lambda_1 = 0. \tag{3.18}$$

Then λ_{12} is also suppressed since it requires again the exchange of a D meson, see Fig. 3.6. Once again, since the $\bar{D}\Sigma_c \to \bar{D}\Sigma_c$ transition is equivalent to $\bar{D}^*\Sigma_c \to \bar{D}^*\Sigma_c$. This implies that

$$\frac{1}{3}(2\lambda_2 + \mu_3) = \frac{1}{9}(2\lambda_2 + 7\mu_3), \tag{3.19}$$

from where we conclude again that

$$\lambda_2 = \mu_3. \tag{3.20}$$

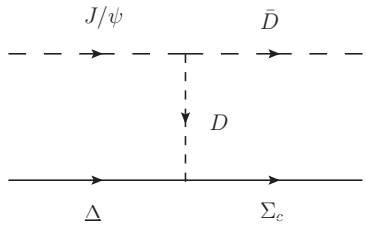

Figure 3.6: Diagrams for the $J/\psi\Delta \to \bar{D}\Sigma_c$ interaction.

Once again the $\bar{D}\Sigma_c \to \bar{D}^*\Sigma_c,\ \bar{D}\Sigma_c^*$ transitions involve pion exchange and we find them negligible, which is compatible with the HQSS requirement since $\mu_3 - \lambda_2 = 0$. The values that we obtain with this isospin combination are then

$$\begin{aligned} \lambda_{12} &= 3\sqrt{3}\ \frac{m_\rho^2}{p_{D^*}^2 - m_{D^*}^2}\ \frac{1}{4f^2}\ (k^0 + k'^0), \\ \mu_3 &= 2\frac{1}{4f^2}(k^0 + k'^0), \quad \lambda_2 = \mu_3, \quad \lambda_1 = 0, \end{aligned} \tag{3.21}$$

which is general for all isospin $I = 3/2$ sectors.

3.1.4 Results

We use the BS equation of Eq. (1.44) in coupled channels to evaluate the scattering amplitudes. We take the usual dimensional regularization formula [194] of Eq. (1.46) for the G function. This formula avoids an undesired behaviour at large energies when one uses a cut off method with a small cut off [195]. As done in Refs. [127, 168], we take $\mu = 1000$ MeV, $a(\mu) = -2.3$ for the parameters in Eq. (1.46), which are the only free parameters in our present study. We solve the BS equation of Eq. (1.44) in coupled channels and look for poles in the second Riemann sheet when there are open channels, or in the first Riemann sheet when one has stable bound states (see [168, 362] for details).

Let $\sqrt{s_p}$ be the complex energy where a pole appears. Close to a pole the amplitude behaves as

$$T_{ij} = \frac{g_i g_j}{\sqrt{s} - \sqrt{s_p}}\ . \tag{3.22}$$

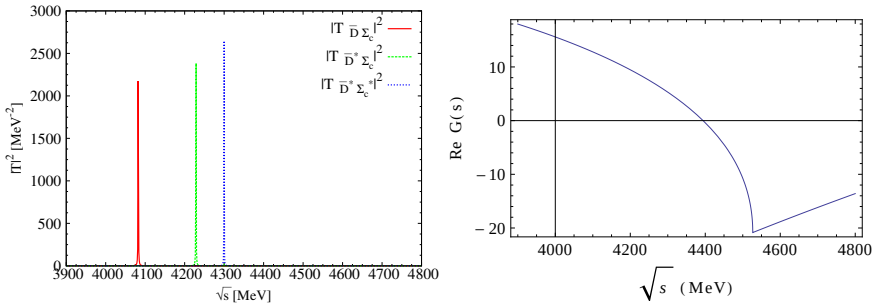

(a) (b)

Figure 3.7: The results of the $J = 1/2,\ I = 3/2$ sector. (a): The squared amplitudes of three channels except for $J/\psi\Delta$ channel. (b): The real parts of G function in $\bar{D}^*\Sigma_c^*$ channel.

where g_i is the coupling of the resonance to the i channel. As one can see in Eq. (3.22), $g_i g_j$ is the residue of T_{ij} at the pole. For a diagonal transitions we have (for meson-baryon interaction)

$$g_i^2 = \lim_{\sqrt{s}\to\sqrt{s_p}} T_{ii}\,(\sqrt{s} - \sqrt{s_p}). \tag{3.23}$$

The determination of the couplings gives us an idea of the structure of the states found, since according to [95, 205], the couplings are related to the wave function at the origin for each channel.

Let us begin with the $J = 1/2,\ I = 3/2$ sector. We can see in Eq. (3.21) that the large potentials are repulsive. So, we should not expect any bound states or resonances. Yet, technically we find bound states in the first Riemann sheet, as one can see in Fig. 3.7(a) for different channels. However, inspection of the energies tell us that these are states bound by about 250 MeV, a large number for our intuition, even more when we started from a repulsive potential. The reason for this, which forces us to reject these poles on physical grounds, is that the G function below threshold turns out to be positive for large binding energies (see Fig. 3.7(b) and discussions in Ref. [128]), contradicting what we would have for the G function evaluated with any cut off, or in Quantum Mechanics with a given range. These poles are then discarded and, thus, we do not find bound states or resonances in $I = 3/2$ in our approach. On the other hand, the WT extended model

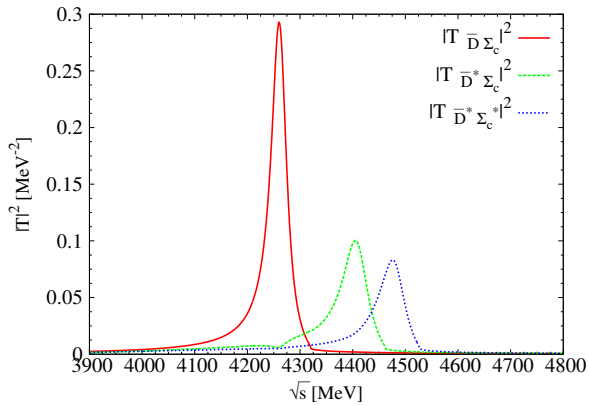

Figure 3.8: The squared amplitudes of the $J = 1/2,\ I = 1/2$ sector.

of Ref. [397] predicts $\mu_3 = -2$, which leads to three odd parity $\Delta-$like resonances with masses around 4 GeV. In addition, two other states show up as cusps very close to the $\Delta J/\psi$ threshold, and their real existence would be unclear.

Our results for the $J = 1/2,\ I = 1/2$ sector are shown in Fig. 3.8. From the squared amplitudes of $|T|^2$, we can find three clear peaks with non zero width around the energy range $4200 \sim 4500$ MeV, which are not far away below the thresholds of $\bar{D}\Sigma_c,\ \bar{D}^*\Sigma_c,\ \bar{D}^*\Sigma_c^*$ respectively. The relatively small width of about 40 MeV of these states allows to distinguish them clearly. We have checked that in the energy ranges where these peaks appear, the real parts of the loop function G, Eq. (1.45), are negative in these channels. Thus these peaks are acceptable as physical ones. Then, we look for the poles corresponding to these peaks in the second Riemann sheet, and find the poles at $(4261.87 + i17.84)$ MeV, $(4410.13 + i29.44)$ MeV, $(4481.35 + i28.91)$ MeV. The couplings to the various coupled channels for these poles are given in Table 3.1. From Table 3.1 we can see that the first pole, $(4261.87 + i17.84)$ MeV, couples mostly to $\bar{D}\Sigma_c$. It could be considered like a $\bar{D}\Sigma_c$ bound state which, however, decays into the open channels $\eta_c N$ and $J/\psi N$. The $\bar{D}\Sigma_c$ threshold is at 4320.8 MeV and, thus, the $\bar{D}\Sigma_c$ state is bound by about 58 MeV. The second pole couples most strongly to $\bar{D}^*\Sigma_c$. In this channel the threshold is 4462.2 MeV and thus we have a state bound by about 52 MeV, much in line with what one expects from heavy quark

Table 3.1: The coupling constants of all channels corresponded certain poles in the $J = 1/2,\ I = 1/2$ sector.

$4261.87 + i17.84$							
	$\eta_c N$	$J/\psi N$	$\bar{D}\Lambda_c$	$\bar{D}\Sigma_c$	$\bar{D}^*\Lambda_c$	$\bar{D}^*\Sigma_c$	$\bar{D}^*\Sigma_c^*$
g_i	$1.04 + i0.05$	$0.76 - i0.08$	$0.02 - i0.02$	$3.12 - i0.25$	$0.14 - i0.48$	$0.33 - i0.68$	$0.16 - i0.28$
$\lvert g_i\rvert$	1.05	0.76	0.02	3.13	0.50	0.75	0.32
$4410.13 + i29.44$							
	$\eta_c N$	$J/\psi N$	$\bar{D}\Lambda_c$	$\bar{D}\Sigma_c$	$\bar{D}^*\Lambda_c$	$\bar{D}^*\Sigma_c$	$\bar{D}^*\Sigma_c^*$
g_i	$0.34 + i0.16$	$1.43 - 0.12$	$0.15 - i0.10$	$0.20 - i0.05$	$0.17 - i0.11$	$3.05 - i0.54$	$0.07 - i0.51$
$\lvert g_i\rvert$	0.38	1.44	0.18	0.20	0.20	3.10	0.51
$4481.35 + i28.91$							
	$\eta_c N$	$J/\psi N$	$\bar{D}\Lambda_c$	$\bar{D}\Sigma_c$	$\bar{D}^*\Lambda_c$	$\bar{D}^*\Sigma_c$	$\bar{D}^*\Sigma_c^*$
g_i	$1.15 - i0.04$	$0.72 + i0.03$	$0.18 - i0.08$	$0.10 - i0.03$	$0.09 - i0.08$	$0.09 - i0.06$	$2.88 - i0.57$
$\lvert g_i\rvert$	1.15	0.72	0.19	0.10	0.12	0.11	2.93

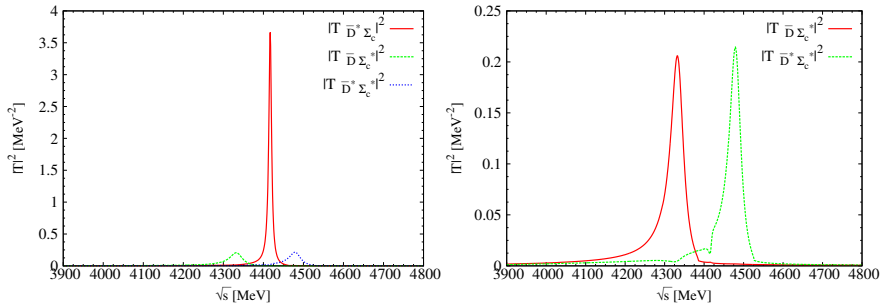

Figure 3.9: The results of $|T|^2$ for the $J = 3/2,\ I = 1/2$ sector. To the right the two small peaks of the left figure magnified.

symmetry comparing this with the former state. This state decays mostly into the $\eta_c N$ and $J/\psi N$ channels again. These two states correspond to those reported in Refs. [127, 168], and also the first one, $\bar{D}\Sigma_c$ state, is consistent with the results using different models [201, 202]. In our work, we get one more new baryon state, $(4481.35 + i28.91)$ MeV, with total momentum $J = 1/2$, which couples mostly to $\bar{D}^*\Sigma_c^*$. Since in Refs. [127, 168] one did not include the baryons of $J^P = 3/2^+$, their consideration here leads to a new resonance. The threshold for the $\bar{D}^*\Sigma_c^*$ channel is 4526.7 MeV and, hence, the state can be considered as a $\bar{D}^*\Sigma_c^*$ bound state by about 46 MeV, which decays mostly in $\eta_c N$ and $J/\psi N$.

For the $J = 3/2,\ I = 1/2$ sector, we show our results in Fig. 3.9. From the results of $|T|^2$, we can also see three clear peaks around the range $4300 \sim 4500$ MeV, which are not far away below the thresholds of $\bar{D}\Sigma_c^*,\ \bar{D}^*\Sigma_c,\ \bar{D}^*\Sigma_c^*$ respectively. The strength of the second peak is 17 times bigger than the other two and the widths are small enough to allow the peaks to show up clearly. We have also checked that in these channels the real parts of the propagator G, Eq. (1.45), are acceptable too. So, these are our predictions for the new baryon states with total momentum $J = 3/2$. We search the poles in the second Riemann sheet, and find $(4334.45 + i19.41)$ MeV, $(4417.04 + i4.11)$ MeV, $(4481.04 + i17.38)$ MeV. The couplings to each coupled channel corresponding to these poles are listed in Table 3.2. From Table 3.2, we find that the first pole, $(4334.45 + i19.41)$ MeV, couples most strongly to the channel $\bar{D}\Sigma_c^*$ and corresponds to a $\bar{D}\Sigma_c^*$ state, bound by 51 MeV with respect to its threshold of 4385.3 MeV,

Table 3.2: The coupling constants to various channels for certain poles in the $J = 3/2,\ I = 1/2$ sector.

$4334.45 + i19.41$	$J/\psi N$	$\bar{D}^*\Lambda_c$	$\bar{D}^*\Sigma_c$	$\bar{D}\Sigma_c^*$	$\bar{D}^*\Sigma_c^*$
g_i	$1.31 - i0.18$	$0.16 - i0.23$	$0.20 - i0.48$	$2.97 - i0.36$	$0.24 - i0.76$
$\lvert g_i \rvert$	1.32	0.28	0.52	2.99	0.80
$4417.04 + i4.11$	$J/\psi N$	$\bar{D}^*\Lambda_c$	$\bar{D}^*\Sigma_c$	$\bar{D}\Sigma_c^*$	$\bar{D}^*\Sigma_c^*$
g_i	$0.53 - i0.07$	$0.08 - i0.07$	$2.81 - i0.07$	$0.12 - i0.10$	$0.11 - i0.51$
$\lvert g_i \rvert$	0.53	0.11	2.81	0.16	0.52
$4481.04 + i17.38$	$J/\psi N$	$\bar{D}^*\Lambda_c$	$\bar{D}^*\Sigma_c$	$\bar{D}\Sigma_c^*$	$\bar{D}^*\Sigma_c^*$
g_i	$1.05 + i0.10$	$0.18 - i0.09$	$0.12 - i0.10$	$0.22 - i0.05$	$2.84 - i0.34$
$\lvert g_i \rvert$	1.05	0.20	0.16	0.22	2.86

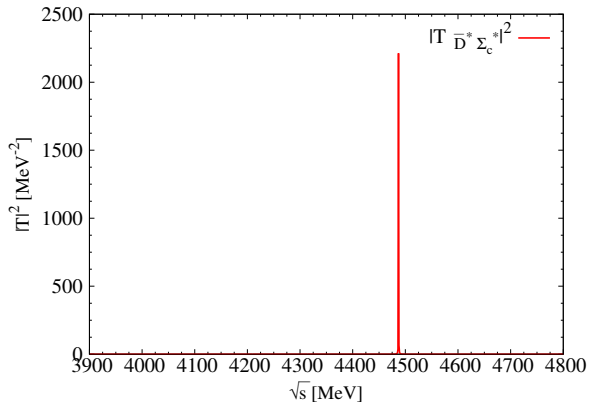

Figure 3.10: The results of $|T|^2$ for the $J = 5/2,\ I = 1/2$ sector.

decaying essentially into $J/\psi N$. The state corresponding to the big peak in Fig. 3.9 (left) couples mostly to $\bar{D}^*\Sigma_c$, it is bound by 45 MeV with respect to the threshold of this channel, 4462.2 MeV and decays mostly into $J/\psi N$. The third state with $J = 3/2,\ I = 1/2$ couples mostly to $\bar{D}^*\Sigma_c^*$, is bound by 45 MeV with respect to the threshold of this channel, 4526.7 MeV and also decays mostly into $J/\psi N$.

Finally, we also find a new bound state of $\bar{D}^*\Sigma_c^*$ around $(4487.10 + i0)$ MeV in the $J = 5/2,\ I = 1/2$ sector, seen in Fig. 3.10. As we can see in the figure, the state has no width, as it corresponds to a single channel, $\bar{D}^*\Sigma_c^*$. It is then a bound state in this channel. The pole appears in the first Riemann sheet and the state is bound by about 40 MeV with respect to the $\bar{D}^*\Sigma_c^*$ threshold.

3.1.5 HQSS and SU(4) symmetry breaking

The results obtained in the former sections rely upon exact HQSS and SU(4) symmetries. We expect some breaking of these symmetries and we study uncertainties of the results tied to these sources.

Yet, when one talks about SU(3) or SU(4) breaking one must be more specific on what magnitude one is talking about. The different masses of the quarks or mesons and baryons associated to the group multiplets are largely responsible for the symmetry breaking of some magnitudes. There is

a clear example of a large SU(3) breaking which is tied to the unitarization and not to elementary vertices [277,419]: when the masses in the two octets are taken as the physical ones the octet splits into two branches and the singlet moves its position, thus, one of the two octets becomes the $\Lambda(1670)$ while the other one gives rise to the second $\Lambda(1405)$ pole at 1420 MeV. This example is telling us that the SU(3) (or SU(4)) symmetry should be assumed in elementary vertices where the masses do not play a role, while one should be ready to accept large breaking in some physical magnitudes where the different scales in the masses are bound to have an effect. A further discussion along these lines can be seen in section II.D of Ref. [168], and uncertainties related to SU(4) breaking are also discussed in section V of Ref. [331].

Contrary to some expectations that SU(4) symmetry should be badly broken by a much larger amount than SU(3), when applied to elementary couplings it works better than expected, as one can see in radiative decays and associated processes [165].

But we want to be more specific here and we concentrate on the vertices that appear in our theory. In the LHG approach the leading term in the meson baryon interaction is provided by the mechanism of Fig. 3.2, exchanging light vector mesons. We will concentrate on the $DD\rho$ vertex for which there are evaluations using the Dyson-Schwinger Equation [413] and QCD lattice gauge simulations [414]. The coupling $g_{DD\rho}$ is obtained in Ref. [413] with the value $g_{DD\rho} \simeq 5$ and in [414], with the value $g_{DD\rho} \simeq 4.9$, which contrasts with the SU(4) value of $g_{DD\rho} = g_{KK\rho} \simeq 2$ obtained in Ref. [408].

One might think that the use of this new coupling, increasing considerably the strength of the potential, will change drastically the results obtained. One can guess that changes would not be so drastic, because, simultaneously with this large coupling, a form factor arises and one has an effective coupling

$$F_{DD\rho}(\vec{q}^{\,2}) \equiv g_{DD\rho}\tilde{F}(\vec{q}^{\,2}), \quad \tilde{F}(\vec{q}^{\,2}) = \frac{\Lambda^2}{\Lambda^2 + \vec{q}^{\,2}}, \tag{3.24}$$

with $\Lambda \simeq 0.7$ GeV, which softens the interaction in the loops. We can actually see the effects of such new couplings in the binding energy in our problem. For this purpose we choose one of the cases, $J = 1/2, \quad I = 1/2$ (for the other cases the effects are similar). Then, following Ref. [206], we

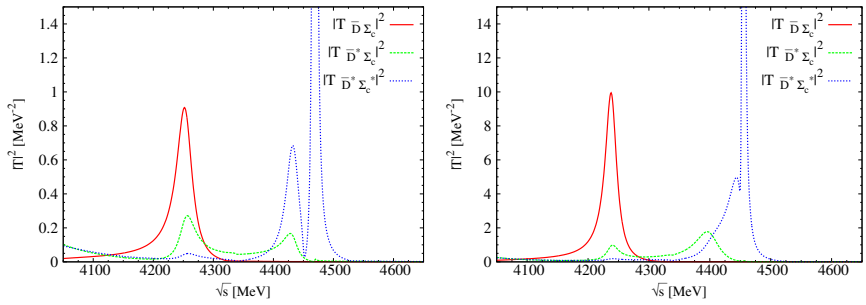

Figure 3.11: The results of squared amplitudes for the $J = 1/2$, $I = 1/2$ sector: (a) With $q_{max} = 820$ MeV; (b) With $q_{max} = 820$ MeV but with the modified potential of Eq. (3.25).

change a bit the present formalism to incorporate the form factor $\tilde{F}(\vec{q}^{\,2})$ of Eq. (3.24). We assume that the lower vertex $BB\rho$ does not change with respect to the one we have. This exercise is sufficient to have a feeling of the uncertainties that we have for adhering to SU(3) or SU(4) symmetry. Then we use Eq. (1.44) to obtain the $\tilde{T}$ matrix but, according to Ref. [206], now we have

$$\begin{aligned} V \to \tilde{V} &\equiv \frac{g_{DD\rho}(new)}{g_{DD\rho}(SU(4))} V, \\ G \to \tilde{G} &= \int \frac{d^3\vec{q}}{(2\pi)^3} \tilde{F}^2(\vec{q}^{\,2}) \frac{\omega_P + \omega_B}{2\,\omega_P\,\omega_B} \frac{2M_B}{P^{0\,2} - (\omega_P + \omega_B)^2 + i\varepsilon}, \end{aligned} \tag{3.25}$$

with ω_P, ω_B, M_B, P^0 the relativitic energy of the pseudoscalar, baryon, mass of the baryon and total energy of the system, respectively. To implement the form factor we have to use an explicit momentum integration for $\tilde{G}$ in Eq. (3.25), instead of the dimensional regularization formula used so far. For this purpose we find first the cut off q_{max}, in the integration, such that the results are similar to those found with dimensional regularization. This q_{max} is found around $q_{max} = 820$ MeV, similar to what was used in Refs. [127, 168].

The results with the modified potential can be seen in Fig. 3.11, compared to those obtained using $q_{max} = 820$ MeV with no modification of the potential (this is obtained using $\tilde{G}$ in Eq. (3.25) with $\tilde{F}(\vec{q}^{\,2}) = 1$). The same three

peaks in $|T|^2$ appear now, albeit with different strength and at different energies. Since our only concern is to see if there are bound states and have an estimate on the binding energy, we can see that this is indeed the case, and the binding energies are changed, but within the same order of magnitude. If we compare the results in Fig. 3.11 with those of dimensional regularization of Fig. 3.8, we can see that the lower and higher peaks have both changed by about 12 MeV. The middle one has changed by a similar amount but in opposite direction (this is consequence of interference of coupled channels). What we see is that we have differences of $\pm(10 \sim 15)$ MeV in the bindings from using different regularization methods on the loop function. We must accept these as systematic uncertainties of our approach.

If now we compare the two figures (a) and (b) in Fig. 3.11, we can see that the effect of using the increased $g_{DD\rho}$ coupling and the form factor simultaneously is an increase of the binding by $12 \sim 14$ MeV for the lower and upper states (the small side structure in the upper peak comes from a numerical artifact of no physical meaning), and the middle one is shifted by 36 MeV, but compared to the results of dimensional regularization by 21 MeV. The changes obtained from this source are of the same order of magnitude as changes from using two different regularization methods.

The other issue we want to discuss is the effect on the breaking of the HQSS. While being a result of QCD for the dominant term in m_Q, the question is how relevant numerically can be the subleading corrections, terms of $\mathcal{O}(m_Q^0)$ in the potential in our formalism. One estimate can be provided by the relevance of the contact terms in the vector-vector interaction in the LHG approach. These terms are indeed one order lower in m_Q in the potential and hence subdominant. Yet, numerically they correspond to corrections of the order of 20 % in the charm sector. In the beauty sector the corrections are much smaller, and HQSS is assumed to be very accurate there. The 20 % violation of this symmetry in the charm sector is in line with findings in lattice QCD, or the Dyson-Schwinger equation. Indeed, in Ref. [414] it is found that $g_{DD\rho} \simeq 4.90$ while $g_{D^*D^*\rho} \simeq 5.42$. Similar breakings are found in the D or D^* decay constants (f_D, f_{D^*}) in Ref. [415] from QCD lattice gauge calculations, comparing g_{D_sDK} and g_{B_sBK} in Ref. [416], evaluated with the Dyson-Schwinger equations, in the QCD lattice evaluation of the D^{*0} magnetic moment [417], or in the QCD sum rule evaluation of the $DD\rho$ and $D^*D^*\rho$ couplings [418].

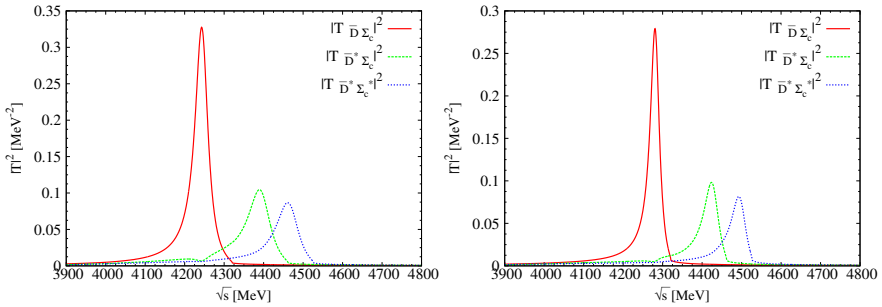

Figure 3.12: The results of squared amplitudes for the $J = 1/2,\ I = 1/2$ sector, which have a modified factor to the potentials. Left: $1.20 \times V$; Right: $0.80 \times V$.

In view of these findings we perform an exercise as the former one, evaluating the T matrix with the interaction used in the former chapter multiplied by 1.20 or 0.80 respectively. The results can be seen in Fig. 3.12 for $J = 1/2,\ I = 1/2$. We can see that with respect to the results with weight unity in the potential, the results with $1.20 \times V$ lead to a binding increased by about 15 MeV, while those with $0.80 \times V$ produce smaller bindings, with energies shifted by about 20 MeV. The former exercises have shown that the changes produced by using different couplings obtained in other approaches to QCD, with a certain amount of SU(4) or HQSS breaking, induce changes of the order of $20-30$ MeV in bindings estimated in our approach to be of the order of 50 MeV. These uncertainties are in line with other systematic uncertainties that we must also admit from our partial ignorance in the scale of regularization in the loops. Yet, with all these uncertainties admitted, the binding of the states remains as a solid conclusion.

3.1.6 Discussion

The results reported in Ref. [397] show a certain parallelism with those found here. There, seven odd parity $N-$like states were also found (three with spin 1/2 and 3/2 and a further one with spin 5/2). Moreover, the dynamics of these resonances is strongly influenced by the $\bar{D}^{(*)}\Sigma_c^{(*)}$ components, as it is the case here. Their masses, however, are quite, differ-

ent, since those found in Ref. [397] lie in the region of 4 GeV, being thus significantly lighter than those found in our work. Besides differences of dynamical origin that can help to understand these changes in the position of the masses, there exists a major difference among both approaches in what concerns the renormalization of the loop function, $G(s)$, in the coupled channels space. The baryon-meson propagator is logarithmically ultraviolet divergent, thus, the loop needed to be renormalized. Here, we use Eq. (1.46) with a scale $\mu = 1000$ MeV and the subtraction constant $a(\mu) = -2.3$, as done in Refs. [127,168]. However in Ref. [397], a subtraction point regularization is chosen such that $G_{ii}(s) = 0$ at a certain energy point, which was first proposed in Refs. [256, 405] and it was successfully used in Refs. [419,420] for three light flavors and in the open charm (bottom) studies carried out in Refs. [237, 238, 396] ([398]). Indeed, a significant part of the differences between the masses of the resonances found here and those reported in Ref. [397] can be attributed to the different renormalization procedure followed in both works. We would like to finish this discussion just stressing again that, ignoring the difference in the mass positions, the isospin 1/2 states found in this work have a clear resemblance with those reported in Ref. [397].

3.1.7 Conclusions

In the present work we have addressed a relevant topic which is to show the consistency of the dynamics of the LHG Lagrangians extrapolated to SU(4) with the LO constraints of HQSS. Once again the requirements of HQSS demanded that we put together pseudoscalar and vector mesons, as well as baryons with $J = 1/2, 3/2$, from which we can obtain the transition potentials between the different meson-baryon channels in different combinations of spin and isospin. After this, we evaluated these matrix elements using the dynamics of the LHG approach and found them to fulfil all the relationships of LO HQSS. We found seven states with different energies or different spin-isospin quantum numbers. Yet, the fact that the interaction that we had for vector-baryon factorizes as $\epsilon \cdot \epsilon'$ produces matrix elements which are degenerate in the different spins allowed by the meson-baryon combinations. Hence, up to some different mixing with subleading channels, we found a very approximate degeneracy in the states that qualify as quasibound $\bar{D}^* B$. In view of this, the seven states that we found could

be more easily classified as four basic states corresponding to a quasibound $\bar{D}\Sigma_c$ state which appears in $J = 1/2$, a $\bar{D}\Sigma_c^*$ state in $J = 3/2$, a $\bar{D}^*\Sigma_c$ state which appears nearly degenerate in $J = 1/2,\ 3/2$ and a $\bar{D}^*\Sigma_c^*$ state which appears nearly degenerate in $J = 1/2,\ 3/2,\ 5/2$. All the states are bound with about 50 MeV with respect to the corresponding $\bar{D}B$ thresholds and the width, except for the $J = 5/2$ state, is also of the same order of magnitude. The $J = 5/2$ state which appears in the single $\bar{D}^*\Sigma_c^*$ channel has the peculiarity that it has zero width in the space of states chosen. All the states found appear in $I = 1/2$ and we found no states in $I = 3/2$. We have also made some exercise estimating uncertainties from the breaking of SU(4) and HQSS. While they introduce indeed changes in the binding energies, the results on the appearance of the bound states are stable under these changes, as well as the order of magnitude of the binding, with binding energies that can increase by $30-50$ %.

3.2 The study of hidden beauty baryons

Under the SU(3) symmetry, the LHG Lagrangian with the coupled channel unitary approach can explain the structure, properties and dynamics of many states which are confirmed in the PDG [9]. With this formalism, the $\rho\rho$ interaction is studied in Ref. [330], and provides a natural explanation of the meson states $f_0(1370)$ and $f_2(1270)$ and one obtains the masses and widths of the two particles in fair agreement with experimental results. Along the same line, the work of Ref. [379] successfully finds 11 states in the vector meson-vector meson interaction, five of which are identified as $f_0(1370)$, $f_0(1710)$, $f_2(1270)$, $f_2(1525)$, and $K_2^*(1430)$, reported in the PDG and regarded as molecular states, and the other ones are predictions. One of the predicted states h_1 $[I^G(J^{PC}) = 0^-(1^{+-})]$ around 1800 MeV finds support from a posterior BES experiment on the $J/\psi \to \eta K^{*0}\bar{K}^{*0}$ [421] as discussed in Refs. [422–424]. An extension of this method to the case of the nonet of vectors interacting with the decuplet baryons is done in Refs. [389, 425], dynamically generating some resonances found in PDG. Turning to the vector nonet-baryon octet interactions, there are results obtained about $J^P = 1/2^-$, $3/2^-$ particles in the work of Ref. [390]. Extension of these ideas to incorporate simultaneously pseudoscalar mesons, vector mesons and baryons is done in Refs. [391–394]. The meson-meson interaction with charm is studied in [331, 383, 384], which dynamically generates the particles $D_2^*(2460)$, $X(3940)$, $Z(3930)$, $X(4160)$ and $D_{s2}^*(2573)$. For the meson-baryon interaction, the works [127, 168] extrapolate the hidden gauge formalism with the coupled channel approach to the hidden charm sector, and dynamically generate some narrow N^* and Λ^* resonances around 4.3 GeV, not listed in the PDG. Analogously, the work of Ref. [128] extends this later formalism to the hidden beauty sector and also predicts several N^* and Λ^* states with narrow width and energies around 11 GeV.

On the other hand, in the heavy quark sectors there is another symmetry, heavy quark spin-flavour symmetry as stated in Refs. [233–236] (seen in the section Sec. 1.5), or only HQSS as described in Ref. [401], which predicts an $\eta_c' f_0(980)$ bound state, suggested as the spin-doublet partner of the $Y(4660)$ theoretically proposed as a $\psi' f_0(980)$ bound state in Ref. [426]. Incorporating the HQSS and the effective field theory, the charmed meson-antimeson system is investigated in Refs. [246, 247, 400, 427], predicting six hidden charm states as HQSS partners of the $D\bar{D}^*$ bound state, $X(3872)$, two of

which are assumed to be $X(3915)$, a $D^*\bar{D}^*$ molecular state, and $Y(4140)$, a $D_s^*\bar{D}_s^*$ molecular state. In Refs. [237, 238, 396–398] an SU(8) spin-flavour symmetry is invoked, within the framework of the unitary coupled channel approach for the meson-baryon interactions, and some charmed and strange baryon resonances are produced dynamically in their theoretical models. A step forward in this direction is given in the former work (Ref. [412]) combining the LHG formalism and HQSS, and using a unitary coupled channel method, making a prediction of four hidden charm states with relatively small widths. In the present work, we extrapolate this later approach to the hidden beauty sector. We also propose a natural way to regularize the loops which removes ambiguities encountered in other works [128].

3.2.1 HQSS and LHG Formalism

Following the former work (Ref. [412]), seen in last section, we extrapolate the formalism to the hidden beauty sector by just changing the $\bar{D}$ meson to a B meson and $\bar{c}$-quark to $\bar{b}$-quark. Therefore we can study baryons with hidden beauty with isospin $I = 1/2,\ 3/2$, and spin $J = 1/2,\ 3/2,\ 5/2$. We take as coupled channels states with η_b, Υ and a N or a Δ, and states with B, B^* and Λ_b, Σ_b or Σ_b^*. For the different I, J quantum numbers we have the following space states.

1) $J = 1/2,\ I = 1/2$
$\eta_b N,\ \Upsilon N,\ B\Lambda_b,\ B\Sigma_b,\ B^*\Lambda_b,\ B^*\Sigma_b,\ B^*\Sigma_b^*$.

2) $J = 1/2,\ I = 3/2$
$\Upsilon\Delta,\ B\Sigma_b,\ B^*\Sigma_b,\ B^*\Sigma_b^*$.

3) $J = 3/2,\ I = 1/2$
$\Upsilon N,\ B^*\Lambda_b,\ B^*\Sigma_b,\ B\Sigma_b^*,\ B^*\Sigma_b^*$.

4) $J = 3/2,\ I = 3/2$
$\eta_b\Delta,\ \Upsilon\Delta,\ B^*\Sigma_b,\ B\Sigma_b^*,\ B^*\Sigma_b^*$.

5) $J = 5/2,\ I = 1/2$
$B^*\Sigma_b^*$.

6) $J = 5/2,\ I = 3/2$
$\Upsilon\Delta,\ B^*\Sigma_b^*$.

Following the results of former work (Ref. [412]), we extrapolate the LHG formalism to the beauty sector as done in Ref. [128]. Thus, combining these matrix elements with the HQSS requirements, for the matrix elements of Eq. (3.6) in the $J = 1/2,\ I = 1/2$ sector, just replacing the $\bar{D}$ meson to a B meson and $\bar{c}$-quark to $\bar{b}$-quark, we analogously obtain the values for the parameters of the low energy constants for $J = 1/2,\ I = 1/2$ (more details seen in our paper [428]),

$$\begin{aligned} \mu_2 &= \frac{1}{4f^2}(k^0 + k'^0), \quad \mu_3 = -\frac{1}{4f^2}(k^0 + k'^0), \\ \mu_{12} &= -\sqrt{6}\ \frac{g^2}{p_{B^*}^2 - m_{B^*}^2}\ (k^0 + k'^0), \\ \mu_1 &= 0, \quad \mu_{23} = 0, \quad \lambda_2 = \mu_3, \quad \mu_{13} = -\mu_{12}, \end{aligned} \tag{3.26}$$

where p_{B^*} is the four momentum of B^* in the VVV or PPV vertex (which will be discussed later). Thus, μ_{12} is small because of the much heavier B^* exchanged. But we keep it since this term is the only one that allows the scattering $\eta_b N \to \eta_b N$ ($\Upsilon N \to \Upsilon N$) through intermediate inelastic states. Similarly, the matrix of Eq. (3.7) for $J = 1/2,\ I = 3/2$ now for beauty sector is given by

$$\begin{aligned} \lambda_{12} &= 3\sqrt{3}\ \frac{g^2}{p_{B^*}^2 - m_{B^*}^2}\ (k^0 + k'^0), \\ \mu_3 &= 2\frac{1}{4f^2}(k^0 + k'^0), \quad \lambda_2 = \mu_3, \quad \lambda_1 = 0. \end{aligned} \tag{3.27}$$

Because the coefficients μ_i^I, μ_{ij}^I and λ_m^I, λ_{mn}^I are isospin dependent but J independent, the results of Eq. (3.26) are also the same for all $I = 1/2$ sectors. The other $I = 3/2$ sectors share the same parameters as Eq. (3.27).

Although we have used coefficients using SU(4), we could have equally obtained them using only SU(3) relationships, invoking the spectator character of the heavy quarks. This means that we treat u, d, s quarks as light quarks and use SU(3) to obtain couplings in this sector. By using the spectator hypothesis for the s or c and b quarks we would obtain the $DD\rho$,

$BB\rho$ couplings equal to the $KK\rho$. This coupling is g in our approach which is taken as $m_V/2f_\pi$, with $m_V \approx m_\rho$, hence $g \approx 4.14$. With this coupling one reproduces the chiral Lagrangians in the light sector by exchanging vector mesons. The spectator hypothesis is challenged in Ref. [413], where they quote a value of $g_{DD\rho} \approx 5$. This should be compared with $g_{\pi\pi\rho}/2 = 3$ used in Refs. [408, 429], or 4.14 that we use here. One should also note that in Ref. [413] they propose in addition an extra form factor

$$F(\vec{q}) = \frac{\Lambda^2}{\Lambda^2 + |\vec{q}|^2}; \quad \Lambda \approx 0.7 \text{ GeV}. \tag{3.28}$$

The value of $g_{DD\rho} \approx 5$ would also agree with results obtained in sum rules in Ref. [414], $g_{DD\rho} \approx 4.84$. On the other hand, by using also sum rules in the light cone in Ref. [430] (after caring about factors in the definition) they get $g_{DD\rho} = 3.81/2 \approx 1.9$ with differs appreciably from the other values. In this same paper and in Ref. [431], they also report a value for $g_{BB\rho} = \sqrt{2} \times 1.89 \approx 2.67$ (after adapting to our normalization). We can see a difference of almost a factor 1.5 with respect to our value. To estimate uncertainties we shall assume uncertainties in the non zero diagonal terms of the interaction of about a factor 1.5 up and down. Larger uncertainties might appear in the non diagonal terms involving the exchange of a B^*. This affects the μ_{12}, λ_{12} terms of Eqs. (3.26), (3.27). Here we must admit larger uncertainties from the SU(4) symmetry used (or implicit SU(3) if we use the analogy of b quarks with s quarks). We shall substitute g^2 in Eqs. (3.26), (3.27) by g_{mmB^*} for the mesonic vertex times g_{bbB^*} for the baryonic vertex. We will accept that g_{mmB^*} in this case can be either a factor of two larger or smaller than the central SU(4) value (this should include possible changes in g_{bbB^*} too).

As we mentioned, the π exchange is subdominant in the heavy quark mass counting and we disregard those terms. One might think of two pion exchange. In the present case, two pion exchange in the scalar isoscalar sector (σ exchange) would not contribute for the non diagonal terms of the interaction, and only induce minor change in the non zero diagonal terms. From the picture of the σ, or two uncorrelated π exchange of Ref. [432], the diagonal $\eta_b N$ and ΥN interaction would be OZI forbidden and one can also neglect it.

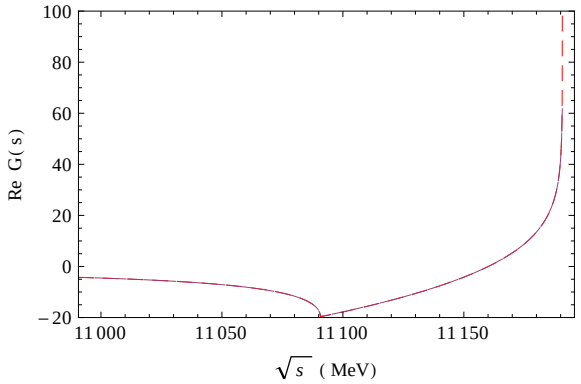

Figure 3.13: Re G as a function of $\sqrt{s}$ for $q_{max} = 745.5$ MeV/c.

3.2.2 The coupled channel approach

The scattering matrix is evaluated by solving the coupled channels BS equation in the on shell factorization approach, Eq. (1.44), seen in the subsection 1.3.1.

Normally, in the low energy the two regularization methods for the loop function G, seen the discussions in the subsection 1.3.1, are compatible and there are relationships between these free parameters, $a(\mu)$, μ and q_{max} (seen Eq. (52) of Ref. [196]). At higher energies, as discussed in Ref. [128], there are large differences even not far away from threshold (see Fig. 2 of Ref. [128]). The cut-off method for the heavy hadrons has obvious deficiencies if the cut off chosen is of the order of the on shell momenta of the propagating pair in the loop function. This can be seen to happen in Fig. 3.13 for about 100 MeV of excitation, where the G function artificially blows up. On the other hand, the use of G in dimensional regularization has its own problems, since matching it to the cut-off formula at threshold develops positive values below threshold, leading to the unphysical generation of states with a repulsive potential when $1 - GV = 0$. The cut-off method, however, does not show this pathology since $G < 0$ below threshold. A satisfactory solution to both problems is accomplished if one uses the cut off regularization but in addition considers the $\vec{q}$ dependence of the vector meson propagator in the t-channel, which provides a physical regularization factor.

Recalling that p^0 is small for large values of $\vec{p}$ in the heavy sector, one can take

$$\frac{1}{p^2 - m_V^2} = \frac{1}{p^{0\,2} - \vec{p}^{\,2} - m_V^2} \approx \frac{1}{-\vec{p}^{\,2} - m_V^2} = -\frac{1}{\vec{p}^{\,2} + m_V^2}. \tag{3.29}$$

For lower momentum transfers one can take the approximation, $\vec{p}^{\,2} \sim 0$, and then Eq. (3.29) becomes $-1/m_V^2$, which can be factorized outside the loop and give rise to the potential of Eq. (3.9). In the heavy quark sector, $\vec{p}$ can be larger than m_V and the $\vec{p}$ dependence of Eq. (3.29) must be taken into account.

We, thus, improve our formalism to solve this problem. As discussed in section VII of Ref. [95], also in the subsection 1.3.2, we can introduce a form factor to the potential,

$$V(\vec{q}\,', \vec{q}) = \langle \vec{q}\,' | \hat{V} | \vec{q} \rangle \equiv v\, f(\vec{q}\,') f(\vec{q}), \tag{3.30}$$

writing it in a separable form. As shown in Ref. [95] and the subsection 1.3.2, the T matrix also factorizes like Eq. (3.30) and one has

$$T(\vec{q}, \vec{q}\,') = \langle \vec{q} | \hat{T} | \vec{q}\,' \rangle \equiv t\, f(\vec{q}) f(\vec{q}\,'), \tag{3.31}$$

and then the Lippmann-Schwinger equation (BS equation now) becomes

$$t = [1 - v\, G]^{-1}\, v, \tag{3.32}$$

but now

$$G(s) = \int \frac{d^3\vec{q}}{(2\pi)^3} f^2(\vec{q}) \frac{\omega_P + \omega_B}{2\,\omega_P\,\omega_B} \frac{2M_B}{P^{0\,2} - (\omega_P + \omega_B)^2 + i\varepsilon}. \tag{3.33}$$

Once again we can put the integral equation as an algebraic equation [155]. Note that Eq. (3.32) has the same format as Eq. (1.44) (and Eq. (1.55)), but, the matrices t, v are defined by Eqs. (3.30) and (3.31), and the loop function $G(s)$ is changed by Eq. (3.33) which absorbs a momentum dependent form factor from the factorized potential. Then, the kernel v is still the same as discussed in the last subsection 3.2.1.

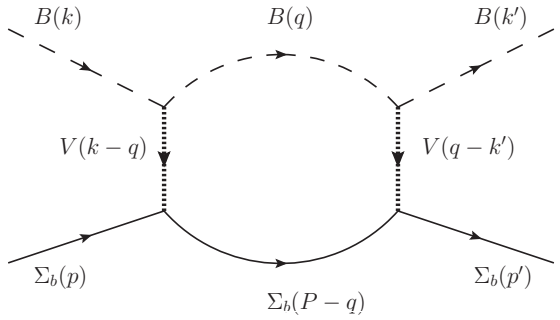

Figure 3.14: Feymann diagram for the transition $B\Sigma_b \to B\Sigma_b$ with one loop.

3.2.3 Application to the heavy quark sector

In the present work, we focus on the beauty sector involving much higher energy than the light quark sector, even than the charm sector. As mentioned in the former subsection 3.2.2, because of the large value of the momentum $\vec{q}$ running in the loop, we should consider the $\vec{q}$ dependence of the vector exchange. For this we use the formalism discussed in the former section.

First, for the channels involving the light vector mesons exchange, such as $B\Sigma_b$ channel, the problem is that the potential has a factor which does not depend on $\vec{q}$ but just on $\vec{k}-\vec{q}$, as shown in Fig. 3.14. However, we should keep in mind that while $\vec{q}$ in the loop can be larger than m_V, we only study states close to threshold where the external momenta are small. Thus, we have

$$f(\vec{k})f(\vec{q}) \equiv \frac{m_V^2}{(\vec{k}-\vec{q})^2+m_V^2} \simeq \frac{m_V^2}{\vec{q}^{\,2}+m_V^2}, \tag{3.34}$$

which defines

$$f(\vec{q}) = \frac{m_V^2}{\vec{q}^{\,2}+m_V^2}, \ f(\vec{k}) \simeq 1. \tag{3.35}$$

For the main potential related to the light vector meson exchange, this form factor should be incorporated into the new G function, Eq. (3.33), thus, there is a factor $f^2(\vec{q})$ in the integral. With the implementation of the form factor in Eq. (3.33) the function G becomes convergent. In Fig. 3.15, we

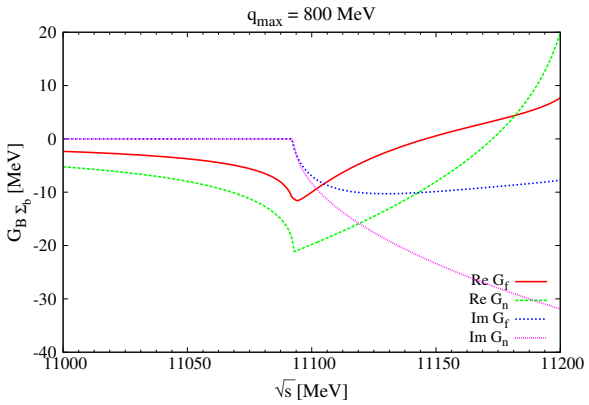

Figure 3.15: The real and imaginary parts of G function with Eq. (1.47) (G_n) and Eq. (3.33) (G_f).

compare the new results for $\mathrm{Re}\, G$ and $\mathrm{Im}\, G$ with the new prescription with the sharp cut-off results with $q_{max} = 800$ MeV/C used in Ref. [128]. As we can see, both $\mathrm{Re}\, G$ and $\mathrm{Im}\, G$ are reduced in the new approach which leads to smaller binding of the states.

As we have seen, we have kept in Eq. (3.26) the term μ_{12}, related to the exchange of a heavy vector. This appears in diagrams of multiple scattering like those shown in Fig. 3.16 (in the figure B means B or B^* meson). Fig. 3.16(a) would produce some small $\eta_b N \to \eta_b N$ amplitude, which is not allowed directly since $\mu_1 = 0$ (see Eq. (3.26)). However, we are more interested in terms of the type of 3.16(b), also small but which contribute to the width of the states, since the mass of the intermediate state is smaller than the external one. Because of this, we pay some special attention to it and investigate the form factor involved in this case related to the exchange of the heavy vector.

To determine the new form factor, $\tilde{f}(\vec{q})$, we should come back to the transition potential μ_{12} of Eq. (3.26), which takes into account the heavy B^* exchange propagator,

$$\frac{1}{p^2_{B^*} - m^2_{B^*}}. \tag{3.36}$$

If we calculate the four momentum $p^2_{B^*}$ by taking on shell approximation,

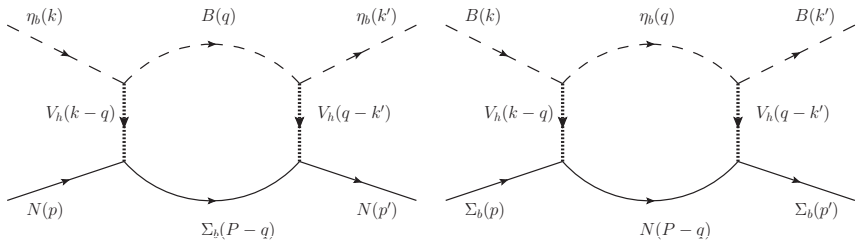

Figure 3.16: Diagram for the transitions coupled with $\eta_b N$ channel in the loop.

we have

$$p_{B^*}^2 = (p_{\eta_b} - p_B)^2 \simeq m_{\eta_b}^2 + m_B^2 - 2E_{\eta_b}E_B, \tag{3.37}$$

where the on shell energies of the particles are given by

$$E_{\eta_b} = \frac{s + m_{\eta_b}^2 - m_N^2}{2\sqrt{s}}; \quad E_B = \frac{s + m_B^2 - m_{\Sigma_b}^2}{2\sqrt{s}}. \tag{3.38}$$

Once again, we take into account that in the loop one can exchange large momenta with small energy transfer. Therefore, we can consider that the energy is the same but there will be an off shell momentum running. Thus, we take

$$p_{B^*}^2 = (p_{\eta_b} - p_B)^2 = (E_{\eta_b} - E_B)^2 - (\vec{p}_{\eta_b} - \vec{p}_B)^2 \simeq (E_{\eta_b} - E_B)^2 - \vec{q}^{\,2}, \tag{3.39}$$

where we have taken the external momentum $\vec{p}_B \approx 0$ as before and $\vec{p}_{\eta_b} = \vec{q}$. Hence, for the transition potential of Eqs. (3.26) and (3.27) we shall use the on shell expression, Eqs. (3.36) and (3.37), as in the charm sector, but now in the $\eta_b N$ channel we should use a form factor in the loop function,

$$\tilde{f}(\vec{q}) = \frac{m_{B^*}^2 - (E_{\eta_b} - E_B)^2}{m_{B^*}^2 - (E_{\eta_b} - E_B)^2 + \vec{q}^{\,2}}, \tag{3.40}$$

where the on shell energies, E_{η_b} and E_B, are given by Eq. (3.38). In practice, for E_B we take average masses of b-baryons and then have a unique form factor $\tilde{f}(\vec{q})$.

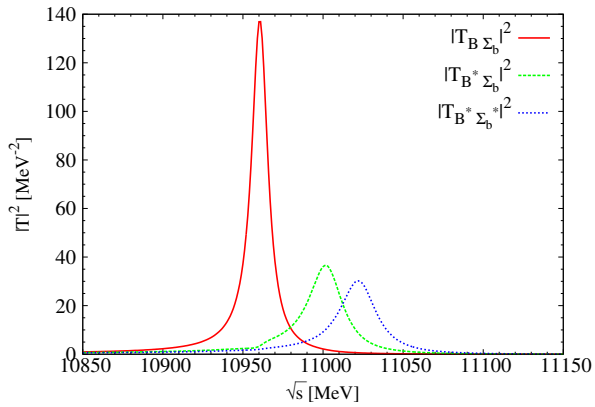

Figure 3.17: The squared amplitudes of the $J = 1/2,\ I = 1/2$ sector.

3.2.4 Results

In our formalism we use the BS equation of Eq. (3.32) in coupled channels to evaluate the scattering amplitudes, where the G function for the meson-baryon interaction is given by Eq. (3.33). We first search the resonance peak in the scattering amplitudes and then look for poles in the second Riemann sheet when there are open channels, or in the first Riemann sheet when one has stable bound states (see [168, 362] for details).

For open channels the second Riemann sheet is obtained in our case by changing

$$G^I \to G^{II} = G^I + \frac{i}{4\pi}\frac{q_{cm}}{\sqrt{s}} f (q_{cm}^2)^2, \tag{3.41}$$

where q_{cm} is defined after Eq. (1.46), and given by Eq. (2.58). Besides, the couplings are defined as before, seen Eq. (3.23).

Similarly to the charm sector before, in all $I = 3/2$ channels we have repulsive potentials as can be seen in Eq. (3.27). So, we should not expect any bound states or resonances.

Next we show the results for the $J = 1/2,\ I = 1/2$ sector in Fig. 3.17. There are three clear peaks with non zero width in the range $10950 \sim 11050$ MeV in the squared amplitudes of $|T|^2$. These peaks are below the thresholds of $B\Sigma_b,\ B^*\Sigma_b,\ B^*\Sigma_b^*$ respectively. From Eq. (3.26), we know that the potentials of these channels are attractive, and the energy ranges

where these peaks appear are reasonable. In Fig. 3.15, one can see that the real parts of the loop function G, Eq. (3.33), are negative below the threshold. Thus these peaks are acceptable as physical ones. We look for the poles corresponding to these peaks in the second Riemann sheet, and find the poles at $(10960.68 + i6.15)$ MeV, $(11002.31 + i12.85)$ MeV, $(11022.77 + i13.77)$ MeV. We can see that the width of the first pole is about 12 MeV, and the last two ones have a width of about $25 \sim 28$ MeV, which is two times bigger than the first one. The couplings to the various coupled channels for these poles are given in Table 3.3. From the couplings in Table 3.3, the first pole, $(10960.68 + i6.15)$ MeV, couples mostly to $B\Sigma_b$, with a threshold of 11092.81 MeV. So, it could be considered like a $B\Sigma_b$ bound state with a binding energy about 133 MeV, which is small compared to the mass of $B\Sigma_b$. The second pole, $(11002.31 + i12.85)$ MeV, couples most strongly to $B^*\Sigma_b$ and thus, is still bound by about 136 MeV below the $B^*\Sigma_b$ threshold, 11138.60 MeV. Finally, the third pole, $(11022.77 + i13.77)$ MeV, couples mostly to $B^*\Sigma_b^*$. It has a binding energy of 136 MeV with respected to the $B^*\Sigma_b^*$ threshold, 11158.80 MeV. We can see that the binding energies of the three poles are similar, close to 130 MeV. We can also see that all the three bound states decay mostly into the open channels $\eta_b N$ and ΥN, and couple most strongly to some other BY_b channels. Note that the former two states correspond to those reported in Ref. [128], which are $(11052 + i0.69)$ MeV for the $B\Sigma_b$ bound state and $(11100 + i0.66)$ MeV for the $B^*\Sigma_b$ bound state. The difference in the binding energies with the results of Ref. [128] are at most of 90 MeV, but the uncertainties in Ref. [128] had a range within this magnitude. The widths obtained in Ref. [128] are smaller but there are more open channels in our approach and we also do not have restrictions from using a small cut-off as used in Ref. [128] in some cases. Note that in the $B\Sigma_b$ decay to $\eta_b N$ the on shell momentum is about 1300 MeV/c and will be missed if a smaller cut-off is chosen to regularize G. The small width obtained in Ref. [128] comes mostly from decay to light channels Refs. [127, 168] that we neglect here. Their results show that because of higher energy in the beauty sector, these light channels have a small influence on the two bound states decay width. In our present work, we include two open channels constrained by the HQSS, $\eta_b N$ and ΥN, which play an important role for the the decay width. This is why we get a wider decay width.

Table 3.3: Couplings of resonances to the different channels in the $J = 1/2,\ I = 1/2$ sector.

$10960.68 + i6.15$							
	$\eta_b N$	ΥN	$B\Lambda_b$	$B\Sigma_b$	$B^*\Lambda_b$	$B^*\Sigma_b$	$B^*\Sigma_b^*$
g_i	$0.83 - i0.22$	$0.51 - i0.22$	$0.05 + i0.01$	$8.48 - i0.27$	$0.05 - i0.04$	$0.20 - i1.71$	$0.13 - i0.75$
$\lvert g_i \rvert$	0.86	0.56	0.05	8.48	0.06	1.72	0.76
$11002.31 + i12.85$							
	$\eta_b N$	ΥN	$B\Lambda_b$	$B\Sigma_b$	$B^*\Lambda_b$	$B^*\Sigma_b$	$B^*\Sigma_b^*$
g_i	$0.45 + i0.29$	$1.40 - 0.16$	$0.11 - i0.03$	$0.08 - i1.02$	$0.09 - i0.00$	$8.82 - i0.57$	$0.03 - i1.53$
$\lvert g_i \rvert$	0.53	1.41	0.11	1.03	0.09	8.84	1.53
$11022.77 + i13.77$							
	$\eta_b N$	ΥN	$B\Lambda_b$	$B\Sigma_b$	$B^*\Lambda_b$	$B^*\Sigma_b$	$B^*\Sigma_b^*$
g_i	$1.28 - i0.11$	$0.76 + i0.12$	$0.16 - i0.00$	$0.13 + i0.37$	$0.06 - i0.02$	$0.05 - i1.20$	$8.72 - i0.63$
$\lvert g_i \rvert$	1.29	0.77	0.16	0.39	0.07	1.20	8.74

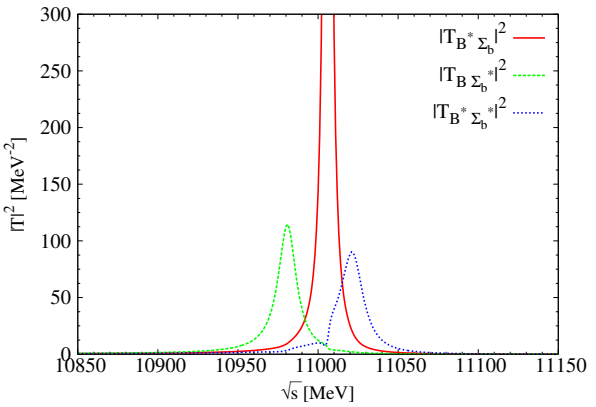

Figure 3.18: The results of $|T|^2$ for the $J = 3/2,\ I = 1/2$ sector.

In Fig. 3.18 we show our results for the $J = 3/2,\ I = 1/2$ sector. From the results of $|T|^2$, we can also see three clear peaks around the range $10950 \sim 11050$ MeV, which are about 130 MeV below the thresholds of $B\Sigma_b^*,\ B^*\Sigma_b,\ B^*\Sigma_b^*$ respectively. The strength of the second peak is about 10 times bigger than the other two and the widths are small enough to allow the peaks to show up clearly. In the second Riemann sheet, we find the poles at $(10981.01 + i6.94)$ MeV, $(11006.12 + i2.13)$ MeV, $(11021.70 + i8.45)$ MeV, showing that the widths are about 14 MeV, 4 MeV, 17 MeV respectively. We list the couplings to each coupled channel corresponding to these poles in Table 3.4. One can see from Table 3.4, that the first pole, $(10981.01+i6.94)$ MeV, couples most strongly to the channel $B\Sigma_b^*$ and corresponds to a $B\Sigma_b^*$ state, bound by 132 MeV with respect to its threshold of 11113.02 MeV. The state, $(11006.12 + i2.13)$ MeV, corresponding to the big peak in the middle of Fig. 3.18, with small width, couples mostly to $B^*\Sigma_b$. Thus, it is bound by 132 MeV with respect to the threshold of the $B^*\Sigma_b$ channel, 11138.60 MeV. The third one, $(11021.70 + i8.45)$ MeV, couples mostly to $B^*\Sigma_b^*$, and is bound by 137 MeV with respect to the threshold of this channel, 11158.80 MeV. Also, we can find that all the three states decay essentially into ΥN channel, couple very weakly to the $B^*\Lambda_b$ channel, and couple more strongly to the other channels.

Table 3.4: Couplings of resonances to the different channels in the $J = 3/2,\ I = 1/2$ sector.

$10981.01 + i6.94$	ΥN	$B^*\Lambda_b$	$B^*\Sigma_b$	$B\Sigma_b^*$	$B^*\Sigma_b^*$
g_i	$1.05 - i0.41$	$0.07 - i0.04$	$0.33 - i1.43$	$8.58 - i0.27$	$0.24 - i2.06$
$\lvert g_i\rvert$	1.13	0.08	1.47	8.59	2.07
$11006.12 + i2.13$	ΥN	$B^*\Lambda_b$	$B^*\Sigma_b$	$B\Sigma_b^*$	$B^*\Sigma_b^*$
g_i	$0.60 - i0.20$	$0.07 - i0.01$	$8.71 - i0.06$	$0.09 + i1.12$	$0.27 - i2.29$
$\lvert g_i\rvert$	0.64	0.07	8.71	1.12	2.31
$11021.70 + i8.45$	ΥN	$B^*\Lambda_b$	$B^*\Sigma_b$	$B\Sigma_b^*$	$B^*\Sigma_b^*$
g_i	$1.25 + i0.23$	$0.13 + i0.00$	$0.09 + i1.93$	$0.29 - i1.20$	$9.02 - i0.30$
$\lvert g_i\rvert$	1.27	0.13	1.93	1.24	9.03

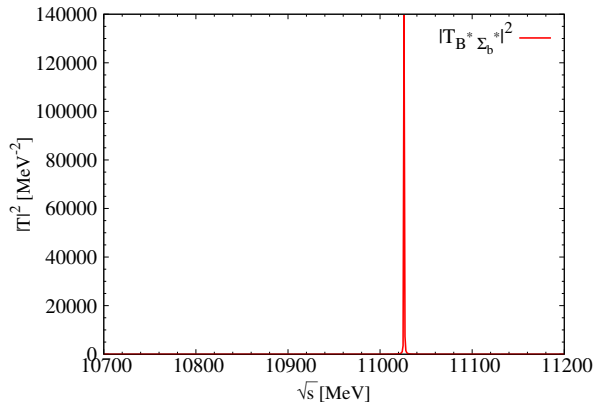

Figure 3.19: The results of $|T|^2$ for the $J = 5/2,\ I = 1/2$ sector.

As shown in Fig. 3.19, we also search for a new state in the $J = 5/2,\ I = 1/2$ sector, which is a bound state of $B^*\Sigma_b^*$ around $(11026.10 + i0)$ MeV. From Fig. 3.19, we can see that, this state has no width, as it corresponds to a single channel, $B^*\Sigma_b^*$. Then it is a bound state of this channel and has no other channels to decay. Therefore we can look for the pole in the first Riemann sheet with zero width. One can see that the state is bound by about 133 MeV with respect to the $B^*\Sigma_b^*$ threshold.

3.2.5 Discussion

We have seen that our procedure to regularize the loops allows sufficiently large momenta to get the imaginary part of the loops of the decay channels. Thus, technically we get a good estimate of the width of the states. Yet, we would like to make some estimate for the uncertainties in the masses and widths of the states obtained.

In a first step we introduce a sharp cut off of $q_{max} = 800$ MeV, as suggested in Ref. [128], in addition to the natural form factors from vector exchange that we have. Because of the caveat about the imaginary parts, we only look at the real parts. We observe that systematically the states are less bound. They are now bound by about 50 MeV. The experimental finding of some of the states predicted would allow us to be more refined on the regularization procedure, but for the time being we can accept the

differences in the binding energies as uncertainties of our theoretical approach. We thus conclude that the states found would be bound by about $50 - 130$ MeV and the widths are of the order of $4 - 28$ MeV.

Finally we would like to evaluate other uncertainties tied to possible changes in the input parameters of the potential. As we discussed at the end of subsection 3.2.1, we will look for changes that come from increasing or decreasing by 50 % de diagonal terms of the potential, or by a factor of two up and down μ_{12} and λ_{12}. We summarize the results for the energies of three states in Tables 3.5 and 3.6.

Table 3.5: The poles corresponding to $J = 1/2,\ I = 1/2$ sector when the diagonal potentials are changed by a factor.

$V_{dig}/1.5$	V_{dig}	$V_{dig}\,1.5$
$11022.00 + i2.58$	$10960.68 + i6.15$	$10877.41 + i17.15$
$11032.73 + i4.32$	$11002.31 + i12.85$	$10897.55 + i18.50$
$11076.37 + i9.59$	$11022.77 + i13.77$	$10905.00 + i17.62$

Table 3.6: The poles corresponding to $J = 1/2,\ I = 1/2$ sector when the non diagonal potentials are changed by a factor.

$(\mu_{12}/2,\ \lambda_{12}/2)$	$(\mu_{12},\ \lambda_{12})$	$(2\mu_{12},\ 2\lambda_{12})$
$10960.51 + i1.39$	$10960.68 + i6.15$	$10974.87 + i9.22$
$11005.13 + i3.12$	$11002.31 + i12.85$	$11005.44 + i54.00$
$11025.31 + i3.37$	$11022.77 + i13.77$	$11033.50 + i54.00$

As we can see in Tables 3.5 and 3.6, the results for the bindings and widths change with the changes made. The changes in the diagonal potentials induce changes in the binding. Increasing the potential by 50 % makes the binding increase by about $60 - 90$ MeV, while by dividing it by 1.5 reduces the binding in about $50 - 70$ MeV. It is interesting to note that even

if we divide the diagonal potential by a factor four we still get weak bound states, which tells us that the prediction on the bound states is rather solid, even if we have large uncertainties about the binding energy.

The widths of these states are also changed with the former changes in the potential. However, the changes are more apparent when we multiply or divide by two the nondiagonal terms of the potential. In this case the binding does not change much, but the widths are roughly multiplied or divided by a factor of four. Even with these uncertainties the widths that we obtain are below 110 MeV.

3.2.6 Conclusions

In the present work we investigate the hidden beauty sector by combining the dynamics of the LHG Lagrangians extrapolated to SU(4) with the constraints of HQSS. We also benefit from the high energies of the problem and find a natural way to regularize the loops using the range provided by the light vector masses, whose exchange in the t-channel provide the source of the interaction in the LHG approach.

After our investigation, we find seven new states of N^* with hidden beauty. All these states are different since they correspond to different energies or different total spin J, and some of them appear at about the same energy with the same channel but different J, which are analogous to those found in our former work on hidden charm. Thus, they are degenerate states that we get in $J = 1/2,\ 3/2$ for $B^*\Sigma_b$ and $J = 1/2,\ 3/2,\ 5/2$ for $B^*\Sigma_b^*$. From this perspective, we report our results as claiming that we get four bound states with about $50 - 130$ MeV binding and isospin $I = 1/2$, corresponding to $B\Sigma_b$ with $J = 1/2$, $B\Sigma_b^*$ with $J = 3/2$, $B^*\Sigma_b$ degenerated with $J = 1/2,\ 3/2$ and $B^*\Sigma_b^*$ degenerated with $J = 1/2,\ 3/2,\ 5/2$. Note that the two states of $B\Sigma_b,\ B^*\Sigma_b$ with $J = 1/2,\ I = 1/2$ are consistent with the ones reported in Ref. [128]. Besides, we found no states in $I = 3/2$. We also estimated uncertainties in binding energies, which were of the order of ± 70 MeV, but found that the bound state character of the states obtained was rather stable. For the width we obtained values around $4 - 28$ MeV with uncertainties of about $\pm^{70}_{20}$ MeV.

3.3 The study of hidden beauty meson molecules

The world of heavy quarks, charm and beauty, is experiencing a fast development, with a plethora of new states being found in facilities as BABAR, CLEO, BELLE, BES [433–436]. The states capturing more attention are those that do not fit within the standard picture of mesons as $q\bar{q}$ or baryons as qqq, and which require more complex structures, like tetraquarks, molecules, or hybrids, and so on. The field of meson molecules in the charm sector has been much studied [90, 93, 247, 259–261, 350, 426, 429, 437–450] and many of the observed states with hidden charm and open charm are shown to be consistent with the molecule interpretation. The work on the charm sector is gradually moving to the beauty sector and there are works dealing with b or hidden b meson molecules built up from other mesons containing some b quark [427, 442, 444, 445, 451–458]. The recent discovery of the hidden beauty $Z_b(10610)$ and $Z_b(10650)$ states in three charge states [114, 459, 460], and hence with isospin I=1, has brought a new stimulus to the molecular idea [427, 442, 444, 456, 458], since they cannot be $b\bar{b}$ quarkonium states.

One of the elements that has allowed progress in the heavy quark sector is the implementation of the HQSS (seen in the section Sec. 1.5), as discussed before. However, the HQSS does not determine the interaction, simply puts some constraints in it, and to proceed further to make predictions one must rely upon some experimental information or use models. In this sense, the work of Ref. [427] uses properties from the X(3872) resonance, which is assumed to be a $D\bar{D}^* - cc$ molecule, and extrapolates this information to make predictions of $B\bar{B}^* - cc$ molecules.

An alternative approach to using empirical data to constrain the interaction is the use of some dynamical model. The use of chiral Lagrangians has been a common thing in this kind of works, but its extension to the heavy quark sector is not straightforward. Conversely, the use of the LHG Lagrangians has allowed much progress in the heavy sector, which introduces pseudoscalar and vector mesons as building blocks, and provides the same information as the chiral Lagrangians (seen in the subsection 1.2.1) up to next to leading order under the assumption of vector meson dominance [378], and additionally introduces explicitly vector mesons and their interaction in the theory.

In the former works, we found that the LHG approach respects HQSS and this is quite relevant since it allows one to be more predictive. Thus, in

the present work, we tackle the interaction of $B\bar{B}$, $B\bar{B}^*$ and $B^*\bar{B}^*$ in the hidden beauty sector and make predictions for bound states.

3.3.1 HQSS Formalism

Following the former work (Ref. [412]) for hidden charm baryons, we extrapolate the formalism to the hidden beauty sector for the mesons. Therefore we can study mesons with hidden beauty with isospin $I = 0,\ 1$, and spin $J = 0,\ 1,\ 2$. We take as coupled channels states with $B,\ B^*,\ B_s,\ B_s^*$ and their corresponding antiparticles. For the different $I,\ J$ quantum numbers we have the following space states.

1) $J = 0,\ I = 0$
$B\bar{B},\ B_s\bar{B}_s,\ B^*\bar{B}^*,\ B_s^*\bar{B}_s^*$.

2) $J = 0,\ I = 1$
$B\bar{B},\ B^*\bar{B}^*$.

3) $J = 1,\ I = 0$
$B\bar{B}^*\ (B^*\bar{B}),\ B_s\bar{B}_s^*\ (B_s^*\bar{B}_s),\ B^*\bar{B}^*,\ B_s^*\bar{B}_s^*$.

4) $J = 1,\ I = 1$
$B\bar{B}^*\ (B^*\bar{B}),\ B^*\bar{B}^*$.

5) $J = 2,\ I = 0$
$B^*\bar{B}^*,\ B_s^*\bar{B}_s^*$.

6) $J = 2,\ I = 1$
$B^*\bar{B}^*$.

With different spin quantum number there are 12 orthogonal states (of which 6 are having hidden strangeness) in the physical basis for $I = 0$. For $I = 1$ there are only 6 states since the hidden strangeness states have $I = 0$. Next we will introduce a HQSS basis, for which it is straightforward to implement the lowest order HQSS constraints. Thus, we have 12 orthogonal states in the physical basis, given by

- $|S_{b\bar{b}}=0,\,\mathcal{L}=0\,;\,J=0\,\rangle$, $|S_{b\bar{b}}=0,\,\mathcal{L}=0\,;\,J=0\,\rangle_s$,
- $|S_{b\bar{b}}=0,\,\mathcal{L}=1\,;\,J=1\,\rangle$, $|S_{b\bar{b}}=0,\,\mathcal{L}=1\,;\,J=1\,\rangle_s$,
- $|S_{b\bar{b}}=1,\,\mathcal{L}=0\,;\,J=1\,\rangle$, $|S_{b\bar{b}}=1,\,\mathcal{L}=0\,;\,J=1\,\rangle_s$,
- $|S_{b\bar{b}}=1,\,\mathcal{L}=1\,;\,J=0\,\rangle$, $|S_{b\bar{b}}=1,\,\mathcal{L}=1\,;\,J=0\,\rangle_s$,
- $|S_{b\bar{b}}=1,\,\mathcal{L}=1\,;\,J=1\,\rangle$, $|S_{b\bar{b}}=1,\,\mathcal{L}=1\,;\,J=1\,\rangle_s$,
- $|S_{b\bar{b}}=1,\,\mathcal{L}=1\,;\,J=2\,\rangle$, $|S_{b\bar{b}}=1,\,\mathcal{L}=1\,;\,J=2\,\rangle_s$,

where, J is total spin of the hidden beauty meson system; $\mathcal{L}$, total spin of the light quarks system; $S_{b\bar{b}}$, total spin of the $b\bar{b}$ subsystem; and the subindex s means that the light quarks are strange. Note that we study ground state mesons, which means that all orbital angular momenta are zero.

In order to take into account the HQSS it is interesting to use the heavy quark basis in which the spins are rearranged such as to combine the spin of the $b\bar{b}$ quarks into $S_{b\bar{b}}$ since the matrix elements do not depend on this spin. One classifies the HQSS in terms of $\vec{S}_{b\bar{b}}$, $\vec{\mathcal{L}}$ and $\vec{J}$. The conservation of $\vec{S}_{b\bar{b}}$ and $\vec{J}$ leads to the conservation of $\vec{\mathcal{L}}=\vec{J}-\vec{S}_{b\bar{b}}$ and then in the HQSS basis the matrix elements fulfil (Similar to Eq. (3.1))

$$\langle S'_{b\bar{b}},\,\mathcal{L}';J',\,\alpha'|H^{QCD}|S_{b\bar{b}},\,\mathcal{L};J,\,\alpha\rangle=\;\delta_{\alpha\alpha'}\delta_{JJ'}\delta_{S'_{b\bar{b}}S_{b\bar{b}}}\delta_{\mathcal{L}\mathcal{L}'}\langle\mathcal{L};\alpha||H^{QCD}||\mathcal{L};\alpha\rangle. \tag{3.42}$$

Thus, in a given α sector, we have a total of six unknown LEC's:

- Three LEC's associated to $\mathcal{L}=0$

$$\lambda_0^\alpha = \langle\mathcal{L}=0;\alpha||H^{QCD}||\mathcal{L}=0;\alpha\rangle \tag{3.43}$$
$$\lambda_{0s}^\alpha = {}_s\langle\mathcal{L}=0;\alpha||H^{QCD}||\mathcal{L}=0;\alpha\rangle_s \tag{3.44}$$
$$\lambda_{0m}^\alpha = \langle\mathcal{L}=0;\alpha||H^{QCD}||\mathcal{L}=0;\alpha\rangle_s \tag{3.45}$$

- Three LEC's associated to $\mathcal{L}=1$

$$\lambda_1^\alpha = \langle\mathcal{L}=1;\alpha||H^{QCD}||\mathcal{L}=1;\alpha\rangle \tag{3.46}$$
$$\lambda_{1s}^\alpha = {}_s\langle\mathcal{L}=1;\alpha||H^{QCD}||\mathcal{L}=1;\alpha\rangle_s \tag{3.47}$$
$$\lambda_{1m}^\alpha = \langle\mathcal{L}=1;\alpha||H^{QCD}||\mathcal{L}=1;\alpha\rangle_s \tag{3.48}$$

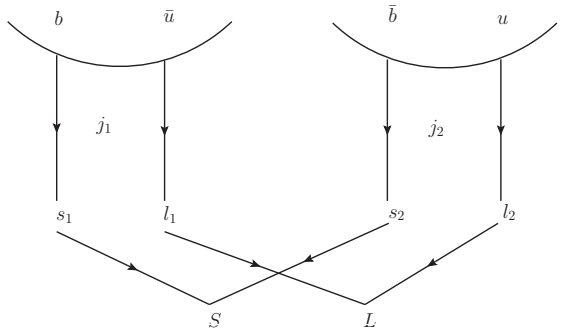

Figure 3.20: Diagrams for the calculation of 9-j coefficients.

Therefore in the HQSS basis, the H^{QCD} is a block diagonal matrix.

To exploit Eq. (3.42), one should express hidden beauty uncoupled meson-meson states in terms of the HQSS basis. Therefore, one needs to use 9-j symbols, seen in Eq. (3.3).

As an example take a meson(M)-antimeson($\bar{M}$) state of the type $B^{(*)}\bar{B}^{(*)}$ and look at the recombination scheme on Fig. 3.20. Thus, in this case we have the correspondence,

generic:	l_1	l_2	s_1	s_2	j_1	j_2	L	S	J
HQSS:	$\frac{1}{2}$	$\frac{1}{2}$	$\frac{1}{2}$	$\frac{1}{2}$	$J_M(0,1)$	$J_{\bar{M}}(0,1)$	$\mathcal{L}(0,1)$	$S_{b\bar{b}}(0,1)$	$J(0,1,2)$.

with J_M and $J_{\bar{M}}$ the total spin of the meson and antimeson respectively. Next, similar to the former work of hidden charm, we can expand the physical states by the HQSS basis (more details can be referred to our paper [461]). Then, we can evaluate the transition matrix elements between the physical states with LEC's by involving the HQSS basis. Using Eqs. (3.42)−(3.48) we obtain the transition matrix elements in the physical basis, as below

- $J = 0$, $I = 0$

$$
\begin{array}{c}
\begin{array}{cccc} B\bar{B} & B^*\bar{B}^* & B_s\bar{B}_s & B_s^*\bar{B}_s^* \end{array} \\
\left(\begin{array}{cccc}
\frac{1}{4}\lambda_0 + \frac{3}{4}\lambda_1 & -\frac{\sqrt{3}}{4}\lambda_0 + \frac{\sqrt{3}}{4}\lambda_1 & \frac{1}{4}\lambda_{0m} + \frac{3}{4}\lambda_{1m} & -\frac{\sqrt{3}}{4}\lambda_{0m} + \frac{\sqrt{3}}{4}\lambda_{1m} \\
-\frac{\sqrt{3}}{4}\lambda_0 + \frac{\sqrt{3}}{4}\lambda_1 & \frac{3}{4}\lambda_0 + \frac{1}{4}\lambda_1 & -\frac{\sqrt{3}}{4}\lambda_{0m} + \frac{\sqrt{3}}{4}\lambda_{1m} & \frac{3}{4}\lambda_{0m} + \frac{1}{4}\lambda_{1m} \\
\frac{1}{4}\lambda_{0m} + \frac{3}{4}\lambda_{1m} & -\frac{\sqrt{3}}{4}\lambda_{0m} + \frac{\sqrt{3}}{4}\lambda_{1m} & \frac{1}{4}\lambda_{0s} + \frac{3}{4}\lambda_{1s} & -\frac{\sqrt{3}}{4}\lambda_{0s} + \frac{\sqrt{3}}{4}\lambda_{1s} \\
-\frac{\sqrt{3}}{4}\lambda_{0m} + \frac{\sqrt{3}}{4}\lambda_{1m} & \frac{3}{4}\lambda_{0m} + \frac{1}{4}\lambda_{1m} & -\frac{\sqrt{3}}{4}\lambda_{0s} + \frac{\sqrt{3}}{4}\lambda_{1s} & \frac{3}{4}\lambda_{0s} + \frac{1}{4}\lambda_{1s}
\end{array} \right)_{I=0}
\end{array}
\tag{3.49}
$$

- $J = 1(C = -)$, $I = 0$

$$\begin{array}{cccc} B\bar{B}^* & B^*\bar{B}^* & B_s\bar{B}_s^* & B_s^*\bar{B}_s^* \end{array}$$
$$\left(\begin{array}{cccc} \frac{1}{2}(\lambda_0+\lambda_1) & \frac{1}{2}(-\lambda_0+\lambda_1) & \frac{1}{2}(\lambda_{0m}+\lambda_{1m}) & \frac{1}{2}(-\lambda_{0m}+\lambda_{1m}) \\ \frac{1}{2}(-\lambda_0+\lambda_1) & \frac{1}{2}(\lambda_0+\lambda_1) & \frac{1}{2}(-\lambda_{0m}+\lambda_{1m}) & \frac{1}{2}(\lambda_{0m}+\lambda_{1m}) \\ \frac{1}{2}(\lambda_{0m}+\lambda_{1m}) & \frac{1}{2}(-\lambda_{0m}+\lambda_{1m}) & \frac{1}{2}(\lambda_{0s}+\lambda_{1s}) & \frac{1}{2}(-\lambda_{0s}+\lambda_{1s}) \\ \frac{1}{2}(-\lambda_{0m}+\lambda_{1m}) & \frac{1}{2}(\lambda_{0m}+\lambda_{1m}) & \frac{1}{2}(-\lambda_{0s}+\lambda_{1s}) & \frac{1}{2}(\lambda_{0s}+\lambda_{1s}) \end{array} \right)_{I=0} \tag{3.50}$$

- $J = 1(C = +)$, $I = 0$

$$\begin{array}{cc} B\bar{B}^* & B_s\bar{B}_s^* \end{array}$$
$$\left(\begin{array}{cc} \lambda_1 & \lambda_{1m} \\ \lambda_{1m} & \lambda_{1s} \end{array} \right)_{I=0} \tag{3.51}$$

- $J = 2$, $I = 0$

$$\begin{array}{cc} B^*\bar{B}^* & B_s^*\bar{B}_s^* \end{array}$$
$$\left(\begin{array}{cc} \lambda_1 & \lambda_{1m} \\ \lambda_{1m} & \lambda_{1s} \end{array} \right)_{I=0} \tag{3.52}$$

For $I = 1$ one removes the B_s, B_s^* states in the former Eqs. (3.49)−(3.52). The coefficients λ_i^I, λ_{is}^I and λ_{im}^I $(i = 0, 1)$ are the six unknown LEC's of HQSS, which depend on isospin and can be related using $SU(3)$ flavour symmetry. The values of these coefficients are also dependent on the model used. As done in the former works before, we also determine them by using the LHG approach.

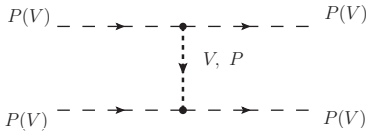

Figure 3.21: Diagrams for interaction of pseudoscalar or vector mesons with themselves by means of meson exchange.

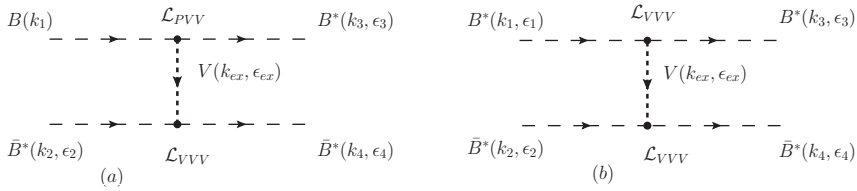

Figure 3.22: Diagrams for interactions of $B\bar{B}^* \to B^*\bar{B}^*$ and $B^*\bar{B}^* \to B^*\bar{B}^*$.

3.3.2 Calculation of the LEC's with the LHG formalism

The formalism of the LHG and the Lagrangians can be seen the subsection 1.2.2. Starting from these Lagrangians, the $PP \to PP$, $PV \to PV$, $VV \to VV$, $PP \to VV$ and $PV \to VV$ interactions can be obtained using the Feynman diagrams by exchanging a vector meson or a pseudoscalar depending on the case, as depicted in Fig. 3.21.

With lowest order HQSS constraints, the six unknown LEC's of λ_i^I, λ_{is}^I and λ_{im}^I $(i = 0, 1)$ are spin independent. Therefore, we can determine them with the hidden gauge approach by some selected channels, taking the transitions $B\bar{B}^* \to B^*\bar{B}^*$ and $B^*\bar{B}^* \to B^*\bar{B}^*$ for example, shown in Fig. 3.22. In the upper vertex of Fig. 3.22 (a), using Eq. (1.37), we can have

$$t_{PVV} \simeq \epsilon^{\mu\nu\alpha\beta}\, k_{3\mu}\, \epsilon_{3\nu}\, k_\alpha^{ex}\, \epsilon_\beta^{ex}. \tag{3.53}$$

For the lower vertex of Fig. 3.22 (a), using Eq. (1.33), we obtain

$$t_{VVV} = \frac{g}{\sqrt{2}}\,(k_2 + k_4)_\mu\, \epsilon_{2\nu}\, \epsilon_4^\nu\, \epsilon_{ex}^\mu. \tag{3.54}$$

Thus, from these results, we can estimate the magnitude of the amplitude for $B\bar{B}^* \to B^*\bar{B}^*$. Working relatively close to threshold, as is our case, the

external momenta are small, which means that $\vec{k}_3 \approx 0$ and then only the $\mu = 0$ component of Eq. (3.53) contributes, $k_3^0 \approx m_{B^*}$. Thus,

$$t_{PVV} \sim \epsilon^{ijk}\, m_{B^*}\, \epsilon_{3i}\, k_j^{ex}\, \epsilon_k^{ex}, \tag{3.55}$$

which implies that the momentum of the exchange vector is only spatial. Next, for the transition of $B\bar{B}^* \to B^*\bar{B}^*$, we can find

$$t_{B\bar{B}^*\to B^*\bar{B}^*} \sim \epsilon^{ijk}\, m_{B^*}\, \epsilon_{3i}\, k_j^{ex}\, (k_2+k_4)_k\, \epsilon_{2\nu}\, \epsilon_4^{\nu} \sim k_l^2\, m_{B^*}, \tag{3.56}$$

where k_l^2 is the magnitude of an external three momenta and is small. On the other hand, for the Fig. 3.22 (b), the transition of $B^*\bar{B}^* \to B^*\bar{B}^*$, we can easily get

$$t_{B^*\bar{B}^*\to B^*\bar{B}^*} \simeq (k_1+k_3)\cdot(k_2+k_4)\, \epsilon_{1\mu}\, \epsilon_3^{\mu}\, \epsilon_{2\nu}\, \epsilon_4^{\nu} \sim 4m_{B^*}^2, \tag{3.57}$$

where we take an approximation of $k_i^0 \approx m_{B^*}$ $(i = 1, 2, 3, 4)$. Comparing with Eqs. (3.56) and (3.57), we can conclude that the contribution of the transition of Fig. 3.22 (a) is anomalous and subleading and then, we can take $t_{B\bar{B}^*\to B^*\bar{B}^*} \approx 0$, which is indeed the case if the actual evaluation is done. In the leading order in the m_Q counting where B and B^* have the same mass, the term would go to zero. Therefore, we obtain

$$\begin{aligned} t_{B\bar{B}^*\to B^*\bar{B}^*} &= \frac{1}{2}(-\lambda_0+\lambda_1) \approx 0, \\ \Longrightarrow \quad & \lambda_0 = \lambda_1. \end{aligned} \tag{3.58}$$

Analogously, we have

$$\lambda_{0s} = \lambda_{1s}, \quad \lambda_{0m} = \lambda_{1m}. \tag{3.59}$$

So, one can see that some non diagonal elements of Eqs. (3.49)−(3.52) are zero in our hidden gauge model.

We can repeat the same arguments in cases where the exchange of a pseudoscalar is allowed, like $VV \to PP$ (see Fig. 3.21) for the case of $B^*\bar{B}^* \to B\bar{B}$. In this case we can exchange a pion. We need the vertices of Eq. (1.34) and we find an interaction for the vertices B^*, $\bar{B}^*$ close to threshold of the type

$$t \approx \frac{2\,\vec{p}_B\,\vec{\epsilon}\,2\,\vec{p}_{\bar{B}}\,\vec{\epsilon}\,'}{(m_{B^*}-m_B)^2 - \vec{p}_B^{\,2} - m_\pi^2}. \tag{3.60}$$

Since $\vec{p}_B \approx 690$ MeV/c and $(m_{B^*} - m_B) = 45$ MeV, the term $\vec{p}_B^{\,2}$ dominates in the denominator and the order of magnitude in Eq. (3.60) is of the order of 4, to be compared with Eq. (3.57), which, considering the vector exchange propagator, is of order $4m_{B^*}^2/m_\rho^2$. There is more than a factor 50 difference in the interaction considering the angle dependence of Eq. (3.60). In the case of $B\bar{B}^* \to B\bar{B}^*$ we can also have pion exchange, but at threshold the three momentum is zero and the pion exchange interaction is further suppressed. Although these derivations are done for the tree level diagram, in loops the terms will survive, but the exercise done is sufficient to show that these terms are subleading in the heavy quark mass counting. An important consequence of this is that in our approach the B and B^* do not mix and then we get states for $B\bar{B}$, $B\bar{B}^*$ and $B^*\bar{B}^*$ independently, but coupled to the corresponding channels with B_s, B_s^*.

The subleading character of pion exchange seems to contrast with the large amount of work done assuming the dynamics of pion exchange [89, 90, 437, 439, 440, 442–445, 451, 462–465]. One indication of the weakness of this potential can be seen in the fact that while in some works the mechanism is enough to bind for instance the $X(3872)$ as a $D\bar{D}^*$ state [437, 439, 440], in other works one reaches the opposite conclusion [462, 463]. The comparison of our work with other work where pion exchange is taken into account is better done with the works of Refs. [442–445, 451, 454] where, in addition to pion exchange, other exchanges are taken into account as σ, η and in particular, vector meson exchange as we have done here. Yet, the conclusions seem to be different than here, indicating a weaker strength for the vector exchange than we find here. In part this is due to cancellations in particular channels (see our discussion below concerning $I = 1$ states), but there is a general stronger reason that we discuss now. Indeed, form factors introduced in the vertices in Refs. [442, 451, 454], produce a dynamics from vector meson exchange that is drastically weaker than that provided by the chiral Lagrangians, which we would like to respect in our work.

Since the LEC's are dependent on the isospin, we should take into account the isospin structure of the states. Thus, we can easily derive $\lambda_1^{I=0}$, $\lambda_1^{I=1}$ for $B^*\bar{B}^* \to B^*\bar{B}^*$ by exchanging ρ, ω using Eq. (1.33), ignor-

ing possible terms with Υ exchange which are negligible, and we find

$$\lambda_1^{I=0} = t^{I=0}_{B^*\bar{B}^*\to B^*\bar{B}^*} = \frac{1}{4}\, g^2(\frac{3}{m_\rho^2}+\frac{1}{m_\omega^2})(4m_{B^*}^2-3s), \tag{3.61}$$

$$\lambda_1^{I=1} = t^{I=1}_{B^*\bar{B}^*\to B^*\bar{B}^*} = \frac{1}{4}\, g^2(-\frac{1}{m_\rho^2}+\frac{1}{m_\omega^2})(4m_{B^*}^2-3s). \tag{3.62}$$

We are also neglecting here the contact terms of the vector vector interactions of the hidden gauge approach. These terms are of order $(m_V/m_{B^*})^2$ with respect to the vector meson exchange terms [383], and hence negligible. In the charm sector they are small but not negligible (of the order of 20 %) and they are kept in Ref. [383].

By taking $m_\rho \approx m_\omega = m_V$ in Eqs. (3.61) and (3.62), we get a general result,

$$\lambda_1^{I=0} = \frac{1}{4}\, g^2(\frac{3}{m_\rho^2}+\frac{1}{m_\omega^2})(m_1^2+m_2^2+m_3^2+m_4^2-3s), \tag{3.63}$$

$$\lambda_1^{I=1} = 0. \tag{3.64}$$

Similarly, taking the interactions of $B_s^*\bar{B}_s^* \to B_s^*\bar{B}_s^*$ and $B^*\bar{B}^* \to B_s^*\bar{B}_s^*$, which now require ϕ and K^* exchange, we also get

$$\lambda_{1s}^{I=0} = \frac{1}{2}\, g^2 \frac{1}{m_\phi^2}(m_1^2+m_2^2+m_3^2+m_4^2-3s), \tag{3.65}$$

$$\lambda_{1s}^{I=1} = 0, \tag{3.66}$$

$$\lambda_{1m}^{I=0} = \frac{1}{\sqrt{2}}\, g^2 \frac{1}{m_{K^*}^2}(m_1^2+m_2^2+m_3^2+m_4^2-3s), \tag{3.67}$$

$$\lambda_{1m}^{I=1} = 0, \tag{3.68}$$

This is a peculiar finding of the hidden gauge approach, which gives a null interaction in the $I = 1$ sector. This would be in contradiction with the finding of the $Z_b(10610)$ and $Z_b(10650)$ resonances which appear very close to the $B\bar{B}^*$ and $B^*\bar{B}^*$ thresholds, such that, assuming they are molecular states, it implies that the interaction is weak or subdominant, as we are finding. In models where λ_0, λ_1 are fitted to some data, as in Ref. [247], one can get $I = 1$ bound states.

Since we are getting an $I = 1$ zero potential in the limit of $m_\rho = m_\omega$, this is one case where the subleading interaction of pseudoscalar exchange,

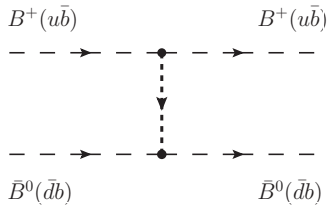

Figure 3.23: Diagrams for interactions of $B^+\bar{B}^0 \to B^+\bar{B}^0$.

as considered in Refs. [442, 444, 445], might be relevant. Yet, it is a more subtle issue than usually acknowledged. Indeed, consider a $B^+\bar{B}^0 \to B^+\bar{B}^0$ interaction, as depicted in Fig. 3.23. We can see that if we exchange a light meson as $(q\bar{q})$ object, we start from the upper vertex with a $u\bar{u}$, but in the lower vertex we should absorb a $d\bar{d}$. This violates the OZI rule and will be forbidden with usual Lagrangians. Indeed, one can see that here and in Ref. [442] the ρ and ω contribution cancel when these masses are equal. The same should happen with the pseudoscalar exchange and one should have an exact cancellation when $\pi,\ \eta,\ \eta'$ are exchanged assuming the same masses. Conversely, for large exchanged momenta where $q > m$, we should find an exact cancellation. In Ref. [442] π and η are explicitly considered and indeed the cancellation for pseudoscalars does not appear. The same can be said about the σ-exchange, unless the σ is considered as a tetraquark or a molecular state. This is why the LHG approach gives zero interaction in $I = 1$, and one needs to get further insight into this problem in future works [2].

3.3.3 The coupled channel approach for the heavy quark sector

The scattering matrix is evaluated by solving the coupled channels BS equation Eq. (1.44), seen in the subsection 1.3.1.

At higher energies for the beauty sector, as discussed in the former work (Ref. [428]) and Ref. [128], there are large differences even not far away from threshold. This is because, for heavy mesons one can accommodate large

[2] Very recently this problem has been retaken in Refs. [107, 466], where the exchanges of heavy vectors are found to lead to very weakly bound states of $D\bar{D}^*$ and $D^*\bar{D}^*$

momentum transfers with small energy, and cut offs of reasonable range, of the order of $500 - 1000$ MeV, already produce distorted G functions at excitation energies of the order of 100 MeV. On the other hand, for energies below threshold the cut off method always gives G negative, while the dimensional regularization can produce G positive, leading to an unwanted result of bound states with repulsive potentials (see discussion in the former work [428]).

We are interested in bound states, so, we will rely upon the cut off method. Then it is useful to recall how the on shell BS equation that we use here are derived with a Quantum Mechanical approach. This is done in Ref. [95] and also discussed in the former work (Ref. [428]). Following the former work, we should introduce a form factor to the potential V, seen Eqs. (3.30−3.32), but now

$$G(s) = \int \frac{d^3\vec{q}}{(2\pi)^3} f^2(\vec{q}) \frac{\omega_1 + \omega_2}{2\,\omega_1\,\omega_2} \frac{1}{P^{0\,2} - (\omega_1 + \omega_2)^2 + i\varepsilon}. \tag{3.69}$$

Thus, the loop function $G(s)$ of Eq. (3.69) absorbs a momentum dependent form factor from the factorized potential. A form factor $f(\vec{q})$ that appears in our approach is discussed in the former work, seen Eq. (3.35), and comes from the light vector meson exchange. It is obtained from the vector meson propagator keeping the three momentum exchange, ignoring the energy exchange. This allows us to keep for v the same potentials that we have used before, and the effect of the form factor of Eq. (3.35) is absorbed in the G function, Eq. (3.69), that now becomes convergent. Certainly, for dynamical reasons, or just to account for missing channels in the approach, one still has some freedom in q_{max} which we shall use in the results section.

Note that the introduction of q_{max} in the G function, is equivalent to multiplying the form factor $f(\vec{q})$ by the step function $\theta(q_{max} - q)$. The potential in coordinate space can be obtained by Fourier transforming Eq. (3.30). A smaller cut off would imply a wider potential and a more spread wave function. The spread of the wave function would be relevant when discussing the variation of the couplings as one changes the cut off (see also [95]).

An important parameter in the analysis is the cutoff used to regularize the loop functions. In the heavy quark limit, the value of q_{max} should be independent of quark flavor. To see this, note that in the heavy quark limit,

the binding energy of states is independent of the heavy quark mass. In terms of the t matrix, this means that the position of the poles of the t matrix with respect to the threshold should be independent of the heavy quark mass, i.e., vG should scale as m_Q^0 in the heavy quark limit. Since the potential v scales as m_Q^2 in the heavy quark limit (as discussed in section Sec. 3.1), the G function should scale as m_Q^{-2} to cancel the m_Q dependence of the potential v. In the definition of the G function, Eq. (1.47), if one makes the following approximations:

$$\frac{1}{(P^0)^2 - (w_1 + w_2)^2 + i\epsilon} \simeq \frac{1}{4Bm_Q}, \tag{3.70}$$

where B is the binding energy and taking approximation $w_i \simeq m_Q$, the G function can be estimated as

$$G \simeq \frac{1}{4Bm_Q^2} \int_{q<q_{max}} \frac{d^3q}{(2\pi)^3} f(q^2)^2. \tag{3.71}$$

Since G has to scale as m_Q^{-2} in the heavy quark limit, the integral has to scale as m_Q^0, and hence q_{max} should be flavor independent in the heavy quark limit.

The molecules appear as the poles of the t matrix given in Eq. (3.32). The coupling of a given resonance of mass m_R to the i^{th} channel can be obtained through (for meson-meson interaction):

$$g_i^2 = \lim_{s \to m_r^2} (s - m_R^2) t_{ii}. \tag{3.72}$$

Instead of taking this limit, which would require a high precision determination of m_R, the limit can be expressed as a loop integral in the complex s plane:

$$g_i^2 = \frac{1}{2\pi i} \oint t_{ii} ds \tag{3.73}$$

where the integral is over a closed path in the complex s plane around the pole at $s = m_R^2$ and not crossing the branch cuts.

3.3.4 Results and discussion

Requiring that the presented formalism predicts a bound state of mass 3720 MeV, as found in Ref. [261], when the B meson masses are replaced by the

analogous D meson masses, yields the value $q_{max} = 415$ MeV. Assuming that this cutoff is independent of the heavy flavor, the same value is used in the B-meson sector. To estimate the errors due to variation of this cutoff, the spectrum is also analyzed using twice this value: $q_{max} = 830$ MeV. These values are also consistent with the typical scales proposed in Ref. [427].

In principle, by exchanging K^* mesons, the hidden strange sector is coupled to the non-strange one. When discussing coupled channels with such a small cut off for coupled channels with different masses, some technical details are in order. If we study bound states of $B\bar{B}$ and we add the $B_s\bar{B}_s$ channel, the G function for $B_s\bar{B}_s$ in the energy region around the $B\bar{B}$ threshold is negligible and then the effect of the $B_s\bar{B}_s$ coupled channel is washed away.

The reverse has technical problems. If we investigate a possible state around the $B_s\bar{B}_s$ threshold, separated by 180 MeV from the $B\bar{B}$ threshold, the $B\bar{B}$ state would have a momentum of 980 MeV/c, which is bigger than the cut-off chosen. This means that the G function for $B\bar{B}$ around the $B_s\bar{B}_s$ threshold will be unrealistic with the small cut-off chosen and we can not use this method. It is better to argue that the $B\bar{B}$ state will not influence any possible $B_s\bar{B}_s$ bound state in the same was as the $B_s\bar{B}_s$ did not influence the bound state $B\bar{B}$. The only difference is that the $B_s\bar{B}_s$ bound state could decay to the $B\bar{B}$ channel, but the disconnection of these states will make its width also small. We can even estimate this width by taking $\mathrm{Re}G_{B\bar{B}} = 0$ around the $B_s\bar{B}_s$ threshold which we expect on physical grounds, but keeping $\mathrm{Im}G_{B\bar{B}}$ which can be calculated analytically to be:

$$\mathrm{Im}G = -\frac{1}{8\pi}\frac{q_{cm}}{\sqrt{s}} f(q_{cm}^2)^2 \tag{3.74}$$

where q_{cm} is defined after Eq. (1.46).

In all the cases analyzed, coupled channels wash away the second pole, which is dominantly a hidden strange state. This second pole has a weak strength even in the single channel case. The origin of the lack of a second pole in the coupled channel case can be traced back to the potential v. When the effects of coupled channel analysis are taken into account, the dominant contribution to the determinant of the potential is proportional to $m_{K^*}^4 - m_\phi^2 m_\rho^2$ with a small correction from the mass difference of the hidden strange sector and the non-strange one (see Eqs.(3.63)−(3.68)). Since

$m^2_{K^*} \simeq m_\phi m_\rho$, this determinant is very small, hence one of the eigenvalues is very close to zero. This means that, in the corresponding channel, which is mostly hidden strange state, the mesons do not interact and hence can not form a bound state.

In the $J^{PC} = 2^{++}$ sector, the available channels are the $B^*\bar{B}^*$ and $B_s^*\bar{B}_s^*$. When the coupled channel effects are taken into account, the t matrix has a single pole which is located at $m_R = 10613$ MeV ($m_R = 10469$ MeV) when $q_{max} = 415$ MeV (830 MeV). This corresponds to a binding energy of 37 MeV (181 MeV) with respect to the $B^*\bar{B}^*$ threshold. In Table 3.7 we present the masses and the couplings of this resonance to various channels for $q_{max} = 415$ MeV and $q_{max} = 830$ MeV. It is observed that both the binding energy and the couplings strongly depend on the value of the cut off chosen. Increasing the cut off from $q_{max} = 415$ MeV to $q_{max} = 830$ MeV changes the binding energy by about 140 MeV whereas the couplings increase by a factor of two. This increase in the couplings is expected since as one increases the cut off, the potential has larger extent in momentum space, and hence the wave functions become narrower in coordinate space. A narrower S-wave wave function necessarily has a larger value at the origin. Since the couplings are proportional to the wave function at the origin, as the wave function gets narrower its value at the origin increases and the coupling grows.

Table 3.7: The couplings to various channels for the poles in the $J^{PC} = 2^{++}$ channel for $q_{max} = 415$ MeV (left panel) and $q_{max} = 830$ MeV (right panel), all units in MeV.

10613	$B^*\bar{B}^*$	$B_s^*\bar{B}_s^*$	10469	$B^*\bar{B}^*$	$B_s^*\bar{B}_s^*$
g_i	86168	45864	g_i	174393	92843

As mentioned before, we deem the value of the lower cut off more realistic, and also in tune with Ref. [427]. The value obtained with $q_{max} = 830$ MeV should be considered a generous upper bound.

In Table 3.8, we present the properties of resonances if the coupled channel effects are ignored. It is seen that the properties of the lighter resonance changes slightly by the removal of the coupled channel effects. Its mass increases by 3 MeV (31 MeV) and its coupling to the $B^*\bar{B}^*$ state

is reduced by about 5% (10%) if the cut off is taken as $q_{max} = 415$ Mev (830 MeV). Since the coupled channel effects are ignored, this resonance does not couple to $B_s^* \bar{B}_s^*$. In this case, a weakly bound second pole is also observed in the $B_s^* \bar{B}_s^*$ channel. This second pole has a binding energy of 2 MeV (18 MeV) when the cut off is taken to be $q_{max} = 415$ MeV (830 MeV). This binding energy is more than ten times smaller than the binding of the lighter resonance. The coupling of this heavier resonance to $B_s^* \bar{B}_s^*$ is also about four times smaller that the coupling of the lighter resonance to the $B^* \bar{B}^*$ channel.

Table 3.8: The couplings to various channels for the poles in the $J^{PC} = 2^{++}$ channel for $q_{max} = 415$ MeV (left panel) and $q_{max} = 830$ MeV (right panel) ignoring coupled channels, all units in MeV.

10616	$B^* \bar{B}^*$	$B_s^* \bar{B}_s^*$	10500	$B^* \bar{B}^*$	$B_s^* \bar{B}_s^*$
g_i	81595	0	g_i	159102	0
10828	$B^* \bar{B}^*$	$B_s^* \bar{B}_s^*$	10812	$B^* \bar{B}^*$	$B_s^* \bar{B}_s^*$
g_i	0	19787	g_i	0	44102

In a $B^* \bar{B}^*$ molecule, the vector mesons can also combine to a total spin 1 ($J^{PC} = 1^{+-}$) or 0 ($J^{PC} = 0^{++}$) state. In the heavy quark limit considered in this work, these channels are degenerate with the total spin 2 state. Hence, their properties are identical to the properties of resonances shown in Tables 3.7 and 3.8.

Besides the $J = 1$ combination in the $B_{(s)}^* \bar{B}_{(s)}^*$ channel, there are four other states with $J = 1$ formed by $B_{(s)} \bar{B}_{(s)}^*$. These states have quantum number $J^{PC} = 1^{++}$ and $J^{PC} = 1^{+-}$ and are $B_{(s)} \bar{B}_{(s)}^* -$ c.c. and $B_{(s)} \bar{B}_{(s)}^* +$ c.c. respectively. These channels are degenerate in the heavy quark limit. The properties of resonances in these channels are shown in Tables 3.9 and 3.10. As in the $J^{PC} = 2^{++}$ channel, if coupled channels are taken into account, there is only one resonance. This resonance has a binding energy of 37 MeV (180 MeV) with respect to the $B\bar{B}^*$ threshold. Compared with the previous case, the binding energy is found to be degenerate with the binding energies obtained in the $J^{PC} = 2^{++}$ channel. Due to the smaller

mass of the $B\bar{B}^*$ system compared to the $B^*\bar{B}^*$, the couplings to various channels are slightly smaller.[3] The results obtained when coupled channel effects are ignored are presented in Table 3.10. As in the case when coupled channel effects are taken into account, the binding energies are degenerate with the corresponding case in $J^{PC} = 2^{++}$ sector, and the couplings are slightly reduced.

Table 3.9: The couplings to various channels for the poles in the $J^{PC} = 1^{+-}$ and $J^{PC} = 1^{++}$ channels for $q_{max} = 415$ MeV (left panel) and $q_{max} = 830$ MeV (right panel), all units in MeV.

10568	$B\bar{B}^*$±c.c.	$B_s\bar{B}_s^*$±c.c.	10425	$B\bar{B}^*$±c.c.	$B_s\bar{B}_s^*$±c.c.
g_i	85433	45560	g_i	172908	92232

Table 3.10: The couplings to various channels for the poles in the $J^{PC} = 1^{+-}$ and $J^{PC} = 1^{++}$ channels for $q_{max} = 415$ MeV (left panel) and $q_{max} = 830$ MeV (right panel) ignoring coupled channels, all units in MeV.

10571	$B\bar{B}^*$±c.c.	$B_s\bar{B}_s^*$±c.c.	10455	$B\bar{B}^*$±c.c.	$B_s\bar{B}_s^*$±c.c.
g_i	80884	0	g_i	157691	0
10783	$B\bar{B}^*$±c.c.	$B_s\bar{B}_s^*$±c.c.	10768	$B\bar{B}^*$±c.c.	$B_s\bar{B}_s^*$±c.c.
g_i	0	19611	g_i	0	43776

In Tables 3.11 and 3.12, we present our results for the $J^{PC} = 0^{++}$ sector. In this sector, the new states are $B\bar{B}$ and $B_s\bar{B}_s$. The similarities that we observed when comparing the $J^{PC} = 2^{++}$ and $J^{PC} = 1^{+\pm}$ sectors also exists when the $J^{PC} = 0^{++}$ channel is compared with the previous cases, i.e. the binding energies are degenerate with the previous cases and due to the even smaller total mass in the $B_{(s)}\bar{B}_{(s)}$, the couplings are smaller. The

[3]The couplings are related to the wave function at the origin. Due to the smaller masses, the wave function spreads more, reducing the value of the wave function at the origin.

Table 3.11: The couplings to various channels for the poles in the $J^{PC} = 0^{++}$ channel for $q_{max} = 415$ MeV (left panel) and $q_{max} = 830$ MeV (right panel), all units in MeV.

10523	$B\bar{B}.$	$B_s\bar{B}_s$	10380	$B\bar{B}$	$B_s\bar{B}_s$
g_i	85045	45257	g_i	172046	91591

Table 3.12: The couplings to various channels for the poles in the $J^{PC} = 0^{++}$ channel for $q_{max} = 415$ MeV (left panel) and $q_{max} = 830$ MeV (right panel) ignoring coupled channel effects, all units in MeV.

10526	$B\bar{B}.$	$B_s\bar{B}_s$	10410	$B\bar{B}$	$B_s\bar{B}_s$
g_i	80528	0	g_i	156968	0
10738	$B\bar{B}$	$B_s\bar{B}_s$	10723	$B\bar{B}$	$B_s\bar{B}_s$
g_i	0	19441	g_i	0	43443

binding obtained here for $B\bar{B}$ with the small cut off is very similar to the one obtained in Ref. [445] using the extended chiral quark model, where vector mesons are allowed to be exchanged between quarks, with clear similarities with the dynamics of the LHG approach.

Note that the observed degeneracies are consistent with the results obtained in Refs. [91, 246, 247]. In these works, it is shown that in the heavy quark limit, in the spectrum of molecules of $\bar{Q}q$ and $\bar{q}Q$ where Q is a heavy quark and q is any other quark, the $J^{PC} = 0^{++}$, 1^{++}, 2^{++} and 1^{+-} states have degenerate binding energies. Furthermore, there are two other states with $J^{PC} = 0^{++}$ and 1^{+-} that have degenerate binding energies which are not necessarily degenerate with the previous four. In our work, we observe that all six states have degenerate binding energies. These degeneracies can be observed from Eqs. (3.49)−(3.52).

3.3.5 Further discussions

From the former section, we find 6 hidden beauty resonances and other 6 possible resonances with hidden beauty-hidden strangeness. In this section we investigate some of their properties. For shortness of the discussion, we only take the results of Table 3.11, $B\bar{B}$ state. Results in other cases are similar.

Following again Refs. [95, 205, 206], one finds that for a resonance or bound state, which is dynamically generated by the interaction, the sum rule

$$-\sum_i g_i^2 \left[\frac{dG_i}{dE}\right]_{E=E_p} = 1 \tag{3.75}$$

is fulfilled, with E_p the position of the pole, and g_i is the coupling, defined in Eq. (3.72). For bound states each term in the sum in Eq. (3.75) is a measure of the probability, P_i, to find the particular channel in the wave function of the given state (subtleties appear for the case of resonances in Ref. [467], but, since this is not the case here, we do not discuss it). For the 0^{++} state that couples mostly to $B\bar{B}$ (see Table 3.11), taking $q_{max} = 415$ MeV, we get $P_{B\bar{B}} = 0.985$, which means that the bound state with mass 10523 MeV is essentially made by $B\bar{B}$ with a minor $B_s\bar{B}_s$ component. This state is also rather stable, taking into account the changes of the free parameters in our formalism, as showed in Table 3.13, where we take different values of q_{max}

Table 3.13: The poles in the $J^{PC} = 0^{++}$ channel when the cut off is changed (units in MeV).

q_{max}	450	500	600	700	800
pole	10513	10498	10464	10427	10389

and always get a pole within a certain range of binding energies.

Another property which is interesting to study is the wave function and radius of the state. According to Eq. (104) of Ref. [205], the wave function is given by

$$\phi(\vec{r}) = \int_{q_{max}} \frac{d^3\vec{p}}{(2\pi)^{3/2}}\, e^{i\vec{p}\cdot\vec{r}} \langle \vec{p}|\Psi\rangle. \tag{3.76}$$

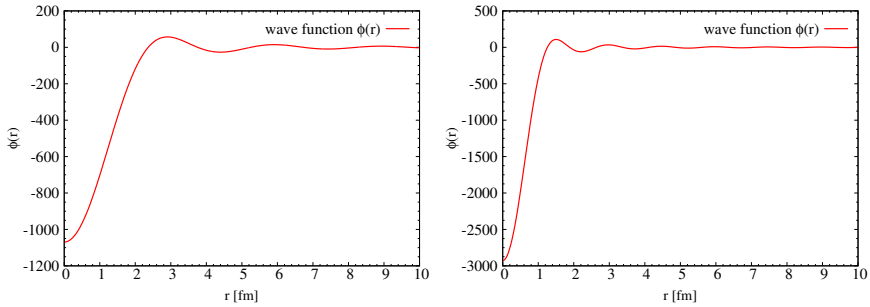

Figure 3.24: The wave functions of $B\bar{B}$ state, Left: $q_{max} = 415$ MeV; Right: $q_{max} = 830$ MeV.

Using the wave function in momentum space given in Refs. [95, 205] suited to our formalism, we obtain after performing the angle integration

$$\phi(\vec{r}\,) = \frac{1}{(2\pi)^{3/2}} \frac{4\pi}{r} \frac{1}{C} \int_{q_{max}} p\, dp\, sin(pr) \frac{\Theta(q_{max} - |\vec{p}|)}{E - \omega_1(\vec{p}) - \omega_2(\vec{p}\,)} \frac{m_V^2}{\vec{q}^{\,2} + m_V^2}, \tag{3.77}$$

where $r \equiv |\vec{r}|$ and $C \equiv \sqrt{\mathcal{N}}$ is the norm of the wave function, obtained demanding that $\int |\phi(r)|^2 d^3r = 1$. For the $B\bar{B}$ state, we show its wave function in Fig. 3.24. The radii are given in the Table 3.14 for two values of the cut off. These radii are of the same order of magnitude as those found for related beauty states in Refs. [442, 445].

Table 3.14: The radii of the states.

states	$q_{max} = 415$ MeV	$q_{max} = 830$ MeV
$B^*\bar{B}^*$	1.46 fm	0.72 fm
$B\bar{B}^*$	1.46 fm	0.72 fm
$B\bar{B}$	1.46 fm	0.72 fm

3.3.6 Conclusions

In the present work we investigate the hidden beauty sector by combining the dynamics of the LHG Lagrangians extrapolated to $SU(4)$ with the constraints of HQSS. The $SU(4)$ symmetry is broken to $SU(3)$ symmetry by taking large masses for the mesons containing a b-quark.

It is shown that in the $I = 1$ sector, the interaction is too weak in the current approach to form any bound states. In the $I = 0$ sector, both the hidden strangeness and non-strange channels are analyzed. The results show that the binding energies in all the possible J^{PC} channels are degenerate.

When the couplings between the hidden strange and non strange sectors are ignored, bound states are observed in both sectors. Hence there are a total of 6 hidden beauty resonances, with binding energies 34 MeV (178 MeV) with respect to the non strange threshold, and 6 hidden beauty-hidden strange resonances, with binding energies 2 MeV (18 MeV) with respect to the hidden strange threshold, for a cut off value of $q_{max} = 415$ MeV ($q_{max} = 830$ MeV). The hidden beauty-hidden strange resonances are found to be weakly bound.

Our prediction of the existence of resonances close to the the hidden strange threshold is not robust with respect to the effects of the coupled channels. When the coupled channel effects are taken into account they disappear, whereas the masses of the other resonances are only slightly modified. Hence we predict with confidence the existence of (at least) 6 resonances in the hidden beauty sector, with possible other 6 heavier resonances which are mainly hidden beauty-hidden strange resonances.

The couplings of each resonance to the various channels are also analyzed and for the lighter resonance in each channel, the couplings are shown to depend very slightly on the couple channel effects. It is also shown that the couplings are quite sensitive to the value of the cut off used, hence they should be taken more as an order of magnitude estimate rather than precise predictions. When any of these states is experimentally found, the tuning of the cut off to the observed energies will also allow to be more precise on the value of these couplings.

Finally, using the Weinberg compositeness condition [204] (Eq. (3.75)), we determine the probability to find a certain channel in the wave function. We also determine the radii of the states, which, within the uncertainties of the approach, are compatible with values obtained in alternative approaches.

3.4 Baryon states with open beauty

Hadron Physics in the charm and beauty sectors is booming, with mounting activity in experiments BABAR, CLEO, BELLE, BES, LHC$_b$, CDF [433–436, 468, 469] and theory [131]. One of the issues that has attracted much attention is the finding of hadronic states which cannot be interpreted in the conventional picture of $q\bar{q}$ for mesons and qqq for baryons. Multiquark states, hybrids or hadronic molecules have been suggested in several works [247, 260, 261, 346, 350, 446, 470–474]. The molecular picture stands on firm grounds once the use of chiral unitary theory in the light quark sector, or its extension through the LHG approach, has shown that many mesonic and baryonic resonances are dynamically generated from the interaction of more elementary hadron components [189, 395]. Concerning baryonic resonances with charm or hidden charm, work on molecules has been done in Refs. [127, 168, 238, 256–258, 397, 412, 475], while in the beauty sector, baryon states with beauty or hidden beauty have also been studied in Refs. [128, 398, 428, 476].

On the experimental side, Λ_b excited states have been reported by the LHC$_b$ collaboration in Ref. [399]. Two states, $\Lambda_b(5912)$ and $\Lambda_b(5920)$ are found in the experiment, with widths smaller than 0.66 MeV in both cases. Although no direct spin and parity have been determined, the states are interpreted as orbitally excited states of the ground state of the $\Lambda_b(5619)$. One of the states, the $\Lambda_b(5920)$, has been confirmed by the CDF collaboration in Refs. [477, 478]. The association to the orbitally excited states of the $\Lambda_b(5619)$ seems most natural since predictions of quark models had been done for these states, as the orbitally excited Λ_b states with $L = 1$ and $J^P = 1/2^-, 3/2^-$ [479, 480]. Compared to the observed results, the Λ_b masses, including that of the ground state, are only off by about 30-35 MeV.

The closest work in spirit to the present one is that of Ref. [398] where these states are dynamically generated from the interaction of mesons and baryons. In Ref. [398] the HQSS is used as an underlying symmetry. According to it, the B, B^* states are degenerate in the heavy quark limit, as well as the $J^P = 1/2^+, 3/2^+$ baryon states, which are then considered together in a coupled channels approach. An extrapolation of the Weinberg Tomozawa interaction in the light sector is then used [238, 398], with elements of an SU(6) spin-isospin symmetry [237]. With suitable choices of the renormalization scheme for the loops, good agreement with the masses

of the newly found Λ_b states is obtained. Our scheme takes advantage of the former works (Refs. [412, 428, 461]), where it was found that the use of the extended LHG approach to the heavy quark sector fully respects the HQSS, but it provided a dynamics different from the one of Ref. [398]. In particular, the connection between B and B^* states (or baryon states with $J^P = 1/2^+, 3/2^+$) requires pion exchange, or anomalous terms, which are found subleading in the large heavy quark mass counting, and numerically small. Similar conclusions are also found in Ref. [427]. In some works [442], pion exchange is found relevant compared to vector meson exchange (the dominant terms in the LHG approach), but as discussed in the former work (Ref. [461]), this is in part due to the use of a type of form factor for vector mesons, not present when the equivalent chiral amplitudes are constructed, that suppresses the vector exchange.

3.4.1 Coupled channel formalism

We will look at the states $\pi\Sigma_b$, $\pi\Lambda_b$, $\eta\Lambda_b$, $\eta\Sigma_b$, $\bar{B}N$ which can couple to $I = 0,\ 1$ which we will investigate. Similarly, we shall look at $\bar{B}^*N$ and $\pi\Sigma_b^*$, $\eta\Sigma_b^*$, $\bar{B}\Delta$, $\bar{B}^*\Delta$, with $\Delta \equiv \Delta(1232)$ and $\Sigma_b^* = \Sigma_b^*(5829)$, belonging to a decuplet of $3/2^+$ states. Since we do not consider states with strangeness or hidden strangeness, thus, all matrix elements of the interaction are formally identical (except for the mass or energy dependence) to those found for the interaction of the analogous states $\pi\Sigma$, $\pi\Lambda$, $\eta\Lambda$, $\eta\Sigma$, $\bar{K}N$, $\bar{K}^*N$, $\pi\Sigma^*$, $\eta\Sigma^*$, $\bar{K}\Delta$, $\bar{K}^*\Delta$. This interaction has been studied in Ref. [155] and Ref. [481].

The transition potential from channel i to channel j is given by [276]

$$V = -C_{ij}\frac{1}{4f^2}(2\sqrt{s} - M_{B_i} - M_{B_j})\sqrt{\frac{M_{B_i}+E_i}{2M_{B_i}}}\sqrt{\frac{M_{B_j}+E_j}{2M_{B_j}}}, \qquad (3.78)$$

with f the pion decay constant, M_{B_i}, E_i (M_{B_j}, E_j) the mass, energy of baryon of i (j) channel. We take $f = f_\pi = 93$ MeV since we exchange light vector mesons. The C_{ij} coefficients are evaluated in Refs. [155, 481] and we quote them below.

For pseudoscalar mesons and $1/2^+$ baryons we have the coupled channels $\bar{B}N$, $\pi\Sigma_b$, $\eta\Lambda_b$ in $I = 0$ and the C_{ij} coefficients are given in Table 3.15.

Table 3.15: C_{ij} coefficients for $I = 0$ and $J^P = 1/2^-$.

C_{ij}	$\bar{B}N$	$\pi\Sigma_b$	$\eta\Lambda_b$
$\bar{B}N$	3	$-\sqrt{\frac{3}{2}}$	$\frac{3}{\sqrt{2}}$
$\pi\Sigma_b$		4	0
$\eta\Lambda_b$			0

In $I = 1$ we have the channels $\bar{B}N$, $\pi\Sigma_b$, $\pi\Lambda_b$, $\eta\Sigma_b$ and the C_{ij} coefficients are given in Table 3.16.

Table 3.16: C_{ij} coefficients for $I = 1$ and $J^P = 1/2^-$.

C_{ij}	$\bar{B}N$	$\pi\Sigma_b$	$\pi\Lambda_b$	$\eta\Sigma_b$
$\bar{B}N$	1	-1	$-\sqrt{\frac{3}{2}}$	$-\sqrt{\frac{3}{2}}$
$\pi\Sigma_b$		2	0	0
$\pi\Lambda_b$			0	0
$\eta\Sigma_b$				0

As one can see, the interaction in $I = 0$ is stronger than that in $I = 1$ and we have more chances to bind states in $I = 0$.

As discussed in section Sec. 3.1 (Ref. [412]), the mixing of states containing baryons of the octet (in u, d, b) like Σ_b and of the decuplet Σ_b^* require pion exchange for their mixing and this is strongly suppressed in the heavy quarks sector, hence, we neglect the mixing in a first step, but we shall come back to it in subsection 3.4.4. Then, if we consider a pseudoscalar meson and a baryon of the decuplet, we have the results for C_{ij} given in Tables 3.17 and 3.18 [481]. We note that the strength of the $\bar{B}\Delta \to \bar{B}\Delta$ coefficient is four times bigger than for $\bar{B}N \to \bar{B}N$ and thus, we expect larger bindings in this case. The interaction $\bar{B}\Delta$ and coupled channels with $I = 2$ is repulsive and we do not consider it.

Table 3.17: C_{ij} coefficients for $I = 0$ and $J^P = 3/2^-$.

C_{ij}	$\pi\Sigma_b^*$
$\pi\Sigma_b^*$	4

Table 3.18: C_{ij} coefficients for $I = 1$ and $J^P = 3/2^-$.

C_{ij}	$\bar{B}\Delta$	$\pi\Sigma_b^*$	$\eta\Sigma_b^*$
$\bar{B}\Delta$	4	1	$\sqrt{6}$
$\pi\Sigma_b^*$		2	0
$\eta\Sigma_b^*$			0

In coupled channels we will use the BS equation Eq. (1.44), seen in subsection 1.3.1. In section Sec. 3.2 (Ref. [428]) we warned about potential dangers of using the dimensional regularization for the G functions (see also [128]) since for values of the energy below threshold G can soon become positive and then one can be misled to obtain bound states with a positive (repulsive) potential when $1 - VG = 0$ (see Eq. (1.44) in one channel). For this reason we also use here the cut off regularization for G given by Eq. (1.47), with only one free parameter, q_{max}, the cut-off of the three-momentum. However, in section Sec. 3.2 (Ref. [428]), we also took into account the form factor from vector meson exchange, seen in Eq. (3.35), in which case we would have to replace Eq. (1.47) by

$$G(s) = \int \frac{d^3\vec{q}}{(2\pi)^3} f(\vec{q}) \frac{\omega_P + \omega_B}{2\,\omega_P\,\omega_B} \frac{2M_B}{P^{0\,2} - (\omega_P + \omega_B)^2 + i\varepsilon}, \tag{3.79}$$

putting the extra $f(\vec{q})$ factor. We would like to make a comment here since in section Sec. 3.2 (Ref. [428]) we put $f^2(\vec{q})$. From the practical point of view, the differences between the two choices are smaller than uncertainties we will accept from other sources. From the theoretical point of view, while the first loop implicit in Eq. (1.44), VGV, contains $f^2(\vec{q})$, the terms in the series go as VGV, $VGVGV$, $VGVGVGV\cdots$ and the ratio of one term to the other is GV. Hence it is more appropriate to take just the one form

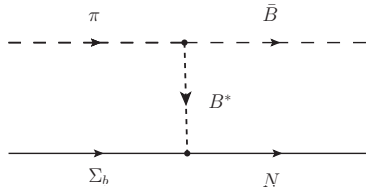

Figure 3.25: Transition potential from $\pi\Sigma_b \to \bar{B}N$.

factor of the potential V and include it in the G function when integrating over $\vec{q}$.

Since the G function in Eq. (1.47) is logarithmically divergent, the inclusion of $f(\vec{q})$ in Eq. (3.79) makes it already convergent. Yet we will put an extra cut off q_{max} that will serve to fine tune our T matrix and the binding of the states. We shall fine tune q_{max} in the integral of Eq. (1.47) and we shall need values q_{max} smaller than $M_V \approx 780$ MeV. Hence, from the practical point of view we can even neglect the factor $f(\vec{q})$ and effectively include its effects with the use of a suited value of q_{max}.

Besides, in most of the cases, we get energies where all the coupled channels are closed and, hence, the width is zero. When there are open channels we look for poles in the second Riemann sheet, which is obtained by changing the G function as Eq. (1.50) [362].

Before closing this sector we must say two words concerning the transition $\pi\Sigma_b \to \bar{B}N$. This is depicted in Fig. 3.25. and it is mediated by B^* exchange in the extended LHG approach. In the strict large heavy quark mass counting this term would be neglected because it involves the exchange of a heavy vector B^* and its propagator would render this term negligible. However, although suppressed, it is not so much as one would expect. Indeed the propagator will be

$$D_{B^*} = \frac{1}{p^2_{B^*} - m^2_{B^*}} \equiv \frac{1}{(p^0_\pi - p^0_{\bar{B}})^2 - (\vec{p}_\pi - \vec{p}_{\bar{B}})^2 - m^2_{B^*}}. \tag{3.80}$$

Conversely, in a diagonal transition $\bar{B}N \to \bar{B}N$ mediated by ρ exchange for instance we would have

$$D_\rho \approx \frac{1}{m^2_V}. \tag{3.81}$$

Close to $\bar{B}N$ threshold the ratio is

$$\frac{D_{B^*}}{D_\rho} \simeq \frac{m_V^2}{(p_\pi^0 - p_{\bar{B}}^0)^2 - \vec{p}_\pi^2 - m_{B^*}^2} \simeq \frac{1}{4}. \tag{3.82}$$

Since the non diagonal terms have a smaller importance in the process than the diagonal ones of the heavy mesons, we simply account for these transitions multiplying by 1/4 the results obtained from Eq. (3.78) and the Tables.

3.4.2 First results for $I = 0$

We first choose the single channel $\pi\Sigma_b^*$ in $I = 0$ and look for the binding energy. The state with $L = 0$ (s-wave) has $J = 3/2$. First we find that with the normal potential and a wide range of cutoffs (up to 3000 MeV) we do not find a bound state. We must look at the reason for this in the fact that the potential is indeed weak. This is so because the potential in Eq. (3.78) is a relativistic form of $k^0 + k'^0$ (the sum of the incoming and outgoing pion energies). The small mass of the π makes its energy small close to threshold and this potential is subleading with respect to the one of $\bar{B}N$ where the energies now are those of the $\bar{B}$.

Next we try to see if increasing the potential by a factor 1.5 or 2 and varying the cut off we can obtain a reasonable binding. The results are chosen in Table 3.19. As we can see, we have to increase the potential by a factor of two and go to very large cutoffs to obtain the desired value of the binding of the $\Lambda_b(5920)$. We might think that and increase by about a factor 1.5 of the potential could be accepted by recalling that such changes appear in models like Dyson Schwinger approach [413] (see also in section Sec. 3.1, Ref. [412]). Indeed, with respect to the coupling we would be using here, the $D\rho D$ coupling used in Ref. [413], or in Ref. [414] obtained with sum rules, is about a factor 1.5 bigger. However, in the same work of Ref. [413], the coupling is accompanied by a form factor which would be equivalent to a cut off q_{max} of about 700 MeV. Hence, we cannot invoke simultaneously an increase of the potential by a factor 2 and a q_{max} of 3000 MeV, and the only conclusion is that the $\pi\Sigma_b^*$ channel by itself cannot account for the $\Lambda_b(5920)$ state.

Table 3.19: Energies for $\pi\Sigma_b^*$ only channel as a function of V and q_{max}. (unit: MeV)

q_{max}	800	1000	1200	1400	1600	1800	2000	3000
$1.5\,V$	5971	5965	5961	5956	5953	5950	5948	5942
$2\,V$	5955	5947	5940	5935	5932	5929	5927	5920

Next we repeat the same exercise with the single channel $\bar{B}N$ and show the results in Table 3.20. What we see in this table is that the binding grows spectacularly (and unrealistically) for bigger V and q_{max}. Obviously the large value of the potential, as we mentioned above, is responsible for this. At this point we should mention that in the study of the $\bar{K}N$ system in coupled channels a cut off of 630 MeV was used in Ref. [155]. In the study of the pseudoscalar mesons with the decuplet of baryons [481] a value of $q_{max} = 700$ MeV was used, while in Ref. [128] in the study of baryons with hidden beauty a value of $q_{max} = 800$ MeV was used. We can also see in Table 3.19, that changes in V can be accommodated by a change in q_{max}. In what follows we shall then use the potential that we get in the approach, without the extra multiplicative factor, but play with values of q_{max} around 700 MeV $-$ 850 MeV, in the range of values used in previous works.

Table 3.20: Energies for $\bar{B}N$ only channel as a function of V and q_{max}. (unit: MeV)

q_{max}	700	800	1000	1200	1400	1600	1800	2000
$1\,V$	6074	6026	5933	5851	5782	5725	5678	5639
$1.5\,V$	5967	5896	5766	5658	5572	5504	5450	5406
$2\,V$	5871	5784	5630	5509	5415	5343	5287	5243

As an example we show next the results without form factor of Eq. (3.35) for $\bar{B}N$, just changing q_{max}, as shown in Table 3.21.

Table 3.21: Energies for a state of $\bar{B}N$ in $I = 0$ as a function of q_{max}. (unit: MeV)

q_{max}	700	750	800	850
V	5987.5	5941.6	5893.5	5843.7

Next we introduce the coupled channels that couple to $\bar{B}N$ in $I = 0$ (see Table 3.15). The results that we obtained for the energy are shown in Table 3.22.

Table 3.22: Energies for a state in coupled channels $\bar{B}N$, $\pi\Sigma_b$, $\eta\Lambda_b$ in $I = 0$ as a function of q_{max}. (unit: MeV)

q_{max}	700	750	800	850
V	5935.3	5897.3	5851.4	5802.0
	$6005.8 + i23.8$	$5988.9 + i26.4$	$5976.9 + i24.4$	$5968.0 + i20.5$

The results are interesting. We see now that we get two states rather than one. In order to get a feeling of the meaning of the states we calculate the coupling of those states to the different coupled channels. We show the results in Table 3.23 for $q_{max} = 800$ MeV. We show the values

Table 3.23: The coupling constants to various channels for certain poles in the $J = 1/2,\ I = 0$ sector.

$5851.4 + i0$	$\bar{B}N$	$\pi\Sigma_b$	$\eta\Lambda_b$
g_i	16.20	0.96	1.47
$g_i\, G_i^{II}$	-20.55	-16.23	-14.31
$5976.9 + i24.4$	$\bar{B}N$	$\pi\Sigma_b$	$\eta\Lambda_b$
g_i	$5.88 - i0.24$	$1.52 + i0.75$	$0.75 + i0.02$
$g_i\, G_i^{II}$	$-9.60 - i0.16$	$-53.13 - i12.34$	$-9.33 - i0.85$

of the couplings (g_i^2 is the residue of the matrix element T_{ii} at the pole,

seen Eq. (3.23)) and of $g_i G_i^{II}$, which, according to Ref. [95], provides the wave function of the origin in coordinate space, the magnitude that shows the relevance of the channel in the short range strong interactions. It is interesting to see that there has been an appreciable mixture of these channels. The lower energy state that originally was formed from $\bar{B}N$ alone, now is still dominated by the $\bar{B}N$ channel but with an appreciable mixture of $\pi\Sigma_b$ and $\eta\Lambda_b$. On the other hand, the higher energy state is shown to be dominated by the $\pi\Sigma_b$ channel. However, the coupling to the $\bar{B}N$ state has been essential to obtain this state, since the single channel $\pi\Sigma_b$ does not produce it.

If one compares the energy of the lower energy state in Table 3.22 with that of the single $\bar{B}N$ channel in Table 3.21, we can see that for $q_{max} =$ 800 MeV the effect of the coupled channels has been a reduction of about 40 MeV. Hence, even if suppressed, the coupled channels to the $\bar{B}N$ have a relevant role in the generation of states. In any case, we see that neither of the states found can qualify as the $\Lambda_b(5912)$, $\Lambda_b(5920)$. This is also the case for the higher energy state.

After this, we exploit another possibility, that these Λ_b states come from $\bar{B}^*N$ and coupled channels. The $\bar{B}^*N$ can lead to two spins, $J^P = 1/2^-$, $3/2^-$ and within the LHG approach the interaction is spin independent [390]. Then we would get two degenerate states with spins 1/2 and 3/2. The 8 MeV difference between $\Lambda_b(5912)$ and $\Lambda_b(5920)$ is small enough to fit into the category of degenerate. The degeneracy is broken with the mixture of the $V\,B$ and $P\,B$ states, which is done in Refs. [391–393], but for the heavier mesons this mixture is smaller [412], which can explain the small difference between the masses of the two states. We shall come back to this point in the next two subsections.

The binding of $\bar{B}N$ in Table 3.21 for $q_{max} \sim 750{-}800$ MeV is of the order of 300 MeV. While this is only 5 % of the total energy, it might surprise us that this amount is about three times bigger than the one obtained in Refs. [128,428] for hidden beauty baryons ($B\Sigma_b$ is the equivalent component), but this is easy to understand, both qualitatively and quantitatively. Indeed, in the exchange of light vectors between $\bar{B}$ and N, the nucleon has three light quarks, while in the exchange of a light vector between B and Σ_b, the Σ_b has only two light quarks. There are, hence, more chances to exchange a light vector between $\bar{B}N$ than in $B\Sigma_b$. More quantitatively, if we take $I = 0$ for

$\bar{B}N$ we have two components, $\bar{B}^0(b\bar{d})\,n(udd)$ and $\bar{B}^-(b\bar{u})\,p(uud)$. We have two d quarks from the n to accommodate the exchange of a light $q\bar{q}$ in the first component and two u quarks in the second component. If we take $B\Sigma_b$ in $I = 1/2$, which was found bound in section Sec. 3.2 (Ref. [428]), we have the components $B^0(\bar{b}d)\,\Sigma_b^+(uub)$ and $B^+(\bar{b}u)\,\Sigma_b^0(udb)$. In the first case we can not exchange a light $q\bar{q}$ vector and in the second case there is only one u quark in the Σ_b^0 that can accommodate it. The strength of light vector exchange in $\bar{B}N$, $I = 0$, should be much large than in $B\Sigma_b$, $I = 1/2$. This is the case in practice since, comparing Table 3.15 of the present paper with Eqs. (2) and (12) of Ref. [428], we find that the relevant C_{ij} coefficient is 3 for $\bar{B}N$ and 1 for $B\Sigma_b$. As a consequence, we have the about three times larger binding found here with respect to the one of Refs. [128, 428].

3.4.3 Vector-baryon channels

The transitions $VB \to VB$ for small momenta of the vector mesons have formally the same expressions as the corresponding $PB \to PB$ substituting the octet of pseudoscalars by the octet of vectors [390], with only one minor change to account for the ϕ and ω SU(3) structure, which is to replace each η by $-\sqrt{2/3}\,\phi$ or $\sqrt{1/3}\,\omega$. The case of vector interaction with the decuplet of baryons is similar [389]. The Tables 3.15, 3.16, 3.18 are changed now to Tables 3.24, 3.25, 3.26. Once again we penalize with a factor 1/4 the transitions from a heavy vector to a light vector as we did before for the pseudoscalar mesons.

Table 3.24: C_{ij} coefficients for $\bar{B}^*N$ and coupled channels for $I = 0$, and $J^P = 1/2^-$, $3/2^-$.

C_{ij}	$\bar{B}^*N$	$\rho\Sigma_b$	$\omega\Lambda_b$	$\phi\Lambda_b$
$\bar{B}^*N$	3	$-\sqrt{\frac{3}{2}}$	$\sqrt{\frac{3}{2}}$	$-\sqrt{3}$
$\rho\Sigma_b$		4	0	0
$\omega\Lambda_b$			0	0
$\phi\Lambda_b$				0

Table 3.25: C_{ij} coefficients for $\bar{B}^*N$ and coupled channels for $I = 1$, and $J^P = 1/2^-, 3/2^-$.

C_{ij}	$\bar{B}^*N$	$\rho\Sigma_b$	$\rho\Lambda_b$	$\omega\Sigma_b$	$\phi\Sigma_b$
$\bar{B}^*N$	1	-1	$-\sqrt{\frac{3}{2}}$	$-\sqrt{\frac{1}{2}}$	1
$\rho\Sigma_b$		2	0	0	0
$\rho\Lambda_b$			0	0	0
$\omega\Sigma_b$				0	0
$\phi\Sigma_b$					0

Table 3.26: C_{ij} coefficients for $\bar{B}^*\Delta$ and coupled channels for $I = 1$, and $J^P = 1/2^-, 3/2^-, 5/2^-$.

C_{ij}	$\bar{B}^*\Delta$	$\rho\Sigma_b^*$	$\omega\Sigma_b^*$	$\phi\Sigma_b^*$
$\bar{B}^*\Delta$	4	1	$\sqrt{2}$	-2
$\rho\Sigma_b^*$		2	0	0
$\omega\Sigma_b^*$			0	0
$\phi\Sigma_b^*$				0

We take again the case of $I = 0$ of Table 3.24 and show the results that obtain in Table 3.27 for $\bar{B}^*N$ single channel, and in Table 3.28 for coupled channels.

Table 3.27: Energies for a state of $\bar{B}^*N$ in $I = 0$ as a function of q_{max}. (unit: MeV)

q_{max}	700	750	800	850
V	6033.1	5987.2	5939.0	5889.3

Table 3.28: Energies for a state in coupled channels $\bar{B}^*N$, $\rho\Sigma_b$, $\omega\Lambda_b$, $\phi\Lambda_b$ in $I = 0$ as a function of q_{max}. (unit: MeV)

q_{max}	700	750	800	850
V	6019.2	5970.6	5919.8	5867.6
	$6364.6 + i0.8$	$6333.3 + i0.8$	$6303.0 + i0.6$	$6274.1 + i0.3$

Once again we see that the consideration of coupled channels leads to two states. In order to see the meaning of the states we calculate again the couplings to the different channels for $q_{max} = 800$ MeV, and the results are shown in Table 3.29. There we can see that the state that couples strongly

Table 3.29: The coupling constants to various channels for certain poles in the $J = 1/2,\ 3/2,\ I = 0$ sector.

$5919.8 + i0$	$\bar{B}^*N$	$\rho\Sigma_b$	$\omega\Lambda_b$	$\phi\Lambda_b$
g_i	16.81	1.04	0.94	1.33
$g_i\, G_i^{II}$	-22.01	-5.46	-6.16	-5.67
$6303.0 + i0.6$	$\bar{B}^*N$	$\rho\Sigma_b$	$\omega\Lambda_b$	$\phi\Lambda_b$
g_i	$0.37 + i0.27$	$5.14 + i0.01$	$0.15 + i0.01$	$0.21 + i0.02$
$g_i\, G_i^{II}$	$-2.73 - i0.27$	$-46.81 - i0.13$	$-2.22 - i0.22$	$-1.50 - i0.15$

to $\bar{B}^*N$ is the one with lower energy. The higher energy state couples mostly to $\rho\Sigma_b$.

It is interesting to compare the results of Tables 3.21 and 3.27 for the states that couple mostly to $\bar{B}N$ and $\bar{B}^*N$. If we calculate with single channel we find a difference in energies between these two levels of 45 MeV, the same as between m_{B^*} and m_B. However, when we include the coupled channels we see some changes. If we compare Tables 3.27 and 3.28 at $q_{max} =$ 800 MeV, the effect of the coupled channels is a reduction of the mass of the lower state by about 20 MeV rather than 40 MeV in the case of $\bar{B}N$. The difference in the masses of the $\pi\Sigma_b$ or $\rho\Sigma_b$ is one of the reasons for it, but also the interaction of these two channels is different. Indeed, the VVV vertices or PPV vertices go as the sum of the external energies, as we saw,

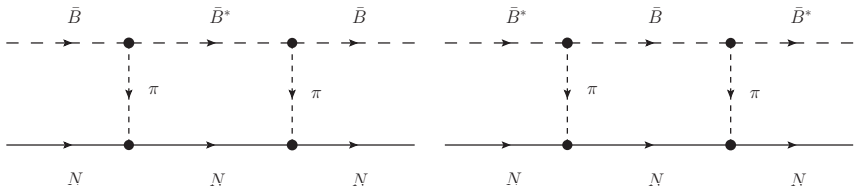

Figure 3.26: Diagrammatic representation of the $\bar{B}^*N$ in intermediate state (left) and the $\bar{B}N$ in intermediate state (right).

but now we have the much larger energy of the ρ instead of the energy of the π.

3.4.4 Breaking the $J = 1/2^-, 3/2^-$ degeneracy in the $\bar{B}^*N$ sector

In this subsection we shall break the degeneracy of the $1/2^-$, $3/2^-$ states of the $\bar{B}^*N$ sector. For this purpose we follow the approach of Ref. [391] and mix states of $\bar{B}^*N$ and $\bar{B}N$ in both sectors. We test first that in the coupled channels like the $\bar{B}^*N$ sector, the important contribution comes from $\bar{B}^*N \to X \to \bar{B}^*N$, where X stands for the other coupled channels. The extra interaction of the X channels among themselves is negligible compared to that of the dominant $\bar{B}^*N$ channel, because of the big value of the $\bar{B}^*$ energy entering the interaction. This means that it is sufficient to evaluate the contribution of the box diagrams of Fig. 3.26, in analogy to the box diagrams evaluated in Ref. [391], and add this contribution, δV, to the $\bar{B}N$ or $\bar{B}^*N$ potential. Using the doublets of isospin (B^+, B^0), $(\bar{B}^0, -B^-)$ the Λ_c state in the $\bar{B}N$ basis is given by

$$|\bar{B}N, I = 0\rangle = \frac{1}{\sqrt{2}}(|\bar{B}^0 n\rangle + |B^- p\rangle), \tag{3.83}$$

and analogously for $\bar{B}^*N$. The $\bar{B}N \to \bar{B}^*N$ transition in $I = 0$ is given by the diagrams of Fig. 3.27.

The $V\,P\,\pi$ vertex in SU(3) is given by the Lagrangian of Eq. (1.34), but, P, V^μ are the ordinary meson octet and vector nonet SU(3) matrix of

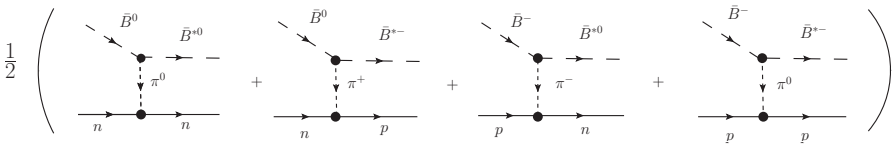

Figure 3.27: Diagrammatic representation of the transition $\bar{B}N \to \bar{B}^* N$ in $I = 0$.

the corresponding fields

$$P = \begin{pmatrix} \frac{\pi^0}{\sqrt{2}} + \frac{\eta_8}{\sqrt{6}} & \pi^+ & K^+ \\ \pi^- & -\frac{\pi^0}{\sqrt{2}} + \frac{\eta_8}{\sqrt{6}} & K^0 \\ K^- & \bar{K}^0 & -\frac{2\eta_8}{\sqrt{6}} \end{pmatrix}, \tag{3.84}$$

$$V_\mu = \begin{pmatrix} \frac{\rho^0}{\sqrt{2}} + \frac{\omega}{\sqrt{2}} & \rho^+ & K^{*+} \\ \rho^- & -\frac{\rho^0}{\sqrt{2}} + \frac{\omega}{\sqrt{2}} & K^{*0} \\ K^{*-} & \bar{K}^{*0} & \phi \end{pmatrix}_\mu . \tag{3.85}$$

One can extend the Lagrangian Eq. (1.34) to the SU(4) space, as done in the former work (Ref. [461]) and in subsection 1.2.2 (or Refs. [127,168]), but it is unnecessary. It is more intuitive and rigorous to follow the derivation below (more justification can be referred to our paper [482]), which allows us to directly connect with the results of heavy quark spin-flavour symmetry [483]. Indeed, all we need to do is to invoke that the leading terms correspond to light meson exchange, in which case the heavy quark plays the role of a spectator at the quark level.

Let us then compare the $K^{*+} \to K^0\pi^+$ and $B^{*+} \to B^0\pi^+$ transitions as shown in Fig. 3.28. As we can see in the figure, the transitions are identical and governed by the light quarks, with the $\bar{s}$ quark in K^{*+} and $\bar{b}$ quark in B^{*+} playing the role of a spectator. The transition amplitudes are thus identical at the quark microscopic level, but we must take into account that when used at the macroscopic level of the K^{*+} or B^{*+} there are normalization factors $(2\omega)^{-1/2}$ which are different for the K^{*+}, K^0 or B^{*+}, B^0 fields. This is taken easily into account by constructing the S matrix at the macroscopic level. At the microscopic level we have (we

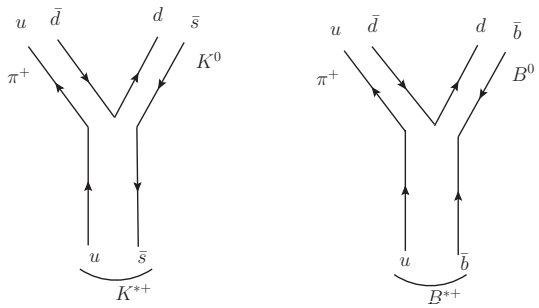

Figure 3.28: Diagram of the transition $K^{*+} \to K^0\pi^+$ (left) and $B^{*+} \to B^0\pi^+$ (right).

follow Mandl + Shaw normalization of the fields [197])

$$S^{mic} = 1 - it\sqrt{\frac{2m_L}{2E_L}}\sqrt{\frac{2m'_L}{2E'_L}}\sqrt{\frac{1}{2\omega_\pi}}\frac{1}{\mathcal{V}^{3/2}}\,(2\pi)^4\delta(P_{in} - P_{out}), \tag{3.86}$$

with m_L, E_L, m'_L, E'_L the masses (constituent) of the incoming and outgoing light quarks, $\mathcal{V}$ the volume of the box where states are normalized to unity, and ω_π the pion energy. At the macroscopic level we have for the K^{*+} and B^{*+}

$$S^{mac}_{K^*} = 1 - it_{K^*}\frac{1}{\sqrt{2\omega_{K^*}}}\frac{1}{\sqrt{2\omega_K}}\frac{1}{\sqrt{2\omega_\pi}}\frac{1}{\mathcal{V}^{3/2}}\,(2\pi)^4\delta(P_{in} - P_{out}), \tag{3.87}$$

$$S^{mac}_{B^*} = 1 - it_{B^*}\frac{1}{\sqrt{2\omega_{B^*}}}\frac{1}{\sqrt{2\omega_B}}\frac{1}{\sqrt{2\omega_\pi}}\frac{1}{\mathcal{V}^{3/2}}\,(2\pi)^4\delta(P_{in} - P_{out}). \tag{3.88}$$

These considerations are common place in the study of three body systems in the FCA [223, 227]. Eqs. (3.86), (3.87), (3.88) allow one to relate t_{B^*} and t_{K^*} with the macroscopic t amplitude, but since we have t_{K^*} given by the effective Lagrangian of Eq. (1.34), we can obtain t_{B^*} in terms of t_{K^*} by means

$$\frac{t_{B^*}}{t_{K^*}} \equiv \frac{\sqrt{m_{B^*}m_B}}{\sqrt{m_{K^*}m_K}} \simeq \frac{m_{B^*}}{m_{K^*}}. \tag{3.89}$$

Now we come back to the evaluation of the box diagrams of Fig. 3.26. The vertex for the $I = 0$ transition $\bar{B}N \to \bar{B}^*N$ of Fig. 3.27, considering

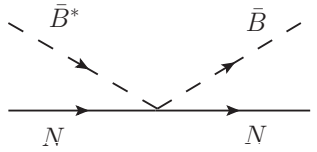

Figure 3.29: Diagram of the Kroll Ruderman term.

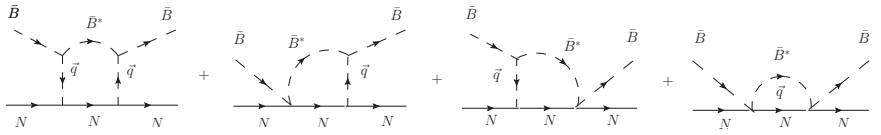

Figure 3.30: All of the diagrams for the $\bar{B}^*N$ in the intermediate state.

the Yukawa coupling for the πNN vertex is given by

$$-it = -\frac{3}{\sqrt{2}} g \frac{m_{B^*}}{m_{K^*}} (q + P_{in})_\mu \epsilon^\mu \frac{1}{q^2 - m_\pi^2} \frac{D+F}{2f_\pi} \vec{\sigma} \cdot \vec{q}, \tag{3.90}$$

with $D = 0.75$ and $F = 0.51$ [313], and since $P_{in} = q + P_{out}$ and $P_{out} \cdot \epsilon = 0$ plus $\epsilon^0 \approx 0$, we get effectively

$$-it = \frac{6}{\sqrt{2}} g \frac{m_{B^*}}{m_{K^*}} \vec{q} \cdot \vec{\epsilon} \frac{1}{q^2 - m_\pi^2} \frac{D+F}{2f_\pi} \vec{\sigma} \cdot \vec{q}. \tag{3.91}$$

In addition to the pion exchange of Fig. 3.27, we have the Kroll Ruderman contact term, depicted in Fig. 3.29. Following Refs. [391, 484], in order to get the Kroll Ruderman term, we must substitute in Eq. (3.90) $\epsilon_\mu (q + P_{in})^\mu \frac{1}{q^2 - m_\pi^2} \vec{\sigma} \cdot \vec{q}$ by $-\vec{\sigma} \cdot \vec{q}$. Then, we must evaluate the diagrams of Fig. 3.30 for the $\bar{B}N \to \bar{B}^*N \to \bar{B}N$ transition, and we obtain

$$\delta V = \delta V^{PP} + 2\delta V^{PC} + \delta V^{CC}, \tag{3.92}$$

where δV^{PP} stands for the first diagram of Fig. 3.30, $2\delta V^{PC}$ for the two middle diagrams and δV^{CC} for the last one. Then, after performing derivations, for the $\bar{B}N \to \bar{B}^*N \to \bar{B}N$ box diagram we only have the $J = 1/2$ case (more details can be seen in our paper [482]). Thus, we have

$$J = 1/2: \quad \delta V = FAC\Big(\frac{\partial}{\partial m_\pi^2} I_1 + 2\, I_2 + I_3\Big) \tag{3.93}$$

where

$$
\begin{aligned}
I_1 &= \int \frac{d^3q}{(2\pi)^3} 4\vec{q}^{\,4} \frac{1}{2\omega_{B^*}(\vec{q})} \frac{M_N}{E_N(\vec{q})} \frac{Num}{Den}, \\
I_2 &= \int \frac{d^3q}{(2\pi)^3} 2\vec{q}^{\,2} \frac{1}{2\omega_{B^*}(\vec{q})} \frac{M_N}{E_N(\vec{q})} \frac{Num}{Den}, \\
I_3 &= \int \frac{d^3q}{(2\pi)^3} \frac{3}{2\omega_{B^*}(\vec{q})} \frac{M_N}{E_N(\vec{q})} \frac{1}{P^0_{in} + K^0_{in} - E_N(\vec{q}) - \omega_{B^*}(\vec{q}) + i\epsilon},
\end{aligned}
\tag{3.94}
$$

with

$$
FAC = \frac{9}{2} g^2 \Big(\frac{m_{B^*}}{m_{K^*}}\Big)^2 \Big(\frac{F+D}{2f_\pi}\Big)^2, \tag{3.95}
$$

$$
Num = K^0_{in} - E_N(\vec{q}) - 2\omega_\pi(\vec{q}) - \omega_{B^*}(\vec{q}) + P^0_{in}, \tag{3.96}
$$

$$
\begin{aligned}
Den = {} & 2\omega_\pi(\vec{q})[P^0_{in} - \omega_\pi(\vec{q}) - \omega_{B^*}(\vec{q}) + i\epsilon][K^0_{in} - E_N(\vec{q}) - \omega_\pi(\vec{q}) + i\epsilon] \\
& \times [P^0_{in} + K^0_{in} - E_N(\vec{q}) - \omega_{B^*}(\vec{q}) + i\epsilon],
\end{aligned}
\tag{3.97}
$$

with P^0_{in}, K^0_{in} the incoming $\bar{B}$, N energies.

For the case of the $\bar{B}^* N \to \bar{B} N \to \bar{B}^* N$ box diagram, the formula is like the former one for $J = 1/2$ exchanging accordingly the masses of $B \leftrightarrow B^*$. Thus, we have

$$
J = 1/2: \quad \delta V = FAC\Big(\frac{\partial}{\partial m_\pi^2} I'_1 + 2\, I'_2 + I'_3\Big), \tag{3.98}
$$

$$
J = 3/2: \quad \delta V = FAC\Big(\frac{\partial}{\partial m_\pi^2} I'_1\Big), \tag{3.99}
$$

where

$$
\begin{aligned}
I'_1 &= \int \frac{d^3q}{(2\pi)^3} \frac{4}{3}\vec{q}^{\,4} \frac{1}{2\omega_B(\vec{q})} \frac{M_N}{E_N(\vec{q})} \frac{Num}{Den}, \\
I'_2 &= \int \frac{d^3q}{(2\pi)^3} 2\vec{q}^{\,2} \frac{1}{2\omega_B(\vec{q})} \frac{M_N}{E_N(\vec{q})} \frac{Num}{Den}, \\
I'_3 &= \int \frac{d^3q}{(2\pi)^3} \frac{3}{2\omega_B(\vec{q})} \frac{M_N}{E_N(\vec{q})} \frac{1}{P^0_{in} + K^0_{in} - E_N(\vec{q}) - \omega_B(\vec{q}) + i\epsilon},
\end{aligned}
\tag{3.100}
$$

with Num, Den having the same expressions but in terms of the proper energies and masses. In the Yukawa vertex it is customary to include a

monopole form factor to agree with the NN peripheral partial waves [485] and thus we introduce a factor

$$FF(\vec{q}) = \Big(\frac{\Lambda^2}{\Lambda^2 + \vec{q}^{\,2}}\Big)^2, \tag{3.101}$$

with $\Lambda \simeq 1$ GeV, which we include in the integrands of Eqs. (3.100), (3.94).

To go to the second Riemann sheet with the box contribution δV, we can do a similar thing as in Eq. (1.50). Yet, when $\sqrt{s}$ is real $G_l^{II} \equiv (G_l^I)^*$ and this is also the case, quite accurately, when we are close to the real axis. In view of this, and the small contribution of the intermediate $\bar{B}N$ states to the width, we use the prescription, $\delta V \to (\delta V)^*$ to go to the second Riemann sheet. In practice, this is equivalent to changing $+i\epsilon \to -i\epsilon$ in the factors of *Den* of Eq. (3.97) (more discussions can be seen in our paper [482]).

Once the formalism has been described, we show the results of including δV in the approach in Tables 3.30, 3.31.

It is interesting to compare the results of Table 3.30 with those of Table 3.28. At 750 MeV the box diagram reduces the mass of the state by about 30 MeV for $J = 1/2$, and 20 MeV for $J = 3/2$. We can see that the value of the masses is rather sensitive to the value q_{max} used. However, it is interesting to remark that the splitting of energies between the $J = 1/2$ and $J = 3/2$ levels is about 10 MeV, rather independent of the cutoff used. We can thus see that the mixing of $\bar{B}^*N$ and $\bar{B}N$ states leads naturally to two states, nearly degenerate in spin, only separated by about 10 MeV, like the $\Lambda_b(5912)$ and $\Lambda_b(5920)$. If we fine tune q_{max} to get the right binding, we find $q_{max} = 776$ MeV, where the energy of the $J = 1/2$ state is 5910 MeV, and the one of the $J = 3/2$ state 5920 MeV. We also observe that the higher energy state, around 6300 MeV, has been practically not affected by the box diagram, which is most logical since this state couples weakly to $\bar{B}^*N$.

For the $\bar{B}N$ state of Table 3.31, comparing it with the results of Table 3.22, the box diagram has reduced the energy by about 50 MeV at $q_{max} =$ 750 MeV. The upper level energy is increased by about 15 MeV for this value of q_{max}.

Table 3.30: Poles with box diagram in coupled channels $\bar{B}^*N$, $\rho\Sigma_b$, $\omega\Lambda_b$, $\phi\Lambda_b$ in $I = 0$ as a function of V and q_{max}. (unit: MeV)

q_{max}	700	750	776	800	850
$J = 1/2$	$5991.9 + i0$	$5939.2 + i0$	$5910.7 + i0$	$5884.0 + i0$	$5827.4 + i0$
	$6364.2 + i1.4$	$6332.6 + i1.4$	$6316.6 + i1.4$	$6301.1 + i1.4$	$6273.0 + i1.2$
$J = 3/2$	$5998.8 + i0$	$5948.0 + i0$	$5920.7 + i0$	$5895.1 + i0$	$5840.9 + i0$
	$6363.5 + i2.1$	$6331.7 + i2.0$	$6315.7 + i1.9$	$6301.2 + i1.7$	$6272.1 + i1.2$

Table 3.31: Poles with box diagram in coupled channels $\bar{B}N$, $\pi\Sigma_b$, $\eta\Lambda_b$ in $I = 0$ as a function of V and q_{max}. (unit: MeV)

q_{max}	700	750	776	800	850
$J = 1/2$	$5902.6 + i0$	$5850.1 + i0$	$5820.9 + i0$	$5793.3 + i0$	$5734.4 + i0$
	$5985.6 + i29.1$	$5974.1 + i26.8$	$5969.5 + i24.6$	$5965.8 + i22.3$	$5959.5 + i17.3$

3.4.5 Results of $I = 1$ states

With the cut off obtained to reproduce the mass of the $\Lambda_b(5912)$ state we proceed now to evaluate the states corresponding to Tables 3.16, 3.18, 3.25, 3.26, which are mostly bound states of $\bar{B}N\,(I = 1,\, J^P = 1/2^-)$, $\bar{B}\Delta\,(I = 1,\, J^P = 3/2^-)$, $\bar{B}^*N\,(I = 1,\, J^P = 1/2^-, 3/2^-)$, $\bar{B}^*\Delta\,(I = 1,\, J^P = 1/2^-, 3/2^-, 5/2^-)$. The results can be seen in Tables 3.34, 3.32, 3.35, 3.33 with $q_{max} = 776$ MeV, together with the couplings to the different coupled channels.

Table 3.32: The coupling constants to various channels for certain poles in the $I = 1$ sector of $\bar{B}\Delta$ and coupled channels.

$5971.9 + i0$	$\bar{B}\Delta$	$\pi\Sigma_b^*$	$\eta\Sigma_b^*$
g_i	10.79	0.61	0.85
$g_i\, G_i^{II}$	-10.89	-16.51	-6.69
$6073.0 + i77.2$	$\bar{B}\Delta$	$\pi\Sigma_b^*$	$\eta\Sigma_b^*$
g_i	$7.67 - i5.14$	$1.43 + i1.36$	$0.81 - i0.36$
$g_i\, G_i^{II}$	$-9.59 + i4.83$	$-70.37 - i20.89$	$-7.87 + i2.27$

Table 3.33: The coupling constants to various channels for certain poles in the $I = 1$ sector of $\bar{B}^*\Delta$ and coupled channels.

$6049.2 + i0$	$\bar{B}^*\Delta$	$\rho\Sigma_b^*$	$\omega\Sigma_b^*$	$\phi\Sigma_b^*$
g_i	21.14	0.85	1.03	1.46
$g_i\, G_i^{II}$	-22.11	-4.70	-5.66	-5.30
$6491.9 + i0$	$\bar{B}^*\Delta$	$\rho\Sigma_b^*$	$\omega\Sigma_b^*$	$\phi\Sigma_b^*$
g_i	0.66	3.76	0.13	0.18
$g_i\, G_i^{II}$	-2.19	-50.69	-1.71	-1.20

With respect to their thresholds, the binding energies for the $\bar{B}N$ channel are now smaller than for $I = 0$, as we anticipated in view of the smaller C_{ij} coefficients, but for $\bar{B}\Delta$ the binding is bigger than for the $\bar{B}N$ state, as discussed earlier. We again see that we get two states in each one of the

Table 3.34: The coupling constants for certain poles in the $I = 1$ sector of $\bar{B}N$ and coupled channels.

$6002.8 + i66.2$	$\bar{B}N$	$\pi\Sigma_b$	$\pi\Lambda_b$	$\eta\Sigma_b$
g_i	$5.69 + i1.62$	$1.80 + i1.00$	$0.39 + i0.21$	$0.37 + i0.20$
$g_i\, G_i^{II}$	$-8.60 - i4.12$	$-72.70 - i12.65$	$-16.12 + i5.73$	$-2.95 - i2.01$
$6179.4 + i61.4$	$\bar{B}N$	$\pi\Sigma_b$	$\pi\Lambda_b$	$\eta\Sigma_b$
g_i	$6.76 - i3.03$	$0.30 + i0.80$	$1.11 - i0.03$	$1.07 - i0.03$
$g_i\, G_i^{II}$	$-21.71 + i1.38$	$-30.00 - i13.31$	$-14.96 + i47.71$	$-12.74 - i1.63$

Table 3.35: The coupling constants for certain poles in the $I = 1$ sector of $\bar{B}^*N$ and coupled channels.

$6202.1 + i0$	$\bar{B}^*N$	$\rho\Sigma_b$	$\rho\Lambda_b$	$\omega\Sigma_b$	$\phi\Sigma_b$
g_i	7.29	1.22	1.05	0.59	0.83
$g_i\, G_i^{II}$	-20.66	-8.67	-11.20	-4.11	-3.62
$6477.2 + i5.0$	$\bar{B}^*N$	$\rho\Sigma_b$	$\rho\Lambda_b$	$\omega\Sigma_b$	$\phi\Sigma_b$
g_i	$0.21 - i0.62$	$3.68 - i0.08$	$0.25 + i0.12$	$0.14 + i0.07$	$0.20 + i0.10$
$g_i\, G_i^{II}$	$4.23 + i2.05$	$-50.58 + i0.19$	$-9.39 + i2.89$	$-1.85 - i0.94$	$-1.29 - i0.64$

cases, but also notice that there is more mixture of the states than for $I = 0$. In the case of the $\bar{B}N$ channels, the lower state is clearly dominated by $\pi\Sigma_b$. For the $\bar{B}\Delta$ channels, the upper state is dominated by $\pi\Sigma_b^*$. For the $\bar{B}^*N$ channels, the lower state is dominated by $\bar{B}^*N$ and the higher one by $\rho\Sigma_b$. For the $\bar{B}^*\Delta$ channels, the lower state is dominated by $\bar{B}^*\Delta$ and the upper one by $\rho\Sigma_b^*$.

3.4.6 Box diagram for $I = 1$ states

We now evaluate the contribution of the box diagram to the $I = 1$ states made from $\bar{B}N$, $\bar{B}^*N$, $\bar{B}\Delta$, $\bar{B}^*\Delta$.

a) $\bar{B}N$, $I = 1$:
The isospin $I = 1$ state is now

$$|\bar{B}N; I = 1, I_3 = 0\rangle = \frac{1}{\sqrt{2}}\big(|\bar{B}^0 n\rangle - |\bar{B}^- p\rangle\big). \tag{3.102}$$

The counting of isospin done before can be repeated and we simply find that a factor $\frac{3}{\sqrt{2}}$ gets converted in $\frac{1}{\sqrt{2}}$ in the $\bar{B}N \to \bar{B}^*N$ transition. We thus get a factor 9 smaller contribution than for $I = 0$ from the box and we neglect it.

b) $\bar{B}^*N$, $I = 1$:
We have the same suppression factor as before and we also neglect it.

c) $\bar{B}\Delta$, $I = 1$:
The state of $\bar{B}\Delta$ with $I = 1$ is given by

$$|\bar{B}\Delta; I = 1, I_3 = 1\rangle = \sqrt{\frac{3}{4}}|\bar{B}^-\Delta^{++}\rangle + \sqrt{\frac{1}{4}}|\bar{B}^0\Delta^+\rangle. \tag{3.103}$$

The diagram under contribution is now in Fig. 3.31. We must also substitute $\frac{f}{m_\pi}\vec{\sigma}\cdot\vec{q}\tau^\lambda$ in the case of nucleons by $\frac{f_\Delta}{m_\pi}\vec{S}_\Delta\cdot\vec{q}T_\Delta^\lambda$, where $\vec{S}_\Delta$, $\vec{T}_\Delta$ are the ordinary spin and isospin matrices of the Δ.

We have [486]

$$\frac{f_\Delta}{f} = \frac{4}{5}, \quad (\text{where} \quad \frac{f}{m_\pi} = \frac{F+D}{2f}). \tag{3.104}$$

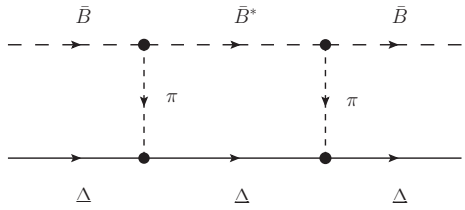

Figure 3.31: Diagrammatic representation of the transition of $\bar{B}\Delta \to \bar{B}^*\Delta \to \bar{B}\Delta$.

Using the appropriate Clebsch-Gordan coefficient for $\vec{T}_\Delta$, we find that the term corresponding the box in diagram Fig. 3.31 is now given by

$$\delta V = FAC\frac{\partial \tilde{I}_1}{\partial m_\pi^2}, \tag{3.105}$$

where

$$\tilde{I}_1 = \frac{5}{9}\int \frac{d^3q}{(2\pi)^3} 4\vec{q}^4 \frac{1}{2\omega_{B^*}(\vec{q})}\frac{M_\Delta}{E_\Delta(\vec{q})}\frac{Num}{Den}, \tag{3.106}$$

with Num, Den the expressions of Eqs. (3.96), (3.97) but putting the appropriate masses.

d) $\bar{B}^*\Delta$, $I = 1$:

In this case we proceed as before, and everything is formulated in the same way but now $I_1' \to \tilde{I}_1'$, with

$$\tilde{I}_1' = \frac{5}{9}\int \frac{d^3q}{(2\pi)^3} \frac{4}{3}\vec{q}^4 \frac{1}{2\omega_B(\vec{q})}\frac{M_\Delta}{E_\Delta(\vec{q})}\frac{Num}{Den}. \tag{3.107}$$

To reach this formula we have made an average over the spins of the initial Δ, taking the same initial and final third spin component of the Δ. This is in consonance with the fact that since we have a reduction factor of about 1/2, the splitting of spin levels is now smaller than for $\bar{B}^*N$ and accepting uncertainties larger than 5 MeV we do not worry about it. Consequently we do not evaluate the I_2, I_3, I_2', I_3' terms that produced the spin splitting.

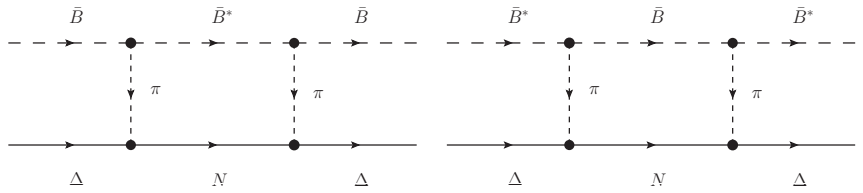

Figure 3.32: Diagrammatic representation of the $\bar{B}^*N$ in intermediate state (left) and the $\bar{B}N$ in intermediate state (right).

3.4.7 Further decay channels of $\bar{B}\Delta$ and $\bar{B}^*\Delta$

In this subsection we evaluate the box diagram corresponding to Figs. 3.32. We thus consider the intermediate $\bar{B}N$ or $\bar{B}^*N$ channels. Should the binding $\bar{B}\Delta$ and $\bar{B}^*\Delta$ states be not bigger than the Δ and N mass differences, there would provide decay channels of the states. In principle we should also consider the $\bar{B}\Delta$ and $\bar{B}^*\Delta$ intermediate states for the $\bar{B}N$ and $\bar{B}^*N$ states, but, considering the binding, these intermediate states are about 600 MeV away in energy and we do not consider them. The changes are also simple: we must substitute

$$\frac{f}{m_\pi}\vec{\sigma}\cdot\vec{q}\,\tau^\lambda \to \frac{f_{\pi N\Delta}}{m_\pi}\vec{S}\cdot\vec{q}\,T^\lambda, \tag{3.108}$$

where now $\vec{S}\,(\vec{T})$ is transition spin (isospin) operator from spin (isospin) 3/2 to 1/2, with the normalization for S^+_μ in spherical basis

$$\langle 3/2\,M|S^+_\mu|1/2\,m\rangle = \mathcal{C}(1/2\;1\;3/2;\;m_\mu\,M), \tag{3.109}$$

with $\mathcal{C}(\cdot)$ a Clebsch-Gordan coefficient, and we have the property [487]

$$\sum_M S_i|M\rangle\langle M|S_j = \frac{2}{3}\delta_{ij} - i\frac{1}{3}\epsilon_{ijk}\sigma_k, \tag{3.110}$$

for S_i, S_j in cartesian basis. Also from Ref. [487] we take $f_{\pi N\Delta}/f = 2.25$. For the isospin transition, in addition to the $I = 1$ $\bar{B}\Delta$ state of Eq. (3.103) we need

$$|\bar{B}N; I = 1, I_3 = 1\rangle = |\bar{B}^0 p\rangle. \tag{3.111}$$

The $\pi^0 p\Delta^+$ vertex for T^λ_Δ gives us $\sqrt{2/3}$ and the $\pi^+ p\Delta^{++}$ gives us (-1) (recall phase used $|\pi^+\rangle = -|1,1\rangle$).

Once again, making the average over Δ spins as before, we obtain the results for δV_2 given by the same formalism as before, substituting

$$I_1 \to \tilde{I}_1 = \frac{8}{81}\Big(\frac{f_{\pi N\Delta}}{f}\Big)^2 \int \frac{d^3q}{(2\pi)^3} 4\vec{q}^{\,4} \frac{1}{2\omega_{B^*}(\vec{q})} \frac{M_N}{E_N(\vec{q})} \frac{Num}{Den}, \tag{3.112}$$

for the $\bar{B}\Delta \to \bar{B}^* N \to \bar{B}\Delta$ process, and

$$I_1' \to \tilde{I}_1' = \frac{8}{81}\Big(\frac{f_{\pi N\Delta}}{f}\Big)^2 \int \frac{d^3q}{(2\pi)^3} \frac{4}{3}\vec{q}^{\,4} \frac{1}{2\omega_{B}(\vec{q})} \frac{M_N}{E_N(\vec{q})} \frac{Num}{Den}, \tag{3.113}$$

for the $\bar{B}^*\Delta \to \bar{B}N \to \bar{B}^*\Delta$ process, with Num and Den given by Eqs. (3.96), (3.97), but substituting the masses by the appropriate ones.

We show our results with the contribution of box diagrams, seen in Figs. 3.31 and 3.32, in Tables 3.36, 3.37 for the $\bar{B}\Delta$, $\bar{B}^*\Delta$ and their coupled channels.

Table 3.36: Poles with box diagram in $I = 1$ sector of $\bar{B}\Delta$ and its coupled channels with $q_{max} = 776$ MeV: δV_1 is the $\bar{B}^*\Delta$ box, δV_2 is the $\bar{B}^* N$ box. (unit: MeV)

no box	$V + \delta V_1$	$V + \delta V_2$	$V + \delta V_1 + \delta V_2$
$5971.9 + i0$	$5957.8 + i0$	$5949.4 + i0$	$5932.9 + i0$
$6073.0 + i77.2$	$6069.1 + i80.7$	$6066.3 + i81.7$	$6063.8 + i83.5$

Table 3.37: Poles with box diagram in $I = 1$ sector of $\bar{B}^*\Delta$ and its coupled channels with $q_{max} = 776$ MeV: δV_1 is the $\bar{B}\Delta$ box, δV_2 is the $\bar{B}N$ box. (unit: MeV)

no box	$V + \delta V_1$	$V + \delta V_2$	$V + \delta V_1 + \delta V_2$
$6049.2 + i0$	$6039.1 + i0$	$6032.2 + i0$	$6022.9 + i0$
$6491.9 + i0$	$6491.4 + i0$	$6493.0 + i1.0$	$6491.7 + i0.8$

We can see that the effect of the box with $\bar{B}\Delta$ or $\bar{B}^*\Delta$ intermediate states is a reduction of the mass of the lower state by bout $10-15$ MeV, with an extra reduction of a about $15-25$ MeV from the box with intermediate $\bar{B}N$ and $\bar{B}^*N$ states. The upper state is not much modified by the box diagrams.

3.4.8 Summary of the results

Finally, since we have many intermediate results, we summarize here the final results that we get for the states, with $q_{max} = 776$ MeV, which we used to fix one of the Λ_b energies. The results are shown in Table 3.38, where we also write for a quick intuition the main channel of the state.

Table 3.38: Energies and widths of the states obtained and the channels to which the states couple most strongly.

main channel	J	I	(E, Γ) [MeV]	Exp.
$\bar{B}N$	1/2	0	5820.9, 0	-
$\pi\Sigma_b$	1/2	0	5969.5, 49.2	-
$\bar{B}^*N$	1/2	0	5910.7, 0	$\Lambda_b(5912)$
$\bar{B}^*N$	3/2	0	5920.7, 0	$\Lambda_b(5920)$
$\rho\Sigma_b$	1/2	0	6316.6, 2.8	-
$\rho\Sigma_b$	3/2	0	6315.7, 3.8	-
$\bar{B}N$, $\pi\Sigma_b$	1/2	1	6179.4, 122.8	-
$\pi\Sigma_b$	1/2	1	6002.8, 132.4	-
$\bar{B}\Delta$, $\pi\Sigma_b^*$	3/2	1	5932.9, 0	-
$\pi\Sigma_b^*$	3/2	1	6063.8, 167.0	-
$\bar{B}^*N$	1/2, 3/2	1	6202.2, 0	-
$\rho\Sigma_b$	1/2, 3/2	1	6477.2, 10.0	-
$\bar{B}^*\Delta$	1/2, 3/2, 5/2	1	6022.9, 0	-
$\rho\Sigma_b^*$	1/2, 3/2, 5/2	1	6491.7, 1.6	-

In summary, we predict 6 states with $I = 0$, two of them corresponding to the $\Lambda_b(5912)$ and $\Lambda_b(5920)$, and 8 states with $I = 1$. The energies of the

states range from about 5800 MeV to 6500 MeV.

It is interesting to compare the results obtained here with those of Ref. [398]. In this later work, the same interaction as here is used for the main diagonal channels, but the transition between different coupled channels is not obtained through vector or pion exchange as done here, but invoking a combined SU(6) and HQSS. In Ref. [398] the states of $I = 1$ are not investigated but for $I = 0$ four states are obtained, two of them, with $J = 1/2,\ 3/2$, are also associated to the $\Lambda_b(5912)$ and $\Lambda_b(5920)$. In spite of the differences in the input, there are common features in the results. The two states associated to the $\Lambda_b(5912)$ and $\Lambda_b(5920)$ exhibit, as here, a substantial coupling to $\bar{B}^* N$. There is also a $1/2^-$ state in Ref. [398] at 5797 MeV which we find at 5820 MeV, only 33 MeV higher, and another state at 6009 MeV that we find at 5969 MeV, 40 MeV below. The mostly $\rho\Sigma_b$ state found here at 6316 MeV, basically degenerate in $J = 1/2,\ 3/2$, was either not found or not searched for in Ref. [398] because of its higher mass. The qualitative agreement between the results of the two approaches is remarkable and gives further support to the common predictions. In addition, we have investigated states of $I = 1$ and we find quite a few, some of them narrow enough for a clear experimental observation.

3.4.9 Conclusions

In this work we examine the interaction of $\bar{B}N$, $\bar{B}\Delta$, $\bar{B}^* N$ and $\bar{B}^*\Delta$ states, together with their coupled channels, using a mapping from the light meson sector. The assumption that the heavy quarks act as spectators at the quark level automatically leads us to the results of the HQSS for pion exchange and reproduces the results of the Weinberg Tomozawa term, coming from light vector exchanges in the extended local hidden gauge approach. With this dynamics we look for states dynamically generated from the interaction and find two states with nearly zero width, which we associate to the $\Lambda_b(5912)$ and $\Lambda_b(5920)$ states. The states couple mostly to $\bar{B}^* N$, which are degenerate. The difference of masses between these two states, with $J = 1/2,\ 3/2$ respectively, is due to pion exchange connecting these states to intermediate $\bar{B}N$ states. In addition to these two Λ_b states, we find three more states with $I = 0$, one of them nearly degenerate in two states of $J = 1/2,\ 3/2$. Furthermore we also find eight more states in $I = 1$, two of them degenerate in $J = 1/2, 3/2$, and other two degenerate in $J = 1/2,\ 3/2,\ 5/2$.

3.5 Baryon states with open charm

In dealing with hadronic states involving heavy quarks (charm or beauty), the HQSS [233–236, 483] plays an important role and serves as a guiding principle to proceed with calculations. HQSS has been applied to calculate baryon spectra in Refs. [41, 237, 238, 397, 398, 412, 475, 488]. The basic idea behind these works is to use HQSS to reduce the freedom in the interaction, which is then written in terms of a few parameters which are adjusted to some experimental data. Then predictions on spectra of baryons with charm or beauty, or hidden charm and beauty are made. In Ref. [237] an SU(8) spin-flavor scheme is used, to account for the spin symmetry, in order to obtain the interaction, and a coupled channel unitary approach is implemented to obtain poles in the scattering matrices, which correspond to the baryon resonance states. In particular the $\Lambda_c(2595)$ state is obtained and shown to couple largely to the D^*N channel. In Ref. [238] the SU(8) scheme is once again used, but with some symmetry breaking, to match with an extension of the Weinberg Tomozawa interaction in SU(3). Among other resonances, the states $\Lambda_c(2595)$ ($J^P = 1/2^-$) and $\Lambda_c(2625)$ ($J^P = 3/2^-$) are obtained.

In the charm sector, many works investigate the properties of the particles with heavy quark [127, 128, 168, 257, 258, 489, 490], such as the Λ_c ($J^P = 1/2^-$) and Σ_c ($J^P = 3/2^-$) resonances. Two well known resonances, the $\Lambda_c(2595)$ ($J^P = 1/2^-$) and $\Lambda_c(2625)$ ($J^P = 3/2^-$) states [9], were dynamically generated in the coupled channel interaction [237, 238, 257, 258], with a different explanation for their properties. The $\Lambda_c(2625)$ ($J^P = 3/2^-$) state is mostly tied to the D^*N channel, and the $\Lambda_c(2595)$ state has a more important coupling to the DN channel. In the present work, following the former work (Ref. [482]), where the states $\Lambda_b(5912)$ and $\Lambda_b(5920)$ ($J^P = 1/2^-, 3/2^-$) were obtained using a unitary scheme with coupled channels and the dynamics based on the LHG approach [156, 159, 163], we extrapolate the approach from the beauty sector to the charm sector, to see if a similar explanation can be given in this case, or see if those states call for a different explanation.

3.5.1 Summary of the formalism

Following the former work (Ref. [482]) in last section, we extrapolate the formalism to the open charm sector by just changing the $\bar{B}^{(*)}$ meson to a $D^{(*)}$ meson and b-quark to c-quark for the baryon. We take coupled channels $\pi\Sigma_c$, $\pi\Lambda_c$, $\eta\Lambda_c$, $\eta\Sigma_c$, DN with $I = 0,\ 1$, and also consider D^*N and $\pi\Sigma_c^*$, $\eta\Sigma_c^*$, $D\Delta$, $D^*\Delta$, with $\Delta \equiv \Delta(1232)$ and $\Sigma_c^* = \Sigma_c^*(2520)$, belonging to a decuplet of $3/2^+$ states. The transition potential is given by Eq. (3.78). The C_{ij} coefficients are similarly obtained as before from Refs. [155,389,390,481]

For the interaction of pseudoscalar mesons and $1/2^+$ baryons, the coupled channels and the C_{ij} coefficients both in $I = 0$ and $I = 1$ are given in Tables 3.39−3.42.

Table 3.39: C_{ij} coefficients for $I = 0$ and $J^P = 1/2^-$.

C_{ij}	DN	$\pi\Sigma_c$	$\eta\Lambda_c$
DN	3	$-\sqrt{\frac{3}{2}}$	$\frac{3}{\sqrt{2}}$
$\pi\Sigma_c$		4	0
$\eta\Lambda_c$			0

Table 3.40: C_{ij} coefficients for $I = 1$ and $J^P = 1/2^-$.

C_{ij}	DN	$\pi\Sigma_c$	$\pi\Lambda_c$	$\eta\Sigma_c$
DN	1	-1	$-\sqrt{\frac{3}{2}}$	$-\sqrt{\frac{3}{2}}$
$\pi\Sigma_c$		2	0	0
$\pi\Lambda_c$			0	0
$\eta\Sigma_c$				0

Table 3.41: C_{ij} coefficient for $I = 0$ and $J^P = 3/2^-$.

C_{ij}	$\pi\Sigma_c^*$
$\pi\Sigma_c^*$	4

Table 3.42: C_{ij} coefficients for $I = 1$ and $J^P = 3/2^-$.

C_{ij}	$D\Delta$	$\pi\Sigma_c^*$	$\eta\Sigma_c^*$
$D\Delta$	4	1	$\sqrt{6}$
$\pi\Sigma_c^*$		2	0
$\eta\Sigma_c^*$			0

For the cases of the transitions $VB \to VB$, the interactions of vector mesons and baryons, analogously, the coupled channels and the C_{ij} coefficients for $I = 0$ and $I = 1$ are given in Tables 3.43−3.45.

Table 3.43: C_{ij} coefficients for D^*N and coupled channels for $I = 0$, and $J^P = 1/2^-$, $3/2^-$.

C_{ij}	D^*N	$\rho\Sigma_c$	$\omega\Lambda_c$	$\phi\Lambda_c$
D^*N	3	$-\sqrt{\frac{3}{2}}$	$\sqrt{\frac{3}{2}}$	$-\sqrt{3}$
$\rho\Sigma_c$		4	0	0
$\omega\Lambda_c$			0	0
$\phi\Lambda_c$				0

Table 3.44: C_{ij} coefficients for D^*N and coupled channels for $I = 1$, and $J^P = 1/2^-, 3/2^-$.

C_{ij}	D^*N	$\rho\Sigma_c$	$\rho\Lambda_c$	$\omega\Sigma_c$	$\phi\Sigma_c$
D^*N	1	-1	$-\sqrt{\frac{3}{2}}$	$-\sqrt{\frac{1}{2}}$	1
$\rho\Sigma_c$		2	0	0	0
$\rho\Lambda_c$			0	0	0
$\omega\Sigma_c$				0	0
$\phi\Sigma_c$					0

Table 3.45: C_{ij} coefficients for $D^*\Delta$ and coupled channels for $I = 1$, and $J^P = 1/2^-, 3/2^-, 5/2^-$.

C_{ij}	$D^*\Delta$	$\rho\Sigma_c^*$	$\omega\Sigma_c^*$	$\phi\Sigma_c^*$
$D^*\Delta$	4	1	$\sqrt{2}$	-2
$\rho\Sigma_c^*$		2	0	0
$\omega\Sigma_c^*$			0	0
$\phi\Sigma_c^*$				0

Once again we suppress with a factor 1/4 the transitions from a heavy vector to a light vector for the non diagonal terms as done before. Furthermore, we also take into account the contribution of the box diagrams as done in the former work, using the former formalism but changing the masses accordingly. More details can be seen in our paper [491].

3.5.2 Results for $I = 0$

In Table 3.46 we show the results that we obtain for $J = 1/2, I = 0$ from the DN and coupled channels as a function of the cut off, q_{max}, used. In the Table we show the results obtained with and without the box. In the s-wave amplitude that we study, the parity of all the states obtained is negative.

Table 3.46: Poles in coupled channels $DN(2806)$, $\pi\Sigma_c(2592)$, $\eta\Lambda_c(2834)$ with $I = 0$ as a function of q_{max}. (The number in brackets after the channel is the mass of the channel. Units: MeV)

q_{max}	630	638	645	700
no box	$2599.7 + i27.8$	$2598.8 + i25.6$	$2597.8 + i23.5$	$2590.8 + i0$
	$2666.8 + i7.7$	$2661.8 + i8.7$	$2657.4 + i9.6$	$2629.4 + i21.5$
with box	$2597.6 + i11.0$	$2592.0 + i4.5$	$2591.2 + i0$	$2547.2 + i0$
	$2625.2 + i22.8$	$2623.3 + i26.4$	$2621.9 + i28.4$	$2612.0 + i31.0$

We can see that for $q_{max} = 638$ MeV, and considering the box, we obtain a state with small width of 9 MeV. This state could be associated with the experimental one $\Lambda_c(2595)$, which has a mass of 2592.25 ± 0.28 MeV and a width of 2.59 MeV. The effect of the box has been a reduction of the mass by about 7 MeV, which indicates a small mixing with D^*N.

It is interesting to observe in this Table that we predict another $J = 1/2, I = 0$ state with a mass of 2623 MeV and a width of 53 MeV.

One may complain that the width of the 2592 MeV state that we get is larger than the experimental one, but we are very close to the $\pi\Sigma_c$ threshold and the results are very sensitive to the precise value of the mass of the state. For these reasons we make a small variation of q_{max} around 640 MeV. We can see that in Table 3.46 taking $q_{max} = 645$ MeV reduces the mass of the state by 0.8 MeV, and being below the $\pi\Sigma_c$ threshold, the width is now zero. The channel $\pi\Sigma_c$ is what gives width to the state and the proximity to the threshold is what makes the width very small.

In Table 3.47 we show now the results for the states of $J = 1/2, 3/2$, $I = 0$, obtained from the D^*N interaction with its coupled channels, both with inclusion or not of the box diagram. We obtain two states, degenerate in spin without the box. The box diagram breaks the degeneracy for the lower energy state but barely changes the result for the higher energy state, something that we shall be able to interpret when we look at the couplings of the states to the different channels. The reason for the breakup of the spin degeneracy is the Kroll Ruderman term that only acts in $J = 1/2$. The effect of the box is a reduction of the mass of this lower energy state by about 60 MeV for values of q_{max} around 800 MeV. The effect of the box is bigger

here than in the former case. First we are choosing q_{max} bigger, but also the mass of DN in the intermediate state is closer here to the energies obtained than the mass of D^*N to the energies of Table 3.46. We are searching for the experimental $J = 3/2$, $\Lambda_c(2625)$, which has a mass of 2628.11 ± 0.19 MeV and a width smaller than 0.97 MeV. We find a candidate with zero width for $q_{max} = 791$ MeV. In addition we obtain three more states, since we obtain two states with $J = 1/2$ and two with $3/2$, all of them with zero or very small width. The effect of the box is very small in the higher energy state, which is then nearly degenerate in $J = 1/2$ and $3/2$. We shall be able to interpret this when we look for the couplings of the states to the different channels.

Table 3.47: Poles in coupled channels $D^*N(2948)$, $\rho\Sigma_c(3229)$, $\omega\Lambda_c(3069)$, $\phi\Lambda_c(3306)$ with $I = 0$ as a function of q_{max}. (Units: MeV)

q_{max}	780	791	810	850
no box	$2683.1 + i0$	$2673.9 + i0$	$2657.9 + i0$	$2624.0 + i0$
	$2966.4 + i0.4$	$2959.8 + i0.3$	$2948.6 + i0.1$	$2926.0 + i0$
with box	$2626.0 + i0$	$2615.4 + i0$	$2596.9 + i0$	$2557.6 + i0$
$(J = 1/2)$	$2965.8 + i0.8$	$2959.1 + i0.7$	$2947.9 + i0.6$	$2925.0 + i0.7$
with box	$2638.0 + i0$	$2628.5 + i0$	$2611.9 + i0$	$2576.5 + i0$
$(J = 3/2)$	$2965.2 + i1.5$	$2958.6 + i1.5$	$2947.4 + i1.4$	$2924.3 + i1.4$

The first striking thing is that we have used two different cut offs in the two sectors. Although they are still rather similar, this might look a bit arbitrary, but the regularization scale does not have to be exactly the same for different sectors. What we have done is to use two free parameters of the theory to fine tune the energies of the two states, but we would not have claimed success if the cut off needed had been outside the natural range. Even then, it is by no means trivial to get the width so small, as in the experiment. Note that in the case of the DN states we also found a state with a mass of the order of 2623 MeV but the width was about 52 MeV. Yet, it is interesting to recall that the values of the cut off needed to get these states are perfectly in line with what was already observed in the light sector. Indeed, in the study of the $\bar{K}N$ interaction with its coupled

channels, two states for the $\Lambda(1405)$ were obtained in Ref. [277] using the input of Ref. [155], the one at 1420 MeV corresponding to the $\Lambda_c(2595)$ obtained here. The cut off needed in Ref. [155] was 630 MeV, much in line with what we have found here. On the other hand, an analogous case to the spin 1/2, 3/2 that we obtain from the D^*N and coupled channels is the one of the resonances $\Delta(1900)(1/2^-), \Delta(1930)(5/2^-), \Delta(1940)(3/2^-)$. These states were studied along the same lines as here in Ref. [492] with the $\rho\Delta$ channel, and with extra coupled channels in Ref. [389], and a cut off of about 770 MeV was needed to reproduce them. In other studies a different regularization procedure is done by making the G function zero at $\sqrt{s} = \sqrt{m_M^2 + m_B^2}$, where m_M, m_B are the meson and baryon masses for the lightest of the coupled channels in a given quantum number [237, 489]. In practice this has a similar effect to the one of the different cut offs.

It is interesting to see in Table 3.47 that we obtain a state at 2615 MeV with $J = 1/2$ and zero width. This is not far away from the $J = 1/2$ state of Table 3.46 at 2592 MeV, and one might think that this could be a candidate for the experimental 2595 MeV state, given the flexibility of the theory to make small changes in the cut off. However, there is one argument against this interpretation. This state is linked to the 2628 MeV, $J = 3/2$ state of Table 3.47. Once this latter energy is fixed, so is the one of the $J = 1/2$ state. One might think that a compromise for the two spin states could be found with a different cut off, but this is not possible because the difference of mass of these two states in the range of $q_{max} = 780 - 850$ MeV (not to spoil too much the agreement for the 3/2 state) ranges within 12-19 MeV, rather stable with the cut off, while the difference between the experimental 1/2 and 3/2 states is 36 MeV. This fact, however, has a repercussion which is that we predict a $J^P = 1/2^-$ state with mass 2615 MeV and zero width, in addition to the state associated to the experimental one at 2592 MeV. We, thus, get two narrow states, one at 2592 MeV and the other one at 2615 MeV. In this range only one narrow state is obtained in Ref. [238] at 2618 MeV.

In order to understand the meaning of the results that we obtain we evaluate the residues, g_i, and wave function at the origin, $g_i G_i$ [95], corresponding to the states with $q_{max} = 638$ MeV. What we can see is that while both states couple appreciably to DN and $\pi\Sigma_c$, the amount of DN, measured by its coupling, or better, the wave function at the origin, is big-

ger for the lower energy state. In our results, we also found that the wave function at the origin for $\pi\Sigma_c$ is rather large, but this is linked to the fact that we are so close to the $\pi\Sigma_c$ threshold. Indeed, if one recalls the shape of the G function, we know that ReG is negative, with a discontinuity in the derivative at threshold, where it has the minimum (largest $|\text{Re}G|$) (see fig. 4 of Ref. [428]). This also tells that the amount of the wave function of $\pi\Sigma_c$ at the origin will be very sensitive to small changes in the mass of the state. Similarly, we also can do the test for the states found with D^*N and coupled channels of Table 3.47 (more discussions can be seen in our paper [491])

It is instructive to compare the results obtained here with those of Ref. [238]. There a $1/2^-$, I=0 state is found at 2618 MeV, with very small width, which is associated to the $\Lambda_c(2595)$. The state couples both to DN and D^*N but the coupling to D^*N is about 50 % bigger than the one to DN. As we have discussed here, this does not mean that the D^*N channel is the dominant in the wave function, because what matters is the wave function at the origin, gG, and, since the D^*N channel is farther away in energy than the DN, the G function is smaller and finally the DN channel stands as dominant, which would be in agreement with our statement in this paper. It is also interesting to note that in Ref. [238] another Λ_c resonance is found around 2617 MeV, but with a width of 90 MeV. We also find a similar state around 2623 MeV and a width of 52 MeV. In both cases, a considerable coupling to the $\pi\Sigma_c$ state is responsible for the width. In addition, in Ref. [238] a state with $J^P = 3/2^-$, $I = 0$ is obtained at 2666 MeV with a width of 54 MeV which is associated to the $\Lambda_c(2625)$. We, instead, get a state at 2628 MeV and with zero width, with the dominant coupling to the D^*N state, while in Ref. [238] there is a large coupling to D^*N but there is also some coupling to $\pi\Sigma_c^*$ which is responsible for the relatively large width. Yet, the width can be drastically reduced if the mass goes down, getting closer to the threshold mass of the $\pi\Sigma_c^*$ channel (2664 MeV). The dynamics of our approach highly suppresses this latter channel, which would involve D exchange instead of π exchange, and is hence further suppressed than the already suppressed pion exchange. Also in the $J^P = 1/2^-$, $I = 0$ sector, in Ref. [238] a state with 2828 MeV and a width of 0.8 MeV is found, which couples to $\rho\Sigma_c$ among other channels. We find a similar state at 2958 MeV of dominant $\rho\Sigma_c$ nature, with a width of about 2 MeV.

The result obtained here for the $\Lambda_c(2595)$ also agrees qualitatively with the one in Ref. [257] or Ref. [489], where also the Weinberg Tomozawa interaction is used, with some small differences in the coupling constants and the use of extra channels in Ref. [257] which are farther away in energy and which we have ignored. The important thing is that in these works, the state associated to the $\Lambda_c(2595)$ couples mostly to DN, like in our case.

In addition, the results for the single channel $\pi\Sigma_c^*$ in $I = 0$ and $J = 3/2$ are shown in Table 3.48.

Table 3.48: Poles in single channel $\pi\Sigma_c^*(2656)$ with $I = 0$ and $J = 3/2$ as a function of q_{max}. (The number in bracket after the channel indicate the mass of the channel. Units: MeV)

q_{max}	700	800	1000	1200
no box	$2664.05 + i28.5$	$2657.26 + i17.1$	$2655.61 + i0$	$2646.76 + i0$

We can see that depending on the value of the cut off we get a state barely above threshold or below. In the first case we have a width and in the second the width is zero. By looking at table III of Ref. [238] this state is likely to be identified to the 3/2 state at 2666 MeV of Ref. [238] which couples strongly to $\pi\Sigma_c^*$ and was associated there to the experimental state at 2628 MeV. In our case the state associated to the experimental 3/2 has a different nature and is mostly a D^*N state. If we force the state in Table 3.48 to correspond to the experimental one with $J = 3/2$ we need $q_{max} = 1530$ MeV, which we could not justify with the ranges found from phenomenology. We stick to the choice of the cut off $q_{max} = 638$ MeV for the PB channels in which case we have a prediction of a state with $I = 0$, $J = 3/2$ of 2668 MeV with $\Gamma = 72$ MeV. We should note that we have obtained a resonant state above threshold with a single channel. This might seem to contradict the findings in Ref. [205] where a single channel with an energy independent potential does not generate resonances above threshold. We have checked that it is the energy dependence of the potential of Eq. (3.78) what makes the appearance of the state possible. Indeed, if we make the potential energy independent by taking its value at the $\pi\Sigma_c^*$ threshold we do not get poles above threshold.

3.5.3 Results for $I = 1$ states

In this section we show the results that we obtain for $I = 1$ from the DN, D^*N, $D\Delta$ and $D^*\Delta$ and coupled channels.

In Table 3.49 we show the pole positions of the states obtained with the DN and coupled channels as a function of the cut off. The idea is that we shall now use the same cut off as for $I = 0$ with the DN channel. Depending on the cut off we find one or two poles. When we take $q_{max} = 638$ MeV, there is only one pole. The 2nd pole gets closer to the DN threshold and disappears.

Table 3.49: Poles in the $I = 1$ sector of DN and coupled channels as a function of q_{max}. Threshold masses: $DN(2806)$, $\pi\Sigma_c(2592)$, $\pi\Lambda_c(2425)$, $\eta\Sigma_c(3001)$. (Units: MeV)

q_{max}	600	638	700	750
no box	$2668.9 + i119.0$	$2669.1 + i112.1$	$2668.1 + i100.7$	$2666.2 + i91.4$
	–	–	$2801.9 + i11.5$	$2795.4 + i16.4$

By taking the pole obtained for $q_{max} = 638$ MeV we show in Table 3.50 the couplings and wave functions at the origin. We observe that the state largely couples to $\pi\Sigma_c$.

Table 3.50: The coupling constants to various channels for the poles in the $I = 1$ sector of DN and coupled channels, taking $q_{max} = 638$ MeV.

$2669.1 + i112.1$	DN	$\pi\Sigma_c$	$\pi\Lambda_c$	$\eta\Sigma_c$
g_i	$-1.33 - i0.79$	$1.72 + i1.44$	$0.05 + i0.08$	$0.04 + i0.07$
$g_i\, G_i^{II}$	$3.18 + i4.01$	$-75.77 - i15.68$	$-3.36 - i0.32$	$-0.17 - i0.48$

In Table 3.51 we show the states obtained with D^*N and its coupled channels as a function of the cut off. We find two states with zero or a small width. The couplings of these states to the coupled channels are shown in Table 3.52 for the cut off that we used with the same D^*N channel in $I = 0$. We see that the state found around 2917 MeV couples mostly to D^*N, while the one at 3125 MeV couples mostly to $\rho\Sigma_c$.

Table 3.51: Poles in the $I = 1$ sector of D^*N and coupled channels as a function of q_{max}. Threshold masses: $D^*N(2948)$, $\rho\Sigma_c(3229)$, $\rho\Lambda_c(3062)$, $\omega\Sigma_c(3236)$, $\phi\Sigma_c(3173)$. (Units: MeV)

q_{max}	750	780	791	810
no box	$2926.4 + i0$	$2920.1 + i0$	$2917.6 + i0$	$2913.0 + i0$
	$3141.0 + i3.8$	$3129.9 + i4.2$	$3125.8 + i4.4$	$3118.6 + i4.6$

Table 3.52: The coupling constants to various channels for the poles in the $I = 1$ sector of D^*N and coupled channels, taking $q_{max} = 791$ MeV.

$2917.62 + i0$	D^*N	$\rho\Sigma_c$	$\rho\Lambda_c$	$\omega\Sigma_c$	$\phi\Sigma_c$
g_i	3.90	-0.95	-0.71	-0.38	0.53
$g_i\, G_i^{II}$	-30.90	7.68	8.22	3.04	-2.64
$3125.8 + i4.4$	D^*N	$\rho\Sigma_c$	$\rho\Lambda_c$	$\omega\Sigma_c$	$\phi\Sigma_c$
g_i	$-0.05 + i0.55$	$3.82 - i0.08$	$-0.17 - i0.11$	$-0.09 - i0.06$	$0.13 + i0.08$
$g_i\, G_i^{II}$	$-6.26 - i3.91$	$-51.06 + i0.32$	$5.95 - i0.19$	$1.21 + i0.79$	$-0.87 - i0.56$

In Table 3.53 we show the states that we obtain in the $D\Delta$ and coupled channels. We obtain two states. Once again we use the cut off corresponding to the pseudoscalar-baryon channels and study the coupling of these states to the different channels. We found that the lower state that we get couples mostly to $\pi\Sigma_c^*$, while the one couples mostly to $D\Delta$.

Table 3.53: Poles in the $I = 1$ sector of $D\Delta$ and coupled channels as a function of q_{max}. Threshold masses: $D\Delta(3099)$, $\pi\Sigma_c^*(2656)$, $\eta\Sigma_c^*(3066)$. (Units: MeV)

q_{max}	600	638	700	750
no box	$2733.9 + i119.4$	$2734.7 + i112.1$	$2737.6 + i99.2$	$2743.1 + i93.0$
	$2882.0 + i3.1$	$2843.5 + i4.5$	$2774.4 + i8.1$	$2712.8 + i6.7$
with box	$2734.4 + i119.2$	$2736.0 + i111.9$	$2740.6 + i102.4$	$2741.2 + i98.2$
	$2829.7 + i3.3$	$2789.1 + i4.8$	$2714.2 + i4.7$	$2653.9 + i0.2$

Finally, in Table 3.54 we show the states that we get from the $D^*\Delta$ and coupled channels. We get two states with zero or a small width. Once again, taking the cut off corresponding to the vector-baryon channels, after investigating the coupling to the different channels, we found that the lower state couples mostly to $D^*\Delta$, while the other one couples most strongly to $\rho\Sigma_c^*$.

Table 3.54: Poles in the $I = 1$ sector of $D^*\Delta$ and coupled channels as a function of q_{max}. Threshold masses: $D^*\Delta(3241)$, $\rho\Sigma_c^*(3293)$, $\omega\Sigma_c^*(3301)$, $\phi\Sigma_c^*(3538)$. (Units: MeV)

q_{max}	750	780	791	810
no box	$2852.1 + i0$	$2816.9 + i0$	$2803.9 + i0$	$2781.5 + i0$
	$3201.4 + i0$	$3189.7 + i0$	$3185.4 + i0$	$3177.7 + i0$
with box	$2791.1 + i0$	$2761.0 + i0$	$2749.2 + i0$	$2728.4 + i0$
	$3201.2 + i1.3$	$3189.3 + i1.2$	$3184.9 + i1.1$	$3177.1 + i1.1$

We have obtained seven states with $I = 1$, corresponding to Σ_c states. In Ref. [238] one also sees three Σ_c states with $J = 1/2$ and two states with

$J = 3/2$. Some of them have strong couplings to particular channels, as we also find here, but the masses of the states differ somewhat. The stronger resemblance is for a state that couples strongly to $\pi\Sigma_c^*$ in Ref. [238] at 2693 MeV with $\Gamma = 67$ MeV, while here we find it at 2736 MeV with $\Gamma = 224$ MeV.

It is curious to see that the $D^*\Delta$ state has smaller mass than the corresponding D^*N state, in spite of the $\Delta - N$ mass difference. The reason has to be seen in the factor 4 in Table 3.26 for $D^*\Delta \to D^*\Delta$ versus the factor 1 for $D^*N \to D^*N$ in Table 3.25.

3.5.4 Summary of the results

Finally, since we have many intermediate results, we summarize here the final results that we get for the states. The results are shown in Table 3.55, where we also write for reference the main channel of the state.

Table 3.55: Energies and widths of the states obtained and the channels to which the states couple most strongly.

main channel	J	I	(E, Γ) [MeV]	Exp.
$DN,\ \ \pi\Sigma_c$	1/2	0	2592, 9	$\Lambda_c(2595)$
$\pi\Sigma_c$	1/2	0	2623, 53	-
D^*N	1/2	0	2615, 0	-
D^*N	3/2	0	2628, 0	$\Lambda_c(2625)$
$\pi\Sigma_c^*$	3/2	0	2668, 70	-
$\rho\Sigma_c$	1/2, 3/2	0	2959, 3	$\Lambda_c(2940)$?
$\pi\Sigma_c$	1/2	1	2669, 224	-
$D\Delta$	3/2	1	2789, 9	-
$\pi\Sigma_c^*$	3/2	1	2736, 224	-
D^*N	1/2, 3/2	1	2917, 0	-
$\rho\Sigma_c$	1/2, 3/2	1	3126, 9	-
$D^*\Delta$	1/2, 3/2, 5/2	1	2749, 0	-
$\rho\Sigma_c^*$	1/2, 3/2, 5/2	1	3185, 2	-

In summary, we predict six states with $I = 0$, two of them corresponding

to the $\Lambda_c(2595)$ and $\Lambda_c(2625)$, and seven states with $I = 1$, some of them degenerate in spin. The energies of the states range from about 2592 MeV to 3185 MeV.

It might seem at first sight that this is a large number of states, but we must recall that for the analogous sector of baryon strange states one finds within the same range of difference of energies six Λ states with spin and parity $J^P = 1/2^-, 3/2^-, 5/2^-$ and six Σ states with the same spin and parity, most of which could be reproduced as dynamically generated states of meson-baryon or vector-baryon [189, 395].

For the moment there is only one Σ_c state reported in the Ref. [9] around 2800 MeV. The state, however, has no spin nor parity assigned. While there are several states in Table 3.38 close in energy to this state, it is worth quoting that the width of the experimental state is around 75 MeV, which is far away from the $\Gamma = 0, 9, 224$ MeV, that we find for the likely states in Table 3.38 according to the mass. We would tentatively conclude that the experimental state corresponds most likely to a positive parity state. On the other hand, the reported state $\Lambda_c(2940)$ with $\Gamma = 17^{+8}_{-6}$ MeV [9], which has no spin parity associated, could correspond to the spin degenerate Λ_c state that we find at 2959 MeV with small width. In other approaches that use a constituent quark model [476] a D^*N structure is suggested for this state. However, as discussed before, this state, which has some coupling to D^*N, couples mostly to $\rho\Sigma_c$. The states dominated by D^*N in our approach appear more bound.

3.5.5 Conclusions

In this work we studied the interaction of DN, $D\Delta$, D^*N and $D^*\Delta$ states with its coupled channels using dynamics extrapolated from the light quark sector to the heavy one. The starting point was to consider the heavy quarks as spectators in the dominant terms of the interaction. The source of interaction was pion exchange, that mixes states of pseudoscalar-baryon with those of vector baryon, and vector exchange. The interaction was extracted mapping from the light sector and respecting the rules of HQSS. Hence, an extrapolation of the results of the LHG approach was used. With these elements of the interaction, adding subleading terms in the large heavy quark mass counting, obtained from the exchange of heavy vectors in the LHG approach, we studied the interaction of the DN, $D\Delta$, D^*N and $D^*\Delta$

with their coupled channels $\pi\Sigma_c$, $\pi\Lambda_c$, $\eta\Sigma_c$ (for the DN); $\pi\Sigma_c^*$, $\eta\Sigma_c^*$ (for the $D\Delta$); $\rho\Sigma_c$, $\omega\Lambda_c$, $\phi\Lambda_c$, $\rho\Sigma_c^*$, $\omega\Sigma_c^*$, $\phi\Sigma_c^*$ (for the D^*N); and $\rho\Sigma_c^*$, $\omega\Sigma_c^*$, $\phi\Sigma_c^*$ (for the $D^*\Delta$), and we searched for poles of the scattering matrix in different states of spin and isospin. We found six states in $I = 0$, with one of them degenerate in spin $J = 1/2,\ 3/2$, and seven states in $I = 1$, two of them degenerate in spin $J = 1/2,\ 3/2$, and two more degenerate in spin $J = 1/2,\ 3/2,\ 5/2$. The coupling of the states to the different channels, together with their wave function at the origin, were evaluated to show which is the weight of the different building blocks in those molecular states. In particular, two of the states, one with spin $1/2$ that couples mostly to DN, and a second one with spin $3/2$ that couples mostly to D^*N were associated to the experimental ones, $\Lambda_c(2595)$ and $\Lambda_c(2625)$ respectively. The rest of states are so far predictions, with a number of states that is similar to the one of negative parity Λ and Σ states in the strange sector. We think that the use of realistic dynamics, with strict respect of heavy quark spin-flavor symmetry, renders the results obtained rather solid and they should serve as a guideline for future experiments searching for baryon states with open charm.

Chapter 4

Particle decay properties

Particle decays is one of important sources of information in high energy hadron experiments. Thus, to understand and explain the properties of resonances theoretically, we also need to investigate the particle decay modes. Inside nuclei we have additional decay modes that come from particle-nucleon reactions. In this chapter, we will investigate the decay properties of some states, predicted in theories or found in experiments, such as the dynamics in the nuclear medium, the experimental suppression, cross section, phase shift of certain partial wave, the structure component of the states, and radiative decay properties, *et al.*.

4.1 J/ψ reaction mechanisms and suppression

The subject of J/ψ suppression in nuclei has a long history [493] and many plausible reasons for it have been given. Reaction mechanisms of J/ψ with the nucleons are suggested in Refs. [494–496]. Parton shadowing in the target nucleus may suppress the probability of producing a J/ψ [497]. Energy loss of the incident parton in the nuclear medium, prior to $c\bar{c}$ production, may alter the J/ψ production cross section [498, 499]. Also, a suppression of the J/ψ has been proposed as a signature of the formation of Quark-Gluon Plasma in ultrarelativistic nucleus-nucleus collisions [500]. The reaction mechanisms producing the J/ψ in a first place are also not well understood [131]. In any case, a proper understanding of what happens in hot nuclear matter in ultrarelativistic nucleus-nucleus collisions demands

that we understand what happens and why in cold matter as mentioned in Ref. [501]. In this sense J/ψ suppression has been extensively searched in p-nucleus collisions in several fixed target experiments (NA3 [502], E772 [503], NA38 [504], E866 [505], E672/E706 [506], NA50 [501,507,508] and more recently in NA60 [509].

Our aim in this work is to exploit recent progress in the theoretical description of the interaction of vectors mesons with nucleons and apply these ideas to study mechanisms of J/ψ absorption in nuclei. We have in mind the depletion of J/ψ in production reactions in nuclei induced by elementary particles, protons, photons, etc. The starting point is to recall recent advances on our theoretical understanding of the interaction of vector mesons with nucleons. At small and intermediate energies the practical tool to deal with vector meson interactions is the use of effective Lagrangians of the LHG theory [156,159,163,329] which incorporate pseudoscalar mesons, vector mesons and photons. Concerning the pseudoscalar interaction these Lagrangians are equivalent to the chiral Lagrangians [160,377] assuming vector meson dominance, thus, they account for chiral symmetry. In addition they allow to extend the theory to provide the interaction of pseudoscalar mesons with vector mesons and vector mesons with themselves. If one considers the coupling of vector mesons to baryons [171, 172] one can then address the interaction of vectors with baryons. Yet, even at low energies the use of perturbation theory becomes inadequate and nonperturbative techniques are demanded to study this interaction. By combining the information from the Lagrangians and unitary in coupled channels, following the pattern of the ChUA [189], a study of the vector-baryon interaction is done in Ref. [390] for the case of the baryons of the octet of the proton and in Ref. [389] for the case of the baryons of the decuplet of the Δ. It is found there that several resonances appear as a consequence of the interaction which can be associated to known states of the PDG [9]. The extrapolation of these works to the charm sector was done in Refs. [127,168], where some N^* and Λ^* resonances in the hidden charm sector were dynamically generated from DN and other coupled channels, $\pi\Sigma_c$ and $\pi\Lambda_c$ among them. These works contain the tools to address the $J/\psi N$ interaction which are used here.

Furthermore, when it comes to study the propagation of vector mesons with nuclei we apply also recent tools developed in the study of the $\bar{K}^*(890)$

in nuclei [510]. This latter work has gone one step forward with respect to the well established works on the issue [511–516] that were constructed to address the problem of vector meson propagation through nuclei [284, 517]. While the latter quoted works concentrated mostly on the modification of the decay channels and the coupling to some resonance-hole components introduced empirically, the dynamical generation of these resonances, to which the vector-nucleon couples so strongly, in the work of Ref. [390], allows to address the problem from a more microscopical point of view. Indeed, in Ref. [510] there are two sources of modification of the $\bar{K}^*$ properties, the modification of its decay channel, $\pi\bar{K}$, and the $\bar{K}$ N interaction modified in the medium, which is studied nonperturbatively in Ref. [510] and gives rise to dynamically generated resonances in the region of 2000 MeV. In this sense the coupling of the $\bar{K}^*$ to hole-resonance components is done automatically, with the strength provided by the same model. This of course has more relevance when we go to the charm sector since experimental information on baryonic resonances is scarce and their coupling to vector meson components is not known.

With these motivation, in order to test the relevance of the J/ψ absorption mechanisms found, in the present work we evaluate the transparency ratio for photoproduction of J/ψ in nuclei. Using beams of around 10 GeV, and energies accessible in the Jefferson Lab upgrade, we look for the rate of production in different nuclei.

4.1.1 Vector-baryon coupled channels approach

Recently, a study of the vector-baryon interaction in the hidden charm sector around energies of 4 GeV, has been tackled in Refs. [127, 168]. In the sector with isospin $I = 1/2$ and strangeness $S = 0$, three channels are considered: $\bar{D}^*\Lambda_c$, $\bar{D}^*\Sigma_c$ and $J/\psi N$. The potential is evaluated using an SU(4) extrapolation of the LHG approach with symmetry breaking ingredients implemented [127, 168]. The amplitudes of Feynmann diagrams like those in Fig. 4.1 a) are evaluated, and the potential after projecting in s-wave takes the form:

$$V_{ij}^{WT} = C_{ij}\frac{1}{4f^2}(E + E')\vec{\epsilon}\,\vec{\epsilon}', \tag{4.1}$$

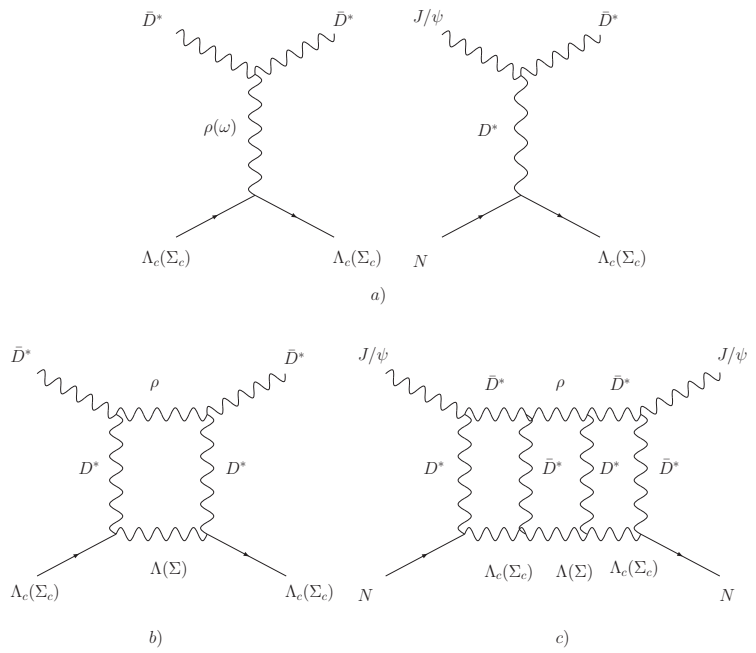

Figure 4.1: a) Vector exchange diagrams for the vector-baryon interaction considered in Refs. [127, 168]. b) Box diagram with $\rho\Lambda(\Sigma)$ in the intermediate state. c) $J/\psi N \to J/\psi N$ like-box diagram with $\rho\Lambda(\Sigma)$ in the intermediate state.

for $i, j = \bar{D}^*\Lambda_c, \bar{D}^*\Sigma_c$, with a minus sign different from Eq. (3.9) absorbed by the present coefficients C_{ij}. In the above formula, E, E' are the energies of vector mesons, $\vec{\epsilon}$, $\vec{\epsilon}'$ the polarization vectors, and $f \equiv f_\pi = 93$ MeV. The transition between these two channels is achieved through the exchange of one ρ or ω mesons. For transitions between $\bar{D}^*\Lambda_c, \bar{D}^*\Sigma_c$ and $J/\psi N$, the full propagator of the D^* meson is taken into account. Thus, we have

$$V_{kl}^{WT}(J/\psi N \to \bar{D}^*\Lambda_c, \bar{D}^*\Sigma_c) = -\frac{C_{kl}g^2}{p_{D^*}^2 - m_{D^*}^2}(E_{D^*} + E_{J/\psi})\vec{\epsilon}\,\vec{\epsilon}', \qquad (4.2)$$

where $g = m_\rho/2f$. Note that the vertices $J/\psi J/\psi\omega$ or $J/\psi J/\psi\rho$ are forbidden by G-parity and isospin respectively, which leads to a zero potential

of the tree order amplitude $J/\psi N \to J/\psi N$. But, when amplitudes are unitarized via the BS equation, the resummation of loops implies indirect reactions $J\psi N \to \bar{D}^* \Lambda_c(\Sigma_c) \to J\psi N$.

The scattering matrix is given by the BS equation in coupled channels, Eq. (1.44), seen in the subsection 1.3.1, with the G function using the dimensional regularization expression, Eq. (1.46), as done in Refs. [127,168], and the potential V given by Eq. (4.1) removing $\vec{\epsilon}\vec{\epsilon}'$. When going to the complex plane of the energy, one resonance is found at the position $\mathrm{Re}(\sqrt{s}) = 4415$ MeV. Pole positions and couplings to the different channels are given in Table 4.1. In addition, there can be transitions from the heavy

Table 4.1: Pole position and coupling constants (g_a) to various channels for the state found in the sector $(I, S) = (1/2, 0)$

(I,S)	$\sqrt{s} = 4415 - 9.5i$	Channels		
$(1/2,0)$		$\bar{D}^*\Sigma_c$	$\bar{D}^*\Lambda_c$	$J/\psi N$
g_a		$2.83 - 0.19i$	$-0.07 + 0.05i$	$-0.85 + 0.02i$

vector-heavy baryon channels to light vector-light baryon channels with a big momentum transfer to the last ones for the energies that we consider. To account for this momentum dependence, the light vector-light baryon channels are implemented through box Feynmann diagrams, see Fig. 4.1 b). This is done because the masses of the intermediate channels are very far from the energies under consideration for $J/\psi N$. This transition potential is derived from the same hidden gauge Lagrangians, and it is given by Refs. [127, 168]

$$\delta \tilde{V}_{ab}^{Box} = \sum_c \tilde{V}_{al}\, G_l\, \tilde{V}_{lb}, \tag{4.3}$$

where l stands for the light channels ρN, ωN, ϕN, $K^*\Lambda$, $K^*\Sigma$, and

$$\tilde{V}_{al} = -C_{al} g^2 \frac{-2E_{V_1} + [(M_{B_3} - M_{B_1})(M_{V_1}^2 + M_{V_1^*}^2 - M_{V_3}^2)]/M_{V_1^*}^2}{M_{V_1}^2 + M_{V_3}^2 - 2E_{V_3}E_{V_1} - M_{V_1^*}^2} \tag{4.4}$$

Here l stands for a different group of $V_3 B_3$, and C_{al} [C_{ij} in Eq. (4.1), C_{kl} in Eq. (4.2)] coefficients given in Refs. [127, 168] or our paper [518]. Then,

the kernel V in the BS equation, Eq. (1.44), becomes now:

$$V_{ab}(V_1B_1 \to V_2B_2) = V_{ab}^{WT} + \delta\tilde{V}_{ab}^{Box} \tag{4.5}$$

with V_{ab}^{WT} given by Eqs. (4.1) and (4.2). Since the light vector-light baryon intermediate channels are very far from the thresholds of $J/\psi N, \bar{D}^*\Lambda_c(\Sigma_c)$, the real part of the box diagrams is small and only the imaginary part matters, but one pays the prize of having the factor $-m_{D^*}^2$ in the denominator of the propagator, which reduces its contribution. Thus, the effect of the inclusion of the potential $\delta\tilde{V}_{acb}^{Box}$ in the BS equation is only a moderate widening of the resonance. With this, the state found with mass $M = 4415$ MeV has a width of 28 MeV added to the 19.2 MeV due to its decay into the $J/\psi N$ channel, which results in a total width of around 50 MeV [127, 168]. The fact that this width is small for a state with such high mass is due to the fact that the transitions are mediated by a heavy vector meson. It is worth noting that the $J/\psi N$ channel, which concerns us in the present article, only can go to the light vector-light baryon channels through intermediate states with $\bar{D}^*\Lambda_c$, $\bar{D}^*\Sigma_c$, see Fig. 4.1 c). Since the depletion has to do with the inelastic $J/\psi N$ cross section, we evaluate it by using the optical theorem that states in our normalization

$$\sigma_{tot} = -\frac{M_N}{P_{CM}^{J/\psi}\sqrt{s}}\text{Im}\ \ T_{J/\psi N\to J/\psi N}, \tag{4.6}$$

hence, by evaluating also the elastic cross section we have

$$\begin{aligned}\sigma_{in} &= \sigma_{tot} - \sigma_{el} \\ &= -\frac{M_N}{P_{CM}^{J/\psi}\sqrt{s}}\text{Im}\ \ T_{J/\psi N\to J/\psi N} - \frac{1}{4\pi}\frac{M_N^2}{s}\overline{\sum}\sum|T_{J/\psi N\to J/\psi N}|^2,\end{aligned} \tag{4.7}$$

where $\sum$, $\overline{\sum}$ stand for sum and average over the spins of the nucleons and J/ψ.

In Fig. 4.2 we plot the results for these cross sections. We observe a peak around 4425 MeV, which corresponds to a hidden charm resonance found in Refs. [127, 168]. Actually, we are interested in the region of J/ψ created in electron nucleus collisions for electrons around 10 GeV which corresponds to J/ψ moving in the rest frame of the nucleons with $\sqrt{s} \simeq 4050 - 5300$ MeV, which includes the resonant peak.

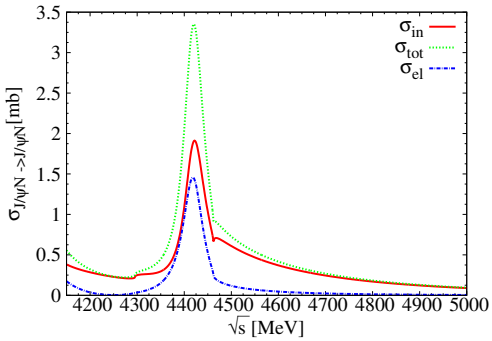

Figure 4.2: The total, elastic and inelastic cross sections in Eqs. (4.6) and (4.8).

4.1.2 The $J/\psi N \to \bar{D}\Lambda_c(\Sigma_c)$ reaction

In the case of the ρ meson the decay channel is $\pi\pi$, and $\pi\bar{K}$ for the $\bar{K}^*$. The equivalent mesonic decay channel of the J/ψ is $D\bar{D}$, but it is closed kinematically. Yet, in the medium there is more available energy for the opening of new decay channels. Indeed, the channel $\bar{D}\Lambda_c$ is slightly above the $J/\psi N$ threshold and can lead to absorption phenomena in the medium. The extrapolation to SU(4) of the coupling of vector mesons to pseudoscalars, as done in Ref. [383], provides a strong coupling of J/ψ to $D\bar{D}$, and the medium related decay channels, with $DN \to \Lambda_c$ or $DN \to \Sigma_c$, are studied in the present work. When implementing vertex corrections in the medium, a contact term $J/\psi N \to \bar{D}\Lambda_c$, which is called Kroll Rudermann (KR) term, must also be taken into account. Altogether, this leads to a relevant source of the J/ψ absorption in the medium through the reaction $J/\psi N \to \bar{D}\Lambda_c$. In addition, one can also consider the creation of one pion in the final state, i. e. $J/\psi N \to \bar{D}\Sigma_c\pi, \bar{D}\Lambda_c\pi$, which will be discussed in next subsection. This reaction requires more energy, however, it is interesting to study it since the $\pi\Sigma_c, \pi\Lambda_c$ channels are decay channels of the $\Lambda_c(2595)$ and $\Sigma_c(2800)$ resonances respectively, which are dynamically generated [256–258].

By analogy to the $\rho \to \pi\pi$ decay or $\bar{K}^* \to \bar{K}\pi$, the J/ψ couples to $D\bar{D}$. Although the channel is not open for decay, the channels $J/\psi N \to \bar{D}\Lambda_c$, $\bar{D}\Sigma_c$ are nearly opened, the thresholds are 4160 and 4290 MeV respectively, which requires a momentum $p^{\rm cm}_{J/\psi} = 405$ MeV for $\bar{D}\Lambda_c$ production. The ver-

tex $J/\psi D\bar{D}$ needed in these diagrams is obtained from the LHG Lagrangian, Eq. (1.34), seen in subsection 1.2.2, in SU(4). The isospin doublets of D are (D^+, D^0), $(-\bar{D}^0, D^-)$, and, thus, we find

$$-it_{J/\psi D^+(q)D^-(P-q)} = -i2g\, q_\mu\, \epsilon^\mu, \tag{4.8}$$

$$-it_{J/\psi D^0(q)\bar{D}^0 q} = -i2g\, q_\mu\, \epsilon^\mu, \tag{4.9}$$

$$-it_{J/\psi D\bar{D}(I=0)} = -i2\sqrt{2}\, q_\mu\, \epsilon^\mu, \tag{4.10}$$

with P the J/ψ momentum.

We then evaluate the cross section for the Feynman diagrams of Figs. 4.3 a). This requires in addition the extension of the Yukawa vertex $DN\Lambda_c(\Sigma_c)$.

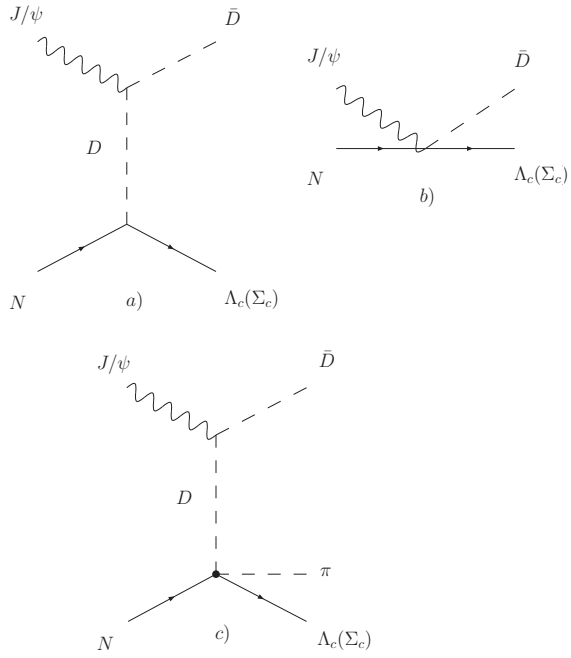

Figure 4.3: Feynman diagrams of $J/\psi N \to \bar{D}\Lambda_c(\Sigma_c)$, a) Vector exchange contribution. b) Kroll Ruderman term. c) The $J/\psi N \to \bar{D}\pi\Lambda_c(\Sigma_c)$ reaction.

One can use SU(4) symmetry or simply assume that the D plays the anal-

ogous role as a $\bar{K}$ and $\Lambda_c(\Sigma_c)$ the role of $\Lambda(\Sigma)$. Then we find

$$-it_{D^0p\to\Lambda_c^+} = -\frac{1}{\sqrt{3}}\left(\frac{D+3F}{2f}\right)\vec{\sigma}\cdot\vec{q}, \tag{4.11}$$

$$-it_{D^0p\to\Sigma_c^+} = \frac{D-F}{2f}\vec{\sigma}\cdot\vec{q}, \tag{4.12}$$

$$-it_{D^+p\to\Sigma_c^{++}} = \sqrt{2}\frac{D-F}{2f}\vec{\sigma}\cdot\vec{q}. \tag{4.13}$$

We use the values $D = 0.795$, $F = 0.465$ [313]. The cross section for the process $J/\psi \to \bar{D}^0\Lambda_c^+$ is given by

$$\sigma = \frac{M_N M_{\Lambda_c}}{4\pi}\frac{1}{s}\frac{p'}{p}\overline{\sum}\sum|T|^2, \tag{4.14}$$

where p', p are the Λ_c and N momentum in the $J/\psi N$ CM frame and $|T|^2$ is given by

$$\begin{aligned}\overline{\sum}\sum|T|^2 &= \frac{4}{3}g_D^2\Big[\frac{(P\cdot p_{\bar{D}})^2}{M_{J/\psi}^2} - m_{\bar{D}}^2\Big]\times\frac{1}{2}\frac{1}{m_N m_{\Lambda_c}}(m_N+m_{\Lambda_c})^2 \\ &\quad\times(pp' - m_N m_{\Lambda_c})\times\frac{1}{(q^2-m_D^2)^2}\times\frac{1}{3}\Big(\frac{3F+D}{2f}\Big)^2\end{aligned} \tag{4.15}$$

with m_N the proton mass and P, $p_{\bar{D}}$ the four-momentum of the J/ψ and $\bar{D}$ respectively and $g_D = m_{D^*}/2f_D$ ($f_D = 206/\sqrt{2}$ MeV).

For reasons of gauge invariance [393, 511, 515, 519, 520] one should add the KR term, this is a contact term for the vector-two-baryon-pseudoscalar particles, see Fig. 4.3 b). The prescription to get the KR term is to substitute the meson pole term: $\vec{\epsilon}(\vec{P}_V + 2\vec{q})\,\frac{1}{(P_V+q)^2-m_D^2}\,\vec{\sigma}\,(\vec{P}_V+q)$ by the KR term: $\vec{\sigma}\cdot\vec{\epsilon}$. In the case of $J/\psi p \to \bar{D}^0\Lambda_c^+$ we get,

$$-it_{p\Lambda_c^+ J/\psi\bar{D}^0} = -\frac{g}{\sqrt{3}}\left(\frac{D+3F}{2f}\right)\vec{\sigma}\cdot\vec{\epsilon} \tag{4.16}$$

In Fig. 4.4 we can see both contributions: D-exchange (dashed line), KR (dot-dashed line), and the sum, which takes into account the interference (continuous line). Whereas the KR contribution remains constant while increasing $\sqrt{s}$, the D-exchange term increases with the momenta of the J/ψ.

We observe that for energies around 4400 MeV the KR term dominates, being about five times bigger than the D-exchange contribution, the latter has $\sigma \sim 1.2$ mb around this energy for $\bar{D}\Lambda_c$. In the case of $\bar{D}\Sigma_c$, the sum is about one order of magnitude smaller than for $\bar{D}\Lambda_c$. The cross section for $J/\psi N \to \bar{D}\Lambda_c$ was also studied in [496] based on the same mechanism of Fig. 4.3 a) and with similar results. We have also included here the KR term following the developments of Refs. [393, 511, 515, 519, 520].

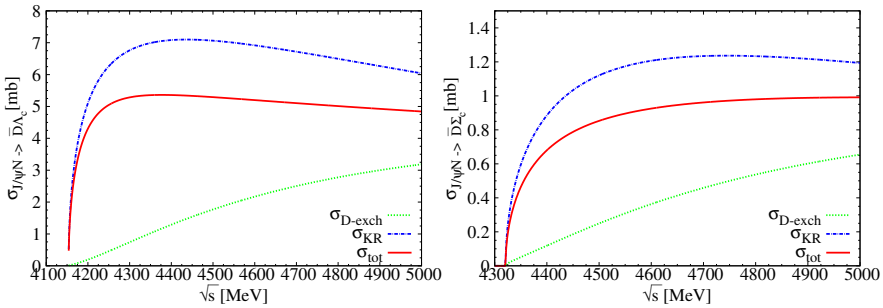

Figure 4.4: The cross section for $J/\psi N \to \bar{D}\Lambda_c$ (left) and $J/\psi N \to \bar{D}\Sigma_c$ (right).

4.1.3 The $J/\psi N \to \bar{D}\pi\Lambda_c, \bar{D}\pi\Sigma_c$

Next we study the reactions $J/\psi N \to \bar{D}\pi\Lambda_c, \bar{D}\pi\Sigma_c$. The diagrams are depicted in Fig. 4.3 c). This process is interesting to study because the DN interaction leads to the $\Lambda_c(2595)$ and $\Sigma_c(2800)$ resonances studied in Refs. [256–258], which have the opened decay channels $\pi\Sigma_c$ and $\pi\Lambda_c$ respectively. The scattering matrix for this process is calculated similarly as in the mechanisms of the former section and we find for $J/\psi N \to \bar{D}\pi\Lambda_c$

$$\sigma = \frac{M_N M_{\Lambda_c}}{4 p_{J/\psi} s} \int dM_{23} \int_{-1}^{1} dcos\theta \frac{p_1 \tilde{p}_2}{(2\pi)^3} \overline{\sum} \sum |T|^2, \tag{4.17}$$

with

$$\overline{\sum} \sum |T|^2 = \frac{4}{3} g_D^2 \Big[\frac{(P \cdot p_{\bar{D}})^2}{M_{J/\psi}^2} - m_{\bar{D}}^2 \Big] \Big(\frac{1}{q^2 - m_D^2} \Big)^2 \times \frac{3}{2} |T^{I=1}_{D\bar{N} \to \pi\Lambda_c}|^2. \tag{4.18}$$

In Eq. (4.17) M_{23} is the invariant mass of $\pi\Lambda_c$ and θ the angle between J/ψ and $\bar{D}$, and

$$p_1 = \frac{\lambda^{1/2}(s, m_{\bar{D}}^2, M_{23}^2)}{2\sqrt{s}}, \quad \tilde{p}_2 = \frac{\lambda^{1/2}(M_{23}^2, M_{\Lambda_c}^2, m_\pi^2)}{2M_{23}}. \tag{4.19}$$

For the case of $J/\psi N \to \bar{D}\pi\Sigma_c$ we take only the $I = 0$ part, which is dominant, and we sum the possible charge processes with this isospin: $J/\psi\ p \to \bar{D}^0\pi^+\Sigma_c^0$; $J/\psi\ p \to \bar{D}^0\pi^0\Sigma_c^+$; $J/\psi\ p \to \bar{D}^0\pi^-\Sigma_c^{++}$. We find

$$\overline{\sum}\sum |T|^2 = \frac{4}{3} g_D^2 \Big[\frac{(P\cdot p_{\bar{D}})^2}{M_{J/\psi}^2} - m_{\bar{D}}^2\Big]\Big(\frac{1}{q^2 - m_D^2}\Big)^2 \times \frac{1}{2}\big|T^{I=0}_{DN\to\pi\Sigma_c}\big|^2. \tag{4.20}$$

The amplitudes $T^{I=1}_{DN\to\pi\Lambda_c}$ and $T^{I=0}_{DN\to\pi\Sigma_c}$ are evaluated using the model of [257, 258]. We show the cross section for Λ_c and Σ_c in the final state in Fig. 4.5. The cross sections found are small. The one for $J/\psi N \to \bar{D}\pi\Lambda_c$ is about 30 times smaller than the one for $J/\psi N \to \bar{D}\Lambda_c$, and the one for $J/\psi N \to \bar{D}\pi\Sigma_c$ about five times smaller than that of $J/\psi N \to \bar{D}\Sigma_c$.

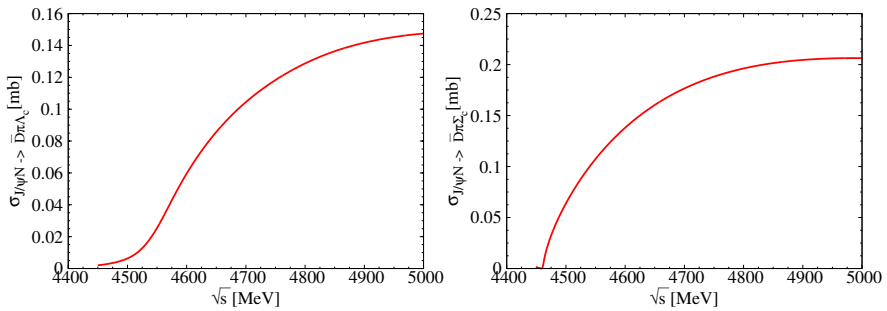

Figure 4.5: The cross section for $J/\psi N \to \bar{D}\pi\Lambda_c(\Sigma_c)$.

4.1.4 Transparency ratio

We now try to see how we can test this prediction. We can for instance take an electron beam of 10 GeV as in the Jefferson lab upgrade and look at $\gamma A \to J/\psi\ X$. Depending on what is the elementary production of J/ψ, like $\gamma N \to J/\psi N$, $J/\psi\pi N, \cdots$. We will have a range of J/ψ energies in the lab frame which covers the range of energies 4000 MeV − 5340 MeV. We

choose this range because we have the resonance peak for σ_{in} in this region. We define the transparency ratio

$$T_A = \frac{\sigma_A(J/\psi)}{A\sigma_N(J/\psi)}, \tag{4.21}$$

but it is customary to normalize to a light nucleus like ^{12}C and define

$$T'_A = \frac{T_A}{T_{^{12}C}}. \tag{4.22}$$

We take several nuclei and evaluate $\sigma_A(J/\psi)$ as a function of A. Given the fact that the J/ψ will move in the nucleus essentially forward in the lab frame of $J/\psi N$, with N a secondary nucleon in the nucleus which we consider at rest, we can use a simple formula derived in Ref. [521] which gives the transparency ratio as

$$T_A = \frac{\pi R^2}{A\sigma_{J/\psi N}}\Big\{1 + \big(\frac{\lambda}{R}\big)exp\big[-2\frac{R}{\lambda}\big] + \frac{1}{2}\big(\frac{\lambda}{R}\big)^2\big(exp\big[-2\frac{R}{\lambda}\big] - 1\big)\Big\}. \tag{4.23}$$

where $\lambda = (\rho_0\sigma_{J/\psi N})^{-1}$, with $\sigma_{J/\psi N}$ the inelastic cross section of $J/\psi N$. In Eq. (4.23) R is the radius of a sphere of uniform density $\rho_0 = 0.17\ fm^{-3}$ with $R = r_0A^{1/3}$, $r_0 = 1.143\ fm$ and A the mass number. This formula works remarkably well in comparison with a more accurate one that takes into account the angle dispersion in the laboratory, as we have checked and is also reported in Ref. [522] in η' photoproduction in nuclei.

We plot in Fig. 4.6 the total $J/\psi N$ inelastic cross section, as the sum of all inelastic cross sections from the different sources discussed before. We can take now various energies of J/ψ and evaluate T_A for this energy as a function of A. We do that in Fig. 4.7 for $\sqrt{s} = 4600$ MeV ($\sigma_{Total(in)} \simeq 6.8\ mb$), a typical energy which is not in the peak of the resonance (4415 MeV). We can see that the values of the transparency ratio are of the order of $0.60 - 0.70$ for heavy nuclei indicating a depletion of about $30 - 35$ % in J/ψ production in nuclei. Normalized to $T_{^{12}C}$ the ratio goes down to 0.75 for heavy nuclei.

In Fig. 4.8 we plot the ratio $T_{^{207}Pb}/T_{^{12}C}$ as a function of energy. We can see that the presence of a resonance results into a dip in the ratio of transparency ratios at the energy of the resonance.

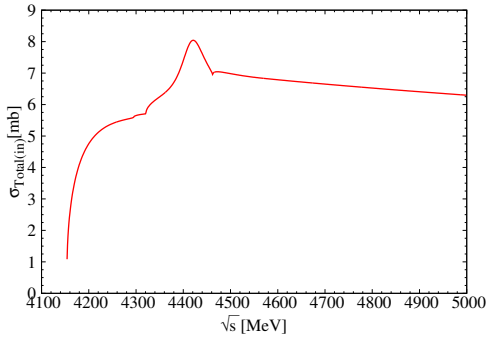

Figure 4.6: The total inelastic cross section of $J/\psi N$.

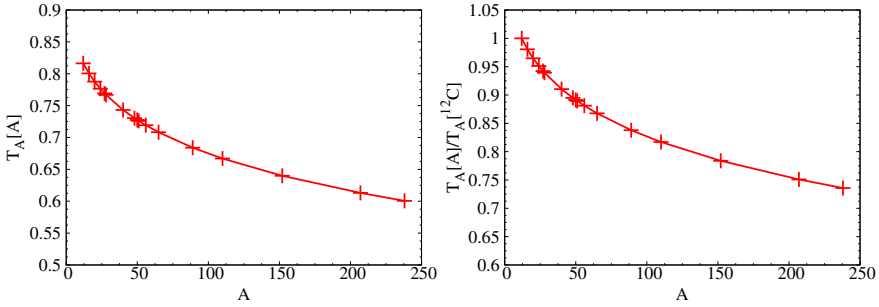

Figure 4.7: The transparency ratio of J/ψ in different nuclei. Left: T_A. Right: $T_A/T_{^{12}C}$

It should be noted that the calculation of the transparency ratio done with Eq. (4.23) does not consider the shadowing of the photons and assumes they can reach every point without being absorbed. However, for γ energies of around 10 GeV, as suggested here, the photon shadowing cannot be ignored. Talking it into account is easy since one can multiply the ratio T'_A by the ratio of N_{eff} for the nucleus of mass A and ^{12}C. This ratio for ^{208}Pb to ^{12}C at $E_\gamma = 10$ GeV is of the order 0.8, but with uncertainties [523]. We should then multiply $T'_A(^{208}Pb)$ in Fig. 4.8 by this extra factor for a proper comparison with experiment. However, this factor does not influence the shape of the results of Fig. 4.8 and the dip due to the resonance. The small dip in Fig. 4.8 would require a high precision experiment to be observed. However, there is one more important reason that makes it not observable,

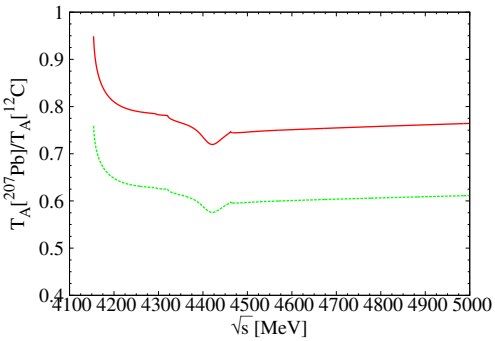

Figure 4.8: The transparency ratio of J/ψ photoproduction as a function of the energy in the CM of J/ψ with nucleons of the nucleus. Solid line: represents the effects due to J/ψ absorption. Dashed line: includes photon shadowing [523].

and this is the Fermi motion of the nucleons [1]. Indeed, in the secondary collisions of the J/ψ with nucleons of the nucleus the argument s of the $J/\psi N$ cross section is given by

$$s_N = (p_{J/\psi} + p_N)^2 = (E_{J/\psi} + E_N)^2 - (\vec{p}_{J/\psi} + \vec{p}_N)^2, \tag{4.24}$$

while $E_N \approx M_N$, the term $2\vec{p}_{J/\psi}\vec{p}_N$ in the expansion of s gives a large span of values of s. For this purpose we substitute the $J/\psi N$ inelastic cross section by the one folded over the nucleon momenta

$$\sigma(s) \to \bar{\sigma} = \int_{|\vec{p}_N|<p_F} \frac{d^3\vec{p}_N}{(2\pi)^3}\sigma(s_N) \Bigg/ \int_{|\vec{p}_N|<p_F} \frac{d^3\vec{p}_N}{(2\pi)^3}, \tag{4.25}$$

where $p_F = (3\pi^2\rho/2)^{1/3}$ and for ρ we take an average density $\rho \approx \rho_0/2$, $\rho_0 = 0.17 fm^{-3}$, the nuclear matter density. The differences are minimal if other realistic densities are used.

The average cross section, $\bar{\sigma}$, is plotted in Fig. 4.9 as a function of $E_{J/\psi}$. We can see that the peak in Fig. 4.6 is washed away by the effect of Fermi motion. Similarly, we redo the calculations of Fig. 4.8 for the transparency

[1] We would like to thank B. Pire for useful remarks concerning the Fermi motion in the transparency ratio.

ratio using the averaged cross section and we find the results of Fig. 4.10. There, again, the dip in the transparency ratio has disappeared, but the values for the J/ψ suppression are essentially the same as before.

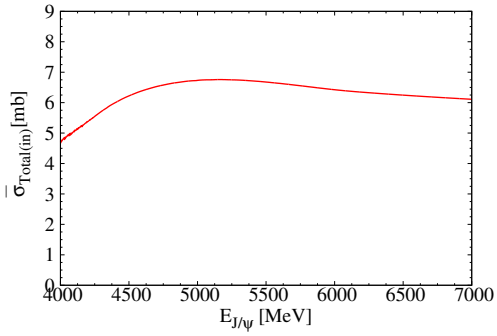

Figure 4.9: The average inelastic cross section of $J/\psi N$.

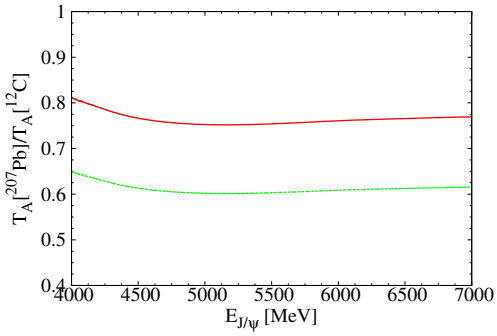

Figure 4.10: The transparency ratio of J/ψ photoproduction as a function of the energy of $E_{J/\psi}$ using the averaged $J/\psi N$ cross section over the Fermi sea of Fig. 4.9. Solid line: represents the effects due to J/ψ absorption. Dashed line: includes photon shadowing [523].

As to the values of the transparency ratio for the different nuclei and different energies, even if the suggested experiment studied here has not been done, the values obtained are in line with the rates of suppression found in many experiments [502–504], where, in spite of using high energies, the J/ψ are produced with momenta in the range studied here.

4.1.5 Conclusions

We have investigated different sources of interaction of J/ψ with nucleons in order to obtain the inelastic $J/\psi N$ cross section. First we have used a model recently developed to study the vector-baryon interaction in the charm and hidden charm sectors. This model produces a resonance which couples to $\bar{D}^*\Lambda_c, \bar{D}^*\Sigma_c, J/\psi N$ at 4415 MeV. The decay of this resonance to light vector-light baryon channels is also incorporated through box Feynman diagrams. Altogether, it gives contribution to the inelastic part of the $J/\psi N \to J/\psi N$ cross section. We have also considered the transitions $J/\psi N \to \bar{D}\Lambda_c$ or $\bar{D}\Sigma_c$ via D-exchange and KR (contact term) diagrams. These processes give a rate large enough to be observed and dominate for the energies that we consider here ($\sqrt{s} \sim 4100 - 5000$ MeV). Furthermore, we evaluate the transitions $J/\psi N \to \bar{D}\pi\Lambda_c$ or $\bar{D}\pi\Sigma_c$. However, these latter processes have a small cross section in the range of energies studied here. We find a total inelastic cross section of the order of a few mb, which is sufficient to produce an appreciable suppression of J/ψ in its propagation through nuclei. We then study theoretically the transparency ratio for J/ψ electroproduction in nuclei, for electrons in the range of 10 GeV, and find values for the transparency ratio which are in consonance with the typical rates of J/ψ suppression found in most experimental reactions. One interesting side effect is that because of the $J/\psi N$ resonance found theoretically around $\sqrt{s} = 4415$ MeV, the J/ψ inelastic cross section has a maximum around the energy of this resonance. The transparency ratio would have a dip around this energy in principle. However, when the Fermi motion of the nucleus is considered the cross section has to be substituted by its average over the nucleon momenta and the dip is washed away. The implementation of such an experiment would be rather valuable, providing information on the J/ψ annihilation modes through the nucleonic components of nuclear matter.

4.2 Small $K\pi$ component in the K^* wave function

Understanding the nature and structure of hadronic particles is an important subject of hadron physics. In principle Quantum Chromodynamics (QCD) should give an answer to these questions. At high energies, because of the asymptotic freedom [142, 143, 524], QCD can be treated perturbatively, but at low energies, needed to interpret the hadron spectrum, QCD is highly non perturbative and calculations become very difficult. Lattice QCD can provide an answer in the future, but so far the determination of the hadron spectrum is finding more problems than anticipated, in particular for particles which decay in several channels, which are the majority of them [525, 526].

Traditionally quark models have tried to find an approach to that problem [2, 527–529] and remarkable progress has been done from this perspective, but in order to understand the particle properties quoted in the PDG [9] it is also becoming clear that hadronic states are more complex than just three quarks for the baryons and $q\bar{q}$ for the mesons [530]. One of the theories that has been remarkably successful dealing with hadron interaction and structure is chiral perturbation theory [376,377]. This theory is an effective field theoretical approach to QCD at low energies and the quark and gluon degrees of freedom are substituted with the baryons and mesons themselves. Yet, it soon became clear that chiral perturbation theory has a very limited energy range of convergence and improvements were made to construct non perturbative unitary extensions of the theory that allowed to deal with hadron interactions at much higher energies. These extensions are commonly known as the ChUA [16, 18, 19, 155, 190, 194, 195, 260, 277, 326–328] (see [189] for a review). With this theory one can study the interaction between hadrons, and some times the interaction leads to poles in the scattering matrix which are interpreted in terms of "dynamically generated" or "composite hadron" states, like the two $\Lambda(1405)$, $\Lambda(1670)$, $N^*(1535)$, etc.

One of the questions that attracts attention is the issue of whether some resonances are "composite" of other hadrons or "genuine" states (other than hadron-hadron molecular states). One answer to this question was early given in the paper of Weinberg [204] (see also Refs. [266, 456, 531]), but it deals with particles bound in s-wave with a very small binding. The generalization to also s-waves but not necessarily so lightly bound and with many coupled channels was given in Ref. [95] for bound states and it was

extended to deal with resonances in Ref. [205]. A further generalization to higher partial waves was done in Ref. [206]. In this latter paper it was found that the ρ meson had a $\pi\pi$ component in the wave function that amounted only to about 20 %, which allows one to claim that the ρ is basically a genuine state rather than a composite state of $\pi\pi$.

In the present work we want to extend the work done in Ref. [206] for the ρ meson to the K^*. The K^* particle was first reported by Ref. [532] and also confirmed in Refs. [533, 534]. It is always exhibited as a resonance in the $K\pi$ scattering [358, 360], which is determined from experiments by the reactions $K^{\pm}p \to K^{\pm}\pi^+ n$, $K^{\pm}p \to K^{\pm}\pi^-\Delta^{++}$ and $K^+p \to K^0\pi^0\Delta^{++}$. The p-wave $K\pi$ scattering was studied by N/D method in Ref. [19] using the ChUA and good agreement was found between theory and experiment. But there are no works focusing on the structure of the K^* resonance from the point of view of its possible $K\pi$ compositeness or otherwise and this is the aim of our present work.

4.2.1 Brief summary of the formalism

Following the formalism of Ref. [206], as discussed in subsection 1.3.2, we have extrapolated the ChUA to higher partial waves, which are used in the present work. With one more step, following again Ref. [206], one finds that for a resonance or bound state, which is dynamically generated by the interaction, the sum rule

$$-\sum_i g_i^2 \left[\frac{dG_i}{dE}\right]_{E=E_p} = 1, \tag{4.26}$$

is fulfilled, with E_p the position of the complex pole (also seen Eq. (3.75)). However, if the state contains some genuine component outside the space of the N wave functions of the coupled channels approach, Eq. (4.26) is generalized to

$$-\sum_i g_i^2 \left[\frac{dG_i}{dE}\right]_{E=E_p} + |\langle\beta|\Psi\rangle|^2 = 1 \ , \tag{4.27}$$

or equivalently to

$$-\sum_i g_i^2 \left[\frac{dG_i}{dE}\right]_{E=E_p} = 1 - Z \ ; \qquad Z = |\langle\beta|\Psi\rangle|^2 \ , \tag{4.28}$$

where $|\beta\rangle$ is the genuine component of the state, and g_i is the coupling, defined as

$$g_i g_j = \lim_{E\to E_p} (E - E_p)\ t_{ij}\ . \tag{4.29}$$

More details can be seen in our paper [535].

4.2.2 Chiral unitary model

Now we investigate the structure of the K^* particle, which shows up as a resonance of $K\pi$, using the formalism discussed before with just one channel. In order to quantify the statement, we first start from the ChUA, and then we use a pure phenomenological method which is independent from any theoretical model to confirm our results, seen in the next subsection.

The p-wave $K\pi$ scattering is studied in Ref. [19] using the N/D method and only the tree level scattering potential. We take the potential from Ref. [19] but taking into account the definition of Eq. (1.53), thus removing the three-momentum factor,

$$v = -\frac{1}{2f^2}\left(1 + \frac{2G_V^2}{f^2}\frac{s}{M_{K^*}^2 - s}\right)\ , \tag{4.30}$$

where M_{K^*} is the bare K^* mass, f is the π decay constant and G_V the coupling to $K\pi$ in the formalism of Ref. [377], where $G_V \simeq f/\sqrt{2}$.

Here, we have explicitly separated the factor $|\vec{p}|^2$ in the potential V to get v which does not depend on the momentum. The formalism using this v kernel requires, as shown in subsection 1.3.2, that the $|\vec{p}|^2$ factor should be included in the loop function (see Eq. (1.56) and the discussion in Ref. [206]). Thus, we can fit the data [19, 358, 360] by using Eq. (1.55) in one channel, but with the loop function G given by

$$G(s) = \int_{|\vec{q}|<q_{max}} \frac{d^3\vec{q}}{(2\pi)^3}\frac{|\vec{q}|^2}{s - (\omega_1+\omega_2)^2 + i\epsilon}\left(\frac{\omega_1+\omega_2}{2\omega_1\omega_2}\right)\ , \tag{4.31}$$

where $\omega_i = \sqrt{m_i^2 + \vec{q}^{\,2}},\ i = \pi,\ K$. The loop function of Eq. (4.31) is regularized by means of a cutoff q_{max}. As also done in Ref. [206], we generalize the formulas of the former subsection to make them relativistic defining $g_i g_j$ as (seen also Eq. (3.72))

$$g_i g_j = \lim_{s\to s_R} (s - s_R)\ t_{ij}\ , \tag{4.32}$$

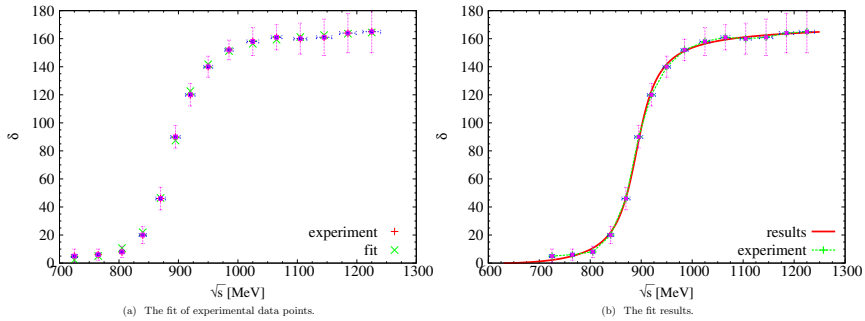

(a) The fit of experimental data points. (b) The fit results.

Figure 4.11: The fit results of the $K\pi$ scattering p-wave phase shift. The data are taken from [19, 358, 360].

The p-wave $K\pi$ phase shift is then given by the formula [206]

$$q_{cm}^2\, t = \frac{-8\pi\sqrt{s}}{q_{cm}\cot\delta(q_{cm}) - i\, q_{cm}} \ , \tag{4.33}$$

with q_{cm} the three-momentum in the center of mass reference frame, which is defined after Eq. (1.46), and given by Eq. (2.58). Then we carry a χ^2 fit to the data [19, 358, 360] using the parameters f, G_V, M_{K^*}, q_{max}, with f, G_V constrained not to differ much from standard values. For the best fit of the data, we find the values of these free parameters:

$$\begin{aligned} f &= 86.22 \text{ MeV} \ , \quad G_V = 53.81 \text{ MeV} \ , \\ M_{K^*} &= 995.76 \text{ MeV} \ , \quad q_{max} = 724.698 \text{ MeV} \ . \end{aligned} \tag{4.34}$$

The best fit results are shown in Fig. 4.11. In Fig. 4.11(a) we show the best fit to data points for the $K\pi$ phase shift which are taken from the experimental data [19, 358, 360]. Fig. 4.11(b) shows the results of the fit using the determined parameters for a continuum of energies. Using the fit parameters, we also get the results for the modulus squared of the scattering amplitudes $|t|^2$ and $|T|^2$, which are shown in Fig. 4.12. From Fig. 4.12, we can see a clear peak in the modulus squared of the amplitudes which corresponds to a resonant structure, with a mass about 890 MeV and a width about 50 MeV. In order to apply the sum rule to the case of a resonance, we should extrapolate the amplitude to the complex plane and look for the complex pole s_0 in the second Riemann sheet. This is done by

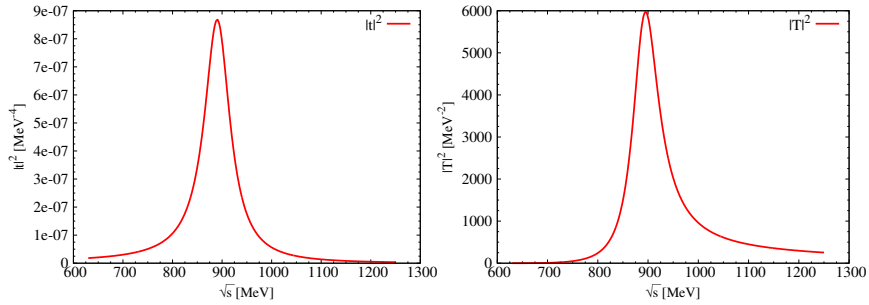

Figure 4.12: Modulus squared of the $K\pi$ scattering amplitudes. Left: $|t|^2$; Right: $|T|^2$ with $cos\theta = 1$.

changing G to G^{II} in Eq. (1.55) to get the complex amplitude in the second Riemann sheet, t^{II}. We proceed as follows:

$G^{II}(s)$ is the analytic continuation to the complex plane of the loop function [16] in p-wave, given by

$$G^{II}(s) = G^{I}(s) + i\frac{q_{cm}^3}{4\pi\sqrt{s}} , \qquad \text{Im } (q_{cm}) > 0 , \tag{4.35}$$

where G^I and G^{II} are the loop functions in the first and second Riemann sheet, G^I is given by Eq. (4.31), and q_{cm} is the complex momentum in the center of mass reference frame, the same as before, given by Eq. (2.58). In the second Riemann sheet, we find the pole of the resonance by solving the equation

$$1 - vG = 0 . \tag{4.36}$$

Thus we are now able to determine the coupling $\tilde{g}_\rho$ as the residue in the pole of the amplitude using Eq. (4.32), as

$$g^2 = \lim_{s \to s_0} (s - s_0) t^{II} . \tag{4.37}$$

Finally, we can use the sum rule of Eq. (4.28) for the single $K\pi$ channel (generalized to the relativistic case) in order to evaluate the contribution of this channel to the wave function of the resonance,

$$-g^2 \left[\frac{dG^{II}(s)}{ds} \right]_{s=s_0} = 1 - Z , \tag{4.38}$$

where Z represents the probability that the K^* is not a $K\pi$ molecule but something else.

Using the determined parameters from the best fit to the data, we find the pole in the second Riemann sheet, which corresponds to the K^* particle,

$$\sqrt{s_0} = (891.0 + i\ 31.3)\ \text{MeV}\ , \tag{4.39}$$

which is consistent with the results of Fig. 4.12. Note that we also get the complex conjugate pole at $(891.0 - i\ 31.3)$ MeV, with a sign convention for the imaginary part as taken in many works looking for poles. We compare the result of Eq. (4.39) with the pole position found in Ref. [536] of $(892.03 - i\ 23.3)$ MeV, and in Ref. [537] of $(892.0 - i\ 23.1)$ MeV. As one can see, the agreement with the mass is very good, but the width obtained is a bit larger. This also happened in the case of the ρ [206]. The value of the coupling at the pole of Eq. (4.39) is

$$g = g_{K\pi} = (7.19 + i\ 0.67)\ . \tag{4.40}$$

Then, we get

$$\begin{aligned} 1 - Z &= (0.122 + i\ 0.193)\ , \\ |1 - Z| &= 0.229\ , \end{aligned} \tag{4.41}$$

which indicates that the amount of $K\pi$ in the wave function is small. One can conclude that the K^* is largely a genuine state other than a $K\pi$ composite molecule.

4.2.3 Phenomenological analysis

As done in Ref. [206], we also use a pure phenomenological analysis to confirm our results only with experimental data. The case for a p-wave resonance is different from the one for s-wave, where the coupling g can be obtained from experiments and $\frac{dG}{dE}$ (or $\frac{dG}{ds}$) is a convergent magnitude, even when $q_{max} \to \infty$.

The phenomenological scattering amplitude in a relativistic form for p-wave can be written as

$$\tilde{t} = \frac{\tilde{g}_{ex}^2}{s - m_{K^*}^2 + i\ m_{K^*}\Gamma_{on}\left(\frac{q_{cm}}{q_{cm}^{on}}\right)^3}\ , \tag{4.42}$$

where q_{cm} is the three-momentum of the $K\pi$ system in the center of mass reference frame, which is given by Eq. (2.58) for real $\sqrt{s}$, and q_{cm}^{on} is the same quantity for $\sqrt{s} = m_{K^*}$,

$$q_{cm}^{on} = q_{cm}(\sqrt{s} = m_{K^*}) \ , \tag{4.43}$$

and the coupling is related to the width through the equation

$$\tilde{g}_{ex}^2 = \frac{8\pi m_{K^*}^2 \Gamma_{on}}{(q_{cm}^{on})^3} \ . \tag{4.44}$$

Besides, the values of the mass m_{K^*} and width Γ_{on} of the K^* for a Breit Wigner distribution are given by experiment, $m_{K^*} = 895.5$ MeV and $\Gamma_{on} = 46.2$ MeV in the PDG [9].

As done in the former subsection, to get the pole and the coupling, we also need to extrapolate the amplitude to the complex plane and search for the pole s_0 in the second Riemann sheet. We obtain $\tilde{t}$ in the second Riemann sheet from Eq. (4.42) by taking s complex, $s = a + i\ b$, and $p \to -p$ in the width term. Thus, we can look for the pole in the second Riemann sheet and then use Eq. (4.37) to evaluate the coupling. We obtain

$$\begin{aligned} \sqrt{s_0} &= (892.0 + i\ 22.4)\ \text{MeV} \ , \\ \tilde{g}_{K\pi} &= (6.08 + i\ 0.50) \ , \end{aligned} \tag{4.45}$$

(and also the complex conjugate ones) which are consistent with those obtained before and closer to the pole positions of $(892.03 - i\ 23.3)$ MeV and $(892.0 - i\ 23.1)$ MeV, found in Refs. [536] and [537], respectively.

For the p-wave, the G function in Eq. (4.31) or Eq. (1.56) is not convergent and $\frac{dG}{ds}$ is also logarithmically divergent [206, 538]. Therefore, when doing the $1 - Z$ calculation, one does not know which value of the cutoff q_{max} should be used to regularize the G function. Hence, as done in [206], we can use natural values of the cutoff and test if the results are stable or not for a certain range of q_{max}.

In Table 4.2, we show the results of our study of the strength $|1 - Z|$ obtained for the K^* by changing the cutoff q_{max} around a certain reasonable range. As we can see, the results are stable and similar to those obtained in the former subsection. Particularly, for $|1 - Z|$ we get the same conclusion as before, which means that, since $|1 - Z|$ is a small number, the K^* is not a $K\pi$ composite state.

Table 4.2: Values of $1 - Z$ for different cutoffs q_{max}.

q_{max} [MeV]	$1 - Z$	$\|1 - Z\|$
724.7	$0.082 - i0.137$	0.160
700.0	$0.077 - i0.138$	0.158
800.0	$0.095 - i0.134$	0.165
900.0	$0.111 - i0.131$	0.172
1000.0	$0.124 - i0.128$	0.179
1100.0	$0.136 - i0.126$	0.186
1200.0	$0.147 - i0.124$	0.192

4.2.4 Conclusions

In the present work, we show the results of our investigation of the K^* structure. We use a method for studying the particle structure by the generalized Weinberg's compositeness condition, which extends the results of Weinberg for s-wave to other partial waves and bound states or resonances. Using this formalism, we first calculate the $K\pi$ coupling with the chiral unitary theory, by means of the tree level chiral potential, and then we make a fit to the experimental data of the phase shifts to determine the free parameters in this model. With the best fit to the experimental data we get the pole of the K^* resonance in the second Riemann Sheet, $(891.0 + i\ 31.3)$ MeV, which is consistent with the PDG data. With the coupling of $K\pi$, we find that the probability of the $K\pi$ component, $|1 - Z|$, is a small value, only 0.229 (about 1/5), which means that the K^* is not a $K\pi$ molecule but something else. Next, we also use a phenomenological method to confirm the former results. The pole in the second Riemann sheet is $(892.0 + i\ 22.4)$ MeV and $|1 - Z|$ has values around $0.158 \sim 0.192$, which are in agreement with the results of the theoretical model analysis within uncertainties, thus, leading to the same conclusion.

4.3 Three methods to detect the $X(3700)$

The use of the ChUA in the meson-meson interaction gives rise to the $f_0(500)$(or σ), $f_0(980)$, $a_0(980)$ scalar mesons [16, 264, 349, 357, 539–541] from the unitarization in coupled channels of the meson-meson interaction provided by the chiral Lagrangians [376,377]. The $f_0(500)$ appears basically as a $\pi\pi$ resonance and the $f_0(980)$, $a_0(980)$ as basically $K\bar{K}$ quasibound states that decay into $\pi\pi$ and $\pi\eta$ respectively. The similarity between $\bar{K}$ and D (K and $\bar{D}$) suggest that there could be also a $D\bar{D}$ quasibound state around 3700 MeV, that we shall call $X(3700)$, decaying into pairs of light pseudoscalars, $\pi\pi$, $\eta\eta$, $\eta\eta'$, $K\bar{K}$. In an extrapolation of the ChUA to the SU(4) sector [261] it was found that, indeed, a quasibound scalar $D\bar{D}$ state with $I = 0$ emerged with a small width, since transition matrix elements from $D\bar{D}$ to the light sector were strongly suppressed. This finding has been corroborated recently in Refs. [246,247] using models that incorporate heavy quark symmetry.

Later on it was found in Ref. [262] that the bump in the $D\bar{D}$ spectrum close to the $D\bar{D}$ threshold observed at Belle in the $e^+e^- \to J/\psi D\bar{D}$ reaction [542] was better interpreted in terms of the bound state below threshold, with $M_X \simeq 3723$ MeV, than with a new resonance as suggested in Ref. [542]. So far, this is the strongest experimental support for this state, in spite of the fact that some other reaction has been suggested to observe it. Indeed, in Ref. [169] a suggestion was made to detect the state in the radiative decay of the $\psi(3770)$. The idea is based in the fact that the $\psi(3770)$ couples strongly to $D\bar{D}$ and with the emission of a photon one can bring the $D\bar{D}$ state below the threshold into the region of the resonance. A width of $\Gamma_{\psi\to\gamma X} = (1.05 \pm 0.41)$ KeV was found which would be in the measurable range. However, a problem of this suggestion is that this peak would have to be seen over a background of $\psi \to \gamma +$ anything, which is estimated to have a branding ratio of the order of 10^{-2}, judging by the rate of some measured channels reported in the PDG [9], while $\Gamma_{\psi\to\gamma X}/\Gamma_\psi \simeq 4 \times 10^{-5}$. The signal would be of the order of 1% of smaller on top of a background and the prospects to see it there would be dim. There is another problem since the peak for the decay appears at small photon momentum where there would be radiative decays displaying Bremsstrahlung of the photons, with accumulated strength at low photon energies, precisely where the peak of the X would appear. The selection of a particular decay channel where

the background would be much reduced would be then much welcome and this is what we do here, suggesting the $\eta\eta'$ channel for reasons that would be clear later on.

On the other hand, with the advent of BESIII the production of the $\psi(4040)$ state is being undertaken and in this case the photon has more energy in the radiative decay, removing the peak from the Bremsstrahlung region, with obvious advantages.

We have also investigated another method, taking the same reaction as performed in Ref. [542] but looking for $e^+e^- \to J/\psi\eta\eta'$. We predict a peak for $\eta\eta'$ production and compare the strength of the peak with the cross sections measured in Ref. [542] for the $J/\psi D\bar{D}$ production.

With all these studies we find out three methods which would allow to see the neat peak for that state and the widths or cross sections are found within present measuring range, such that devoted experiments would be most opportune.

4.3.1 Decay model with the ChUA

In Ref. [169] the radiative decay of $\psi(3770)$ into $\gamma X(3700)$ was studied. The work of Ref. [261] was redone including the channels D^+D^-, $D^0\bar{D}^0$, $D_s^+D_s^-$, $\pi^+\pi^-$, K^+K^-, $\pi^0\pi^0$, $K^0\bar{K}^0$, $\eta\eta$, $\eta\eta'$, $\eta'\eta'$, $\eta_c\eta$, $\eta_c\eta'$. Using a potential derived from an SU(4) extension of the SU(3) chiral Lagrangians [376, 377] with an explicit SU(4) breaking for terms exchanging charm, the BS equations of Eq. (1.44) were solved to obtain the scattering matrix. With this formalism a pole was obtained for the T matrix around 3722 MeV below the $D\bar{D}$ threshold. The accuracy as well as limitations in the case of SU(4) symmetry in the basic vertices is discussed in section II D of Ref. [168]. Note that the inclusion of the η' involves also an assumption about U(3) symmetry. One should also in principle mix states of D and D^* in the coupled channels, but the transition of D and D^* in our approach is given by π exchange and one can easily prove the π exchange term is subleading in the m_Q counting (potential in Quantum Mechanics going as $\mathcal{O}(m_Q^{-1})$), with m_Q the mass of the heavy quark, while the leading diagonal terms are of order $\mathcal{O}(1)$ in this counting (see Ref. [412]), as discussed in last chapter. And more discussion can be found in our paper [543].

What is of relevance for the present work is the coupling of this state to the different channels. In Table 4.3 we show the results obtained in

Ref. [169]: As we can see, the largest couplings are for $D\bar{D}$ and $D_s\bar{D}_s$.

Table 4.3: Coupling of the pole at $(3722 - i18)$ MeV to the channels.

channel	Re(g_X) [MeV]	Im(g_X) [MeV]	$\|g_X\|$ [MeV]
$\pi^+\pi^-$	9	83	84
K^+K^-	5	22	22
D^+D^-	5962	1695	6198
$\pi^0\pi^0$	6	83	84
$K^0\bar{K}^0$	5	22	22
$\eta\eta$	1023	242	1051
$\eta\eta'$	1680	368	1720
$\eta'\eta'$	922	-417	1012
$D^0\bar{D}^0$	5962	1695	6198
$D_s^+D_s^-$	5901	-869	5965
$\eta_c\eta$	518	659	838
$\eta_c\eta'$	405	9	405

However, the separation in energy of the $D_s\bar{D}_s$ component makes the $D\bar{D}$ component to stand as the more relevant meson-meson component of this state, which qualifies approximately as a $D\bar{D}$ quasibound state. The width obtained from the decay of this state in all the allowed channels is 36 MeV. Note that the transition to light, open, channels is suppressed and this determines the large lifetime of the state. We observe from the Table that the largest coupling to the light channels is to $\eta\eta'$ which also contains two different particles, hence, this will be the channel that we will adopt to have the $X(3700)$ state detected.

In Ref. [169] the decay of $\psi(3770)$ to γX was evaluated recalling that the $\psi(3770)$ decays basically to $D\bar{D}$. This allows one to obtain the coupling of $\psi(3770)$ to D^+D^- and then, from the triangular diagram of Fig. 4.13, the $\psi(3770) \to \gamma X$ transition amplitude was evaluated. We do not repeat here the steps of the calculations in Ref. [169] and quote the final results.

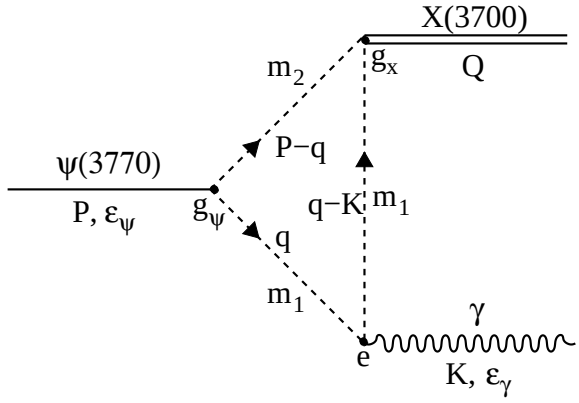

Figure 4.13: Diagram for $\psi(3770) \to \gamma X$ that contains the d term.

The transition amplitude for the diagram of Fig. 4.13 is given by

$$i\mathcal{M} = i\epsilon_{\psi}^{\mu}(P)\epsilon_{\gamma}^{\nu}(K)\mathcal{T}_{\mu\nu}, \tag{4.46}$$

and since the problem has two independent four momenta, by Lorentz invariance one may write

$$\mathcal{T}_{\mu\nu} = ag_{\mu\nu} + bP_{\mu}P_{\nu} + cP_{\mu}K_{\nu} + dP_{\nu}K_{\mu} + eK_{\mu}K_{\nu}. \tag{4.47}$$

Due to gauge invariance only the structures $ag_{\mu\nu}$ and $dP_{\nu}K_{\mu}$ (with P, K the ψ and γ momentum), which leads to a convergent integral, survive, and, in addition, one has $a = -d\,K \cdot P$. The d coefficient is evaluated using the Feynman parameterization of the loop function corresponding to the diagram of Fig. 4.13 and one finds

$$d = -\sum_{j} \frac{g_{\psi}g_{X,j}e}{2\pi^2} \int_0^1 dx \int_0^x dy \frac{y(1-x)}{s + i\epsilon}, \tag{4.48}$$

with s given by

$$s = (1-x)(xM_{\psi}^2 - m_2^2 - 2yP \cdot K) - xm_1^2, \tag{4.49}$$

with e the electron charge ($e^2/4\pi = \alpha = 1/137$), g_{ψ} the coupling of $\psi(3770)$ to D^+D^-, $g_{\psi} = 11.7$, and j summing over the two relevant channels D^+D^-

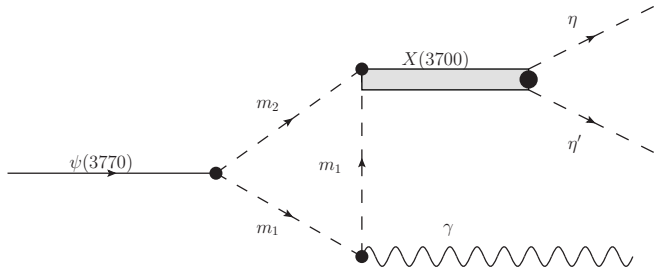

Figure 4.14: Diagram for $\psi(3770) \to \gamma X \to \gamma\eta\eta'$.

and $D_s^+ D_s^-$. The partial decay width for $\psi(3770) \to \gamma X$ is given by

$$\Gamma_{\psi\to\gamma X} = \frac{|\vec{K}|}{12\pi M_\psi^2} \, (P \cdot K)^2 \, |d|^2. \tag{4.50}$$

The result obtained in [169], which we reproduce here, is

$$\Gamma_{\psi\to\gamma X} = 0.65 \text{ KeV}. \tag{4.51}$$

As mentioned in the Introduction, determining the peak corresponding to this process over a background of γX events is problematic and thus we choose the $\eta\eta'$ to detect the X peak. For this the diagram of Fig. 4.13 has to be changed to the one of Fig. 4.14. Technically all we have to do is substitute d by d' where

$$d' = d \frac{1}{M_{inv}^2 - M_X^2 + iM_X\Gamma_X} g_{X,\eta\eta'}, \tag{4.52}$$

with d defined in Eq. (4.48),

$$M_{inv}^2 = (p_\eta + p_{\eta'})^2, \tag{4.53}$$

and $g_{X,\eta\eta'}$ the coupling of the X to the $\eta\eta'$ channel given in Table 4.3. Since the width Γ_X is small (~ 36 MeV) and there is relatively large phase space for $\eta\eta'$ decay, we can simply take Γ_X constant in Eq. (4.52).

The relevant magnitude now is

$$\frac{d\Gamma}{dM_{inv}} = \frac{1}{4(2\pi)^3} \frac{1}{M_\psi^2} \, p_\gamma \, \tilde{p}_\eta \, \overline{\sum} \sum |T|^2, \tag{4.54}$$

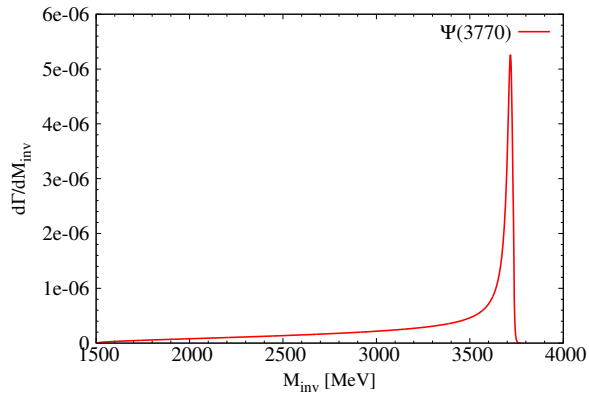

Figure 4.15: The mass distribution of the $\eta\eta'$ in the decay of $\psi(3770)$ to $\gamma X(3700) \to \gamma\eta\eta'$.

which provides the invariant mass distribution, where

$$p_\gamma = \frac{\lambda^{1/2}(M_\psi^2, 0, M_{inv}^2)}{2M_\psi}, \tag{4.55}$$

$$\tilde{p}_\eta = \frac{\lambda^{1/2}(M_{inv}^2, m_\eta^2, m_{\eta'}^2)}{2M_{inv}}, \tag{4.56}$$

$$\overline{\sum}\sum |T|^2 = \frac{2}{3}|d'|^2(K\cdot P)^2, \tag{4.57}$$

with p_γ, $\tilde{p}_\eta$ the γ momentum in the $\psi(3770)$ rest frame and the η momentum in the $\eta\eta'$ rest frame respectively.

In Fig. 4.15 we show this distribution, and we see a clear peak at $M_{inv} \simeq 3722$ MeV, which has a narrow width. The peak is still around the upper threshold for the invariant mass. However, the fact that we have chosen a neutral channel to identify the X state prevents Bremsstrahlung to occur and the identification of a peak there would be a clear signal of a state. The integrated width around the peak ($3600 < M_{inv} < 3770$ MeV) gives

$$\Gamma = \int_{3600}^{3770} \frac{d\Gamma}{dM_{inv}} dM_{inv} = 0.293 \text{ KeV}, \tag{4.58}$$

which is smaller than the total width of Eq. (4.51) which integrates over the whole range of M_{inv}.

The largest contribution comes from the D^+D^- channel which by itself provides 73% of the rate. The coherent sum with the $D_s^+D_s^-$ contribution makes up for the rest of the rate.

The width of Eq. (4.58) represents a branching ratio of 10^{-5}. In this sense one should note that CLEO has set thresholds of the order of magnitude of 10^{-4} and at BESIII one can get a production $\psi(3770)$ of about a factor one hundred times bigger, which would make this measurement feasible in that Lab.

4.3.2 Radiative decay of the $\psi(4040)$

The $\psi(4040)$ shares the same quantum numbers as the $\psi(3770)$, however the largest branching ratio is not to $D\bar{D}$ but to $D^*\bar{D}+cc$. From the data in the PDG we find that

$$\frac{\Gamma(D\bar{D})}{\Gamma(D^*\bar{D}+cc)} = 0.24 \pm 0.05 \pm 0.12, \tag{4.59}$$

$$\frac{\Gamma(D^*\bar{D}^*)}{\Gamma(D^*\bar{D}+cc)} = 0.18 \pm 0.14 \pm 0.03, \tag{4.60}$$

Assuming that the $D^*\bar{D}+cc$, $D\bar{D}$ and $D^*\bar{D}^*$ provide most of the contribution, this allows us to get the coupling

$$g_{\psi(4040),D^+D^-} = 2.15, \tag{4.61}$$

and then we can recalculate the invariant mass distribution and width for $\psi(4040) \to \gamma X(3700)$. In Fig. 4.16 we show the results for the invariant mass distribution. We find now a neat peak around the mass of the X. The novelty here is that the peak is far away from all thresholds which could eventually be seen in the spectrum of inclusive $d\Gamma/dE_\gamma$ without the risk to confuse the peak with Bremsstrahlung like in the case of the $\psi(3770) \to \gamma X$. In any case, as advocated here, the direct measurement of the $\eta\eta'$ channel should drastically reduce the background and allow a clear peak to be identified. The integrated width around this peak ($3600 < M_{inv} < 3800$ MeV) gives

$$\Gamma = \int_{3600}^{3800} \frac{d\Gamma}{dM_{inv}} dM_{inv} = 0.496 \text{ KeV}, \tag{4.62}$$

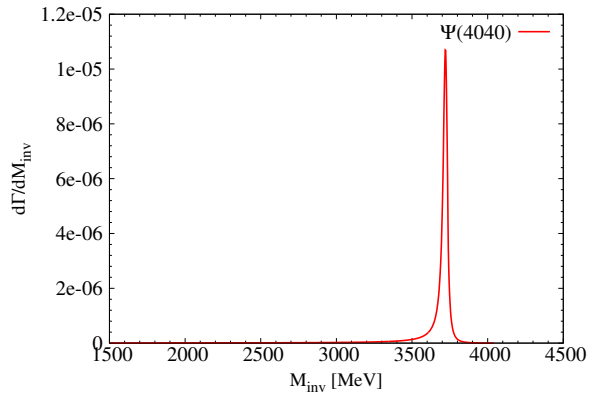

Figure 4.16: The mass distribution of $\eta\eta'$ in the $\psi(4040)$ decay to $\gamma X(3700) \to \gamma\eta\eta'$.

which is about double than in the case of the $\psi(3770)$. In this case, the larger phase space for decay has overcome the reduction due to the reduced coupling of Eq. (4.61).

We should note that the largest contribution comes from the D^+D^- channel, this channel alone providing about half the rate of Eq. (4.62) while $D_s^+D_s^-$ alone only given 19% of this rate.

The width of Eq. (4.62) is a bit bigger than the one obtained for the $\psi(3770)$, yet, the rate of production at BESIII is smaller. Present plans are to produce 2.8 million $\psi(4040)$ events and no plans are made for the future yet [2]. With this statistics and the width of Eq. (4.62), which corresponds to a branching ratio of 6.2×10^{-6}, one could get about 17 events of this radiative decay. It is clear that more statistics would be needed to see a clear peak.

It should be clear that we have only evaluated the cross section for the production of the $\eta\eta'$ in the peak of the $X(3700)$ resonance. There will be for sure background for the reactions studied, but we should note that in all of them there is an OZI suppression since we either destroy $c\bar{c}$ or create $c\bar{c}$. Hence, cross sections from other non resonant mechanisms can be of the same order of magnitude as from the resonance mechanism described, only

[2]We would like to thank Cheng-Ping Shen for providing us the information.

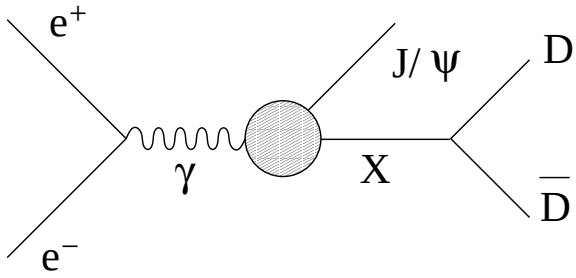

Figure 4.17: Feynman diagram of the reaction $e^+e^- \to J/\psi X \to J/\psi D\bar{D}$.

the strength will be distributed over a large phase space where the peak due to the $X(3700)$ excitation should be clearly visible due to its small width.

4.3.3 The $e^+e^- \to J/\psi X \to J/\psi\eta\eta'$ reaction

In Ref. [262] the $e^+e^- \to J/\psi X \to J/\psi D\bar{D}$ reaction was studied and it was concluded that the data on the $D\bar{D}$ invariant mass distribution was better described in terms of the $X(3700)$ resonance than in terms of a new state suggested in Ref. [542]. The mechanism for this reaction is given in Fig. 4.17. The differental cross section is given by [262]

$$\frac{d\sigma}{dM_{inv}(D\bar{D})} = \frac{1}{(2\pi)^3}\frac{m_e^2}{s\sqrt{s}}|\vec{k}|\ |\vec{p}|\ |T|^2, \tag{4.63}$$

with

$$|\vec{k}| = \frac{\lambda^{1/2}(M_{inv}^2(D\bar{D}), m_D^2, m_D^2)}{2M_{inv}(D\bar{D})}, \tag{4.64}$$

$$|\vec{p}| = \frac{\lambda^{1/2}(s, M_{J/\psi}^2, M_{inv}^2(D\bar{D}))}{2\sqrt{s}}, \tag{4.65}$$

where T is given by

$$T = C\frac{1}{M_{inv}^2(D\bar{D}) - M_X^2 + i\Gamma_X M_X}. \tag{4.66}$$

As in Ref. [262] we restrain from giving absolute values but we can give relative values with respect to $D\bar{D}$ production simply multiplying T of Eq.

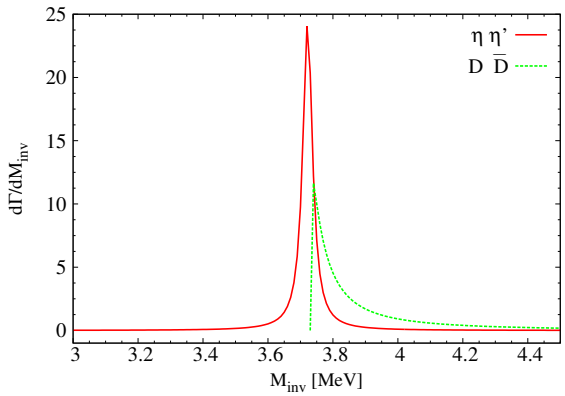

Figure 4.18: The mass distribution of the final states $J/\psi\eta\eta'$ compared to $J/\psi D\bar{D}$.

(4.66) by $g_{X,\eta\eta'}/\sqrt{2}g_{X,D^+D^-}$, where the factor $\sqrt{2}$ will take into account in $|T|^2$ that we compare $\eta\eta'$ production versus $D^+D^- + D^0\bar{D}^0$ production. In Fig. 4.18 we show the results for $\eta\eta'$ production with the same scale as for $D\bar{D}$ production. We can see that the strength of the peak is bigger for $\eta\eta'$ production than for $D\bar{D}$, in spite of having a smaller coupling to $X(3700)$. The reason is that the $\eta\eta'$ production is not suppressed by the threshold factors that inhibit $D\bar{D}$ production. The peak seen in the $\eta\eta'$ mass spectrum is neat and the strength larger than for $D\bar{D}$ production. Since $D\bar{D}$ has been observed in Ref. [542], this guarantees that the $\eta\eta'$ peak is within present measurable range.

4.3.4 Conclusions

In the present work, we have investigated some reactions by means of which one could observe the predicted scalar meson formed as a quasibound state of $D\bar{D}$. This state appears in analogy to the $f_0(500)$ and $f_0(980)$ states which are described within the ChUA as a $\pi\pi$ resonance and a quasibound $K\bar{K}$ state respectively. Some suggestion had been made before to observe this state in the $\psi(3770) \to \gamma X(3700)$ decay by looking at the γ energy distribution. Yet, this has the inconvenience of having to observe a small peak in a large background. In order to suppress the background we have

chosen one of the main decay channels of the $X(3700)$ state, the $\eta\eta'$ channel, and suggest to look at the $\eta\eta'$ invariant mass distribution in the reaction $\psi(3770) \to \gamma X(3700) \to \gamma\eta\eta'$. Since BESIII already can produce the $\psi(4040)$, we also suggest to look at the $\psi(4040) \to \gamma X(3700) \to \gamma\eta\eta'$ decay channel. A third reaction was motivated by the only indirect experimental "evidence" of this state. Indeed, in the BELLE reaction $e^+e^- \to J/\psi D\bar{D}$ [542], a peak was observed in the $D\bar{D}$ invariant mass distribution close to the $D\bar{D}$ threshold, which was interpreted in [262] as a signal of a $D\bar{D}$ resonance below the $D\bar{D}$ threshold. In the present work we have suggested to look at the reaction $e^+e^- \to J/\psi\eta\eta'$, allowing the $X(3700)$ to be produced and decay into $\eta\eta'$.

We find clear peaks in all the invariant mass distributions of $\eta\eta'$. In the two radiative decays, the rates are within present measurable range at BESIII, although in the case of $\psi(4040)$ radiative decay the statistics with presently planned $\psi(4040)$ production would be very low. In the case of the e^+e^- reaction we do not evaluate absolute cross sections and we find more instructive to compare the cross section of the $e^+e^- \to J/\psi\eta\eta'$ reaction with the one of $e^+e^- \to J/\psi D\bar{D}$ already measured. We observe that the cross section for the former reaction is bigger than for the latter one and produces a clear peak that does not have the ambiguity of a threshold enhancement as in the $e^+e^- \to J/\psi D\bar{D}$ reaction. This is the best guarantee that the reaction is within measurable range.

The experimental search for this state is timely and its observation would clarify issues concerning the interaction of hadrons in the charm sector, which is not so well known as the non charmed one, and which would be much welcome.

Chapter 5

Conclusion

In our work, we have made some investigations on the hadronic spectrum, mostly in the heavy quark sector, focusing mainly on the baryonic states with charm and beauty. Besides, we also did some works on the mesonic states both in the light and the heavy quark sectors. First, we explore the recently developed three-body interaction formalism, the fix center approximation to the Faddeev equations, to study some strong interaction of the three-body hadronic systems. Second, we investigate the two-body interactions in the charm and beauty sector with the coupled channel approach, by taking into account the constraints of heavy quark spin symmetry. Third, we study the decay models and properties of some resonances, theoretically predicted in the strong interactions of low energy QCD. Now, we make a conclusion about the three aspects of our research.

I). The Faddeev equations under the fixed center approximation are accurate when dealing with bound states and successfully explain the structure properties of some states dynamically reproduced in the three-body interactions. And it is technically simple, and allows one to deal with three-body hadron interactions effectively without introducing any free parameters, based on the two-body interaction with the chiral unitarized approach. Thus, with this effective tool, we get some results in our studies.

- The results of $\bar{K}DN$, NDK and $ND\bar{D}$ systems

  In the three body systems that have one D meson or $D\bar{D}$, together with one baryon, $\bar{K}DN$, NDK and $ND\bar{D}$, we find bound or quasi-

bound states, relatively narrow, with energies 3150 MeV, 3050 MeV and 4400 MeV, respectively. All these states have $J^P = 1/2^+$ and isospin $I = 1/2$ and differ by their charm or strangeness content, $S = -1, C = 1$, $S = 1, C = 1$, $S = 0, C = 0$, respectively. The first state could perhaps be associated to the $\Xi(3123)$, which has unknown J^P, but the width obtained is a bit too large. The second state is a new state of exotic nature. The third state is like a new regular N^* state, but it contains hidden charm.

- A quasi-bound state in the DNN system

  We have used two methods for the study of the DNN system. The first one used the fixed center approximation for the Faddeev equations and the second one employs the variational approach with hadronic potentials in coordinate space. We found a quasi-bound state in the DNN system with $I = 1/2$, which is bound and rather stable, with a width of about 20-40 MeV. We obtained a clear signal of the quasi-bound state for the total spin $J = 0$ channel around 3500 MeV. The $J = 1$ channel is more subtle, and the precise DN amplitude in the $I = 1$ channel is important for a robust prediction in this channel. The mesonic decay width of the quasi-bound state turned out to be less than 40 MeV.

- New states in the D^*-multi-ρ systems

  In the study of the many-body interaction between a D^* and multi-ρ, we find several clear resonant structures above 2800 MeV in the multi-body scattering amplitudes. They would correspond to new charmed resonances, D_3^*, D_4^*, D_5^* and D_6^*, not listed in the PDG, which are our theoretical predictions, and would be analogous to the $\rho_3(1690)$, $f_4(2050)$, $\rho_5(2350)$, $f_6(2510)$ and $K_3^*(1780)$, $K_4^*(2045)$, $K_5^*(2380)$ described before as multi-ρ and K^*-multi-ρ states respectively.

- The study of the $\eta K\bar{K}$ and $\eta' K\bar{K}$ systems

  For the three-body systems of $\eta K\bar{K}$ and $\eta' K\bar{K}$, we find a clear and stable resonance structure around 1490 MeV in the squared $\eta K\bar{K}$ scattering amplitude, which is not sensitive to the renormalization parameters and is associated to the $\eta(1475)$ in the PDG. Conversely,

we get only an enhancement effect of the threshold in the $\eta' K\bar{K}$ amplitude that indicates the difficulty to bind the $\eta' K\bar{K}$ system as a consequence of a weaker $\eta' K$ interaction than the ηK one.

- The $\rho K\bar{K}$ interaction

  Since the $K\bar{K}$ system with isospin $I = 0$, is found to be a dominant component of the $f_0(980)$ resonance, as many theoretical results claim, we study the $\rho K\bar{K}$ system applying the fixed center approximation to the Faddeev equations. We find a clear peak in the three-body amplitude around 1732 MeV and a width of about 161 MeV, by taking into account the effect of the width of the ρ and $f_0(980)$. We associate this peak to the $\rho(1700)$ which has a mass of 1720 ± 20 MeV and a width of 250 ± 100 MeV.

II). In the low energy QCD interaction, the chiral unitarized approach is successful to understand the interaction information, such as resonance structure, cross section, phase shifts, scattering lengths, and so on. But, in the heavy charm and beauty sector, the heavy quark spin symmetry should also be taken into account. Therefore, with the chiral unitarized approach, combining the coupled channel effect and the heavy quark spin symmetry constraints, we have made some predictions on the heavy baryonic spectrum.

- Hidden charm baryons dynamically generated

  With the constraints of heavy quark spin symmetry and the dynamics of the local hidden gauge for the interaction potential, using a coupled channel unitary approach to evaluate the scattering amplitude for the meson-baryon interaction with hidden charm (taking the coupled channels: $\eta_c N$, $\eta_c \Delta$, $J/\psi N$, $J/\psi \Delta$, $\bar{D}\Lambda_c$, $\bar{D}\Sigma_c$, $\bar{D}^*\Lambda_c$, $\bar{D}^*\Sigma_c$, $\bar{D}^*\Sigma_c^*$), we look for states dynamically generated and find four basic bound states, not list in the PDG too, corresponding to $\bar{D}\Sigma_c$, $\bar{D}\Sigma_c^*$, $\bar{D}^*\Sigma_c$ and $\bar{D}^*\Sigma_c^*$, decaying mostly into $\eta_c N$ and $J/\psi N$. All the states appear in isospin $I = 1/2$ and we find no bound states or resonances in $I = 3/2$. The $\bar{D}\Sigma_c$ state appears in $J = 1/2$, the $\bar{D}\Sigma_c^*$ in $J = 3/2$, the $\bar{D}^*\Sigma_c$ appears nearly degenerate in $J = 1/2,\ 3/2$ and the $\bar{D}^*\Sigma_c^*$ appears nearly degenerate in $J = 1/2,\ 3/2,\ 5/2$, with the peculiarity that in $J = 5/2$ the state has zero width in the space of states chosen. All the states are bound with about 50 MeV with respect to the thresholds

of the corresponding channels, and the width, except for the $J = 5/2$ state, is also of the same order of magnitude.

- New hidden beauty baryon states

  Following the same line and formalism of the hidden charm sector in the former work, we investigate the meson-baryon interaction with hidden beauty and obtain several new states of N^* around 11 GeV. Under the constraints of heavy quark spin symmetry, we consider the coupled channels: $\eta_b N$, ΥN, $B\Lambda_b$, $B\Sigma_b$, $B^*\Lambda_b$, $B^*\Sigma_b$, $B^*\Sigma_b^*$, and find four basic bound states of isospin $I = 1/2$, which correspond to $B\Sigma_b$, $B\Sigma_b^*$, $B^*\Sigma_b$ and $B^*\Sigma_b^*$, decaying mostly into $\eta_b N$ and ΥN. The $B\Sigma_b$ state appears in $J = 1/2$, the $B\Sigma_b^*$ in $J = 3/2$, the $B^*\Sigma_b$ appears nearly degenerate in $J = 1/2,\ 3/2$ and the $B^*\Sigma_b^*$ appears nearly degenerate in $J = 1/2,\ 3/2,\ 5/2$. All these states that we found, have a binding energy about $50 - 130$ MeV with respect to the thresholds of the corresponding channel, and a width from $2 - 110$ MeV, except for the one in $J = 5/2$ with zero width since there is no coupled channel to decay. Finally, we find no bound states or resonances in $I = 3/2$.

- Hidden beauty mesonic molecules

  Following the same line, we investigate the meson-meson interaction in the hidden beauty sector: $B_{(s)}^{(*)}\bar{B}_{(s)}^{(*)}$, and obtain several new states. Both $I = 0$ and $I = 1$ states are analyzed and it is shown that in the $I = 1$ sector, the interactions are too weak to create any bound states within our framework. In total, we predict with confidence the existence of 6 bound states, with binding energies 34 MeV (178 MeV) for $q_{max} = 415$ MeV (830 MeV), and weakly bound 6 more possible states, with binding energies 2 MeV (18 MeV). The existence of these weakly bound states depends on the influence of the coupled channel effects.

- Baryon states in the open beauty sector

  With one more step, we examine the interaction of $\bar{B}N$, $\bar{B}\Delta$, $\bar{B}^*N$ and $\bar{B}^*\Delta$ states, together with their coupled channels: $\pi\Sigma_b$, $\pi\Lambda_b$, $\eta\Sigma_b$ (for the $\bar{B}N$); $\pi\Sigma_b^*$, $\eta\Sigma_b^*$ (for the $\bar{B}\Delta$); $\rho\Sigma_b$, $\omega\Lambda_b$, $\phi\Lambda_b$, $\rho\Sigma_b^*$, $\omega\Sigma_b^*$, $\phi\Sigma_b^*$ (for the $\bar{B}^*N$); and $\rho\Sigma_b^*$, $\omega\Sigma_b^*$, $\phi\Sigma_b^*$ (for the $\bar{B}^*\Delta$). Using a mapping from

the light meson sector and a assumption that the heavy quarks act as spectators at the quark level, with the scattering potential coming from light vector exchanges in the extended local hidden gauge approach, we look for states dynamically generated from the interaction and find two states with nearly zero width, which we associate to the $\Lambda_b(5912)$ and $\Lambda_b(5920)$ states, coupled mostly to $\bar{B}^* N$. The difference of masses between these two degenerate states, with $J = 1/2,\ 3/2$ respectively, is due to pion exchange connecting these states to intermediate $\bar{B} N$ states. In addition to these two Λ_b states, we find three more states with $I = 0$, one of them nearly degenerate in two states of $J = 1/2,\ 3/2$. Furthermore we also find eight more states in $I = 1$, two of them degenerate in $J = 1/2, 3/2$, and the other two degenerate in $J = 1/2,\ 3/2,\ 5/2$.

- The open charm baryon states

  Analogously, following the last work, by changing the $\bar{B}^{(*)}$ meson to a $D^{(*)}$ meson and the b-quark to a c-quark for the baryon, we also investigate the interaction of DN, $D\Delta$, D^*N and $D^*\Delta$ states, together with their coupled channels: $\pi\Sigma_c$, $\pi\Lambda_c$, $\eta\Sigma_c$ (for the DN); $\pi\Sigma_c^*$, $\eta\Sigma_c^*$ (for the $D\Delta$); $\rho\Sigma_c$, $\omega\Lambda_c$, $\phi\Lambda_c$, $\rho\Sigma_c^*$, $\omega\Sigma_c^*$, $\phi\Sigma_c^*$ (for the D^*N); and $\rho\Sigma_c^*$, $\omega\Sigma_c^*$, $\phi\Sigma_c^*$ (for the $D^*\Delta$). The pion exchange and the Weinberg Tomozawa interactions are generalized and with this dynamics we look for states generated from the interaction, finding two states with nearly zero width which are associated to the $\Lambda_c(2595)$ and $\Lambda_c(2625)$. The lower state couples mostly to DN, and the second to D^*N. Additionally, we find four more states with $I = 0$, one of them nearly degenerate in two states of $J = 1/2,\ 3/2$; in the $I = 1$ sector, we find seven states, two of them degenerate in $J = 1/2, 3/2$, and the other two degenerate in $J = 1/2,\ 3/2,\ 5/2$.

III). Furthermore, to understand and explain the properties of the states found in experiment or theory, we also investigate the particle decay modes and the decay properties of some particles.

- J/ψ reaction in the nuclear medium

  Recent studies of the interaction of vector mesons with nuclei make possible and opportune the study of the interaction of the J/ψ with

nuclei and the investigation of the origin of the J/ψ suppression in its propagation thorough a nuclear medium. We observe that the transition of $J/\psi N$ to VN with V being a light vector, ρ, ω, ϕ, together with the inelastic channels, $J/\psi N \to \bar{D}\Lambda_c$ and $J/\psi N \to \bar{D}\Sigma_c$ leads to a particular shape of the inelastic cross section. Analogously, we consider the mechanisms where the exchanged D collides with a nucleon and gives $\pi\Lambda_c$ or $\pi\Sigma_c$. The cross section has a peak around $\sqrt{s} = 4415$ MeV, where the $J/\psi N$ couples to a resonance predicted recently. However, when the Fermi motion of the nucleus is considered the cross section has to be substituted by its average over the nucleon momenta and the peak is washed away. We study the transparency ratio for electron induced J/ψ production in nuclei at about 10 GeV and find that 30 - 35 % of the J/ψ produced in heavy nuclei are absorbed inside the nucleus. This ratio is in line with depletions of J/ψ through matter observed in other reactions.

- $K\pi$ component in the K^* wave function

  Using the Weinberg's compositeness condition to partial waves higher than s-wave in order to determine the weight of a $K\pi$ component in the K^* wave function, we first make a fit to the $K\pi$ phase shifts in p-wave, from where the coupling of K^* to $K\pi$ and the $K\pi$ loop function are determined. Then, with these ingredients, we determine the weight of the $K\pi$ component, $|1 - Z| \sim 0.2$, a small value, and conclude that the K^* is a genuine state, different to a $K\pi$ component, in a proportion of about 80 %.

- How to detect the predicted $D\bar{D}$ scalar meson $X(3700)$

  In the charm sector, a quasibound $D\bar{D}$ state is predicted around 3720 MeV by the chiral unitary approach, and named as $X(3700)$, which is analogous to the $f_0(500)$, appearing as a $\pi\pi$ resonance in chiral unitary theory, and the $f_0(980)$, appearing as a quasibound $K\bar{K}$ state. There is some experimental support seen in the $e^+e^- \to J/\psi D\bar{D}$ reaction close to the $D\bar{D}$ threshold. In our work we propose three different experiments to observe it as a clear peak. The first one is the radiative decay of the $\psi(3770)$, $\psi(3770) \to \gamma X(3700) \to \gamma\eta\eta'$. The second one proposes the analogous reaction $\psi(4040) \to \gamma X(3700) \to \gamma\eta\eta'$ and the third reaction is the $e^+e^- \to J/\psi X(3700) \to J/\psi\eta\eta'$. Neat peaks

are predicted for all the reactions and the calculated rates are found within measurable range in present facilities.

From the former description, one can see that in our research, in addition to describing some known states, we have also theoretically predicted some states which are not listed in the PDG. The approach that we use to investigate, is reliable, thus, our results are accurate, with certain theoretical uncertainties and the resonances found are stable since their width is not very large. Therefore, our results should serve as a guideline for future experimental searches of these new resonances. We hope that the future experiments in the BES, BELLE, J-PARC, RHIC, LHC, FAIR and other facilities will search for these states predicted in our work.

Resumen de la Tesis

La Física de hadrones ha tenido un desarrolo espectacular en los últimos años debido a la plétora de estados nuevos que han sido descubiertos en laboratorios como BES en Beijing, la colaboración Babar en USA, Belle en Japón, CLEO en USA y el CERN en Europa, entre otros. El modelo de quarks, según el cual los mesones están formados de quark antiquark y los bariones de tres quarks, tuvo en su día un valor incalculable, al permitir entender los hadrones en términos de unos pocos componentes elementales. Las predicciones que hizo, y fueron confirmadas, puso este modelo de los hadrones en un lugar incuestionable de la Historia de la Física. Sin embargo, el paso del tiempo nos ha ido enseñando que la Naturaleza es más sutil que nuestros modelos y una una parte de los estados observados recientemente no pueden explicarse en los términos convencionales y exigen estructuras más complejas.

Por otra parte, una vez establecidos los bloques básicos constituyentes de los hadrones, quedaba describir su interacción y entonces se desarrolló la Cromodinámica Cuántica (QCD) que describía la interacción entre los quarks en términos de unos mediadores, los gluones. La descripción de la interacción fuerte y los estados hadrónicos estaba en principio terminada. Sin embargo las propiedades de esa interacción eran sutiles. A grandes energías y transferencia de momento la interacción era débil, pero a bajas energías y transferencias de momento la interacción se volvía muy intensa, debido a dos propiedades, libertad asintótica y confinamiento, respectivamente. Desde el punto de vista de explicación teórica de fenómenos eso significa que a altas energías se pueden hacer cálculos perturbativos, mientras que a bajas energías hay que recurrir a métodos no perturbativos y

entonces la resolución de la QCD se hace técnicamente impracticable. Ello no ha impedido que, con ingentes cantidades de tiempo de ordenador, diversos grupos hayan tratado de obtener propiedades de hadrones partiendo directamente del Lagrangiano de QCD, en lo que hoy llamamos Lattice gauge theories. El avance en ese campo ha sido espectacular, aunque conviene mencionar el excesivo e injustificado entusiasmmo de unos cálculos iniciales con aproximaciones "quenched", que hoy damos por inexactos. Incluso hoy dia, el cálculo del espectro de masas de los hadrones puede hacerse con relativa fiabilidad para los hadrones estables, pero los estados excitados que pueden desintegrarse son mucho más conflictivos debido al hecho que los cálculos unquenched, que en principio mezclan todas las componentes posibles de los estados, dan lugar a energías de estados que no son mas que los estados de colisión de esas componentes que han sido discretizados por la necesaria eleccción de un volumen finito para llevar a cabo los cálculos. Hay técnicas basadas en la fórmula de Lüescher para pasar de esas energías a corrimientos de fase en el continuo, pero las aplicaciones a problemas realistas de estados con varios canales de desintegración está sólo en su fase inicial.

Los modelos de quarks se basan en potenciales efectivos entre los quarks con potenciales confinantes, y otras interacciones que tratan de simular la dinámica de QCD y dan lugar a estructuras de hadrones, muchas veces más complejas que las básicas descritas el principio.

Asi las cosas, una nueva línea de trabajo ha supuesto un gran avance en la descripción de los hadrones y los procesos hadrónicos: las teorías efectivas. En ellas se cambian los grados de liberdad elementales, quarks y gluones, por bloques establecidos en la Naturaleza a bajas energías: los mismos hadrones de más baja energía y más estables. Entonces se derivan Lagrangianos efectivos con esas componentes que respetan las simetrías básicas de QCD. A bajas energías, y tomando como componentes los mesones pseudoscalares y los bariones de más baja energía, aparecen los Lagrangianos quirales y es posible hacer desarrollos perturbativos con ellos, asumiendo una convergenia en potencias del momento de los hadrones. Sin embargo esta teoría, que ha tenido un enorme impacto en la física hadrónica y describe con precisión un gran número de observables, tiene también sus límites. Si nos fijamos en la interacción pion-pion, por ejemplo, un desarrollo perturbativo de la

matriz de colisión sólo tiene sentido hasta la energía de la primera singularidad que en ese caso es el polo de la resonancia $f_0(500)$ (σ popularmente). Mucho antes de los 500 MeV de energía los cálculos perturbativos ya no son significativos.

Hacía falta un paso adelante para hacer cálculos no perturbativos rescatando la dinámica que hay en los Lagrangianos quirales y ese paso se dio con la Teoría quiral Unitaria, también llamada chiral unitary approach. En esa teoría se obtiene la amplitud de colisión a partir de la amplitud a orden más bajo resumando todos los términos de la ecuación de Schrödinger (Lippmann Schwinger en este caso), aunque normalmente los cálculos se hacen relativistas y se usa la ecuación de Bethe Salpeter. La interacción a orden más bajo, u órdenes más bajos, se interpreta como un potencial y hay un rango que se convierte en una escala de regularización en los loops de la ecuación, que tiene un tamaño natural, pero que normalmente se ajusta a algún observable para pasar luego a hacer predicciones en otros observables. El éxito de este desarrollo ha sido innegable y con él pueden obtenerse amplitudes de colisión realistas para procesos hadrónicos. En algunos casos esas mismas amplitudes presentan polos que se interpretan como estados ligados o resonancias. Se dice entonces que se ha generado dinámicamente una resonancia, que puede interpretarse como un estado molecular de otros dos hadrones más elementales que interaccionan entre sí, del mismo modo que un protón y un neutrón interaccionan para dar el deuterón.

Un punto quedaba por describir, pues en los Lagrangianos quirales no aparecen explícitamente los mesones vectoriales. Una solución a este problema ha venido de la introducción de los Lagrangianos de local hidden gauge symmetry. Estos Lagrangianos introducen los vectores junto con los pseudoscalares. La interacción de los pseudoscalares es la misma que en los Lagrangianos quirales, y órdenes superiores de esta teoría dan lugar a los Lagrangianos quirales de orden superior, con la hipótesis de dominancia vectorial de Sakurai.

Con las herramientas del local hidden gauge, que extiende los lagrangianos quirales, y las técnicas de la Teoría quiral unitaria, uno tiene las puertas abiertas al estudio de la mayoría de los procesos hadrónicos. La presente

Tesis ha usado esos elementos para hacer incursiones en diversos campos, como el estudio de posibles estados ligados o resonancias formadas por tres hadrones y la interacción de estados con charm o beauty.

La tesis tiene cuatro capítulos básicos: uno de ellos dedicado a la introducción de la teoría y las técnicas a ser usadas a lo largo de la Tesis. Otro en el que se recopilan los trabajos sobre tres hadrones. Otro en el que se describen los trabajos en los que se usa la simetría de Heavy Quark Spin Symmetry, HQSS, para describir o predecir mesones y bariones con charm o beauty or hidden charm y hidden beauty. En esos trabajos se observa que la extensión del local hidden gauge approach al campo de los quarks pesados es compatiblle con HQSS. Otro capítulo recopila trabajo hecho sobre otros temas como J/ψ suppresion, el estudio de la componente $K\pi$ en la función de onda del K^* o el estudio de diversas reacciones para observar el mesón predicho X(3700) formado por la interacción de $D\bar{D}$.

Estados de tres o más hadrones

La técnica general para estudiar sistemas de tres cuerpos es el uso de las ecuaciones de Faddeev, que a pesar de su sencillez formal son difíciles de resolver y todos los esquemas actuales contienen aproximaciones. En nuestro caso hemos untilizado una aproximación a esas ecuaciones que es fiable sólo cuando el estado resultante es ligado en sus componentes más importantes. Esa aproximación es conocida como el Fixed Center Approximation, FCA, y se basa en el hecho de que dos de las componentes ligan para formar un estado y una tercera partícula interacciona luego con esas dos componentes permitiendo la reinteracción un número ilimitado de veces alternativamente con cada una de las componentes del "cluster" original, que se supone no cambia apreciablemente por esa interacción con terceros. Primero se estudian algunos casos que pueden ser comparados con cálculos más finos realizados utilizando las ecuaciones de Faddeev. Un vez determinadas las condiciones para el éxito de la FCA, se pasa a estudiar nuevos sistemas donde se hacen predicciones.

En uno de los trabajos se estudian los estados de tres hadrones formados por NDK, $\bar{K}DN$ and $NDD\bar{D}$. El estudio se basa en la constatación de que

en trabajos anteriores los estados DN y KD dan lugar a resonancias bien establecidas. En el caso de DN se obtiene la resonancia $\Lambda_c(2595)$ y en el caso de la KD la resonancia $D_{s0}(2317)$. Luego se estudia la interacción de la tecera partícula con ese "cluster" hadrónico y se determina la amplitud de colisión para el sistema de tres cuerpos. Una representación del módulo al cuadrado de esa amplitud, con la observación de picos, nos indica donde hay estados, que en un estudio experimental serían interpretados como bariones. Se obtienen estados con energías 3150 MeV, 3050 MeV y 4400 MeV con números cuánticos $J^P = 1/2^+$ e isospin $I = 1/2$ que difieren en su contenido en charm o strangeness, $S = -1, C = 1$, $S = 1, C = 1$, $S = 0, C = 0$, respectivamente. De momento no se conocen estados con esos números cuánticos y esas energías, y los resultados son predicciones de bariones en un régimen de energías que no está todavía explotado.

Otro trabajo es la predicción de estado con un meson D^* y varios mesones ρ. Estudios anteriores probaron que la interacción de vectores con los spines alineados para dar spin 2 es muy fuerte, de modo que era posible añadir varios mesones ρ con sus spines alineados dando lugar a varios estados mesónicos de spin creciente. Esos estados pudieron ser contrastados con éxito con varios estados conocidos en la Tabla de partículas, hasta un f_6 que estaría formado por seis ρ. Del mismo modo se había comprobado que un K^* y diversos ρ con sus spines alineados daban lugar a estados que también se podían contrastar con estados K^* conocidos. Asi pues, se estudió el sistema de interacción de un D^* con varios ρ dando lugar a picos en la amplidud que se asocian con estados, de momento no observados, por lo que quedan como predicciones de mesones con alto spin y charm, que esperamos sean investigados experimentalmente en el futuro.

Uno de los estados estudiados que ha tenido cierta repercusión es el estado DNN. La relevancia de ese estado radica en que su análogo con strangeness ha sido largamente debatido en la Literatura. Es el estado $\bar{K}NN$. Ha habido grandes debates sobre si ese estado está ligado o si puede ser observado experimentalmente. La conclusión desde el punto de vista teórico es que ese estado está ligado pero que la anchura de desintegración es mayor que la ligadura, lo cual pone grandes dificultades para su observación experimental. Uno puede pensar en ese estado como un estado ligado

de $\Lambda(1405)$ con otro nucleón, pero la $\Lambda(1405)$ tiene una anchura de unos 30-50 MeV, que se traduce en una anchura mayor en el estado $\bar{K}NN$, cuando su ligadura es del orden de unos 20 MeV. Sin embargo, la resonancia equivalente en el caso de DN es la $\Lambda_c(2595)$ que tiene una anchura del orden de 2 MeV, de modo que en ese caso la situación podría ser revertida, con una energía de ligadura mucho mayor que su anchura de desintegración. El estudio, que fue hecho en colaboración con un grupo japonés, usando ellos una técnica variacional, dio lugar como esperado, a un estado ligado y con una anchura de desintegración mucho menor que la ligadura, por lo que pensamos que ese estado debería ser claramente identificable, y en el trabajo se exponen varios posibles experimentos para su observación.

Otro tabajo en esa línea es el estudio del sistema $\rho K\bar{K}$. En ese caso, el sistema $K\bar{K}$ interacciona para formar la $f_0(980)$ y luego el ρ interacciona con K y $\bar{K}$. Es interesante observar que un estado aparece nítido en ese caso y es claramente identificable con el mesón $\rho(1700)$.

En la misma línea estudiamos estados de $\eta K\bar{K}$ y $\eta' K\bar{K}$. En este caso observamos que mientras en el primer caso se obtiene un pico ancho que podría identificarse con la resonancia $\eta(1475)$, en el segundo no obtenemos ningún pico sino un débil cusp en el umbral por lo que pensamos que eso no corresponde a ningún estado observado.

Estudio de mesones y bariones usando la simetría de HQSS

Este tema ha dado lugar a varios artículos. En el primero de ellos se aplica la simetría de HQSS, que nos dice que la interacción es independiente del spin y sabor de los quarks pesados. Sabido eso, se rearreglan los spines de los quarks para dar lugar a sumas de spines de los cuales la interacción es independiente. Ello supone cambiar de base de estados que se lleva a cabo con coeficients de 9j. Luego podemos hacer uso del Teorema de Wigner Eckart y con unos pocos elementos de matriz reducidos somos capaces de describir la interacción. A continuación elegimos un modelo para calcular esos elementos de matriz reducidos y obervamos que la extensión de la teoría de local hidden gauge al sector de quarks pesados satisface las reglas de la HQSS. Usando sólamente los términos dominantes en la

HQSS determinamos entonces las amplitudes de colisión de pares de mesón-barión con charm oculto y a partir de ahí, buscado polos en la segunda hoja de Riemann, determinamos los estados moleculares que se obtienen de la teoría. Observamos varios estados que corresponden básicamente a $\bar{D}\Sigma_c$, $\bar{D}\Sigma_c^*$, $\bar{D}^*\Sigma_c$ y $\bar{D}^*\Sigma_c^*$, y que se desintegran esencialmente en $\eta_c N$ and $J/\psi N$. Algunos de esos estados están degenerados en spin en nuestros modelos. Posteriormente comparamos con resultados obtenidos en otros estudios y vemos analogías y diferencias. Varios de los estados obtenidos son comunes a todos los estudios lo que nos da una gran fiabilidad sobre su existencia y futura observación.

Tras este tema estudiamos estados bariónicos con beauty oculta. De nuevo se obtienen estados que corresponden básicamente a $B\Sigma_b$, $B\Sigma_b^*$, $B^*\Sigma_b$ and $B^*\Sigma_b^*$, y que se desintegran en $\eta_b N$ and ΥN, con una energía de ligadura de unos $50-130$ MeV con respecto al umbral de los correspondientes canales. Todos ellos tienen isospin $I = 1/2$, y no se encuentran estados ligados para $I = 3/2$. Algunos de esos estados, como en el caso anterior, están degenerados en spin.

Siguiendo la misma línea se estudian los estados mesónicos de beauty oculta y de nuevo se obtienen seis estados. También se observa que en el orden dominante de HQSS no aparecen estados de I=1. Ello contrasta con la observacion de estados Z recientemente, lo cual indica que debe haber una interaccion más allá del término dominante. El hecho de que esos estados Z se encuentren muy cerca del umbral de canales es a nuestro entender una señal de la débil interacción, y otros integrantes del grupo de investigación están trabajando en ese tema en la actualidad.

En ese mismo capítulo se estudian dos nuevos sistemas, que son bariones con charm y con beauty. En el primero de ellos se estudian estados de un mesón pseudoscalar y un barión y se mezclan con estados de vector baryon. En el contaje estricto de HQSS y usando la teoría de local hidden gauge, la conexión entre vector-barión y pseudoscalar-barión se hace por intercambio de piones, u otros mesones pseudoscalares, que resultan subdominantes en el estricto contaje de HQSS. Sin embargo en este trabajo retomamos el tema introduciendo explicitamente esa conexión. Entonces observamos que hay

una mezcla apreciable de estados $\bar{B}N$ y $\bar{B}^*N$. Encontramos dos estados con anchura prácticamente nula, que asociamos a los estados descubiertos $\Lambda_b(5912)$ and $\Lambda_b(5920)$ con spines $J = 1/2,\ 3/2$, que se acoplan mayormente a $\bar{B}^*N$. Por otra parte encontramos también otros tres estados de I=0 y ocho estados de I=1, algunos de ellos degenerados en spin. En este trabajo también hacemos una observación esclarecedora del significado de la HQSS, desde el punto de vista de tener los quarks pesados como observadores, deduciendo de una manera sencilla los acoplamientos $D^*D\pi$ y $B^*B\pi$, en perfecto acuerdo con los resultados experimentales en el primer caso, y con resultados de lattice QCD en el segundo.

Tras ese trabajo estudiamos sistemas de mesón barión con charm, de nuevo mezclando vector-barión y pseudoscalar-barión. Nuevamente obtenemos dos estados $\Lambda_c(2595)$ y $\Lambda_c(2625)$ con spin 1/2 y 3/2 respectivamente. En este caso el de menos energía se acopla a DN mayormente, mientras que el de mayor energía se acopla básicamente a D^*N. Por otra parte encontramos cuatro estados más con I=0 y siete con I=1, algunos de ellos degenerados en spin.

Problemas relacionados

En este capítulo estudiamos tres nuevos temas:

a) J/ψ depletion.

b) Tres métodos para la observación de un estado ligado de $D\bar{D}$, X(3700).

c) Componente de $K\pi$ en la función de onda de $\bar{K}^*$.

a) El estudio de la interacción de vectores con nucleones en el sector de charm y charm oculto nos permite tener una mejor visión de la interacción $J/\psi N$ que en otros modelos, al tener acceso a canales acoplados de ese canal en los que puede desintegrarse. De ese modo podemos calcular la anchura de desintegración de J/ψ en núcleos y aportar nuestra contribución al problema del J/ψ depletion, que ha dado lugar a gran número de interpretaciones.

b) En la Tesis de Daniel Gamermann se obtuvo un estado ligado de $D\bar{D}$ con masa alrededor de 3700, que se nombró X(3700). Posteriormente en otros estudios se llega a la misma conclusión. Por ser un estado ligado de esas componentes es difícil de observar. En este trabajo se proponen tres métodos diferentes para su observación experimental. El primero es la desintegración radiativa de $\psi(3770)$, $\psi(3770) \to \gamma X(3700) \to \gamma\eta\eta'$. El segundo propone la reacción análoga $\psi(4040) \to \gamma X(3700) \to \gamma\eta\eta'$ y la tercera reacción es $e^+e^- \to J/\psi X(3700) \to J/\psi\eta\eta'$. En todas las reacciones se obtienen picos nítidos y las secciones eficaces o anchuras de desintegración estan dentro del rango de medidas posibles en los Laboratorios actuales.

c) El chiral unitary approach provee las amplitudes de colisión para diversos procesos. Sin embargo en dicha versión no proporciona información sobre las funciones de onda. En varios trabajos del grupo se ha establecido esa conexión, dando significado a los aclopamientos de los estados a los canales de interacción. Primero se hizo para estados ligados en onda s. Luego se extendió a estados resonantes, y finalmente a estados resonantes en cualquier onda parcial. El resultado para estados resonantes es sutil pues las funciones de onda de los canales abiertos divergen. Entonces hay que reinterpretar el significado de las magnitudes que aparecen en el estudio. En particular hay una regla de suma que generaliza el resultado del compositeness condition de Weinberg, en donde los diversos términos pueden interpretarse como probabilidades de diversos canales, que suman a uno para estados ligados. Sin embargo, ese no es el caso para estados resonantes donde las probabilidad de los canales abiertos es infinita. Una nueva reinterpretación de los términos aparece en ese caso ligado a su uso en los polos de la segunda hoja de Riemann. Los términos están asociados a la integral del cuadrado de la función de onda en una prescripcion de fase concreta, que converge en ese caso, y que nos da una idea del peso que esa componente tiene en la función de onda, aunque no es una probabilidad. En el presente trabajo se han utilizado esas ideas para determinar el peso de la componente πK en la resonancia K^*. El estudio permite no obstante determinar con fiabilidad que al menos un 80 % de la función de onda de esa resonancia no corresponde a un estado πK y está asociado a otros canales, que llamamos genuinos, presumiblemente $q\bar{q}$, aunque la teoría no puede precisar la naturaleza de lo que le falta a la regla de suma respecto de la unidad.

Consideraciones generales: La Tesis se ha desarrollado en torno al estudio de la naturaleza de estados hadrónicos, utilizando para ello las técnicas de teorías efectivas adecuadas a ese tipo de estudios, muchas de las cuales han sido desarrolladas anteriormente en el grupo en el que he realizado la Tesis. Hemos sido capaces de describir varios estados existentes como agregados de dos o tres hadrones más elementales y hemos hecho muchas predicciones, en los sectores de charm y beauty, donde los experimentos están conduciendo a la observación de nuevos estados a un ritmo frenético. Esperamos y deseamos que muchos de esos estados sean observados en un futuro próximo, y a un tiempo más corto esperamos que nuestro estudio sirva de orientación y referencia para otros grupos que trabajan en los mismos temas, de cuyos trabajos nos hemos también beneficiado como se verá a lo largo de esta Tesis.

El trabajo ha dado lugar a 13 publicaciones científicas en revistas internacionales y un trabajo más que está en proceso de revisión. Asímismo ha dado también lugar a diez presentaciones en Congresos Internacionales.

Bibliography

[1] W. J. Marciano, Phys. Rev. D **20**, 274 (1979).

[2] R. P. Feynman, M. Gell-Mann and G. Zweig, Phys. Rev. Lett. **13**, 678 (1964).

[3] M. Gell-Mann, Phys. Lett. **8**, 214 (1964).

[4] J. J. Aubert *et al.* [E598 Collaboration], Phys. Rev. Lett. **33**, 1404 (1974).

[5] J. E. Augustin *et al.* [SLAC-SP-017 Collaboration], Phys. Rev. Lett. **33**, 1406 (1974).

[6] R. M. Barnett, Phys. Rev. Lett. **34**, 41 (1975).

[7] L. A. Copley, N. Isgur and G. Karl, Phys. Rev. D **20**, 768 (1979) [Erratum-ibid. D **23**, 817 (1981)].

[8] C. Hayne and N. Isgur, Phys. Rev. D **25**, 1944 (1982).

[9] J. Beringer *et al.* [Particle Data Group Collaboration], Phys. Rev. D **86**, 010001 (2012).

[10] S. L. Olsen, arXiv:1403.1254 [hep-ex].

[11] S. Choi, arXiv:1403.1832 [hep-ex].

[12] S. L. Glashow, Nucl. Phys. **22**, 579 (1961).

[13] S. Weinberg, Phys. Rev. Lett. **19**, 1264 (1967).

[14] S. Prelovsek, T. Draper, C. B. Lang, M. Limmer, K. -F. Liu, N. Mathur and D. Mohler, Phys. Rev. D **82**, 094507 (2010).

[15] F. Giacosa, Phys. Rev. D **75**, 054007 (2007).

[16] J. A. Oller and E. Oset, Nucl. Phys. A **620**, 438 (1997) [Erratum-ibid. A **652**, 407 (1999)].

[17] J. A. Oller, E. Oset and J. R. Pelaez, Phys. Rev. Lett. **80**, 3452 (1998).

[18] J. A. Oller, E. Oset and J. R. Pelaez, Phys. Rev. D **59**, 074001 (1999) [Erratum-ibid. D **60**, 099906 (1999)] [Erratum-ibid. D **75**, 099903 (2007)].

[19] J. A. Oller and E. Oset, Phys. Rev. D **60**, 074023 (1999).

[20] E. Oset and M. J. Vicente Vacas, Nucl. Phys. A **678**, 424 (2000).

[21] F. -K. Guo, L. Liu, U. -G. Meissner and P. Wang, Phys. Rev. D **88**, 074506 (2013).

[22] F. Okiharu, H. Suganuma and T. T. Takahashi, Phys. Rev. D **72**, 014505 (2005).

[23] A. Esposito, M. Papinutto, A. Pilloni, A. D. Polosa and N. Tantalo, Phys. Rev. D **88**, 054029 (2013).

[24] C. -F. Qiao and L. Tang, Eur. Phys. J. C **74**, 2810 (2014).

[25] Z. -G. Wang, arXiv:1312.1537 [hep-ph].

[26] W. Chen, T. G. Steele and S. -L. Zhu, Phys. Rev. D **89**, 054037 (2014).

[27] T. Nakano *et al.* [LEPS Collaboration], Phys. Rev. Lett. **91**, 012002 (2003).

[28] J. Barth *et al.* [SAPHIR Collaboration], Phys. Lett. B **572**, 127 (2003).

[29] I. Abt *et al.* [HERA-B Collaboration], Phys. Rev. Lett. **93**, 212003 (2004).

[30] S. -L. Zhu, Phys. Rev. Lett. **91**, 232002 (2003).

[31] J. Sugiyama, T. Doi and M. Oka, Phys. Lett. B **581**, 167 (2004).

[32] M. Praszalowicz, Phys. Lett. B **575**, 234 (2003).

[33] F. Csikor, Z. Fodor, S. D. Katz and T. G. Kovacs, JHEP **0311**, 070 (2003).

[34] S. Capstick, P. R. Page and W. Roberts, Phys. Lett. B **570**, 185 (2003).

[35] C. E. Carlson, C. D. Carone, H. J. Kwee and V. Nazaryan, Phys. Lett. B **573**, 101 (2003).

[36] D. Cabrera, Q. B. Li, V. K. Magas, E. Oset and M. J. Vicente Vacas, Phys. Lett. B **608**, 231 (2005).

[37] H. Nagahiro, S. Hirenzaki, E. Oset and M. J. Vicente Vacas, Phys. Lett. B **620**, 125 (2005).

[38] B. McKinnon *et al.* [CLAS Collaboration], Phys. Rev. Lett. **96**, 212001 (2006).

[39] K. Shirotori, T. N. Takahashi, S. Adachi, M. Agnello, S. Ajimura, K. Aoki, H. C. Bhang and B. Bassalleck *et al.*, Phys. Rev. Lett. **109**, 132002 (2012).

[40] T. Hyodo, A. Hosaka and M. Oka, Prog. Theor. Phys. **128**, 523 (2012).

[41] F. -K. Guo, C. Hidalgo-Duque, J. Nieves and M. P. Valderrama, Phys. Rev. D **88**, 054014 (2013).

[42] P. Bicudo, N. Cardoso and M. Cardoso, Prog. Part. Nucl. Phys. **67**, 440 (2012).

[43] N. Cardoso and P. Bicudo, Phys. Rev. D **87**, no. 3, 034504 (2013).

[44] R. M. Albuquerque, S. H. Lee and M. Nielsen, Phys. Rev. D **88**, 076001 (2013).

[45] T. Liu, Y. Mao and B. -Q. Ma, Int. J. Mod. Phys. A **29**, no. 13, 1430020 (2014).

[46] T. Nakano *et al.* [LEPS Collaboration], Phys. Rev. C **79**, 025210 (2009).

[47] A. Martinez Torres and E. Oset, Phys. Rev. Lett. **105**, 092001 (2010).

[48] Yuji Katyo et al, in the 20th International IUPAP Conference on Few-Body Problems in Physics (FB20), held at Fukuoka, Japan.

[49] R. L. Jaffe, Phys. Rev. Lett. **38**, 195 (1977) [Erratum-ibid. **38**, 617 (1977)].

[50] K. Maltman and N. Isgur, Phys. Rev. Lett. **50**, 1827 (1983).

[51] T. Sakai and H. Suganuma, Phys. Lett. B **430**, 168 (1998).

[52] S. R. Beane *et al.* [NPLQCD Collaboration], Phys. Rev. Lett. **106**, 162001 (2011).

[53] T. Inoue *et al.* [HAL QCD Collaboration], Phys. Rev. Lett. **106**, 162002 (2011).

[54] J. Haidenbauer and U. -G. Meissner, Phys. Lett. B **706**, 100 (2011).

[55] J. K. Ahn *et al.* [KEK-PS E224 Collaboration], Phys. Rev. C **62**, 055201 (2000).

[56] C. J. Yoon, H. Akikawa, K. Aoki, Y. Fukao, H. Funahashi, M. Hayata, K. Imai and K. Miwa *et al.*, Phys. Rev. C **75**, 022201 (2007).

[57] B. H. Kim *et al.* [Belle Collaboration], Phys. Rev. Lett. **110**, no. 22, 222002 (2013).

[58] E. Fermi and C. -N. Yang, Phys. Rev. **76**, 1739 (1949).

[59] H. J. Lipkin, Phys. Lett. B **74**, 399 (1978).

[60] H. -M. Chan and H. Hogaasen, Nucl. Phys. B **136**, 401 (1978).

[61] H. -M. Chan and H. Hogaasen, Phys. Lett. B **72**, 400 (1978).

[62] J. Z. Bai *et al.* [BES Collaboration], Phys. Rev. Lett. **91**, 022001 (2003).

[63] M. Ablikim *et al.* [BESIII Collaboration], Phys. Rev. Lett. **108**, 112003 (2012).

[64] M. -L. Yan, S. Li, B. Wu and B. -Q. Ma, Phys. Rev. D **72**, 034027 (2005).

[65] S. -L. Zhu and C. -S. Gao, Commun. Theor. Phys. **46**, 291 (2006).

[66] N. Kochelev and D. -P. Min, Phys. Lett. B **633**, 283 (2006).

[67] Z. -G. Wang and S. -L. Wan, J. Phys. G **34**, 505 (2007).

[68] M. -L. Yan, hep-ph/0605303.

[69] Z. -G. Wang, Eur. Phys. J. A **47**, 71 (2011).

[70] S. Chen and J. Ping, Chin. Phys. C **33**, 1 (2009).

[71] C. Deng, J. Ping, Y. Yang and F. Wang, Phys. Rev. D **86**, 014008 (2012).

[72] C. Shen, arXiv:1402.6589 [hep-ex].

[73] J. Haidenbauer, U. -G. Meissner and A. Sibirtsev, Phys. Rev. D **74**, 017501 (2006).

[74] L. Zhao, N. Li, S. -L. Zhu and B. -S. Zou, Phys. Rev. D **87**, 054034 (2013).

[75] A. Martinez Torres, K. P. Khemchandani, L. S. Geng, M. Napsuciale and E. Oset, Phys. Rev. D **78**, 074031 (2008).

[76] G. Cotugno, R. Faccini, A. D. Polosa and C. Sabelli, Phys. Rev. Lett. **104**, 132005 (2010).

[77] Y. D. Chen and C. F. Qiao, Phys. Rev. D **85**, 034034 (2012).

[78] Y. -D. Chen, C. -F. Qiao, P. -N. Shen and Z. -Q. Zeng, Phys. Rev. D **88**, 114007 (2013).

[79] S. K. Choi *et al.* [Belle Collaboration], Phys. Rev. Lett. **91**, 262001 (2003).

[80] D. Acosta *et al.* [CDF Collaboration], Phys. Rev. Lett. **93**, 072001 (2004).

[81] V. M. Abazov *et al.* [D0 Collaboration], Phys. Rev. Lett. **93**, 162002 (2004).

[82] B. Aubert *et al.* [BaBar Collaboration], Phys. Rev. D **71**, 071103 (2005).

[83] RAaij *et al.* [LHCb Collaboration], Phys. Rev. Lett. **110**, no. 22, 222001 (2013).

[84] K. K. Seth, Prog. Part. Nucl. Phys. **67**, 390 (2012).

[85] K. Zhu, arXiv:1212.2169 [hep-ex].

[86] G. Tatishvili, arXiv:1305.0590 [hep-ex].

[87] T. Barnes and S. Godfrey, Phys. Rev. D **69**, 054008 (2004).

[88] E. J. Eichten, K. Lane and C. Quigg, Phys. Rev. D **69**, 094019 (2004).

[89] M. Suzuki, Phys. Rev. D **72**, 114013 (2005).

[90] X. Liu, Z. -G. Luo, Y. -R. Liu and S. -L. Zhu, Eur. Phys. J. C **61**, 411 (2009).

[91] C. Hidalgo-Duque, J. Nieves, A. Ozpineci and V. Zamiralov, Phys. Lett. B **727**, 432 (2013).

[92] F. -K. Guo, U. -G. Meiner and W. Wang, arXiv:1402.6236 [hep-ph].

[93] D. Gamermann and E. Oset, Eur. Phys. J. A **33**, 119 (2007).

[94] D. Gamermann and E. Oset, Phys. Rev. D **80**, 014003 (2009).

[95] D. Gamermann, J. Nieves, E. Oset and E. Ruiz Arriola, Phys. Rev. D **81**, 014029 (2010).

[96] F. Aceti, R. Molina and E. Oset, Phys. Rev. D **86**, 113007 (2012).

[97] S. K. Choi *et al.* [BELLE Collaboration], Phys. Rev. Lett. **100**, 142001 (2008).

[98] R. Mizuk *et al.* [Belle Collaboration], Phys. Rev. D **78**, 072004 (2008).

[99] M. Ablikim *et al.* [BESIII Collaboration], Phys. Rev. Lett. **110** (2013) 25, 252001.

[100] Z. Q. Liu *et al.* [Belle Collaboration], Phys. Rev. Lett. **110**, no. 25, 252002 (2013).

[101] T. Xiao, S. Dobbs, A. Tomaradze and K. K. Seth, Phys. Lett. B **727**, 366 (2013).

[102] M. Ablikim *et al.* [BESIII Collaboration], Phys. Rev. Lett. **112**, 132001 (2014).

[103] M. Ablikim *et al.* [BESIII Collaboration], Phys. Rev. Lett. **111**, 242001 (2013).

[104] M. Ablikim *et al.* [BESIII Collaboration], Phys. Rev. Lett. **112**, 022001 (2014).

[105] M. Nielsen and F. S. Navarra, Mod. Phys. Lett. A **29**, no. 5, 1430005 (2014).

[106] A. Martinez Torres, K. P. Khemchandani, F. S. Navarra, M. Nielsen and E. Oset, Phys. Rev. D **89**, 014025 (2014).

[107] F. Aceti, M. Bayar, E. Oset, A. M. Torres, K. P. Khemchandani, F. S. Navarra and M. Nielsen, arXiv:1401.8216 [hep-ph].

[108] B. Aubert *et al.* [BaBar Collaboration], Phys. Rev. Lett. **95**, 142001 (2005).

[109] T. E. Coan *et al.* [CLEO Collaboration], Phys. Rev. Lett. **96**, 162003 (2006).

[110] C. Z. Yuan *et al.* [Belle Collaboration], Phys. Rev. Lett. **99**, 182004 (2007).

[111] X. H. Mo, G. Li, C. Z. Yuan, K. L. He, H. M. Hu, J. H. Hu, P. Wang and Z. Y. Wang, Phys. Lett. B **640**, 182 (2006).

[112] W. -S. Hou, Phys. Rev. D **74**, 017504 (2006).

[113] K. F. Chen *et al.* [Belle Collaboration], Phys. Rev. Lett. **100**, 112001 (2008).

[114] A. Bondar *et al.* [Belle Collaboration], Phys. Rev. Lett. **108**, 122001 (2012).

[115] Q. Wang, C. Hanhart and Q. Zhao, Phys. Rev. Lett. **111**, 132003 (2013).

[116] E. Wilbring, H. -W. Hammer and U. -G. Meiner, Phys. Lett. B **726**, 326 (2013).

[117] Q. -Y. Lin, X. Liu and H. -S. Xu, Phys. Rev. D **88**, 114009 (2013).

[118] F. -K. Guo, C. Hidalgo-Duque, J. Nieves and M. P. Valderrama, Int. J. Mod. Phys. Conf. Ser. **26**, 1460073 (2014).

[119] T. Mehen and J. Powell, Phys. Rev. D **88**, no. 3, 034017 (2013).

[120] M. B. Voloshin, Phys. Rev. D **87**, no. 9, 091501 (2013).

[121] Z. -G. Wang and T. Huang, Phys. Rev. D **89**, 054019 (2014).

[122] X. Li and M. B. Voloshin, Phys. Rev. D **86**, 077502 (2012).

[123] C. -Y. Cui, Y. -L. Liu and M. -Q. Huang, Phys. Rev. D **85**, 074014 (2012).

[124] M. Ablikim *et al.* [BESIII Collaboration], Phys. Rev. Lett. **110**, 022001 (2013).

[125] Y. Yamaguchi, S. Ohkoda, S. Yasui and A. Hosaka, Phys. Rev. D **84**, 014032 (2011).

[126] Y. Yamaguchi, S. Ohkoda, S. Yasui and A. Hosaka, Phys. Rev. D **85**, 054003 (2012).

[127] J. -J. Wu, R. Molina, E. Oset and B. S. Zou, Phys. Rev. Lett. **105**, 232001 (2010).

[128] J. -J. Wu, L. Zhao, and B. S. Zou, Phys. Lett. B **709**, 70 (2012).

[129] J. Haidenbauer and U. G. Meissner, Nucl. Phys. A **881**, 44 (2012).

[130] T. F. Carames, A. Valcarce and J. Vijande, Phys. Lett. B **709**, 358 (2012).

[131] N. Brambilla, S. Eidelman, B. K. Heltsley, R. Vogt, G. T. Bodwin, E. Eichten, A. D. Frawley and A. B. Meyer *et al.*, Eur. Phys. J. C **71**, 1534 (2011).

[132] S. Godfrey, arXiv:0910.3409 [hep-ph].

[133] G. T. Bodwin, E. Braaten, E. Eichten, S. L. Olsen, T. K. Pedlar and J. Russ, arXiv:1307.7425.

[134] G. Aad *et al.* [ATLAS Collaboration], Phys. Lett. B **716**, 1 (2012).

[135] S. Chatrchyan *et al.* [CMS Collaboration], Phys. Lett. B **716**, 30 (2012).

[136] S. L. Wu, Mod. Phys. Lett. A **29**, 1330027 (2014).

[137] A. Khodjamirian, hep-ph/0403145.

[138] P. Skands, arXiv:1207.2389 [hep-ph].

[139] U. Aglietti, hep-ph/9705277.

[140] S. Bethke, J. Phys. G **26**, R27 (2000).

[141] D. E. Kharzeev and J. Raufeisen, nucl-th/0206073.

[142] D. J. Gross and F. Wilczek, Phys. Rev. Lett. **30**, 1343 (1973).

[143] H. D. Politzer, Phys. Rev. Lett. **30**, 1346 (1973).

[144] U. Van Kolck, L. J. Abu-Raddad and D. M. Cardamone, nucl-th/0205058.

[145] H. D. Politzer and M. B. Wise, Phys. Lett. B **208** (1988) 504.

[146] H. Georgi, Phys. Lett. B **240**, 447 (1990).

[147] E. Epelbaum, H. -W. Hammer and U. -G. Meissner, Rev. Mod. Phys. **81**, 1773 (2009).

[148] S. Scherer, Adv. Nucl. Phys. **27**, 277 (2003).

[149] J. Goldstone, Nuovo Cim. **19**, 154 (1961).

[150] J. Goldstone, A. Salam and S. Weinberg, Phys. Rev. **127**, 965 (1962).

[151] J. Gasser and H. Leutwyler, Nucl. Phys. B **250**, 465 (1985).

[152] U. G. Meissner, Rept. Prog. Phys. **56**, 903 (1993).

[153] A. Pich, Rept. Prog. Phys. **58**, 563 (1995).

[154] G. Ecker, Prog. Part. Nucl. Phys. **35**, 1 (1995).

[155] E. Oset and A. Ramos, Nucl. Phys. A **635**, 99 (1998).

[156] M. Bando, T. Kugo, S. Uehara, K. Yamawaki and T. Yanagida, Phys. Rev. Lett. **54**, 1215 (1985).

[157] M. Bando, T. Kugo and K. Yamawaki, Prog. Theor. Phys. **73**, 1541 (1985).

[158] M. Bando, T. Kugo and K. Yamawaki, Nucl. Phys. B **259**, 493 (1985).

[159] M. Bando, T. Kugo and K. Yamawaki, Phys. Rept. **164**, 217 (1988).

[160] S. Weinberg, Phys. Rev. **166**, 1568 (1968).

[161] G. Ecker, J. Gasser, H. Leutwyler, A. Pich and E. de Rafael, Phys. Lett. B **223**, 425 (1989).

[162] G. Ecker, J. Gasser, A. Pich and E. de Rafael, Nucl. Phys. B **321**, 311 (1989).

[163] U. G. Meissner, Phys. Rept. **161**, 213 (1988).

[164] M. C. Birse, Z. Phys. A **355**, 231 (1996).

[165] Daniel Gamermann, Ph. D thesis of Valencia University, 2010: http://ific.uv.es/nucth/tesis_DanGam.pdf

[166] Raquel Molina Peralta, Ph. D thesis of Valencia University, 2012: http://ific.uv.es/nucth/tesis_raquel.pdf

[167] H. Nagahiro, L. Roca, A. Hosaka and E. Oset, Phys. Rev. D **79**, 014015 (2009).

[168] J. -J. Wu, R. Molina, E. Oset and B. S. Zou, Phys. Rev. C **84**, 015202 (2011).

[169] D. Gamermann, E. Oset and B. S. Zou, Eur. Phys. J. A **41**, 85 (2009).

[170] A. Bramon, A. Grau and G. Pancheri, Phys. Lett. B **283**, 416 (1992).

[171] F. Klingl, N. Kaiser and W. Weise, Nucl. Phys. A **624**, 527 (1997).

[172] J. E. Palomar and E. Oset, Nucl. Phys. A **716**, 169 (2003).

[173] V. Bernard, N. Kaiser and U. -G. Meissner, Int. J. Mod. Phys. E **4**, 193 (1995).

[174] E. E. Jenkins and A. V. Manohar, Phys. Lett. B **259**, 353 (1991).

[175] F. E. Close, An Introduction to Quarks and Partons, Academic Press, 1979.

[176] J. B. Kogut, Rev. Mod. Phys. **55**, 775 (1983).

[177] M. Luscher, S. Sint, R. Sommer and P. Weisz, Nucl. Phys. B **478**, 365 (1996).

[178] M. Luscher, S. Sint, R. Sommer, P. Weisz and U. Wolff, Nucl. Phys. B **491**, 323 (1997).

[179] D. Mohler, S. Prelovsek and R. M. Woloshyn, Phys. Rev. D **87**, no. 3, 034501 (2013).

[180] M. A. Shifman, A. I. Vainshtein and V. I. Zakharov, Nucl. Phys. B **147**, 385 (1979).

[181] L. J. Reinders, H. Rubinstein and S. Yazaki, Phys. Rept. **127**, 1 (1985).

[182] J. M. Dias, R. M. Albuquerque, M. Nielsen and C. M. Zanetti, Phys. Rev. D **86**, 116012 (2012).

[183] C. D. Roberts and A. G. Williams, Prog. Part. Nucl. Phys. **33**, 477 (1994).

[184] P. Maris and C. D. Roberts, Int. J. Mod. Phys. E **12**, 297 (2003).

[185] C. S. Fischer, J. Phys. G **32**, R253 (2006).

[186] A. Manohar and H. Georgi, Nucl. Phys. B **234**, 189 (1984).

[187] Z. Y. Zhang, Y. W. Yu, P. N. Shen, L. R. Dai, A. Faessler and U. Straub, Nucl. Phys. A **625**, 59 (1997).

[188] José Antonio Oller Berber, Ph. D thesis of Valencia University, 1999: http://ific.uv.es/nucth/tesisoller.pdf

[189] J. A. Oller, E. Oset and A. Ramos, Prog. Part. Nucl. Phys. **45**, 157 (2000).

[190] N. Kaiser, P. B. Siegel and W. Weise, Nucl. Phys. A **594**, 325 (1995).

[191] N. Kaiser, P. B. Siegel and W. Weise, Phys. Lett. B **362**, 23 (1995).

[192] H. -X. Chen, A. Hosaka and S. -L. Zhu, Phys. Rev. D **76**, 094025 (2007).

[193] Y. -R. Liu and S. -L. Zhu, Phys. Rev. D **75**, 034003 (2007).

[194] J. A. Oller and U. G. Meissner, Phys. Lett. B **500**, 263 (2001).

[195] F. -K. Guo, R. -G. Ping, P. -N. Shen, H. -C. Chiang and B. -S. Zou, Nucl. Phys. A **773**, 78 (2006).

[196] C. Garcia-Recio, L. S. Geng, J. Nieves and L. L. Salcedo, Phys. Rev. D **83**, 016007 (2011).

[197] F. Mandl and G. Shaw, *Quantum Field Theory (Wiley-Interscience, New York, 1984).*

[198] A. M. Badalian, L. P. Kok, M. I. Polikarpov and Y. .A. Simonov, Phys. Rept. **82**, 31 (1982).

[199] J. Nieves and E. Ruiz Arriola, Phys. Rev. D **64**, 116008 (2001).

[200] J. Nieves and E. Ruiz Arriola, Nucl. Phys. A **679**, 57 (2000).

[201] J. -J. Wu, T. -S. H. Lee and B. S. Zou, Phys. Rev. C **85**, 044002 (2012).

[202] W. L. Wang, F. Huang, Z. Y. Zhang and B. S. Zou, Phys. Rev. C **84**, 015203 (2011).

[203] M. Altenbuchinger and L. -S. Geng, arXiv:1310.5224 [hep-ph].

[204] S. Weinberg, Phys. Rev. **137**, B672 (1965).

[205] J. Yamagata-Sekihara, J. Nieves, E. Oset, Phys. Rev. D **83**, 014003 (2011).

[206] F. Aceti and E. Oset, Phys. Rev. D **86**, 014012 (2012).

[207] J. Fujita and H. Miyazawa, Prog. Theor. Phys. **17**, 360 (1957).

[208] L. D. Faddeev, Sov. Phys. JETP **12**, 1014 (1961) [Zh. Eksp. Teor. Fiz. **39**, 1459 (1960)].

[209] W. Glockle, T. S. H. Lee and F. Coester, Phys. Rev. C **33**, 709 (1986).

[210] S. Weinberg, Phys. Lett. B **295**, 114 (1992).

[211] J. M. Richard, Phys. Rept. **212**, 1 (1992).

[212] A. Martinez Torres, K. P. Khemchandani and E. Oset, Phys. Rev. C **77**, 042203 (2008).

[213] A. Martinez Torres, K. P. Khemchandani, M. Nielsen and F. S. Navarra, Phys. Rev. D **87**, 034025 (2013).

[214] Alberto Martínez Torres, Ph. D thesis of Valencia University, 2010: http://ific.uv.es/nucth/TesisAlMar.pdf

[215] K. P. Khemchandani, A. Martinez Torres and E. Oset, Eur. Phys. J. A **37**, 233 (2008).

[216] A. Martinez Torres, K. P. Khemchandani, D. Gamermann and E. Oset, Phys. Rev. D **80**, 094012 (2009).

[217] A. Martinez Torres and E. Oset, Phys. Rev. C **81**, 055202 (2010).

[218] G. Toker, A. Gal and J. M. Eisenberg, Nucl. Phys. A **362**, 405 (1981).

[219] R. C. Barrett and A. Deloff, Phys. Rev. C **60**, 025201 (1999).

[220] A. Deloff, Phys. Rev. C **61**, 024004 (2000).

[221] S. S. Kamalov, E. Oset and A. Ramos, Nucl. Phys. A **690**, 494 (2001).

[222] A. Gal, Int. J. Mod. Phys. A **22**, 226 (2007).

[223] L. Roca and E. Oset, Phys. Rev. D **82**, 054013 (2010).

[224] J. Yamagata-Sekihara, L. Roca and E. Oset, Phys. Rev. D **82**, 094017 (2010) [Erratum-ibid. D **85**, 119905 (2012)].

[225] J. -J. Xie, A. Martinez Torres, E. Oset and P. Gonzalez, Phys. Rev. C **83**, 055204 (2011).

[226] J. -J. Xie, A. Martinez Torres and E. Oset, Phys. Rev. C **83**, 065207 (2011).

[227] M. Bayar, J. Yamagata-Sekihara and E. Oset, Phys. Rev. C **84**, 015209 (2011).

[228] M. Bayar and E. Oset, Nucl. Phys. A **883**, 57 (2012).

[229] A. Martinez Torres, K. P. Khemchandani and E. Oset, Phys. Rev. C **79**, 065207 (2009).

[230] D. Jido and Y. Kanada-En'yo, Phys. Rev. C **78**, 035203 (2008).

[231] E. Oset, D. Jido, T. Sekihara, A. Martinez Torres, K. P. Khemchandani, M. Bayar and J. Yamagata-Sekihara, Nucl. Phys. A **881**, 127 (2012).

[232] A. Martinez Torres, E. J. Garzon, E. Oset and L. R. Dai, Phys. Rev. D **83**, 116002 (2011).

[233] N. Isgur and M. B. Wise, Phys. Lett. B **232**, 113 (1989).

[234] N. Isgur and M. B. Wise, Phys. Lett. B **237**, 527 (1990).

[235] M. Neubert, Phys. Rept. **245**, 259 (1994).

[236] A.V. Manohar and M.B. Wise, *Heavy Quark Physics*, Cambridge Monographs on Particle Physics, Nuclear Physics and Cosmology, vol. 10 (Cambridge University Press, Cambridge, England, 2000).

[237] C. Garcia-Recio, V. K. Magas, T. Mizutani, J. Nieves, A. Ramos, L. L. Salcedo and L. Tolos, Phys. Rev. D **79**, 054004 (2009).

[238] O. Romanets, L. Tolos, C. Garcia-Recio, J. Nieves, L. L. Salcedo and R. G. E. Timmermans, Phys. Rev. D **85**, 114032 (2012).

[239] E. Eichten and B. R. Hill, Phys. Lett. B **234**, 511 (1990).

[240] T. Mannel, Nucl. Phys. Proc. Suppl. **39BC**, 426 (1995).

[241] E. Eichten and B. R. Hill, Phys. Lett. B **243** (1990) 427.

[242] A. F. Falk, B. Grinstein and M. E. Luke, Nucl. Phys. B **357**, 185 (1991).

[243] T. -M. Yan, H. -Y. Cheng, C. -Y. Cheung, G. -L. Lin, Y. C. Lin and H. -L. Yu, Phys. Rev. D **46** (1992) 1148 [Erratum-ibid. D **55** (1997) 5851].

[244] G. Burdman and J. F. Donoghue, Phys. Lett. B **280**, 287 (1992).

[245] M. T. AlFiky, F. Gabbiani and A. A. Petrov, Phys. Lett. B **640**, 238 (2006).

[246] J. Nieves and M. P. Valderrama, Phys. Rev. D **86**, 056004 (2012).

[247] C. Hidalgo-Duque, J. Nieves and M. P. Valderrama, Phys. Rev. D **87**, no. 7, 076006 (2013).

[248] P. U. Sauer, A. Deltuva, A. C. Fonseca, AIP Conf. Proc. **1296**, 219-224 (2010).

[249] E. Epelbaum, PoS **CONFINEMENT8**, 187 (2008).

[250] E. Hiyama, M. Kamimura, A. Hosaka, H. Toki, M. Yahiro, Few Body Syst. **38**, 91-96 (2006).

[251] A. Martinez Torres, D. Jido, Phys. Rev. C **82**, 038202 (2010).

[252] A. Gal and H. Garcilazo, Nucl. Phys. A **864**, 153 (2011).

[253] L. Alvarez-Ruso, J. A. Oller, J. M. Alarcon, Phys. Rev. D **80**, 054011 (2009).

[254] A. Martinez Torres, D. Jido and Y. Kanada-En'yo, Phys. Rev. C **83**, 065205 (2011).

[255] A. Martinez Torres, K. P. Khemchandani, D. Jido and A. Hosaka, Phys. Rev. D **84**, 074027 (2011).

[256] J. Hofmann, M. F. M. Lutz, Nucl. Phys. A **763**, 90-139 (2005).

[257] T. Mizutani, A. Ramos, Phys. Rev. C **74**, 065201 (2006).

[258] L. Tolos, A. Ramos, T. Mizutani, Phys. Rev. C **77**, 015207 (2008).

[259] J. Hofmann, M. F. M. Lutz, Nucl. Phys. A **733**, 142-152 (2004).

[260] F. -K. Guo, P. -N. Shen, H. -C. Chiang, R. -G. Ping, Phys. Lett. B **641**, 278-285 (2006).

[261] D. Gamermann, E. Oset, D. Strottman, M. J. Vicente Vacas, Phys. Rev. D **76**, 074016 (2007).

[262] D. Gamermann, E. Oset, Eur. Phys. J. A **36**, 189-194 (2008).

[263] J. D. Weinstein, N. Isgur, Phys. Rev. D **41**, 2236 (1990).

[264] N. Kaiser, Eur. Phys. J. A **3**, 307 (1998).

[265] J. R. Pelaez, Phys. Rev. Lett. **92**, 102001 (2004).

[266] V. Baru, J. Haidenbauer, C. Hanhart, Y. .Kalashnikova, A. E. Kudryavtsev, Phys. Lett. B **586**, 53-61 (2004).

[267] C. Hanhart, Eur. Phys. J. A **31**, 543-548 (2007).

[268] Y. Ikeda and T. Sato, Phys. Rev. C **76**, 035203 (2007).

[269] N. V. Shevchenko, A. Gal and J. Mares, Phys. Rev. Lett. **98**, 082301 (2007).

[270] N. V. Shevchenko, A. Gal, J. Mares and J. Revai, Phys. Rev. C **76**, 044004 (2007).

[271] A. Dote, T. Hyodo and W. Weise, Nucl. Phys. A **804**, 197 (2008).

[272] A. Dote, T. Hyodo and W. Weise, Phys. Rev. C **79**, 014003 (2009).

[273] Y. Ikeda and T. Sato, Phys. Rev. C **79**, 035201 (2009).

[274] C. W. Xiao, M. Bayar and E. Oset, Phys. Rev. D **84**, 034037 (2011).

[275] L. Tolos, C. Garcia-Recio, V. K. Magas, T. Mizutani, J. Nieves, A. Ramos and L. L. Salcedo, Chin. Phys. C **33**, 1323 (2009).

[276] E. Oset, A. Ramos and C. Bennhold, Phys. Lett. B **527**, 99 (2002) [Erratum-ibid. B **530**, 260 (2002)].

[277] D. Jido, J. A. Oller, E. Oset, A. Ramos and U. G. Meissner, Nucl. Phys. A **725**, 181 (2003).

[278] R. Molina, D. Gamermann, E. Oset and L. Tolos, Eur. Phys. J. A **42**, 31 (2009).

[279] M. Krell, T. E. O. Ericson, Nucl. Phys. B **11**, 521-550 (1969).

[280] H. Toki, S. Hirenzaki, T. Yamazaki, R. S. Hayano, Nucl. Phys. A **501**, 653 (1989).

[281] J. Nieves, E. Oset, C. Garcia-Recio, Nucl. Phys. A **554**, 509-553 (1993).

[282] C. J. Batty, E. Friedman, A. Gal, Phys. Rept. **287**, 385-445 (1997).

[283] S. Hirenzaki, Y. Okumura, H. Toki, E. Oset and A. Ramos, Phys. Rev. C **61**, 055205 (2000).

[284] R. S. Hayano, T. Hatsuda, Rev. Mod. Phys. **82**, 2949 (2010).

[285] S. Hirenzaki, H. Toki, T. Yamazaki, Phys. Rev. C **44**, 2472-2479 (1991).

[286] J. Nieves, E. Oset, Phys. Lett. B **282**, 24-30 (1992).

[287] K. J. Raywood, J. B. Lange, G. Jones, M. Pavan, M. E. Sevior, D. A. Hutcheon, A. Olin, D. Ottewell *et* al., Phys. Rev. C **55**, 2492-2500 (1997).

[288] M. Lutz, Phys. Lett. B **426**, 12-20 (1998).

[289] A. Ramos and E. Oset, Nucl. Phys. A **671**, 481 (2000).

[290] J. Schaffner-Bielich, V. Koch, M. Effenberger, Nucl. Phys. A **669**, 153-172 (2000).

[291] A. Cieply, E. Friedman, A. Gal, J. Mares, Nucl. Phys. A **696**, 173-193 (2001).

[292] E. Friedman, A. Gal, C. J. Batty, Nucl. Phys. A **579**, 518-538 (1994).

[293] A. Baca, C. Garcia-Recio and J. Nieves, Nucl. Phys. A **673**, 335 (2000).

[294] V. K. Magas, E. Oset, A. Ramos, H. Toki, Phys. Rev. C **74**, 025206 (2006).

[295] E. Oset, V. K. Magas, A. Ramos, H. Toki, nucl-th/0701023. On the 9th International Conference On Hypernuclear And Strange Particle Physics (HYP 2006), 10-14 Oct 2006, Mainz, Germany.

[296] R. H. Dalitz and S. F. Tuan, Phys. Rev. Lett. **2**, 425 (1959); Annals Phys. **10**, 307 (1960).

[297] M. F. M. Lutz and E. E. Kolomeitsev, Nucl. Phys. A **700**, 193 (2002).

[298] T. Hyodo and D. Jido, Prog. Part. Nucl. Phys. **67**, 55 (2012), 1104.4474.

[299] Y. Ikeda, T. Hyodo and W. Weise, Phys. Lett. B **706**, 63 (2011); Nucl. Phys. A, **881**, 98 (2012).

[300] T. Yamazaki and Y. Akaishi, Phys. Lett. B **535**, 70 (2002).

[301] Y. Ikeda, H. Kamano, T. Sato, Prog. Theor. Phys. **124**, 533-539 (2010).

[302] N. Barnea, A. Gal and E. Z. Liverts, Phys. Lett. B **712** (2012) 132-137.

[303] L. Tolos, C. Garcia-Recio, J. Nieves, Phys. Rev. C **80**, 065202 (2009).

[304] C. Garcia-Recio, J. Nieves, L. Tolos, Phys. Lett. B **690**, 369-375 (2010).

[305] T. Sekihara, D. Jido, Y. Kanada-En'yo, Phys. Rev. C **79**, 062201 (2009).

[306] M. Bayar and E. Oset, Nucl. Phys. A **914**, 349 (2013).

[307] T. Hyodo and W. Weise, Phys. Rev. C **77**, 035204 (2008).

[308] R. Chand, R. H. Dalitz, Annals Phys. **20**, 1-19 (1962).

[309] U. -G. Meissner, U. Raha, A. Rusetsky, Eur. Phys. J. C **47**, 473-480 (2006).

[310] M. Bayar, C. W. Xiao, T. Hyodo, A. Dote, M. Oka and E. Oset, Phys. Rev. C **86**, 044004 (2012).

[311] R. Machleidt, Phys. Rev. C **63**, 024001 (2001).

[312] E. Oset, A. Ramos, Nucl. Phys. A **679**, 616-628 (2001).

[313] B. Borasoy, Phys. Rev. D **59**, 054021 (1999).

[314] A. L. Fetter, J. D. Walencka, Quantum Theory of Many-particle Systems, McGRAW-HILL, 1971.

[315] A. Hasegawa and S. Nagata, Prog. Theor. Phys. **45**, 1786 (1971).

[316] D. R. Thompson, M. Lemere, and Y. C. Tang, Nucl. Phys.A **286**, 53 (1977).

[317] R. B. Wiringa, V. G. J. Stoks, and R. Schiavilla, Phys. Rev. C **51**, 38 (1995).

[318] T. Yamazaki and Y. Akaishi, Phys. Rev. C **76**, 045201 (2007).

[319] A. Arai, M. Oka, and S. Yasui, Prog. Theor. Phys. **119**, 103 (2008).

[320] T. Uchino, T. Hyodo, and M. Oka, Nucl. Phys. A **868-869**, 53 (2011).

[321] A. B. Kaidalov, P. E. Volkovitsky, Z. Phys. C **63**, 517-524 (1994).

[322] A. Khodjamirian, C. .Klein, T. .Mannel, Y. -M. Wang, Eur. Phys. J. A **48**, 31 (2012).

[323] U. Wiedner, Prog. Part. Nucl. Phys. **66**, 477-518 (2011).

[324] S. Cho *et al.* [ExHIC Collaboration], Phys. Rev. Lett. **106**, 212001 (2011).

[325] S. Cho *et al.* [ExHIC Collaboration], Phys. Rev. C **84**, 064910 (2011).

[326] C. Garcia-Recio, J. Nieves, E. Ruiz Arriola and M. J. Vicente Vacas, Phys. Rev. D **67**, 076009 (2003).

[327] C. Garcia-Recio, J. Nieves and L. L. Salcedo, Phys. Rev. D **74**, 034025 (2006).

[328] T. Hyodo, S. I. Nam, D. Jido and A. Hosaka, Phys. Rev. C **68**, 018201 (2003).

[329] M. Harada and K. Yamawaki, Phys. Rept. **381**, 1 (2003).

[330] R. Molina, D. Nicmorus and E. Oset, Phys. Rev. D **78**, 114018 (2008).

[331] R. Molina, H. Nagahiro, A. Hosaka and E. Oset, Phys. Rev. D **80**, 014025 (2009).

[332] C. W. Xiao, M. Bayar and E. Oset, Phys. Rev. D **86**, 094019 (2012).

[333] N. A. Tornqvist and M. Roos, Phys. Rev. Lett. **76**, 1575 (1996).

[334] N. A. Tornqvist, Z. Phys. C **68**, 647 (1995).

[335] E. van Beveren, T. A. Rijken, K. Metzger, C. Dullemond, G. Rupp and J. E. Ribeiro, Z. Phys. C **30**, 615 (1986).

[336] M. Boglione and M. R. Pennington, Phys. Rev. D **65**, 114010 (2002).

[337] T. Branz, L. S. Geng and E. Oset, Phys. Rev. D **81**, 054037 (2010).

[338] G. Rupp, S. Coito and E. van Beveren, Acta Phys. Polon. Supp. **5**, 1007 (2012).

[339] W. -C. Chang and J. -C. Peng, Phys. Lett. B **704**, 197 (2011).

[340] W. -C. Chang and J. -C. Peng, Phys. Rev. Lett. **106**, 252002 (2011).

[341] G. T. Garvey and J. -C. Peng, Prog. Part. Nucl. Phys. **47**, 203 (2001).

[342] A. Valcarce and J. Vijande, Chin. Phys. C **34**, 1290 (2010).

[343] J. Vijande, A. Valcarce and N. Barnea, Phys. Rev. D **79**, 074010 (2009).

[344] J. Vijande, A. Valcarce and J. M. Richard, Phys. Rev. D **85**, 014019 (2012).

[345] V. Crede and W. Roberts, Rept. Prog. Phys. **76**, 076301 (2013).

[346] E. Klempt and J. -M. Richard, Rev. Mod. Phys. **82**, 1095 (2010).

[347] L. Y. Dai, X. G. Wang and H. Q. Zheng, Commun. Theor. Phys. **57**, 841 (2012).

[348] T. Inoue, E. Oset and M. J. Vicente Vacas, Phys. Rev. C **65**, 035204 (2002).

[349] M. P. Locher, V. E. Markushin and H. Q. Zheng, Eur. Phys. J. C **4**, 317 (1998).

[350] E. E. Kolomeitsev and M. F. M. Lutz, Phys. Lett. B **582**, 39 (2004).

[351] L. Li, B. -S. Zou and G. -L. Li, Phys. Rev. D **67**, 034025 (2003).

[352] J. A. Oller, Phys. Rev. D **71**, 054030 (2005).

[353] M. Ablikim *et al.* [BESIII Collaboration], Phys. Rev. Lett. **107**, 182001 (2011).

[354] M. Ablikim *et al.* [BESIII Collaboration], Phys. Rev. Lett. **106**, 072002 (2011).

[355] M. Albaladejo, J. A. Oller and L. Roca, Phys. Rev. D **82**, 094019 (2010).

[356] W. Liang, C. W. Xiao and E. Oset, Phys. Rev. D **88**, 114024 (2013).

[357] J. R. Pelaez and G. Rios, Perturbation Theory," Phys. Rev. Lett. **97**, 242002 (2006).

[358] R. Mercer, P. Antich, A. Callahan, C. Y. Chien, B. Cox, R. Carson, D. Denegri and L. Ettlinger *et al.*, Nucl. Phys. B **32**, 381 (1971).

[359] H. H. Bingham, W. M. Dunwoodie, D. Drijard, D. Linglin, Y. Goldschmidt-Clermont, F. Muller, T. G. Trippe and F. Grard *et al.*, Nucl. Phys. B **41**, 1 (1972).

[360] P. Estabrooks, R. K. Carnegie, A. D. Martin, W. M. Dunwoodie, T. A. Lasinski and D. W. G. S. Leith, Nucl. Phys. B **133**, 490 (1978).

[361] A. Martinez Torres, K. P. Khemchandani, D. Jido and A. Hosaka, Phys. Rev. D **84**, 074027 (2011).

[362] L. Roca, E. Oset and J. Singh, Phys. Rev. D **72**, 014002 (2005).

[363] L. S. Geng, E. Oset, L. Roca and J. A. Oller, Phys. Rev. D **75**, 014017 (2007).

[364] Y. Zhou, X. -L. Ren, H. -X. Chen and L. -S. Geng, arXiv:1404.6847 [nucl-th].

[365] M. Bayar, W. H. Liang, T. Uchino and C. W. Xiao, Eur. Phys. J. A **50**, 67 (2014).

[366] S. Ceci, M. Doring, C. Hanhart, S. Krewald, U. -G. Meissner and A. Svarc, Phys. Rev. C **84**, 015205 (2011).

[367] S. R. Coleman, J. Wess and B. Zumino, Phys. Rev. **177**, 2239 (1969).

[368] L. Castillejo, R. H. Dalitz and F. J. Dyson, Phys. Rev. **101**, 453 (1956).

[369] David J. Griffiths, *Introduction to quantum mechanics*, 2005, Pearson Education, Inc.

[370] V. Baru, C. Hanhart, A. E. Kudryavtsev and U. G. Meissner, Phys. Lett. B **589**, 118 (2004).

[371] V. Lensky, V. Baru, J. Haidenbauer, C. Hanhart, A. E. Kudryavtsev and U. -G. Meissner, Eur. Phys. J. A **26**, 107 (2005).

[372] V. Baru, E. Epelbaum and A. Rusetsky, Eur. Phys. J. A **42**, 111 (2009).

[373] E. J. Garzon, J. J. Xie and E. Oset, Phys. Rev. C **87**, 055204 (2013).

[374] C. -H. Oh, R. A. Arndt, I. I. Strakovsky and R. L. Workman, Phys. Rev. C **56**, 635 (1997).

[375] A. Martinez Torres, K. P. Khemchandani, U. -G. Meissner and E. Oset, Eur. Phys. J. A **41**, 361 (2009).

[376] S. Weinberg, Physica A **96**, 327 (1979).

[377] J. Gasser and H. Leutwyler, Annals Phys. **158**, 142 (1984).

[378] J. J. Sakurai, Currents and Mesons (University of Chicago Press, Chicago, 1969).

[379] L. S. Geng and E. Oset, Phys. Rev. D **79**, 074009 (2009).

[380] H. Nagahiro, J. Yamagata-Sekihara, E. Oset, S. Hirenzaki and R. Molina, Phys. Rev. D **79**, 114023 (2009).

[381] A. Martinez Torres, L. S. Geng, L. R. Dai, B. X. Sun, E. Oset and B. S. Zou, Phys. Lett. B **680**, 310 (2009).

[382] L. S. Geng, F. K. Guo, C. Hanhart, R. Molina, E. Oset and B. S. Zou, Eur. Phys. J. A **44**, 305 (2010).

[383] R. Molina and E. Oset, Phys. Rev. D **80**, 114013 (2009).

[384] R. Molina, T. Branz and E. Oset, Phys. Rev. D **82**, 014010 (2010).

[385] Y. Dong, A. Faessler, T. Gutsche and V. E. Lyubovitskij, J. Phys. G **40**, 015002 (2013).

[386] T. Branz, T. Gutsche and V. E. Lyubovitskij, Phys. Rev. D **82**, 054010 (2010).

[387] T. Branz, T. Gutsche and V. E. Lyubovitskij, Phys. Rev. D **82**, 054025 (2010).

[388] I. W. Lee, A. Faessler, T. Gutsche and V. E. Lyubovitskij, Phys. Rev. D **80**, 094005 (2009).

[389] S. Sarkar, B. -X. Sun, E. Oset and M. J. Vicente Vacas, Eur. Phys. J. A **44**, 431 (2010).

[390] E. Oset, A. Ramos, Eur. Phys. J. A **44**, 445-454 (2010).

[391] E. J. Garzon and E. Oset, Eur. Phys. J. A **48**, 5 (2012).

[392] K. P. Khemchandani, H. Kaneko, H. Nagahiro and A. Hosaka, Phys. Rev. D **83**, 114041 (2011).

[393] K. P. Khemchandani, A. Martinez Torres, H. Kaneko, H. Nagahiro and A. Hosaka, Phys. Rev. D **84**, 094018 (2011).

[394] K. P. Khemchandani, A. Martinez Torres, H. Nagahiro and A. Hosaka, Phys. Rev. D **85**, 114020 (2012).

[395] E. Oset, A. Ramos, E. J. Garzon, R. Molina, L. Tolos, C. W. Xiao, J. J. Wu and B. S. Zou, Int. J. Mod. Phys. E **21**, 1230011 (2012).

[396] D. Gamermann, C. Garcia-Recio, J. Nieves, L. L. Salcedo and L. Tolos, Phys. Rev. D **81**, 094016 (2010).

[397] C. Garcia-Recio, J. Nieves, O. Romanets, L. L. Salcedo and L. Tolos, Phys. Rev. D **87**, 074034 (2013).

[398] C. Garcia-Recio, J. Nieves, O. Romanets, L. L. Salcedo and L. Tolos, Phys. Rev. D **87**, 034032 (2013).

[399] RAaij *et al.* [LHCb Collaboration], Phys. Rev. Lett. **109**, 172003 (2012).

[400] C. Hidalgo-Duque, J. Nieves and M. Pavn Valderrama, Nucl. Phys. A **914**, 482 (2013).

[401] F. -K. Guo, C. Hanhart and U. -G. Meissner, Phys. Rev. Lett. **102**, 242004 (2009).

[402] F. -K. Guo, C. Hidalgo-Duque, J. Nieves and M. P. Valderrama, Phys. Rev. D **88**, 054007 (2013).

[403] M. F. M. Lutz and E. E. Kolomeitsev, Nucl. Phys. A **730**, 110 (2004).

[404] M. F. M. Lutz and E. E. Kolomeitsev, Nucl. Phys. A **755**, 29 (2005).

[405] J. Hofmann and M. F. M. Lutz, Nucl. Phys. A **776**, 17 (2006).

[406] L. Tolos, J. Schaffner-Bielich and A. Mishra, Phys. Rev. C **70**, 025203 (2004).

[407] C. E. Jimenez-Tejero, A. Ramos and I. Vidana, Phys. Rev. C **80**, 055206 (2009).

[408] J. Haidenbauer, G. Krein, U. -G. Meissner and A. Sibirtsev, Eur. Phys. J. A **33**, 107 (2007).

[409] J. Haidenbauer, G. Krein, U. -G. Meissner and A. Sibirtsev, Eur. Phys. J. A **37**, 55 (2008).

[410] J. Haidenbauer, G. Krein, U. -G. Meissner and L. Tolos, Eur. Phys. J. A **47**, 18 (2011).

[411] M. E. Rose, Elementary Theory of Angular Momentum, John Wiley, 1957.

[412] C. W. Xiao, J. Nieves and E. Oset, Phys. Rev. D **88**, 056012 (2013).

[413] B. El-Bennich, G. Krein, L. Chang, C. D. Roberts and D. J. Wilson, Phys. Rev. D **85**, 031502 (2012).

[414] K. U. Can, G. Erkol, M. Oka, A. Ozpineci and T. T. Takahashi, Phys. Lett. B **719**, 103 (2013).

[415] D. Becirevic, V. Lubicz, F. Sanfilippo, S. Simula and C. Tarantino, JHEP **1202**, 042 (2012).

[416] B. El-Bennich, C. D. Roberts and M. A. Ivanov, arXiv:1202.0454 [nucl-th].

[417] D. Becirevic and B. Haas, Eur. Phys. J. C **71**, 1734 (2011).

[418] M. E. Bracco, M. Chiapparini, F. S. Navarra and M. Nielsen, Prog. Part. Nucl. Phys. **67**, 1019 (2012).

[419] C. Garcia-Recio, M. F. M. Lutz and J. Nieves, Phys. Lett. B **582**, 49 (2004).

[420] D. Gamermann, C. Garcia-Recio, J. Nieves and L. L. Salcedo, Phys. Rev. D **84**, 056017 (2011).

[421] M. Ablikim *et al.* [BES Collaboration], Phys. Lett. B **685**, 27 (2010).

[422] J. -J. Xie, M. Albaladejo and E. Oset, Phys. Lett. B **728**, 319 (2014).

[423] W. Liang, M. Albaladejo and E. Oset, Phys. Rev. D **88**, 074027 (2013).

[424] X. -L. Ren, L. -S. Geng, E. Oset and J. Meng, arXiv:1405.0153 [nucl-th].

[425] E. E. Kolomeitsev and M. F. M. Lutz, Phys. Lett. B **585**, 243 (2004).

[426] F. -K. Guo, C. Hanhart and U. -G. Meissner, Phys. Lett. B **665**, 26 (2008).

[427] J. Nieves and M. P. Valderrama, Phys. Rev. D **84**, 056015 (2011).

[428] C. W. Xiao and E. Oset, Eur. Phys. J. A **49**, 139 (2013).

[429] Y. -J. Zhang, H. -C. Chiang, P. -N. Shen and B. -S. Zou, Phys. Rev. D **74**, 014013 (2006).

[430] Z. -H. Li, T. Huang, J. -Z. Sun and Z. -H. Dai, Phys. Rev. D **65**, 076005 (2002).

[431] Z. -H. Li, W. Liu and H. -Y. Liu, Phys. Lett. B **659**, 598 (2008).

[432] E. Oset, H. Toki, M. Mizobe and T. T. Takahashi, Prog. Theor. Phys. **103**, 351 (2000).

[433] A. Ali, PoS BEAUTY **2011**, 002 (2011).

[434] M. Gersabeck, Mod. Phys. Lett. A **27**, 1230026 (2012).

[435] S. L. Olsen, Prog. Theor. Phys. Suppl. **193**, 38 (2012).

[436] L. Li [BESIII Collaboration], Nucl. Phys. B, Proc. Suppl. **225-227**, 107 (2012).

[437] N. A. Tornqvist, Phys. Rev. Lett. **67**, 556 (1991).

[438] N. A. Tornqvist, Z. Phys. C **61**, 525 (1994).

[439] E. S. Swanson, Phys. Lett. B **588**, 189 (2004).

[440] C. E. Thomas and F. E. Close, Phys. Rev. D **78**, 034007 (2008).

[441] M. B. Voloshin and L. B. Okun, JETP Lett. **23**, 333 (1976) [Pisma Zh. Eksp. Teor. Fiz. **23**, 369 (1976)].

[442] Z. -F. Sun, J. He, X. Liu, Z. -G. Luo and S. -L. Zhu, Phys. Rev. D **84**, 054002 (2011).

[443] N. Li and S. -L. Zhu, Phys. Rev. D **86**, 074022 (2012).

[444] M. T. Li, W. L. Wang, Y. B. Dong and Z. Y. Zhang, J. Phys. G **40**, 015003 (2013).

[445] M. T. Li, W. L. Wang, Y. B. Dong and Z. Y. Zhang, Int. J. Mod. Phys. A **27**, 1250161 (2012).

[446] T. Branz, T. Gutsche and V. E. Lyubovitskij, Phys. Rev. D **80**, 054019 (2009).

[447] A. Faessler, T. Gutsche, V. E. Lyubovitskij and Y. -L. Ma, Phys. Rev. D **76**, 014005 (2007).

[448] J. Segovia, A. M. Yasser, D. R. Entem and F. Fernandez, Phys. Rev. D **78**, 114033 (2008).

[449] T. Fernandez-Carames, A. Valcarce and J. Vijande, Phys. Rev. Lett. **103**, 222001 (2009).

[450] T. Gutsche and V. E. Lyubovitskij, AIP Conf. Proc. **1257**, 385 (2010).

[451] G. -J. Ding, J. -F. Liu and M. -L. Yan, Phys. Rev. D **79**, 054005 (2009).

[452] M. B. Voloshin, JETP Lett. **37**, 69 (1983) [Pisma Zh. Eksp. Teor. Fiz. **37**, 58 (1983)].

[453] A. E. Bondar, A. Garmash, A. I. Milstein, R. Mizuk and M. B. Voloshin, Phys. Rev. D **84**, 054010 (2011).

[454] S. Ohkoda, Y. Yamaguchi, S. Yasui, K. Sudoh and A. Hosaka, Phys. Rev. D **86**, 034019 (2012).

[455] X. Liu, Y. -R. Liu, W. -Z. Deng and S. -L. Zhu, Phys. Rev. D **77**, 034003 (2008).

[456] M. Cleven, F. -K. Guo, C. Hanhart and U. -G. Meissner, Eur. Phys. J. A **47**, 120 (2011).

[457] N. Li, Z. -F. Sun, X. Liu and S. -L. Zhu, Phys. Rev. D **88**, 114008 (2013).

[458] M. Cleven, Q. Wang, F. -K. Guo, C. Hanhart, U. -G. Meissner and Q. Zhao, Phys. Rev. **87**, 074006 (2013).

[459] I. Adachi *et al.* [Belle Collaboration], arXiv:1209.6450 [hep-ex].

[460] I. Adachi *et al.* [Belle Collaboration], arXiv:1207.4345 [hep-ex].

[461] A. Ozpineci, C. W. Xiao and E. Oset, Phys. Rev. D **88**, 034018 (2013).

[462] Y. -R. Liu, X. Liu, W. -Z. Deng and S. -L. Zhu, Eur. Phys. J. C **56**, 63 (2008).

[463] Y. .S. Kalashnikova and A. V. Nefediev, JETP Lett. **97**, 70 (2013) [JETP Lett. **97**, 70 (2013)].

[464] T. Mehen and J. W. Powell, Phys. Rev. D **84**, 114013 (2011).

[465] V. Baru, A. A. Filin, C. Hanhart, Y. .S. Kalashnikova, A. E. Kudryavtsev and A. V. Nefediev, Phys. Rev. D **84**, 074029 (2011).

[466] F. Aceti, M. Bayar and E. Oset, arXiv:1401.2076 [hep-ph].

[467] F. Aceti, L. R. Dai, L. S. Geng, E. Oset and Y. Zhang, Eur. Phys. J. A **50**, 57 (2014).

[468] P. De Simone [LHCb Collaboration], Nucl. Phys. B, Proc. Suppl. **233**, 18 (2012).

[469] P. Palni [CDF Collaboration], Nucl. Phys. B, Proc. Suppl. **233**, 151 (2012).

[470] L. Maiani, V. Riquer, F. Piccinini and A. D. Polosa, Phys. Rev. D **72**, 031502 (2005).

[471] E. Swanson, Int. J. Mod. Phys. A **21**, 733 (2006) [AIP Conf. Proc. **814**, 203 (2006)].

[472] J. L. Rosner, J. Phys. Conf. Ser. **69**, 012002 (2007).

[473] M. Nielsen, F. S. Navarra and S. H. Lee, Phys. Rept. **497**, 41 (2010).

[474] P. G. Ortega, D. R. Entem and F. Fernandez, J. Phys. G **40**, 065107 (2013).

[475] O. Romanets, L. Tolos, C. Garca-Recio, J. Nieves, L. L. Salcedo and R. Timmermans, Nucl. Phys. A **914**, 488 (2013).

[476] P. G. Ortega, D. R. Entem and F. Fernandez, Phys. Lett. B **718**, 1381 (2013).

[477] T. A. Aaltonen *et al.* [CDF Collaboration], Phys. Rev. D **88**, 071101 (2013).

[478] P. Palni [for the CDF Collaboration], arXiv:1309.6269 [hep-ex].

[479] S. Capstick and N. Isgur, Phys. Rev. D **34**, 2809 (1986).

[480] H. Garcilazo, J. Vijande and A. Valcarce, J. Phys. G **34**, 961 (2007).

[481] S. Sarkar, E. Oset and M. J. Vicente Vacas, Nucl. Phys. A **750**, 294 (2005) [Erratum-ibid. A **780**, 78 (2006)].

[482] W. H. Liang, C. W. Xiao and E. Oset, Phys. Rev. D **89**, 054023 (2014).

[483] M. B. Wise, Phys. Rev. D **45**, 2188 (1992).

[484] R. C. Carrasco and E. Oset, Nucl. Phys. A **536**, 445 (1992).

[485] R. Machleidt, K. Holinde and C. Elster, Phys. Rept. **149**, 1 (1987).

[486] E. Oset and M. J. Vicente-Vacas, Nucl. Phys. A **446**, 584 (1985).

[487] E. Oset, H. Toki and W. Weise, Phys. Rept. **83**, 281 (1982).

[488] J. M. Flynn, E. Hernandez and J. Nieves, Phys. Rev. D **85**, 014012 (2012).

[489] M. F. M. Lutz and C. L. Korpa, Phys. Lett. B **633**, 43 (2006).

[490] L. Tolos, J. Schaffner-Bielich and H. Stoecker, Phys. Lett. B **635**, 85 (2006).

[491] W. H. Liang, T. Uchino, C. W. Xiao and E. Oset, arXiv:1402.5293 [hep-ph].

[492] P. Gonzalez, E. Oset and J. Vijande, Phys. Rev. C **79**, 025209 (2009).

[493] R. Vogt, Phys. Rept. **310**, 197 (1999).

[494] R. Vogt, Nucl. Phys. A **700**, 539 (2002).

[495] B. Z. Kopeliovich and B. G. Zakharov, Phys. Rev. D **44**, 3466 (1991).

[496] A. Sibirtsev, K. Tsushima and A. W. Thomas, Phys. Rev. C **63**, 044906 (2001).

[497] K. J. Eskola, H. Paukkunen and C. A. Salgado, JHEP **0904**, 065 (2009).

[498] S. Gavin and J. Milana, Phys. Rev. Lett. **68**, 1834 (1992).

[499] E. Marco and E. Oset, Nucl. Phys. A **645**, 303 (1999).

[500] T. Matsui and H. Satz, Phys. Lett. B **178**, 416 (1986).

[501] B. Alessandro *et al.* [NA50 Collaboration], Eur. Phys. J. C **48**, 329 (2006).

[502] J. Badier *et al.* [NA3 Collaboration], Z. Phys. C **20**, 101 (1983).

[503] D. M. Alde, H. W. Baer, T. A. Carey, G. T. Garvey, A. Klein, C. Lee, M. J. Leitch and J. Lillberg *et al.*, Phys. Rev. Lett. **66**, 133 (1991).

[504] M. C. Abreu *et al.* [NA38 Collaboration], Phys. Lett. B **444**, 516 (1998).

[505] M. J. Leitch *et al.* [FNAL E866/NuSea Collaboration], Phys. Rev. Lett. **84**, 3256 (2000).

[506] A. Gribushin *et al.* [E672 and E706 Collaborations], Phys. Rev. D **62**, 012001 (2000).

[507] B. Alessandro *et al.* [NA50 Collaboration], Phys. Lett. B **553**, 167 (2003).

[508] B. Alessandro *et al.* [NA50 Collaboration], Eur. Phys. J. C **33**, 31 (2004).

[509] R. Arnaldi *et al.* [NA60 Collaboration], Phys. Lett. B **706**, 263 (2012) [arXiv:1004.5523 [nucl-ex]].

[510] L. Tolos, R. Molina, E. Oset and A. Ramos, Phys. Rev. C **82**, 045210 (2010).

[511] R. Rapp, G. Chanfray and J. Wambach, Nucl. Phys. A **617**, 472 (1997).

[512] W. Peters, M. Post, H. Lenske, S. Leupold and U. Mosel, Nucl. Phys. A **632**, 109 (1998).

[513] R. Rapp and J. Wambach, Adv. Nucl. Phys. **25**, 1 (2000).

[514] M. Urban, M. Buballa, R. Rapp and J. Wambach, Nucl. Phys. A **673**, 357 (2000).

[515] D. Cabrera, E. Oset and M. J. Vicente Vacas, Nucl. Phys. A **705**, 90 (2002).

[516] D. Cabrera and M. J. Vicente Vacas, Phys. Rev. C **67**, 045203 (2003).

[517] S. Leupold, V. Metag and U. Mosel, Int. J. Mod. Phys. E **19**, 147 (2010).

[518] R. Molina, C. W. Xiao and E. Oset, Phys. Rev. C **86**, 014604 (2012).

[519] K. P. Khemchandani, A. Hosaka, H. Kaneko and H. Nagahiro, AIP Conf. Proc. **1388**, 310 (2011).

[520] E. J. Garzon and E. Oset, Eur. Phys. J. A **48**, 5 (2012).

[521] P. Muhlich and U. Mosel, Nucl. Phys. A **773**, 156 (2006).

[522] M. Nanova [CBELSA/TAPS Collaboration], arXiv:1111.6006 [nucl-ex], submitted to Phys. Lett. B.

[523] N. Bianchi *et al.*, Phys. Rev. C **54**, 1688 (1996).

[524] H. D. Politzer, Phys. Rept. **14**, 129 (1974).

[525] C. B. Lang, L. Leskovec, D. Mohler and S. Prelovsek, Phys. Rev. D **86**, 054508 (2012).

[526] Z. Fu and K. Fu, Phys. Rev. D **86**, 094507 (2012).

[527] N. Isgur and G. Karl, Phys. Rev. D **18**, 4187 (1978).

[528] S. Capstick and W. Roberts, Prog. Part. Nucl. Phys. **45**, S241 (2000).

[529] A. Valcarce, H. Garcilazo, F. Fernandez and P. Gonzalez, Rept. Prog. Phys. **68**, 965 (2005).

[530] J. Vijande, F. Fernandez, A. Valcarce and B. Silvestre-Brac, Eur. Phys. J. A **19**, 383 (2004).

[531] C. Hanhart, Y. .S. Kalashnikova and A. V. Nefediev, Phys. Rev. D **81**, 094028 (2010).

[532] S. G. Wojcicki, Phys. Rev. **135**, B484 (1964).

[533] P. M. Dauber, P. E. Schlein, W. E. Slater and H. K. Ticho, Phys. Rev. **153**, 1403 (1967).

[534] N. Barash, L. Kirsch, D. Miller and T. H. Tan, Phys. Rev. **156**, 1399 (1967).

[535] C. W. Xiao, F. Aceti and M. Bayar, Eur. Phys. J. A **49**, 22 (2013).

[536] D. R. Boito, R. Escribano and M. Jamin, JHEP **1009**, 031 (2010).

[537] D. R. Boito, R. Escribano and M. Jamin, Eur. Phys. J. C **59**, 821 (2009).

[538] F. K. Guo, lectures in the Hadron Physics Summer School 2012 (HPSS2012), Germany.

[539] C. Hanhart, J. R. Pelaez and G. Rios, Phys. Rev. Lett. **100**, 152001 (2008).

[540] J. Nieves and E. Ruiz Arriola, Phys. Lett. B **455**, 30 (1999).

[541] J. Nieves and E. Ruiz Arriola, Phys. Rev. D **80**, 045023 (2009).

[542] P. Pakhlov *et al.* [Belle Collaboration], Phys. Rev. Lett. **100** (2008) 202001.

[543] C. W. Xiao and E. Oset, Eur. Phys. J. A **49**, 52 (2013).